



PhD-FSTC-2019-46
The Faculty of Sciences, Technology and Communication

DISSERTATION

Defence held on 20/06/2019 in Esch-sur-Alzette
to obtain the degree of

DOCTEUR DE L'UNIVERSITÉ DU LUXEMBOURG

EN *SCIENCES DE L'INGENIEUR*

by

Khalid Ibnou Walid KANE

Born on 2 April 1990 in Dakar (Senegal)

AUTOMATED OPTIMISATION OF STEM CELL-DERIVED NEURONAL CELL CULTURE IN THREE-DIMENSIONAL MICROFLUIDIC DEVICES

Dissertation defence committee

Dr Jens Christian Schwamborn, dissertation supervisor
Professor, Université du Luxembourg

Dr Achim Wixforth
Professor, University of Augsburg

Dr Rejko Krüger, Chairman
Professor, Université du Luxembourg

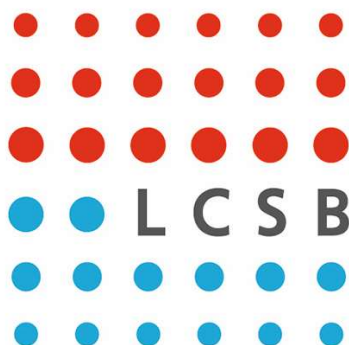
Dr Christian Wagner
Professor, Universität des Saarlandes

Dr Andreas Zilian, Vice Chairman
Professor, Université du Luxembourg

Luxembourg Centre for Systems Biomedicine

Faculty of Life Sciences, Technology and Communication

Supported by the European Union's Horizon 2020 research and innovation programme under grant agreement No 668738



Affidavit

I hereby confirm that the PhD thesis entitled “Automated optimisation of neuronal cell culture in microfluidic devices” has been written independently and without any other than cited.

Luxembourg, July 8, 2019



Khalid Ibnou Walid Kane

Contents

AFFIDAVIT

List of figures

NOMENCLATURE

ABSTRACT

SCIENTIFIC OUTPUT

- A. *Publications in peer-review journals*
- B. *Invention disclosure in preparation at the University of Luxembourg Patent office*
- C. *Manual book*
- D. *Manuscripts in preparation*
- E. *Poster presentations in scientific conferences*

1. INTRODUCTION

- 1.1. *Parkinson's disease and neuronal cell culture*
- 1.2. *Microfluidic cell culture*
- 1.3. *3D Microfluidic neuronal culture*
- 1.4. *Extracellular matrix and its properties in microfluidic cell culture*
- 1.5. *Flow characteristics*
- 1.6. *Laboratory automation*
- 1.7. *Aim of the thesis*
- 1.8. *References*

2. DETERMINATION OF THE RHEOLOGICAL PROPERTIES OF MATRIGEL FOR OPTIMUM SEEDING

- 2.1. *Abstract*
- 2.2. *Introduction*
- 2.3. *Experimental*
- 2.4. *Results and discussion*
- 2.5. *Conclusions*
- 2.6. *Supplementary Materials*
- 2.7. *Acknowledgements*
- 2.8. *References*

3. PASSIVE CONTROLLED FLOW FOR NEURONAL CELL CULTURE IN 3D MICROFLUIDIC DEVICES

- 2.1. *Abstract*
- 2.2. *Nomenclature*
- 2.3. *Introduction*
- 2.4. *Materials and Methods*
- 2.5. *Results and Discussion*
- 2.6. *Conclusions*
- 2.7. *References*

4. AUTOMATED MICROFLUIDIC CELL CULTURE OF STEM CELL DERIVED

- 4.1. *Abstract*
- 4.2. *Introduction*
- 4.3. *Results*
- 4.4. *Discussion*
- 4.5. *Methods*

- 4.6. *References*
- 4.7. *Acknowledgements*
- 4.8. *Competing interests*
- 4.9. *Author Contributions Statement*
- 4.10. *Data availability*

5. NEURONAL HYPERACTIVITY IN A LRRK2-G2019S CELLULAR MODEL OF PARKINSON'S DISEASE

- 5.1. *Abstract*
- 5.2. *Introduction*
- 5.3. *Materials and methods*
- 5.4. *Results*
- 5.5. *Discussion*
- 5.6. *Conclusion*
- 5.7. *Acknowledgements*
- 5.8. *References*

6. CONCLUSIONS AND OUTLOOK

7. SUPPLEMENTARY MATERIAL FOR CHAPTER 2

8. SUPPLEMENTARY MATERIAL FOR CHAPTER 3

9. SUPPLEMENTARY MATERIAL FOR CHAPTER 4

10. SUPPLEMENTARY MATERIAL FOR CHAPTER 5

11. PELICAN USER MANUAL

12. CV

List of figures

Figure 1.1: Does connectivity predict Lewy pathology in clinical Parkinson disease?

Figure 1.2: Parkinson's disease motor symptoms caused by degeneration of neurons in the substantia nigra

Figure 1.3: Parkinson's disease dopaminergic neuronal dysfunction

Figure 1.4: Example of a Lab on chip. A biochip for identifying proteins, Lab on Chip - systems all process for analysis of a sample are integrated into one glass plate

Figure 1.5: schematic representation of a lab-on-a-chip

Figure 1.6: Laminar and turbulent flow profiles

Figure 1.7: Standard communication between devices in an automation plant. HTTP=Hypertext Transfer Protocol. Telnet=Teletype Over Network Protocol for Local Area network or internet. USB=Universal Serial Bus. CAN=Controller Area Network. RS232=Recommend Standard 232

Figure 2.1: . Melting transition of pure Matrigel as seen by Differential Scanning Calorimetry (DSC). Heating rate: 10 K/min)

Figure 2.2: Schematic representation of the OrganoPlate

Figure 2.3: Experimental setup for the rheological measurements (plate radius $R=12.5$ mm; gap width $h=0.5$ to 1 mm). A torque M is applied to the upper plate leading to a rotation. The lower plate is fixed.

Figure 2.4: Determination of the linear response regimes: G' (filled symbols) and G'' (open symbols) as a function of strain amplitude; the strain amplitude runs were carried out under isothermal conditions at the temperatures indicated in the legend.

Figure 2.5: Gelation of Matrigel: G' (filled symbols) and G'' (open symbols) as a function of oscillation frequency; measured isothermally at the temperatures indicated in the legend. For details see text.

Figure 2.6: Flow curves. First scan with increasing shear rates (\nearrow): filled symbols. Second scan with decreasing shear rates (\searrow): open symbols. For more details see text.

Figure 2.7: Velocity profile across the culture lane (for the definition of the r -axis see Figure 2). Filled symbols: PIV data used for fitting. Empty symbols: PIV data not used for fitting (see text). Solid line: Fit using a power law model function. Dashed line: Fit using a Hagen-Poiseuille model. For all fits: $R=87\mu\text{m}$

Figure 2.8: Shear rates at 8°C and 2°C . Shear rates at 8°C are determined from the velocity profiles. Shear rates at 2°C are calculated from the 8°C curves with the help of the flow curves (Fig. 2.6). ΔP =pressure drop, Q =volumetric flow rate

Figure 3.1: Schematic representation of the media section of the media lane. Scheme of a single 2-lane bioreactor composed of a gel inlet (1), a perfusion inlet (2), an optical readout window (3) and a perfusion outlet (4)

Figure 3.2: Flow rate in the medium lane for 24 hours

Figure 3.3: Targeted flow rate for dynamic similarity between the brain and the OrganoPlate

Figure 3.4: Sensitivity analysis of the design variable

Figure 3.5: Ease of change ranking of parameters of hydraulic resistance

Figure 3.6: 3D microfluidic device optimised for neuronal cell culture. (A) Optimum design. (B) Modification for manufacturing of a bioreactor. (C) The new design applied to a 384 microtiter plate

Figure 3.7: Flow rates inside the new microfluidic medium lane

Figure 4.1: Pelican automated cell culture observatory. (A) Top view inside the Pelican automation workstation without housing: (1) Wide angle lens image of the automated

enclosure. (2) Wide angle lens image of the adjacent manual cell culture bench. (B) Outside view of automated culture system (top). Front (bottom left) and rear (bottom right) views of Pelican with housing. Yellow (imaging station), light blue (liquid handling station), green (level of stainless steel work surface) and orange (waste containers). The colour codes of the devices labels in (A) and Fig. S1 match.

Figure 4.2: Microfluidic cell culture device: OrganoPlate. (A) Photograph of underside (left) and upper views (right) of an OrganoPlate. (B) bottom plate of OrganoPlate with selective chips. (C) A schematic of a single 2-lane chip; 1 = Gel inlet, 2 = Medium inlet, 3 = Observation window, 4 = Medium outlet. (D) A transverse section of a culture chamber showing the direction of the flow in the medium lane (yellow arrow), the phaseguide and the culture lane with suspended spheres representing cells embedded in Matrigel. (E) Top view of transverse section of a culture chamber with phaseguide, medium and culture lanes. All dimensions in μm .

Figure 4.3: Semi-automated image acquisition pipeline. See Supplementary Fig. S5 for more details.

Figure 4.4: Automated media change pipeline. See Supplementary Fig. S4 for more details.

Figure 4.5: Dopaminergic neuronal differentiation. Bright field images of hNESCs with media components at (A) 1 day (B) 4 days and (C) 21 days after seeding. (D) Calcium imaging frame of a firing event taken at day 24 after seeding. (E) Immunofluorescence image illustrating the neuronal composition inside a culture chamber. All scale bars are 50 μm . Legend as in Fig. 6.

Figure 4.6: Immunostaining and automated cell segmentation of calcium time-series hNEESC differentiated in chips of the OrganoPlate inside the Pelican. (A) Top view of an entire chip in the OrganoPlate showing differentiated wild type neurons (K7 cell line) immunostained for nuclei with Hoechst (blue), TUB β III (green) and tyrosine hydroxylase (red); scale bar 300 μm . (B) Enlarge top (B) and front (C) views of selected area; scale bar 50 μm . (D) Differentiation efficiency of neurons positive for TUB β III and tyrosine hydroxylase. (E) Mean fluorescence frame of a calcium time-series of WT population with segmented regions of interest corresponding to individual neurons and (F) their corresponding fluorescence traces. (G)

Mean fluorescence frame of a calcium time-series of PINK1 mutants with segmented regions of interest corresponding to individual neurons and their corresponding fluorescence traces (H).

Figure 4.7: CAD drawing of automated workstation. (a) Top view inside the Pelican without housing. (b) Front view of the Pelican with housing. Yellow (imaging station), light blue (liquid handling station), green (level of stainless steel work surface) and orange (waste containers). Perforated surface = work surface. (1) Storage incubator. (2) Liquid-handler. (3) Hotels (manual working bench). (4) Position of microscopy station. (5) Position of liquid dispenser. (6) Automated work bench. Coordinates shown here are consistent with the remainder of the manuscript. See also Figs S1 and S2.

Figure 5.1: Automated image analysis pipeline for calcium imaging data to quantify neuronal activity. Cells are cultured in an automated cell culture observatory (a). Calcium imaging data of a neuronal population are acquired (b). Regions of interest (ROIs) corresponding to individual neurons are identified (c). Fluorescence traces (black traces) and their underlying spike trains (red lines) are measured for each ROI (d). Calcium transients are detected and their properties are estimated, as shown below in Figure 2 (e). Statistical analysis is performed to estimate differences in calcium transient parameters between two neuronal populations.

Figure 5.2: Description of the measured calcium transient features.

Figure 5.3: Automated segmentation, fluorescence trace estimation and spike train inference of calcium time-series of a neuronal population. (a) Mean fluorescence frame of a calcium time-series (top) and numbered segmentation of individual neuronal somata (bottom). (b) Fluorescence baseline correction. (c) Fluorescence traces corresponding to the segmented neurons in (a).

Figure 5.4: Effect of wavelet scale size on segmentation. (a) Different wavelet scale sizes have different effects on the image in the preprocessing step. The purpose of the wavelet function is to smooth the image and give more intensity to round shapes such as cell bodies. (b) The effect of different wavelet scales on segmentation of somas of an average diameter of 12 μm . Clearly, wavelet scale 5, compared with 3 and 4, induces a more accurate segmentation as

the somata are well delineated. (c) The effect of different wavelet scales on segmentation of somas of an average diameter of 8 μm . Clearly, wavelet scale 4 performs better than 3, where some somata are subdivided into several parts and 5, where some somata are merged in one segment. (d) Effect of intensity threshold on segmentation.

Figure 5.5: Classification of mean interspike interval (ISI) values (K7 and K7M cell-lines). (a) Scatter plot of merged inter-spike intervals (ISI, seconds) from control and LRRK2-G2019S mutants. (b) Classification of inter-spike intervals into 10-sec interval groups, colours correspond to individual classes (1 - 3). (c) Scatter plots of the merged inter-spike intervals from control and LRRK2-G2019S neurons for each class. (d) Pie charts showing relative proportions of neurons in each inter-spike interval class colour-coded same as in (b).

Figure 5.6: Hyperactivity of LRRK2-G2019S mutant neurons. (a) Mean fluorescence frames of K7 (control) and K7M (LRRK2-G2019S) cell-lines overlaid with activity maps (top) and examples of traces from each class (bottom). (b) Comparison of the fractions of LRRK2-G2019S neurons in each class relative to wild-type (for both cell-lines).

Figure 9.1: Pelican hardware and software control architecture. Standard on arrow = type of physical connection between a device and the computer. CAN = Controller Area Network. PCI = Peripheral Component Interconnect. RS232 = Recommend Standard number 232. TCP/IP = Transmission Control Protocol/Internet Protocol.

Figure 9.2: Left and right views of Pelican with housing illustrating the manual work bench and hotels (Left) that connect the Pelican to the outside world and the automated liquid handling station (Right).

Figure 9.3: Liquid handler data model for pipetting protocols. Blue (physical action of pipette), red (passive action of pipette: reading from liquid-handler database) and green (passive action of pipette: determining well geometry). QPM=Qualitative Pipette Monitoring. LLD=Liquid Level Detection. The automated pipetting follows this order: pickup a disposable tip, detect the liquid level, aspirate liquid, dispense the liquid into the destination well and finally discard the tip.

Figure 9.4: Automated media change pipeline. W = Washer, P = Peristaltic, 0 = Method not applied to column, 1 = Method applied to column, -1 = search position. Curved connection = Plate movement. Straight connection = Device specific method.

Figure 9.5: Automated image acquisition pipeline. Abbreviations as in Figure S4.

Figure 10.1 : Differentiation of hNESC into dopaminergic neurons. (a) Protocol using small molecules. Bright field images of (b) hNESC 1 day after seeding, cultured in maintenance media containing N2B27 medium, ascorbic acid, PMA and CHIR. (c) hNESC 3 days after seeding, cultured in differentiation media containing N2B27 medium ascorbic acid, BDNF, GDNF, TGF β 3, dbcAMP and PMA. (d) hNESC 10 days after seeding, cultured in differentiation media as in (c) but without PMA. (e) hNESC differentiated into neurons in a well of a 96 well plate after 1 month differentiation. (f) Immunostaining of selected region in the well, showing neurons positive for nuclei with Hoechst (blue), TUB β III (green) and TH (red); scale bar 50 μ m.

Figure 10.2 : Additional calcium transient features of LRRK2-G2019S mutants and controls (K7 and K7M cell lines). No significant differences were observed.

Figure 10.3 : Additional calcium transient features of LRRK2-G2019S mutants and controls, T4 and T4GC cell lines respectively. No significant differences were observed.

Figure 11.1: Pelican devices inventory

Figure 11.2: Warning information

Figure 11.3: Warning of potential misuse Risk of process outage or damage to the system

Figure 11.4: View of safety technology elements of the Pelican. PSEnmag=Non-contact, magnetic safety switches ([http://brochures.pilz.nl/bro_pdf/PSEN Safety Switches Technical Catalogue EN.pdf](http://brochures.pilz.nl/bro_pdf/PSEN_Safety_Switches_Technical_Catalogue_EN.pdf)). 1: Mode selection switch, system ON and enable button 2: PSEnmag safety switch – contactless (upper front doors) 3: PSEnmag safety switch – contactless (upper rear doors) 4: PSEnmag safety switch – contactless (incubator) 5: Main current switch

Figure 11.5: Mechanical installation areas

Figure 11.6: Electrical installation areas

Figure 11.7: Top view inside the Pelican Automation Workstation without housing. For more clarity, the colour codes of Figures 7 and 9 are matched

Figure 11.8: Tips waste station

Figure 11.9: Pelican hardware and software control architecture. Standard on arrow = type of physical connection between a device and the computer. CAN = Controller Area Network. PCI = Peripheral Component Interconnect. RS232 = Recommend Standard number 232. TCP/IP = Transmission Control Protocol/Internet Protocol.

Figure 11.10: List of consumables. List to be continuously updated as more labware are added to the Pelican

Figure 11.11: Main switch

Figure 11.12: Operating button and emergency stop button

Figure 11.13: Mode selection switch (left) and acknowledgement button (right)

Figure 11.14: Operating mode selector switch with operating mode selector chip 2

Figure 11.15: Control elements for operating mode 3

Figure 11.16: Loading of samples and tips into the Pelican. A: Hotels. B: Closed hotel locking mechanism. C: Open hotel locking mechanism

Figure 11.17: Safety feature while system enabled

Figure 11.18: Teaching Master/Sub positions and defining the safe gripping width

Figure 11.19: Robot routing in the Pelican

Figure 11.20: Architecture of the EKI module in the Pelican

Figure 11.21: VCI driver interface

Figure 11.22: VCI3 Device Server Control

Figure 11.23: weidmuller Hub

Figure 11.24: Weidmuller Communication Platform

Nomenclature

PD	Parkinson's Disease
DA	Dopamine / Dopaminergic
DN	Dopaminergic Neurons
SNc	Substantia Nigra pars compacta
iPSCs	induced Pluripotent Stem Cells
hNESCs	human NeuroEpithelial Stem Cells
ER	Endoplasmic Reticulum
LRRK2	Leucine-Rich Repeat Kinase 2
PIV	Particle Image Velocimetry
ROI	Region Of Interest
GECI	Genetically Encoded Calcium Indicator
PCA	Principle Component Analysis
ICA	Independent Component Analysis
NMF	Non-negative Matrix Factorisation
CNMF	Constrained Non-negative Matrix Factorisation
FOOPSI	Optimal Optical Spike Inference
SAOS	Small Amplitude Oscillatory Shear
DSC	Differential Scanning Calorimetry
TH	Tyrosine Hydroxylase
SeNeCa	Search for Neural Cells Accelerated
CNN	Convolutional Neural Network
TPP	Two-Photon Processor
GUI	Graphical User Interface
SIMA	Sequential IMaging Analysis
FluoroSNNP	Fluorescence Single Neuron and Network Analysis Package

OnACID	Online framework for the Analysis of streaming Calcium Imaging Data
FASP	Functional Astrocyte Phenotyping
FIU	Functionally Independent Unit
ALS	Amyotrophic Lateral Sclerosis
FAST	Features from Accelerated Segment Test
TPS	Thin-Plate Spine
LK	Lucas-Kanade
GUI	Graphical User Interface
SiLA	Standardisation in Laboratory Automation
LACS	Laboratory Automation Control Suite
ISI	Inter-Spike Interval

Abstract

This dissertation is a compilation of publications and manuscripts that aim 1) to integrate an automated platform optimised for long term in vitro cell culture maintenance for Parkinson's disease, long term live cell imaging and the handling of many cell lines, 2) to combine physics principles with imaging techniques to optimise the seeding of Matrigel embedded human neuroepithelial stem cells into a three-dimensional microfluidic device, and 3) to combine engineering principles with cell biology to optimise the design of a three-dimensional microfluidic system based on phaseguide technology.

In the first publication manuscript, we investigated Matrigel as a surrogate extracellular matrix in three-dimensional cell culture systems, including microfluidic cell culture. The study aimed at understanding and characterising the properties of Matrigel. Using classical rheological measurements of Matrigel (viscosity versus shear rate) in combination with fluorescence microscopy and fluorescent beads for particle image velocimetry measurements (velocity profiles), the shear rates experienced by cells in a microfluidic device for three-dimensional cell culture was characterised. We discussed how the result of which helped to mechanically optimise the use of Matrigel in microfluidic systems to minimise the shear stress experienced by cells during seeding in a microchannel.

The second manuscript proposes a methodology to passively control the flow of media in a three-dimensional microfluidic channel. We used the fluid dynamic concept of similitude to dynamically replicate cerebral blood flow in a rectangular cross-sectional microchannel. This similarity model of a target cell type and a simple fluid flow mathematical prediction model was used to iterate the most optimum dimensions within some manufacturing constraints to adapt the design of the OrganoPlate, a cell culture plate fully compatible with laboratory automation, which allowed its re-dimension to achieve over 24h of flow for the culture of human neuroepithelial stem cells into midbrain specific dopaminergic neurons.

In the third publication manuscript, we propose an automated cell culture platform optimised for long-term maintenance and monitoring of different cells in three-dimensional microfluidic cell culture devices. The system uses Standard in Laboratory Automation or SiLA, an open source standardisation which allows rapid software integration of laboratory automation

hardware. The automation platform can be flexibly adapted to various experimental protocols and features time-lapse imaging microscopy for quality control and electrophysiology monitoring to assess cellular activity. It was biologically validated by differentiating Parkinson's disease patient derived human neuroepithelial stem cells into midbrain specific dopaminergic neurons. This system is the first example of an automated Organ-on-a-Chip culture and has the potential to enable a versatile array of in vitro experiments for patient-specific disease modelling.

Finally, the fourth manuscript initiates the assessment of the neuronal activity of induced pluripotent stem cell derived neurons from Parkinson's Disease patients with LRRK2-G2019S mutations and isogenic controls. A novel image analysis pipeline that combined semi-automated neuronal segmentation and quantification of calcium transient properties was developed and used to analyse neuronal firing activity. It was found that LRRK2-G2019S mutants have shortened inter-spike intervals and an increased rate of spontaneous calcium transient induction than control cell lines.

Scientific output

Major chapters of this dissertation are based on studies that have been published, are currently under review or in preparation with the candidate as first author or contributing author. In addition, the candidate has filed an invention disclosure statement at the University of Luxembourg for the microfluidic plate design optimised for the culture of mid brain like neurons:

A. Publications in peer-review journals

- **K. I.W. Kane**, E. Lucumi Moreno, S. Hachi, M. Walter, J. Jarazo, T. Hankemeier, P. Vulto, J. C. Schwamborn, M. Thoma, R.M.T. Fleming, Automated microfluidic cell culture of stem cell derived dopaminergic neurons, *Scientific Reports*, volume 9, Article number: 1796 (2019); doi: 10.1038/s41598-018-34828-3
- **K. I.W. Kane**, E. Lucumi Moreno, C. M. Lehra, S. Hachi, R. Dannert, R. Sanctuary, C. Wagner, R. M.T. Fleming and J. Baller, Determination of the rheological properties of Matrigel for optimum seeding conditions in microfluidic cell cultures, *AIP Advances* 8, 125332 (2018); doi: 10.1063/1.5067382

B. Invention disclosure in preparation at the University of Luxembourg Patent office

- **K. I.W. Kane**, Ronan M.T. Fleming, Jens Schwamborn. Invention Disclosure Statement "Neuronal optimum 3D microfluidic device" (*KTT 180052*)

C. Manual book

- **K. I.W. Kane**, M. Walter, M. Thoma, Pelican user manual (2017).

D. Manuscripts in preparation

- **K. I.W. Kane**, Javier Jarazo, Edinson Lucumi Moreno, Paul Vulto, Ronan M.T. Fleming, Bas Trietsch, Jens Schwamborn, Passive controlled flow for neuronal cell culture in 3D microfluidic devices.
- Siham Hachi, Edinson Lucumi Moreno, Sarah L. Nickels, **K. I.W. Kane**, Masha Moein, Jens C. Schwamborn, Alex Skupin, Pieter Vanden Berghe, Ronan M.T. Fleming, Neuronal hyperactivity in LRRK2-G2019S mutation of cellular models of Parkinson's Disease.

E. Poster presentations in scientific conferences

- Engineering flow in a phaseguide-based 3D microfluidic cell culture device to optimise cell culture protocols for an automated cell culture observatory, *Basel Congress 2016*, Basel, Switzerland.

1. Introduction

1.1. Parkinson's disease and neuronal cell culture

PD is the second most common neurodegenerative disease in the world with more than 10 million people affected [1, 2]. The answer to the very important question to what is the real cause of PD is not known. Similar to many other neurodegenerative diseases, the onset of PD symptoms, is more prevalent with age. With an ever-aging population, especially in the developed world where its prevalence is susceptible to substantially increase in the coming years. Therefore, PD has become a global issue for which a solution must be found. In the brain the connectivity of cells is somewhat associated with how information is processed and stored in neural networks. PD is characterised by cell death in different levels of the nervous system [1]. These neuronal losses include cholinergic neurons in the pedunculopontine nucleus, noradrenergic neurons in the locus coeruleus and dopaminergic neurons (DNs) from the substantia nigra pars compacta [3, 4]. The substantia nigra is located in the inferior mid brain tegmentum. The connectivity as it relates to the pathogenesis of PD is summarised in Figure 1.

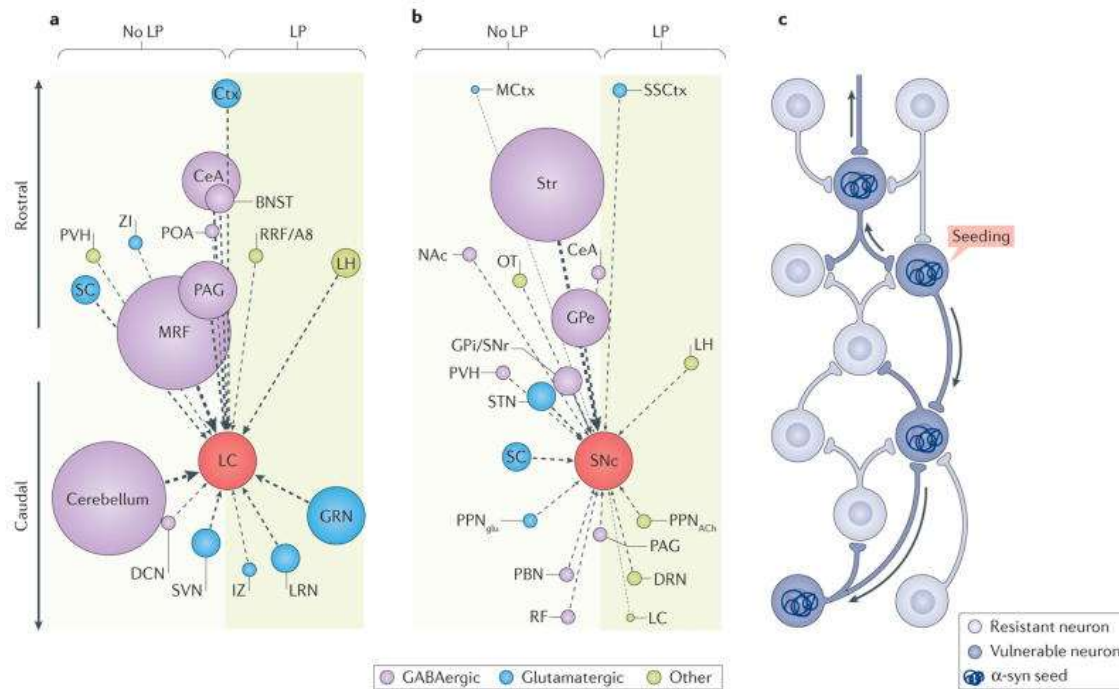


Figure 1: Does connectivity predict Lewy pathology in clinical Parkinson disease?

The connectomes of the mouse locus coeruleus (LC) (part a) and substantia nigra pars compacta (SNc) (part b) do not predict the pattern of postsynaptic, intraneuronal Lewy pathology (LP) that is observed in clinical Parkinson disease (cPD). Because data on the human connectome are not available and because there have been no direct comparisons between the mouse connectome and the spread of LP, a thought experiment was conducted. This thought experiment, as depicted in the figure, assumes that the mouse and human connectomes are largely similar and that retrograde spread of α -synuclein (α -syn) is dictated by the number or strength of synaptic connections. a | A plot of the afferent connectome of mouse LC adrenergic neurons, based on data presented by Schwarz et al.¹, is shown. Nuclei projecting to the LC are represented as circles distributed along a rostrocaudal vertical axis. The diameter of the circle represents the strength of the projection as estimated by the number of retrogradely labelled neurons; the dominant transmitter (GABA, glutamate or other) in each nucleus is coded by a given colour. Nuclei with postsynaptic, intraneuronal LP in late-stage cPD are positioned in the shaded box on the right; nuclei with little or no LP are on the left. The plot reveals that the strength of the synaptic connection to the LC is not correlated with LP; most of the larger circles are located on the left of the plot. b | A plot of the connectome of mouse SNc dopamine neurons as in part a, based on the work of Ogawa et al.² and Watabe-Uchida et al.³, is shown. Again, there is no clear correlation between the strength of the synaptic connection with SNc and the probability of manifesting postsynaptic, intraneuronal LP

¹ Schwarz LA, et al. Viral-genetic tracing of the input– output organization of a central noradrenaline circuit. *Nature*. 2015;524:88–92.

² Ogawa SK, Cohen JY, Hwang D, Uchida N, Watabe-Uchida M. Organization of monosynaptic inputs to the serotonin and dopamine neuromodulatory systems. *Cell Rep*. 2014;8:1105–1118.

³ Watabe-Uchida M, Zhu L, Ogawa SK, Vamanrao A, Uchida N. Whole-brain mapping of direct inputs to midbrain dopamine neurons. *Neuron*. 2012;74:858–873.

in humans with cPD. c | The schematic summarizes the conclusion that, if there is spread of α -syn, it is not strictly determined by synaptic connectivity, but rather must be dictated by other factors, such as vulnerability. In the diagram, a synaptic network is depicted with neurons that are resistant to α -syn spread (light blue) and those that are vulnerable (dark blue). An α -syn seeding event will then result in the spread of LP in a retrograde manner only through vulnerable neurons (depicted by the arrows). BNST, bed nucleus of the stria terminalis; CeA, central nucleus of the amygdala; Ctx, cortex; DCN, deep cerebellar nuclei; DRN, dorsal raphe nucleus; GPe, globus pallidus externa; GPi/SNr, GP interna–SN pars reticulata; GRN, gigantocellular reticular nucleus; IZ, intermediate reticular zone; LH, lateral hypothalamus; LRN, lateral reticular nucleus; MCtx, motor region of the cerebral cortex; MRF, midbrain reticular nucleus; NAc, nucleus accumbens; OT, olfactory tubercle; PAG, periaqueductal grey; PBN, parabrachial nucleus; POA, preoptic area; PPNglu, glutamatergic neurons of the pedunclopontine nucleus; PPNACH, cholinergic neurons of the pedunclopontine nucleus; PVH, paraventricular hypothalamic nucleus; RF, reticular formation; RRF/A8, retrorubral fields/A8 dopaminergic cell group; SC, superior colliculus; SSCtx, somatosensory cortex; STN, subthalamic nucleus; Str, striatum; SVN, spinal vestibular nucleus; ZI, zona incerta.

Reprint from Surmeier DJ, Obeso JA, Halliday GM. Selective neuronal vulnerability in Parkinson disease. *Nat Rev Neurosci.* 2017;18(2):101–113. doi:10.1038/nrn.2016.178

The onset of most cases of PD are sporadic, however, multiple risk factors have been postulated to be the cause of PD. These include genetic factors, environmental triggers, age, occupation, race, serious head injuries, gender (men tend to suffer more from PD than women) and living conditions (the rural population and people living around heavy metals tend to suffer from PD more than people living in cities). 10 to 15% of all PD patients are due to monogenetic mutations [5]. Currently, there is no therapeutic treatment against PD, nor is there any cure capable of slowing down the progression of disease. However, treatments can be used to alleviate PD symptoms with the most prevalent being levodopa therapy. The other symptomatic treatments include: dopamine agonists, monoamine oxidase type B inhibitors, beta-adrenergic antagonists (beta-blockers), amantadine anticholinergics [5]. Each of which is used depending on which symptoms of PD are being targeted. Levodopa is a chemical substance that is converted into dopamine in the brain, and is the standard motor symptoms therapy of PD.

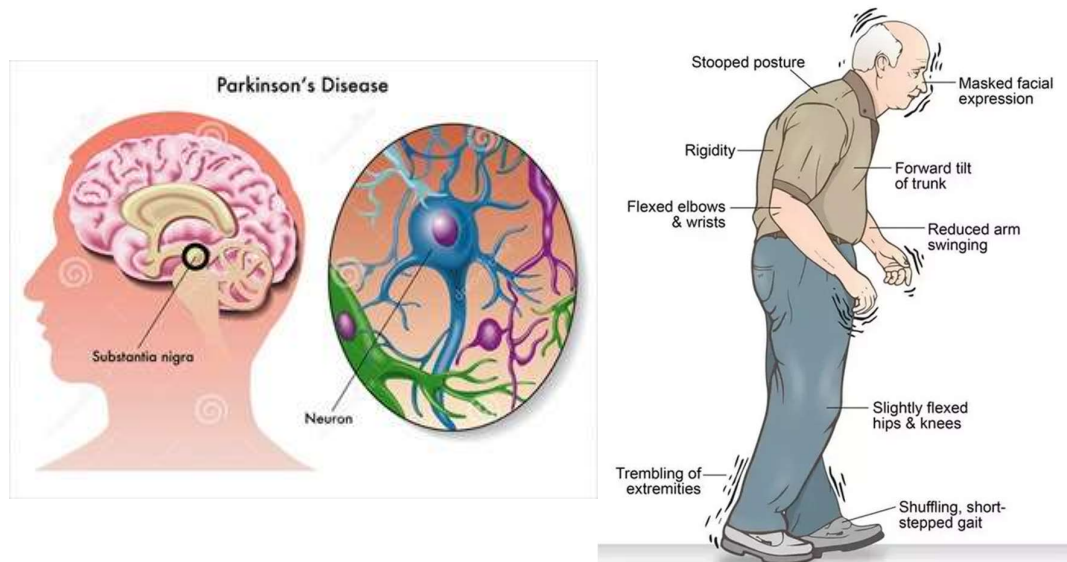


Figure 2: Parkinson's disease motor symptoms caused by degeneration of neurons in the substantia nigra

Downloaded from the Shutterstock.com in January 2019

There have been many genes associated with Parkinson's disease. These include Parkin, PINK1, DJ-1, ATP13A2, α -synuclein, LRRK-2 and GBA. The genetic predispositions associated with heightened risk of PD is summarised in Table 1. In addition, certain cells including DNs play a critical role in brain function by releasing a neurotransmitter called dopamine [6, 7, 8]. It is believed that the loss of DNs is the main reason behind the motor symptoms (rigidity, tremors and postural instability) of PD patients [9] (Figure 2). However, the full symptoms of PD include non-motor symptoms such as mood disorder, anxiety, irritability, hallucination, language, memory difficulties and loss of attention. The vulnerability of DNs in PD is associated with multiple cellular mechanism, including mitochondrial dysfunction, oxidative stress and the homeostasis of calcium [10].

Table 1: Genes associated with Parkinson's Disease

Gene locus	Disorder	Inheritance	Gene	Status and remarks	Mode of identification
4q21-22	EOPD	AD	SNCA	Confirmed; Synuclein Alpha; Lewy Body; Dominant point mutations and duplications. Genetic variability contributes to disease	Linkage analysis
6q25.2-q27	EOPD	AR	Parkin	Confirmed	Linkage analysis
2p13	Classical PD	AD	HGNC	Confirmed; Lewy Body	Linkage analysis
4q21-q23	EOPD	AD	SNCA	Erroneous locus (identical to PARK1)	Linkage analysis
4p14	Classical PD	AD	UCHL1	Moderate evidence	Functional candidate gene approach
1p35-p36	EOPD	AR	PINK1	Confirmed; located in the mitochondria; young onset	Linkage analysis
1p36	EOPD	AR	DJ-1	Confirmed; young onset	Linkage analysis
12q12	Classical PD	AD	LRRK2	Confirmed; variations in LRRK2 gene include risk-conferring variants and disease-causing mutations	Linkage analysis
1p36	Kufor-Rakeb syndrome; atypical PD with dementia, spasticity, and supranuclear gaze palsy	AR	ATP13A2	Confirmed; but complex phenotype that would not be mistaken for early-onset or classical parkinsonism	Linkage analysis
1p32	Classical PD	Risk factor	AAOPD	Confirmed susceptibility locus, however; conflicting results	Linkage analysis
2q36-q37	Late-onset PD	AD	GIGYF2	Recent studies in different populations have been unable to replicate its association with PD; possibly represents a risk factor	Linkage analysis
Xq21-q25	Classical PD	Risk factor	Unknown	Confirmed susceptibility locus; possibly represents a risk factor	Linkage analysis
2p12	Classical PD	AD or risk factor	HTRA2	Confirmed; thought to induce apoptosis; regulates PINK1	Candidate gene approach
22q13.1	Early-onset dystonia-parkinsonism	AR	PLA2G6	Confirmed	Linkage analysis (homozygosity mapping)
22q12-q13	Early-onset parkinsonian-pyramidal syndrome	AR	FBX07	Confirmed	Linkage analysis
1q32	Classical PD	Risk factor	Unknown	Confirmed susceptibility locus	Genome-wide association studies
16q11.2	Classical PD	AD	VPS35	Confirmed	Exome sequencing
3q27.1	Classical PD	AD	EIF4G1	Confirmed	Linkage analysis

1q22	Classical PD	AD	GBA	Suggest that changes in this gene may contribute to the faulty breakdown of toxic substances in neurons; Lewy bodies
------	--------------	----	-----	--

Adapted and updated from Klein C, Westenberger A. Genetics of Parkinson's disease. Cold Spring Harb Perspect Med. 2012;2(1):a008888. doi:10.1101/cshperspect.a008888

On their paper on “The energy cost of action potential propagation in dopamine neurons: clues to susceptibility in Parkinson’s disease”, Pissadaki et al. [11] have demonstrated through the use of a computational model of the axons of individual dopamine neurons, that the energy cost of axon potential propagation and recovery of the membrane exponentially increases with the size and complexity of the axonal arbour. In other words, the high complexity of DNs network, and the high length of DNs put an excessive stress on the mitochondria because of high energy demand to keep DNs cellular integrity. The mitochondria can be thought off as the engine of a cell as it is responsible for the generation of energy to maintain cellular integrity. This is the energy imbalance hypothesis to PD pathogenesis (Figure 3): DNs are susceptible to neurodegeneration due to the high demand for energy to maintain tonic firing that can go from 2 up to 5 firings every second [11, 3].

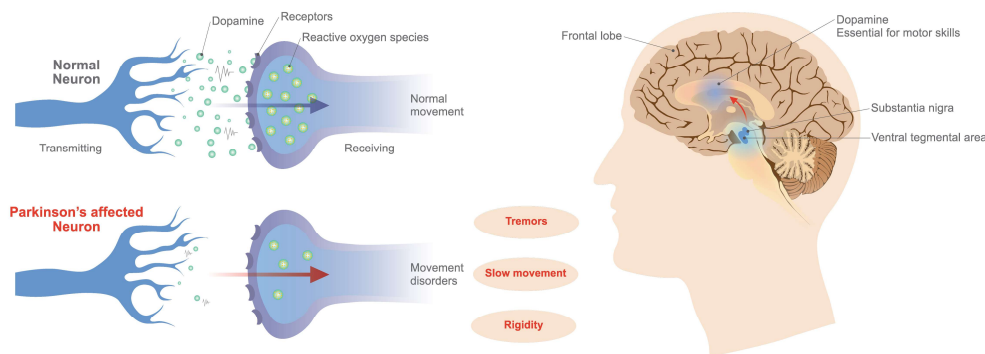


Figure 3: Parkinson’s disease dopaminergic neuronal dysfunction

Downloaded from the Shutterstock.com in January 2019

One of the most important hurdle to PD research has been the use of post-mortem samples for which access is difficult and have a short lifespan for testing in the laboratory. In addition, the impossibility to use samples from living PD patients which could have allowed to better

understand cellular changes of neurons and neuronal networks makes it very difficult to truly understand PD's complex mechanism. To remedy this problem, scientists have tried to use multiple other models to better understand PD. These include animal and most importantly cellular models of the disease. The latter has been boosted by the Nobel Prize winning discovery of induced pluripotent stem cells (iPSCs) by Takahashi et Yamanaka [12] which has revolutionised biomedical research as a whole.

An iPSC is a skin (fibroblast) or a blood cell that has been reprogrammed into an embryonic like stem cell that is capable of becoming any type of human cell including DNs. The techniques to generate iPSCs have been replicated and improved over time using fibroblasts from mice embryos, adult mice and humans to generate stem cells using different factors [13, 14]. The iPSC generation technique offers an unparalleled avenue to create cellular models with specific disease markings to better understand disease progression and find therapeutic cures. This is especially important for neurodegenerative diseases, especially PD and Alzheimer.

In the case of PD research, fibroblasts from PD patients, especially from older patients, with specific genetic mutations have been reprogrammed into neuronal populations of DNs. Many protocols have been developed over the years to efficiently generate DNs from iPSCs [15, 16, 17]. For instance, Swistowski et al [15] adapted a xeno-free system previously developed for generating human embryonic stem cell into an efficient protocol to generate functional DNs from iPSCs. First, they generated iPSCs from somatic cell types and verified its human embryonic stem cell like behaviour by studying their pluripotency and genomic stability. Then, they differentiated the iPSCs into neural stem cells, and subsequently dopaminergic neurons. In addition, Reinhardt et al. [17] have developed a method to generate neural epithelial stem cells (hNESCs) using small molecules. These hNESCs can in turn be differentiated into many neuronal cell types, including midbrain like DNs vital in PD therapeutic study. The dopaminergic phenotype has been confirmed by the expression of tyrosine hydroxylase (TH),

a cellular marker specific to DNs. As a result, it is now possible to differentiate iPSCs into hNESCs, then into midbrain like DNs with the same genetic background of PD patients.

1.2. Microfluidic cell culture

The microfluidic cell culture (Figure 4) field is about the design of devices and protocols for the culture, maintenance and experiment of cells in micro-scale volumes (micrometre, microliter). The reasons behind the popularity of microfluidic cell culture are both economical and scientific. Reagents are expensive items, the amounts used in microscopic cultures are much less than in macroscopic ones [18, 19]. The low volume of reagents used in microfluidics is cheaper and it has the potential to reduce the ratio of the extracellular volume (media) to the intracellular volumes (extracellular matrix embedded cells). The reduction of this ratio allows an increase in extracellular metabolic concentrations, making easier the detection of metabolic changes in an extrametabolic study [20, 21]. Microfluidic cell cultures better resemble the natural environment of a cell because it is easier to generate three dimensional micro-cultures than macro ones [22]. In addition, the miniaturisation of cell culture has allowed scientists to run multiple experiments in a single plate. This promotes reproducibility by keeping environmental conditions constant between replicate experiments. However, this comes at a steep increase in labour cost as one has to deal with more wells than in macro-cell culture. Furthermore, the combination of automated and microfluidic technologies allows the application of the same experimental conditions to different cell lines [23, 24] and to establish live cell culture monitoring [25, 26]. Hence, the combination of laboratory automation with microfluidic cell culture is such an important perspective to explore.



Figure 4: Example of a Lab on chip. A biochip for identifying proteins, Lab on Chip - systems all process for analysis of a sample are integrated into one glass plate

Downloaded from shutterstock.com

1.3. 3D Microfluidic neuronal culture

Moreno et al. recently succeeded in differentiating hNECs into DNs in a stratified 3D microfluidic cell culture bioreactor developed by Trietsch et al. [27, 28]. The microfluidic device (Figure 5) used for the experiment was a 2-lane OrganoPlate 9603-200B (Mimetas BV, Leiden, The Netherlands). It consists of an array of 96 chips embedded in a customised 384-well plate format [28]. Each bioreactor consists of a single microfluidic chip contained between two pieces of glass: a top plate with holes corresponding to the underside of selected wells, and a bottom plate. Each chip has 4 wells and 2 lanes: one gel inlet well for loading of gel-embedded cells into the culture lane, one medium inlet well connected to one medium outlet well through a medium lane where the flow of media is driven by a pressure drop between the 2 wells, and one well used as an observation window for monitoring the quality of cells through an inverted microscope. The culture and medium lanes are separated by a phaseguide, preventing the flow of gel embedded cells from flowing into the medium lane forcing it to stay on the culture lane. A phaseguide is a patterned pinning barrier that controls the liquid-air interface by forcing it to align with the ridge, hence guiding the fluid

flow into the needed lane [29]. Cells are mixed with a liquefied surrogate extracellular matrix. This mixture is dispensed into the gel inlet connected to the culture lane. Then, the bioreactor is incubated at a temperature allowing the gelation of the mixture. Upon gelation, fresh media is loaded into the medium inlet well connected to the medium lane allowing the perfusion of the media over time. This promotes the diffusion of nutrients to the cells and the collection of waste metabolites in the media. The OrganoPlate is fully compatible with laboratory automation. The functionality of this 3D microfluidic device in neuronal differentiation has already been proven, however, it is very time consuming and labour intensive making imperative the need to automate the protocol.

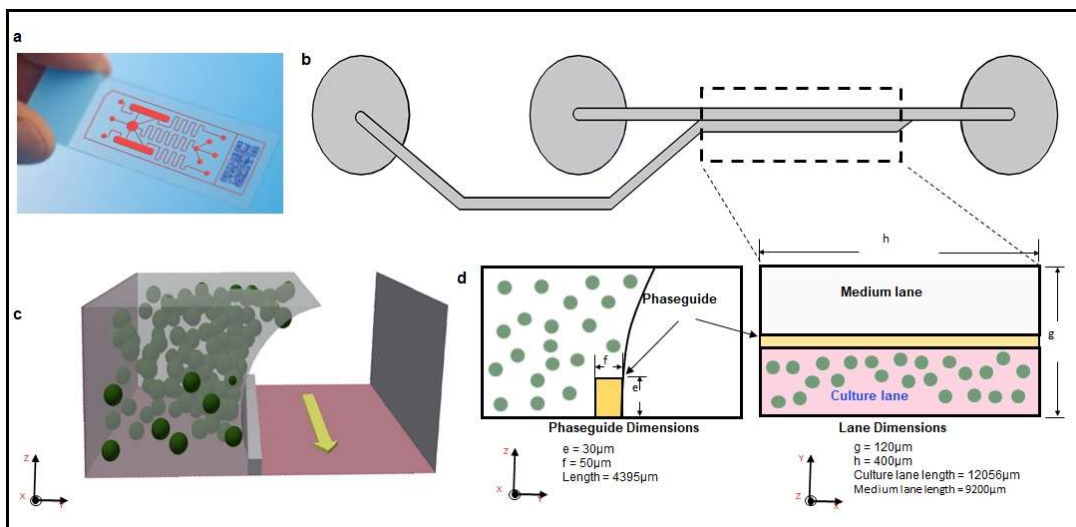


Figure 5: schematic representation of a lab-on-a-chip

Lab on chip (LOC) is device that integrates laboratory functions on nano chip (part a downloaded from shutterstock.com), 2D representation of a single bioreactor of a 2 lane OrganoPlate (part b), 3D representation of a bioreactor section of a 2 lane OrganoPlate with arrow representing the direction of flow of media (part c), 2D cross-sections of a 2 lane OrganoPlate with exact dimensions in mm (part d). Extracellular matrix and its properties in microfluidic cell culture.

1.4. Extracellular matrix and its properties in microfluidic cell culture

3D Microfluidic cell culture requires an appropriate extracellular matrix (ECM) system for the cells to grow and proliferate [30, 31, 32, 33]. The ECM must provide the right mechanical, biochemical and physical scaffold influencing cell movement and orientation as well as, the biochemical signalling environment to control gene expression [31]. In addition to water as the major component of ECM, the main macromolecular constituents of ECM are fibrous

protein (collagen, elastin and fibrillin) and proteoglycans [31, 33]. Several ECM surrogates from natural and synthetic origins have been developed in the form of hydrogels, for cell culture applications [34].

Hydrogels are physically or chemically cross-linked polymer networks that are able to absorb large amounts of water [35]. Because of their biomechanical and biochemical properties, they are used as a surrogate extracellular matrix for 2D and 3D cell culture. Moreover, they are compatible with microscopy techniques. Hydrogels of natural origins are from membrane-based gel preparations; some examples include fibrin gel, collagen gel, alginate gel and Matrigel [27]. Matrigel is a commercial hydrogel of natural origins. It is a reconstituted basement membrane preparation extracted from the Engelbreth-Holm-Swarm (EHS) mouse sarcoma that is biologically active and therefore, widely used in a variety of 2D and 3D cell cultures, including stem cells, cancer cells, induce pluripotent stem cells (iPSCs) and neuronal cells, among other applications.

Rheology is the study of the flow of matter. It is utilised to determine physical properties of a material such as its viscosity or its shear moduli. Liquids (e. g. water and Matrigel) can be divided into two groups: *Newtonian* and *non-Newtonian fluids*. On one hand, a non-Newtonian fluid is a fluid in which the viscosity is dependent on the applied shear stress. On the other hand, for a Newtonian fluid, the applied shear stress and shear rate have a linear relationship, which goes through the origin, with the effective viscosity as the constant of proportionality. A rheometer can be used to determine the physical properties of a fluid. A rheometer is composed of two plates separated by a space to fill liquid samples. A rheometer can be used to apply shear stress into a liquid sample by the rotation of the plates. The sample deforms as a result of the applied shear stress. In addition, due to the first law of thermodynamics the temperature of the sample will increase due to the applied work into the sample. When, the sample deforms easier than its temperature increases, then the sample is said to be liquid. When, the opposite happens, that is the temperature substantially increases while there is minimal deformation, the sample is said to exhibit a more gel like behaviour.

Matrigel has unique properties as a non-Newtonian, *viscoelastic fluid*. A viscoelastic fluid is one that exhibits both a viscous and an elastic behaviour. Matrigel exhibits a Lower Critical

Solution Temperature (LCST) [35] of about 6°C, it maintains a liquid state at temperatures lower than 4°C and transitions to a gel like state at temperatures above 22°C [36, 37]. Hydrogels have similar mechanical properties to soft tissues [34, 36] making them suitable for use as substitutes for ECM in microfluidic devices [38, 27, 36]. However, cells flowing in 3D microfluidic devices are exposed to different physical variables (mechanical stresses) that play a role in their adaptation and survival to the new 3D environment. Cells usually have *poroelastic* mechanical properties. A poroelastic material deforms because of its elasticity [39]. When it is subjected to mechanical stresses, it temporarily loses some fluid content because of the porous nature of the cellular membrane [40]. Therefore, there is a need to quantify the shear stress that cells are exposed to in a given microfluidic device under particular conditions (temperature, applied external pressure, etc.). This requires knowledge of the rheological properties of the working fluid, along with insights into the flow behaviour of the fluid inside the microfluidic device.

1.5. Flow characteristics

Many physics fundamentals are important in the characterisation of the flow of fluid inside a vessel such as inside the medium or culture lane of the OrganoPlate. These are of two groups: the conservation group which comprises the energy, mass and linear momentum conservations from Newton second law based on classical mechanics through Reynolds transport [41], and the continuum hypothesis which assumes that fluids are continuous and are not distinct molecules. Fluids can be compressible or incompressible. A compressible fluid is one in which the density is a function of temperature and pressure, while the density of an incompressible fluid does not depend on pressure, nor does it depend on temperature.

In fluid dynamics, the flow of a fluid can be either *laminar* or *turbulent* (Figure 6). When the flow rate is low enough for the fluid to flow in parallel layers, with no disruption between the layers; then the flow is called laminar or streamlined flow. In laminar flow, the viscous forces dominate the mode of transport of fluid. On the other hand, when the flow is so fast that it is characterised by recirculation, eddies and by randomness; then the flow is said to be turbulent. The flow of a fluid can be modelled using the Navier-Stokes equations which are based on Newton Second law and the fact that the stress in the fluid is due to the viscosity and the pressure. To determine whether a fluid is laminar or turbulent, the Reynolds number

can be used. It is the ratio of inertial forces to viscous forces of a fluid. Above a certain value of the Reynolds number, a flow is said to be turbulent, below this critical number, it is laminar. The critical number is usually empirically determined for many cross-sectional shapes such as for circular or rectangular pipes.

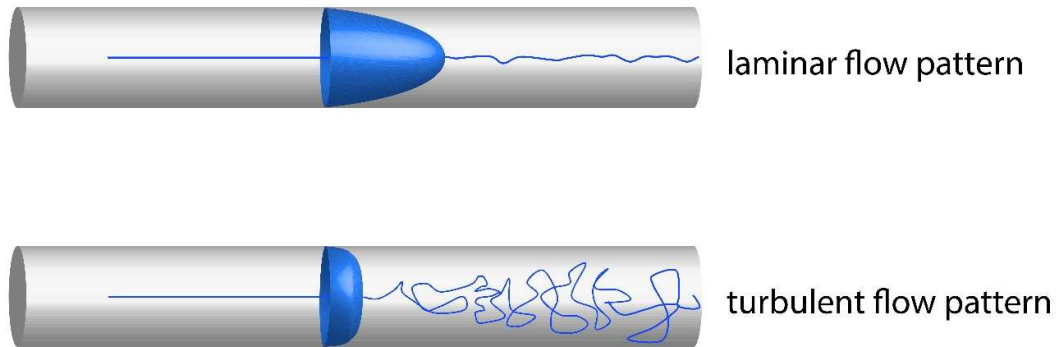


Figure 6: Laminar and turbulent flow profiles

Downloaded from the Shutterstock.com in February 2019

1.6. Laboratory automation

In the field of life sciences, laboratory automation has become a very popular undertaking [42, 43]. The reason being, automated cell culture has the potential to increase the quantity and the quality of experiments that can be completed in parallel and enables long-term cell culture maintenance with reduced manual labour [44]. A robot can work all the time without fatigue and with the same consistency and high accuracy [43]. Laboratory automation promotes reproducibility because, first, it helps reveal the cell culture environmental conditions. Second, it keeps environmental conditions and cell culture parameters constant throughout experiments [45]. There is less variance between replicates. Third, it helps to control most parameters such as dispensing speed, aspirating temperature and precise image acquisition. Automation allows to better replicate *in vivo* physiological conditions by having more control over experimental parameters such as “continuous perfusion, study of low number of cells or single cells in high temporal and/or spatial resolution and parallelization” [46]. This improves the interoperability between *in vitro* and *in vivo* models, accelerating research in biomedicine.

1.6.1. Laboratory automation hardware

In advanced laboratory automation, two main types of robots can be selected based on its functional motion: one with a fixed sample and one with a movable sample. A system where there is a fixed sample is cheaper and does not require a great deal of space. However, it is very limited in terms of the space it can cover. A platform with a movable sample offers more flexibility because it allows a robotic arm to move plates around. In fact, the trend has been to use commercially available industrial robots and combine these with a gripper to integrate them into a plant [43]. The reason being, in industry, there are robots with more and more degrees of freedom. Even though, the selection of an industrial robot with more degrees of freedom consumes more space, it allows the operator to install more devices because any location the arm and/or gripper can reach is a space that can be used to integrate a new component adding to the flexibility of the platform.

The grippers should be manufactured in a fashion that allows many types of substrates to be handle able, minimising human intervention while running processes. The selective-compliance-articulated robot arm (SCARA), offers more flexibility because it has two rotating points compared to one rotating point from the most advanced gantry robot which has only one. However, it is also more expensive.

In liquid handling, most of the technological advances are concentrated in the dispensing side as opposed to the aspiration side [43]. There are two main types of dispensing technologies: *contact dispensing* and *non-contact dispensing*. Contact dispensing requires the physical contact between the dispensing medium and the receiving well for the dispensing to occur. Contact dispensing is very precise for dispensing small volumes. However, this precision is dependent on dispensing at an exact location, which is not always possible [42]. This is particularly problematic for small dispensing in microfluidic devices where gravity is usually not enough to overcome the surface adhesion to drive the flow of fluid. In addition, the force generated by the contact of the tip may damage the well. Well cross-contamination is also likely as there is direct contact between the tip and the well. The integration of contact dispensing in a laboratory automation plant might require the implementation of a decontamination protocol after each dispensing step. This does not promote speed and high-throughput capabilities so sought after in laboratory automation. Non-contact dispensing

does not require any contact between the dispensing tip and the well. This helps to avoid cross-contamination, and promotes the integrity of the well. Non-contact dispensing is very popular in laboratory automation because it is versatile, and it is easy to dispense to any area of a well regardless of geometry such as undercuts, so long as there is an opening on the well [47]. There are many techniques to achieve noncontact dispensing, among which the most popular are solenoid and piezoelectric methods. In solenoid technology, a solenoid valve is used to keep the fluid inside the tip. A force is applied into the back-end of the fluid. This force opens the solenoid valve to eject the fluid [48, 49, 50, 51]. In piezoelectric technology, a piezoelectric crystal is used as a collar around a glass tube containing the fluid. Applying voltage onto the collar leads to contraction of the collar. This force causes pressure on the tube, which ejects the fluid [52, 53, 50]. Research to develop new non-contact dispensing technologies is very vibrant. More non-contact dispensing techniques such as acoustic, gas drive, super-paramagnetic beads, surface tension of the liquid, light, and optically driven have been introduced in recent years [43, 54, 55, 56, 57, 58, 59].

1.6.2. Laboratory automation software

Designing a flexible modular automated system requires not only a flexible hardware, but also it requires the possibility to be able to acquire devices from different companies. The trend in laboratory automation has been established to acquire the different devices of a laboratory plant from different companies as it is difficult to find a single company that is able to supply all components. In addition, easy integration to an existing plant has not always been a point of emphasis of device suppliers [43]. However, when one acquires components from different suppliers, all these devices must be able to be integrated to a single plant connected to one computer where they are all controlled in a synchronous manner. This is only possible if all the devices function in a standard fashion. Many methods have been developed over the years to address the issue of standard and easy integration of new devices into existing plants. These include, first, the ASTM 1394, a standard communication process from the American Society for Testing and Material, however, its lack of some important features such as the initialisation of devices is the reason behind its failure [60]. Second, Health Level Seven 7 standardises clinical diagnostics, however, it lacks a methodology to describe the behaviour of devices such as the state of devices at any given times [61]. Third, Laboratory Equipment

Control Interface Specification is a standard for device control developed in 2002 and has not been used since then because it uses an outdated technical platform and the fact that it is an enterprise wide standardisation making it unfit for open source and academic use [62]. In addition, once a standard device control system has been established, the way that data are sent to and generated by devices are represented must also be agreed upon. The Analytical Information Markup Language (AnIML) is an XML based data representation standard. However, it requires two XML schemas (AnIML Core Scheme and AnIML Technique Definition) and a validation schematic [63] which made its use in an academic setting very challenging. Standardisation in Laboratory Automation (SiLA) solves these problems by standardising the interfacing, integration and data representation in a simple single XML schema for all devices [64, 65]. SiLA standardises the communication between a process management software and one or more devices (Figure 7). SiLA defines common commands per device class and the common device states. These are commonly used functionalities in nearly every laboratory which include incubating and exchanging media of culture plates for instance. SiLA defines the common device classes to achieve these functionalities such as an incubator and a liquid-handler. Each device class will have the required commands for the core functionalities as well as optional commands i.e. extended functionalities that are not necessarily present in every device of the same class. In this regard, a SiLA standard common command dictionary [66] was developed for every single device class where the commands such as setParameter and getParameter and the expected return are known. This allows a process management software to automatically generate the required commands for every device class.

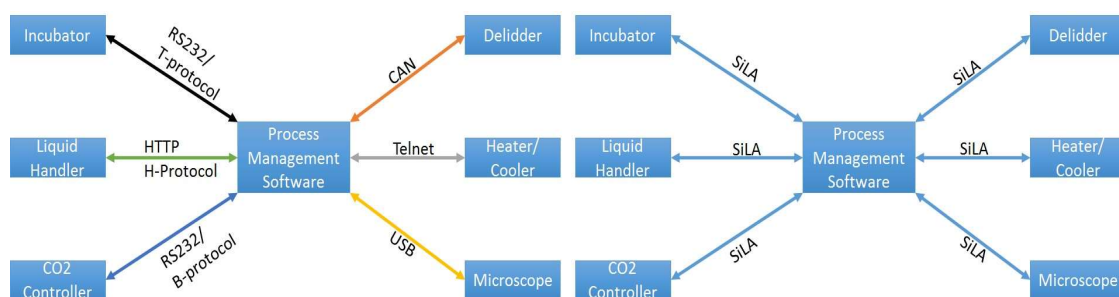


Figure 7: Standard communication between devices in an automation plant. HTTP=Hypertext Transfer Protocol. Telnet=Teletype Over Network Protocol for Local Area network or internet. USB=Universal Serial Bus. CAN=Controller Area Network. RS232=Recommend Standard 232

1.7. Aim of the thesis

The main aim of this interdisciplinary thesis was to integrate an automated platform with a 3D microfluidic system based on phaseguide technology, with a neuronal differentiation protocol based on iPSC technology, and to dynamically optimise the microfluidic used to differentiate human neuro-epithelial stem cell (hNESc) lines into dopaminergic neurons (DNs). This 3D cellular model of PD depends upon the differentiation of dopaminergic (DA) neurons from hNESc using small molecules within microfluidic bioreactors of the OrganoPlate and using Matrigel as surrogate extracellular matrix (ECM). This thesis focuses on three main goals:

Goal 1: Software and hardware integration of an automated platform optimised for long term in vitro cell culture maintenance for Parkinson's disease, long term live cell imaging and the handling of many cell lines.

Goal 2: Combine physics principles with imaging techniques to optimise the seeding of Matrigel embedded hNESCs into the culture lane of the OrganoPlate.

Goal 3: Combine engineering principles with cell biology to optimise the design of a 3D microfluidic system based on phaseguide technology.

1.8. References

1. Lees AJ, Hardy J, Revesz T. Parkinson's disease. *The Lancet*. 2009 Jun;373(9680):2055–2066. Available from: <http://www.sciencedirect.com/science/article/pii/S014067360960492X>.
2. Abdullah R, Basak I, Patil KS, Alves G, Larsen JP, Møller SG. Parkinson's disease and age: The obvious but largely unexplored link. *Experimental Gerontology*. 2015 Aug; 68:33–38. Available from: <http://www.sciencedirect.com/science/article/pii/S053155651400271X>.
3. Surmeier DJ, Schumacker PT. Calcium, Bioenergetics, and Neuronal Vulnerability in Parkinson's Disease. *J Biol Chem*. 2013 Apr;288(15):10736–10741. Available from: <http://www.jbc.org/content/288/15/10736>.
4. Bellucci A, Mercuri NB, Venneri A, Faustini G, Longhena F, Pizzi M, et al. Review: Parkinson's disease: from synaptic loss to connectome dysfunction. *Neuropathol Appl*

Neurobiol. 2016 Feb;42(1):77–94. Available from:

<http://onlinelibrary.wiley.com/doi/10.1111/nan.12297/abstract>.

5. Hindle JV. Ageing, neurodegeneration and Parkinson's disease;39(2):156–161. Available from: <https://academic.oup.com/ageing/article-lookup/doi/10.1093/ageing/afp223>.
6. Chinta SJ, Andersen JK. Dopaminergic neurons. The International Journal of Biochemistry & Cell Biology. 2005 May;37(5):942–946. 00102. Available from: <http://www.sciencedirect.com/science/article/pii/S1357272504003711>.
7. Schondorf DC, Aureli M, McAllister FE, Hindley CJ, Mayer F, Schmid B, et al. iPSC-derived neurons from GBA1-associated Parkinson's disease patients show autophagic defects and impaired calcium homeostasis. Nat Commun. 2014 Jun;5. 00002. Available from: <http://www.nature.com/ncomms/2014/140606/ncomms5028/full/ncomms5028.html>.
8. Munoz P, Huenchuguala S, Paris I, Segura-Aguilar J. Dopamine Oxidation and Autophagy. Parkinsons Dis. 2012;2012. 00000. Available from: <http://www.ncbi.nlm.nih.gov/pmc/articles/PMC3433151/>.
9. Meiser J, Weindl D, Hiller K. Complexity of dopamine metabolism. Cell Communication and Signaling. 2013;11(1):1. Available from: <https://biosignaling.biomedcentral.com/articles/10.1186/1478-811X-11-34>.
10. Obeso JA, Rodriguez-Oroz MC, Goetz CG, Marin C, Kordower JH, Rodriguez M, et al. Missing pieces in the Parkinson's disease puzzle. Nature Medicine. 2010 Jun;16(6):653–661. 00276. Available from: <http://www.nature.com/doi/10.1038/nm.2165>.
11. Pissadaki EK, Bolam JP. The energy cost of action potential propagation in dopamine neurons: clues to susceptibility in Parkinson's disease. Front Comput Neurosci. 2013 Mar; 7:13. Available from: <http://www.ncbi.nlm.nih.gov/pmc/articles/PMC3600574/>.
12. Takahashi K, Yamanaka S. Induction of Pluripotent Stem Cells from Mouse Embryonic and Adult Fibroblast Cultures by Defined Factors;126(4):663–676. Available from: <https://linkinghub.elsevier.com/retrieve/pii/S0092867406009767>.
13. Takahashi K, Tanabe K, Ohnuki M, Narita M, Ichisaka T, Tomoda K, et al. Induction of Pluripotent Stem Cells from Adult Human Fibroblasts by Defined Factors. Cell. 2007 Nov;131(5):861–872. 08307. Available from: <http://www.sciencedirect.com/science/article/pii/S0092867407014717>.
14. Yu J, Vodyanik MA, Smuga-Otto K, Antosiewicz-Bourget J, Frane JL, Tian S, et al. Induced Pluripotent Stem Cell Lines Derived from Human Somatic Cells. Science. 2007 Dec;318(5858):1917–1920. Available from: <http://www.sciencemag.org/content/318/5858/1917>.
15. Swistowski A, Peng J, Liu Q, Mali P, Rao MS, Cheng L, et al. Efficient Generation of Functional Dopaminergic Neurons from Human Induced Pluripotent Stem Cells Under

Defined Conditions. STEM CELLS. 2010;28(10):1893–1904. 00151. Available from: <http://onlinelibrary.wiley.com/doi/10.1002/stem.499/abstract>.

16. Kriks S, Shim JW, Piao J, Ganat YM, Wakeman DR, Xie Z, et al. Dopamine neurons derived from human ES cells efficiently engraft in animal models of Parkinsons disease;480(7378):547–551. Available from: <http://www.nature.com/articles/nature10648>.
17. Reinhardt P, Glatza M, Hemmer K, Tsytsyura Y, Thiel CS, Hoing S, et al. Derivation and Expansion Using Only Small Molecules of Human Neural Progenitors for Neurodegenerative Disease Modeling. PLoS ONE. 2013 Mar;8(3):e59252. 00023. Available from: <http://dx.plos.org/10.1371/journal.pone.0059252>.
18. Gomez-Sjoberg R, Leyrat AA, Pirone DM, Chen CS, Quake SR. Versatile, Fully Automated, Microfluidic Cell Culture System. Analytical Chemistry. 2007 Nov;79(22):8557–8563. 00446. Available from: <http://pubs.acs.org/doi/abs/10.1021/ac071311w>.
19. Lecault V, Vaninsberghe M, Sekulovic S, Knapp D, Wohrer S, Bowden W, et al. High-throughput analysis of single hematopoietic stem cell proliferation in microfluidic cell culture arrays. Nat Methods. 2011 Jul;8(7):581– 586. 00174. Available from: <http://www.ncbi.nlm.nih.gov/pubmed/21602799>.
20. Croushore C, Supharoek S, Lee C, Jakmunee J, Sweedler J. Microfluidic device for the selective chemical stimulation of neurons and characterization of peptide release with mass spectrometry. Anal Chem. 2012 Nov;84(21):9446–9452. Available from: <http://www.ncbi.nlm.nih.gov/pubmed/23004687>.
21. Shintu L, Baudoin R, Navratil V, Prot J, Pontoizeau C, Defernez M, et al. Metabolomics-on-a-chip and predictive systems toxicology in microfluidic bioartificial organs. Anal Chem. 2012 Feb;84(4):1840–1848. 00053. Available from: <http://www.ncbi.nlm.nih.gov/pubmed/22242722>.
22. JW H. 3D cell culture: a review of current approaches and techniques. Methods Mol Biol. 2011; 695:1–15. Available from: <http://www.ncbi.nlm.nih.gov/pubmed/21042962>.
23. Grossmann G, Guo W, Ehrhardt D, Frommer W, Sit R, Quake S, et al. The RootChip: an integrated microfluidic chip for plant science. Plant Cell. 2011 Dec;23(12):4234–4240. Available from: <http://www.ncbi.nlm.nih.gov/pubmed/22186371>.
24. Antia M, Herricks T, Rathod P. Microfluidic modeling of cell-cell interactions in malaria pathogenesis. PLoS Pathog. 2007 Jul;3(7):0939–0948. 00064. Available from: <http://www.ncbi.nlm.nih.gov/pubmed/17658948>.
25. Ho SY, Chao CY, Huang HL, Chiu TW, Charoenkwan P, Hwang E. NeurphologyJ: An automatic neuronal morphology quantification method and its application in

- pharmacological discovery. *BMC Bioinformatics*. 2011 Jun; 12:230. Available from: <http://www.ncbi.nlm.nih.gov/pmc/articles/PMC3121649/>.
26. Vedel S, Tay S, Johnston DM, Bruus H, Quake SR. Migration of cells in a social context. *Proceedings of the National Academy of Sciences*. 2013 Jan;110(1):129–134. Available from: <http://www.pnas.org/cgi/doi/10.1073/pnas.1204291110>.
27. Lucumi Moreno E, Hachi S, Hemmer K, Trietsch SJ, Baumuratov AS, Hankemeier T, et al. Differentiation of neuroepithelial stem cells into functional dopaminergic neurons in 3D microfluidic cell culture. *Lab Chip*. 2015 May;15(11):2419–2428. Available from: <http://pubs.rsc.org/en/content/articlelanding/2015/lc/c5lc00180c>.
28. Trietsch SJ, Israels GD, Joore J, Hankemeier T, Vulto P. Microfluidic titer plate for stratified 3D cell culture. *Lab on a Chip*. 2013;13(18):3548. Available from: <http://xlink.rsc.org/?DOI=c3lc50210d>.
29. Vulto P, Podszun S, Meyer P, Hermann C, Manz A, Urban GA. Phaseguides: a paradigm shift in microfluidic priming and emptying. *Lab Chip*. 2011 May;11(9):1596–1602. 00031. Available from: <http://pubs.rsc.org/en/content/articlelanding/2011/lc/c0lc00643b>.
30. Frantz C, Stewart KM, Weaver VM. The extracellular matrix at a glance. *Journal of Cell Science*. 2010 Dec;123(24):4195–4200. 00329. Available from: <http://jcs.biologists.org/cgi/doi/10.1242/jcs.023820>.
31. Lu P, Weaver VM, Werb Z. The extracellular matrix: A dynamic niche in cancer progression. *J Cell Biol*. 2012 Feb;196(4):395–406. 00788. Available from: <http://jcb.rupress.org/content/196/4/395>.
32. Bittar EE, Bittar N. *Cellular organelles and the extracellular matrix*. JAI Press; 2007. OCLC: 903588222.
33. Miner JH. *Extracellular Matrix in Development and Disease*. Elsevier; 2005. 00004 Google-Books-ID: owZbhFgg1V0C.
34. Caliri SR, Burdick JA. A practical guide to hydrogels for cell culture. *Nat Meth*. 2016 May;13(5):405–414. Available from: <http://www.nature.com/nmeth/journal/v13/n5/abs/nmeth.3839.html>.
35. Van Vlierberghe S, Dubrue P, Schacht E. Biopolymer-Based Hydrogels As Scaffolds for Tissue Engineering Applications: A Review. *Biomacromolecules*. 2011 May;12(5):1387–1408. 00378. Available from: <http://pubs.acs.org/doi/abs/10.1021/bm200083n>.
36. Zhang X, Li L, Luo C. Gel integration for microfluidic applications. *Lab Chip*. 2016 May;16(10):1757–1776. Available from: <http://pubs.rsc.org/en/content/articlelanding/2016/lc/c6lc00247a>.
37. Benton G, Kleinman HK, George J, Arnaoutova I. Multiple uses of basement membrane-like matrix (BME/Matrigel) in vitro and in vivo with cancer cells. *Int J Cancer*. 2011

Apr;128(8):1751–1757. Available from:
<http://onlinelibrary.wiley.com/doi/10.1002/ijc.25781/abstract>.

38. Yanagawa F, Sugiura S, Kanamori T. Hydrogel microfabrication technology toward three dimensional tissue engineering. *Regenerative Therapy*. 2016 Mar;3:45–57. Available from: <http://www.sciencedirect.com/science/article/pii/S2352320416000201>.
39. Moeendarbary E, Valon L, Fritzsche M, Harris AR, Moulding DA, Thrasher AJ, et al. The cytoplasm of living cells behaves as a poroelastic material;12(3):253–261. Available from: <http://www.nature.com/articles/nmat3517>.
40. Chen J. Nanobiomechanics of living cells: a review. *Interface Focus*. 2014 Apr;4(2). Available from: <http://www.ncbi.nlm.nih.gov/pmc/articles/PMC3982446/>.
41. Reynolds O, Brightmore AWB, Moorby WHB. *Papers on Mechanical and Physical Subjects*; v. 3. WENTWORTH Press;. Available from: <https://books.google.com.sa/books?id=aY5OvgAACAAJ>.
42. Dunn DA, Feygin I. Challenges and solutions to ultra-high-throughput screening assay miniaturization: submicroliter fluid handling. *Drug Discovery Today*. 2000 Dec; 5(12, Supplement 1):84–91. Available from: <http://www.sciencedirect.com/science/article/pii/S1359644600000647>.
43. Kong F, Yuan L, Zheng YF, Chen W. Automatic Liquid Handling for Life Science: A Critical Review of the Current State of the Art. *J Lab Autom*. 2012 Jun;17(3):169–185. Available from: <http://dx.doi.org/10.1177/2211068211435302>.
44. Dauwalder O, Landrieve L, Laurent F, de Montclos M, Vandenesch F, Lina G. Does bacteriology laboratory automation reduce time to results and increase quality management? *Clinical Microbiology and Infection*. 2016 Mar;22(3):236–243. Available from: <http://www.sciencedirect.com/science/article/pii/S1198743X15009787>.
45. Triaud F, Clenet DH, Cariou Y, Le Neel T, Morin D, Truchaud A. Evaluation of Automated Cell Culture Incubators. *JALA: Journal of the Association for Laboratory Automation*. 2003 Dec;8(6):82–86. Available from: <http://journals.sagepub.com/doi/abs/10.1016/s1535-5535%2803%2900018-2>.
46. Halldorsson S, Lucumi E, Gómez-Sjöberg R, Fleming RMT. Advantages and challenges of microfluidic cell culture in polydimethylsiloxane devices. *Biosensors and Bioelectronics*. 2015 Jan;63:218–231. 00126. Available from: <http://www.sciencedirect.com/science/article/pii/S0956566314005302>.
47. Piracci A. Advantages of Non-Contact Dispensing in SMT Assembly Processes. In: *SMTA International Conference Proceedings*; 2000. Available from: http://www.smta.org/knowledge/proceedings_abstract.cfm?PROC_ID=619.
48. Mueller U, Nyarsik L, Horn M, Rauth H, Przewieslik T, Saenger W, et al. Development of a technology for automation and miniaturization of protein crystallization. *Journal of*

- Biotechnology. 2001 Jan;85(1):7–14. Available from:
<http://www.sciencedirect.com/science/article/pii/S0168165600003497>.
49. Cooley P, Wallace D, Antohe B. Applications of Ink-Jet Printing Technology to BioMEMS and Microfluidic Systems. JALA: Journal of the Association for Laboratory Automation. 2002 Oct;7(5):33–39. Available from:
<http://journals.sagepub.com/doi/abs/10.1016/S1535-5535-04-00214-X>.
50. Boehm RD, Gittard SD, Byrne JMH, Doraiswamy A, Wilker JJ, Dunaway TM, et al. Piezoelectric inkjet printing of medical adhesives and sealants. JOM. 2010 Jul;62(7):56–60. Available from: <https://link.springer.com/article/10.1007/s11837-010-0109-4>.
51. Lemmo AV, Rose DJ, Tisone TC. Inkjet dispensing technology: applications in drug discovery. Current Opinion in Biotechnology. 1998 Dec;9(6):615–617. Available from:
<http://www.sciencedirect.com/science/article/pii/S0958166998801390>.
52. KH L, CL S, KW K, HL C. Piezoelectric dispenser based on a piezoelectric-metal-cavity actuator. Review of Scientific Instruments. 2009 Jul;80(7):075110. Available from:
<http://aip.scitation.org/doi/abs/10.1063/1.3187220>.
53. Liu Y, Chen L, Sun L. Automated Precise Liquid Dispensing System for Protein Crystallization. In: 2007 International Conference on Mechatronics and Automation; 2007. p. 3616–3621.
54. Wixforth A. Acoustically Driven Programmable Microfluidics for Biological and Chemical Applications. JALA: Journal of the Association for Laboratory Automation. 2006 Dec;11(6):399–405. Available from: <http://journals.sagepub.com/doi/abs/10.1016/j.jala.2006.08.001>.
55. Amirzadeh A, Chandra S. Small droplet formation in a pneumatic drop-on-demand generator: Experiments and analysis. Experimental Thermal and Fluid Science. 2010 Nov;34(8):1488–1497. Available from: <http://www.sciencedirect.com/science/article/pii/S0894177710001421>.
56. Jetha NN, Marzali A. Liquid-Handling Technology and the Method of Electrostatic Drop Transfer to Improve Dispensing Performance. JALA: Journal of the Association for Laboratory Automation. 2006 Aug;11(4):278–280. Available from:
<http://journals.sagepub.com/doi/abs/10.1016/j.jala.2006.05.010>.
57. Husband B, Melvin T, Evans AGR. A superparamagnetic bead driven fluidic device (Invited Paper). vol. 5836; 2005. p. 607–616. Available from:
<http://dx.doi.org/10.1117/12.608699>.
58. Tseng FG, Lin KH, Hsu HT, Chieng CC. A surface-tension-driven fluidic network for precise enzyme batch dispensing and glucose detection. Sensors and Actuators A: Physical. 2004 Mar;111(1):107–117. Available from:
<http://www.sciencedirect.com/science/article/pii/S0924424703005429>.

59. Braun D, Weinert FM. Optically driven fluid flow along arbitrary microscale patterns using thermoviscous expansion. *Journal of Applied Physics*. 2008 Nov;104(10):104701. Available from: <http://aip.scitation.org/doi/abs/10.1063/1.3026526>.
60. American Society for Testing and Material. Standard Specification for Transferring Information Between Clinical Instruments and Computer Systems (Withdrawn 2002). In: *Annual Book of ASTM Standards*. vol. 14.01. West Conshohocken, PA; 1997. Available from: <https://www.astm.org/DATABASE.CART/WITHDRAWN/E1394.htm>.
61. Smith B, Ceusters W. HL7 RIM: an incoherent standard. *Stud Health Technol Inform*. 2006;124:133–138.
62. Joshi S, Pillai R. LECIS Commentary; 2002. Available from: https://www.ergotech.com/lecis.org/documents/UserSpace/LECIS_commentary.pdf.
63. Roth A, Jopp R, Schafer R, Kramer GW. Automated Generation of Animl Documents by Analytical Instruments. *JALA: Journal of the Association for Laboratory Automation*. 2006 Aug;11(4):247–253. Available from: <http://journals.sagepub.com/doi/abs/10.1016/j.jala.2006.05.013>.
64. Bar H, Hochstrasser R, Papenfub B. SiLA: Basic standards for rapid integration in laboratory automation. *J Lab Autom*. 2012 Apr;17(2):86–95.
65. Bar H, Syr'e U. Infoteam SiLA Library Simplifies Device Integration. *JALA: Journal of the Association for Laboratory Automation*. 2011 Oct;16(5):371–376. Available from: <http://journals.sagepub.com/doi/abs/10.1016/j.jala.2011.05.003>.
66. Command Dictionary Specification | SiLA Rapid Integration. Available from: <http://www.sila-standard.org/standards/command-dictionary-specification/>.

2. Determination of the rheological properties of Matrigel for optimum seeding

Title	Determination of the rheological properties of Matrigel for optimum seeding
Author(s) & Affiliation(s)	<p>K. I. W. Kane¹, E. Lucumi Moreno¹, C. M. Lehr², S. Hachi¹, R. Dannert², R. Sanctuary², C. Wagner^{2,3}, R.M.T. Fleming¹ and J. Baller²</p> <p>¹Luxembourg Centre for Systems Biomedicine, University of Luxembourg, 7 avenue des Hauts-Fourneaux, L-4362 Esch-sur-Alzette, Grand-Duchy of Luxembourg</p> <p>²Physics and Materials Science Research Unit, Laboratory for the Physics of Advanced Materials, University of Luxembourg, 162A avenue de la Faïencerie, L1511 Luxembourg, Grand-Duchy of Luxembourg.</p> <p>³Department of Experimental Physics, Saarland University, Campus E2.6, 66123 Saarbrücken, Germany</p>
Publication Outlet	American Institute of Physics
Publication Type	Peer Reviewed Journal
Publication Year	2018
Publication Status	Published
Preface	<p>In this article, we study the rheological properties of the extracellular matrix, a hydrogel, used for the differentiation of human neuroepithelial stem cells into mid brain like dopaminergic neurons. Hydrogels are increasingly used as a surrogate extracellular matrix in three-dimensional cell culture systems, including microfluidic cell culture. Matrigel is a hydrogel of natural origin widely used in cell culture, particularly in the culture of stem cell-derived cell lines. The use</p>

	<p>of Matrigel as a surrogate extracellular matrix in microfluidic systems is challenging due to its biochemical, biophysical, and biomechanical properties. Therefore, understanding and characterising these properties is a prerequisite for optimal use of Matrigel in microfluidic systems. We used rheological measurements and particle image velocimetry to characterise the fluid flow dynamics of liquefied Matrigel during loading into a three-dimensional microfluidic cell culture device. Using fluorescence microscopy and fluorescent beads for particle image velocimetry measurements (velocity profiles) in combination with classical rheological measurements of Matrigel (viscosity versus shear rate), we characterised the shear rates experienced by cells in a microfluidic device for three-dimensional cell culture. This study provides a better understanding of the mechanical stress experienced by cells, during seeding of a mixture of hydrogel and cells, into three-dimensional microfluidic cell culture devices. I contributed to this paper by running the particle image velocimetry experiments and analysis in the automated platform with Edinson Lucumi Moreno and Siham Hachi. In collaboration with Jorg Baller, I shaped the overall direction of the analysis and the narrative of the manuscript. Together with Jorg Baller, the first co-authors wrote the manuscript.</p>
Citation	Kane KIW, Moreno EL, Lehr CM, Hachi S, Dannert R, Sanctuary R, et al. Determination of the rheological properties of Matrigel for optimum seeding conditions in microfluidic cell cultures. AIP Advances. 2018 Dec; 8(12):125332.

Determination of the rheological properties of Matrigel for optimum seeding conditions in microfluidic cell cultures

K. I. W. Kane, E. Lucumi Moreno, C. M. Lehr, S. Hachi, R. Dannert, R. Sanctuary, C. Wagner, R. M. T. Fleming, and J. Baller

Citation: *AIP Advances* **8**, 125332 (2018); doi: 10.1063/1.5067382

View online: <https://doi.org/10.1063/1.5067382>

View Table of Contents: <http://aip.scitation.org/toc/adv/8/12>

Published by the *American Institute of Physics*



Don't let your writing
keep you from getting
published!

AIP | Author Services

Learn more today!

Determination of the rheological properties of Matrigel for optimum seeding conditions in microfluidic cell cultures

K. I. W. Kane,^{1,a} E. Lucumi Moreno,^{1,a} C. M. Lehr,^{2,a} S. Hachi,^{1,a} R. Dannert,² R. Sanctuary,² C. Wagner,^{2,3} R. M. T. Fleming,¹ and J. Baller^{2,b}

¹Luxembourg Centre for Systems Biomedicine, University of Luxembourg,

7 avenue des Hauts-Fourneaux, L-4362 Esch-sur-Alzette, Grand-Duchy of Luxembourg

²Physics and Materials Science Research Unit, Laboratory for the Physics of Advanced Materials, University of Luxembourg, 162A avenue de la Faiëncerie, L-1511 Luxembourg, Grand-Duchy of Luxembourg

³Department of Experimental Physics, Saarland University, Campus E2.6, 66123 Saarbrücken, Germany

(Received 17 October 2018; accepted 17 December 2018; published online 28 December 2018)

Hydrogels are increasingly used as a surrogate extracellular matrix in three-dimensional cell culture systems, including microfluidic cell culture. Matrigel is a hydrogel of natural origin widely used in cell culture, particularly in the culture of stem cell-derived cell lines. The use of Matrigel as a surrogate extracellular matrix in microfluidic systems is challenging due to its biochemical, biophysical, and biomechanical properties. Therefore, understanding and characterising these properties is a prerequisite for optimal use of Matrigel in microfluidic systems. We used rheological measurements and particle image velocimetry to characterise the fluid flow dynamics of liquefied Matrigel during loading into a three-dimensional microfluidic cell culture device. Using fluorescence microscopy and fluorescent beads for particle image velocimetry measurements (velocity profiles) in combination with classical rheological measurements of Matrigel (viscosity versus shear rate), we characterised the shear rates experienced by cells in a microfluidic device for three-dimensional cell culture. This study provides a better understanding of the mechanical stress experienced by cells, during seeding of a mixture of hydrogel and cells, into three-dimensional microfluidic cell culture devices. © 2018 Author(s). All article content, except where otherwise noted, is licensed under a Creative Commons Attribution (CC BY) license (<http://creativecommons.org/licenses/by/4.0/>). <https://doi.org/10.1063/1.5067382>

INTRODUCTION

In vivo cellular microenvironment

In a human soft tissue, all cells reside within a three-dimensional extracellular matrix, a viscous gel that mechanically strengthens the tissue and supports the cells within it. The extracellular matrix consists of a ground substance formed from large complex macromolecules, especially polysaccharides and proteoglycans, which attract water and ions, and fibrous proteins, especially collagen and elastin, which provide tensile strength and elasticity.^{1,2} The cellular microenvironment consists of the extracellular matrix and the molecular species that can diffuse between cells and the microvasculature. The extracellular matrix permits free diffusion of molecules between cells and the microvasculature. Nevertheless, it has a strong influence on cellular phenotype.¹ Therefore, when attempting to mimic an *in vivo* microenvironment with an *in vitro* cell culture system, it is important to provide an appropriate surrogate extracellular matrix. An *in vivo* system refers to an experiment conducted within

^aThese authors contributed equally to this work.

^bAuthor to whom correspondence should be addressed: joerg.baller@uni.lu. Tel.: ++352 466 644 6755.

a whole living organism while an *in vitro* system is one that is conducted in the laboratory within, for example, a petri dish.

Surrogate extracellular matrices

Several extracellular matrix surrogates from natural and synthetic origins have been developed in the form of hydrogels, for cell culture applications.³ Hydrogels are physically or chemically cross-linked polymer networks that absorb large amounts of water.⁴ Because of their biomechanical and biochemical properties, they are used as a surrogate extracellular matrix for 2D and 3D cell culture. Moreover, they are compatible with microscopy techniques. Hydrogels of natural origins are basement membrane-based gel preparations; some examples include fibrin gel, collagen gel, alginate gel and Matrigel.⁵ Matrigel is a commercial hydrogel of natural origins. It is a reconstituted basement membrane preparation extracted from Engelbreth-Holm-Swarm (EHS) mouse sarcoma that is biologically active and therefore, widely used in a variety of 2D and 3D cell cultures, including stem cells, cancer cells, induced pluripotent stem cells (iPSCs) and neuronal cells, among other applications.

Microfluidic cell culture

Microfluidic cell culture concerns the development of devices and techniques for culturing, maintaining, analysing and experimenting with cells in micro-scale volumes.^{6,7} Microfluidic cell culture in three-dimensions resembles the cellular microenvironment experienced by cells *in vivo*.⁸ Hydrogels have similar mechanical properties to soft tissues^{3,9} making them suitable for use as substitutes for extracellular matrix in microfluidic devices.^{5,9,10} Automated microfluidic cell culture has the potential to increase the quantity of experiments that can be completed in parallel and enables long-term cell culture maintenance with reduced manual labour. However, such systems rely on precise programming of robotics and liquid handlers, which first requires quantitative characterisation of the chemical and rheological properties of the fluids involved.

Matrigel in microfluidic devices

Matrigel is frequently used as a surrogate extracellular matrix in microfluidic cell culture, see e.g. Trietsch *et al.*¹¹ and Lucumi *et al.*⁵ As Matrigel is a liquid at low temperatures and a gel at room temperature it is suited for seeding of microfluidic cell culture devices, where the cell culture chamber is usually remote from the accessible input of the microfluidic cell culture device. The fluid properties of Matrigel for its application in 3D microfluidics have not been fully characterized yet.¹²⁻¹⁴ In Trietsch *et al.*¹¹ and Lucumi *et al.*,⁵ a low temperature mixture of Matrigel and cells is used to seed each three dimensional microfluidic cell culture chamber, prior to restoration to body temperature and juxtaposed perfusion with liquid cell culture medium.

Rheology

Rheology is the study of the flow of matter. It is utilised to determine physical properties of a material such as its viscosity or its shear moduli. Liquids (e. g. water and Matrigel) can be divided into two groups: Newtonian and non-Newtonian fluids. Non-Newtonian fluids are fluids for which the viscosity is dependent on the amount of applied shear stress, while the viscosity of Newtonian fluids is independent of the applied shear stress.

Our contribution

Cells have poroelastic mechanical properties: subjected to mechanical stress, they elastically deform and temporarily lose some fluid content. This behaviour is due to the porous nature of the cellular membrane.¹⁵ Therefore, it is important to quantify the shear stress and shear rates that cells are exposed to in a given microfluidic device under particular conditions. Herein, we employ rheology on isolated Matrigel to characterise its rheological properties at different temperatures. We also quantify the velocity field of Matrigel flow during seeding of an established three dimensional microfluidic cell culture device (OrganoPlate)¹¹ using particle image velocimetry. Combining the results of both techniques allows the prediction of the shear rates that cells are exposed to in a microfluidic device at different temperatures. To the best of our knowledge, this approach has never been reported for

gels used in cell culture devices. In addition, through this study, we aim to provide the optimum conditions of flow of Matrigel to minimise the stresses experienced by cells as they are seeded into 3D microfluidic systems. This should allow to decrease the mortality of the cells and thus increase the applicability of hydrogels in microfluidic cell culture.

EXPERIMENTAL

Matrigel and fluorescent beads

Matrigel was obtained from BD biosciences (Germany). Fluorescent polystyrene beads (PS-FluoGreen-Fi226) in an aqueous suspension (2.5 wt%) with an average diameter of 10 μm were purchased from Microparticles GmbH (Berlin, Germany).

Matrigel consists of about 60% laminin, 30% collagen IV, and 8% entactin. Entactin is a bridging molecule that interacts with laminin and collagen IV, and contributes to the structural organization of Matrigel. The latter is a non-Newtonian viscoelastic fluid that exhibits a Lower Critical Solution Temperature⁴ of about 6°C. In other terms, below that temperature it is liquid and can be filled into microfluidic devices using a pipette. The exact water content of Matrigel is unknown. Therefore, we performed a standard Differential Scanning Calorimetry (DSC) scan in the vicinity of the melting point of water (see Fig. 1). Since the difference between the measured *heat of fusion* (334.8 J/g) of Matrigel and the corresponding value for pure water (332.8 J/g)¹⁶ is below the experimental error, the water content of Matrigel can be assumed to be higher than 99 wt %.

For Particle Image Velocimetry (PIV) measurements, 2 μL of the aqueous suspension containing the polystyrene beads was mixed with 8 μL of Matrigel.

For all experimental studies, the same batch of Matrigel was used.

Microfluidic device and microscopy setup

A 2-lane OrganoPlate (Mimetas BV, Leiden, The Netherlands) consists of an array of 96 chips embedded in a customised 384-well plate format, illustrated in Fig. 2. Each microfluidic chip is contained between two sheets of glass with the top sheet of glass having holes complementary to the underside of selected wells. Each chip is juxtaposed to 3 wells, one gel inlet well (Fig. 2 b1) for loading gel-embedded cells into the culture lane by capillary forces, one readout window (Fig. 2 b3) for monitoring the culture lane by inverted light microscopy. In addition, each bioreactor has a perfusion inlet well (Fig. 2 b2) connected to a perfusion outlet (Fig. 2 b4) well via a media perfusion lane. In each culture chamber, during cell loading a phaseguide prevents liquefied gel-embedded cells from leaving the culture lane and entering the medium lane.

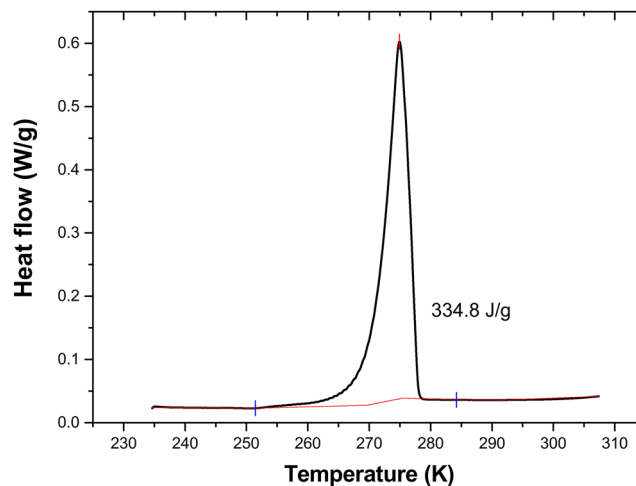


FIG. 1. Melting transition of pure Matrigel as seen by Differential Scanning Calorimetry (DSC). Heating rate: 10 K/min).

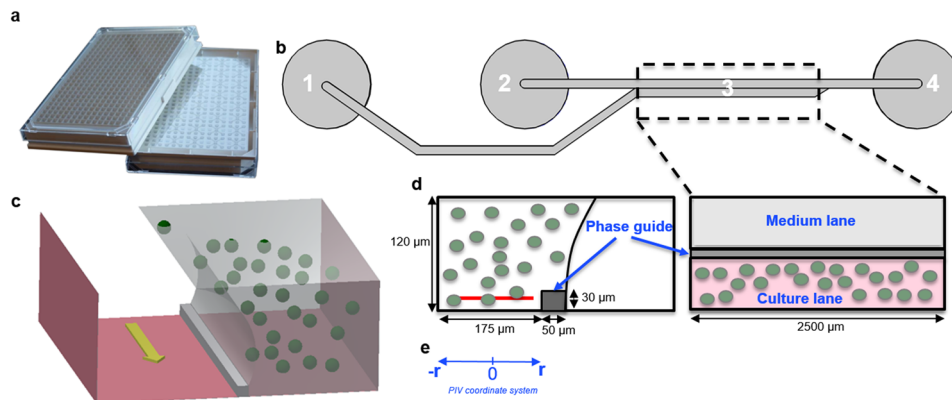


FIG. 2. Schematic representation of the OrganoPlate. (a) Overall view of an OrganoPlate. (b) Schematic of a single 2-lane chip: 1=gel inlet, 2=medium inlet, 3=observation window, 4=medium outlet. (c) Transverse section of a culture chamber showing the direction of the flow (yellow arrow) in the medium lane, the phaseguide and the culture lane with suspended spheres. (d) Detailed view of the culture chamber with dimensions. Red line: Focal plane of the PIV measurements (e) Coordinate system used for the PIV measurements (Fig. 7 and Fig. 8).

A phaseguide is a patterned pinning barrier that controls the liquid-air interface by forcing it to align with the ridge and therefore allowing the filling of microfluidic structures. An inverted epifluorescence microscope (Leica DMI6000B) equipped with a cooled sCMOS camera (Neo 5.5, Andor Technology), within a temperature controlled incubation chamber (Incubator BLX, Pecon), was used to perform PIV during seeding. An ice bath was used to keep Matrigel from gelation while loading it into the OrganoPlate.

Rheology

Rheological measurements were performed with an Anton Paar rheometer MCR 302. A schematic representation of the experimental setup is shown in Fig. 3. All measurements were done using parallel-plate configuration. The sample temperature was controlled with a liquid nitrogen cryostat. Measurement of the torque M and the angle φ allows to determine the shear stress $\sigma(t)$ as well as the strain $\gamma(t)$ or the shear rate $\dot{\gamma}(t)$ respectively.¹⁷

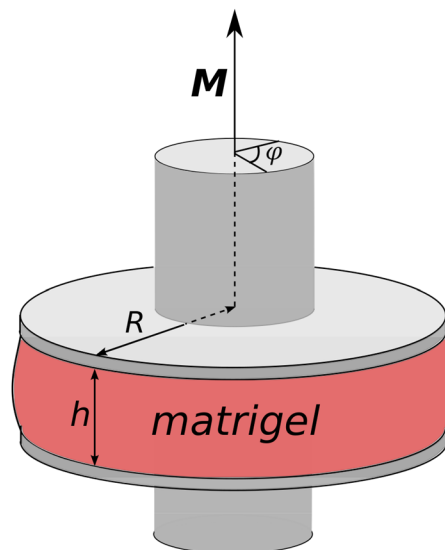


FIG. 3. Experimental setup for the rheological measurements (plate radius $R=12.5$ mm; gap width $h=0.5$ to 1 mm). A torque M is applied to the upper plate leading to a rotation. The lower plate is fixed.

Filling of the sample

Matrigel was kept at a temperature of -12°C until the start of the measurements. It was then put on the pre-cooled rheometer plates using a syringe. Due to the fact, that this process had to be done as fast as possible in order to avoid gelation of Matrigel and heating of the rheometer plates (the furnace has to be opened) the filling was not as homogeneous as possible. This certainly affects the absolute values of the viscosity and shear moduli. The power law behaviour of the viscosity as well as the gelation behaviour (gelation temperature) is not affected.

Flow curves

The flow properties, i.e. the dependency of the shear stress σ or the viscosity η on the shear rate $\dot{\gamma}$ can be determined by recording so-called *flow-curves*.^{17,18} A flow curve is a graph representing the shear stress or the viscosity of a sample as a function of the shear rate at constant temperatures. The following measurement protocol was applied while keeping the sample temperature constant at a defined value T : The viscosity of the samples has first been measured while increasing the shear rate from 0.1 s^{-1} to 10 s^{-1} (flow curves \nearrow). The recording time τ for each data point has always been chosen such that $\tau > \dot{\gamma}^{-1}$ in order to assure the establishment of the desired shear field throughout the entire sample.¹⁹ Then the same measurement has been done with decreasing shear rates (flow curves \searrow). Thereby, besides the shear rate dependency of the viscosity, the thixotropic character of the material or the dependency of the viscosity on the shear history can be determined.²⁰

Small amplitude oscillatory shear (SAOS) measurements

SAOS measurements can be used to determine the storage and loss shear moduli of viscoelastic samples. A sinusoidal strain $\gamma(t) = \gamma_0 \sin(\omega t)$ with amplitude γ_0 and angular frequency ω is applied to the samples.²¹ The resulting stress $\sigma(t)$ is measured and linear response theory is used to calculate the real (storage) and imaginary (loss) parts G' and G'' of the complex shear modulus respectively. The following measurement protocol has been used for the SAOS measurements presented in this work: For each temperature T , an *amplitude sweep* has been performed in order to determine the maximum value of the strain amplitude γ_0 for which linear response conditions (shear moduli independent of strain amplitude) hold. Then, isothermal frequency sweeps have been performed to determine the dynamic rheological properties.

Particle image velocimetry

To determine the velocity profiles of fluorescent beads mixed with Matrigel flowing in the culture lane of an OrganoPlate, Particle Image Velocimetry measurements were performed. Images were sampled at a rate of 50Hz and with a pixel size of $0.33\mu\text{m}/\text{pixel}$. To accurately estimate the velocity fields, out-of-focus beads were first removed. A bandpass was then applied to smoothen the images and subtract the background.²² A threshold for pixel intensities was set to suppress out-of-focus beads. The flow velocities were then determined using an open source framework for particle image velocimetry analysis, OpenPIV,²¹ which is implemented in MATLAB, C++ and Python (www.openpiv.net). Each image was subdivided into smaller areas termed interrogation windows. Interrogation windows having the size of 512×128 pixels with an overlap of 128×32 pixels were used. This determines the number of pixels by which adjacent windows overlap. For the same interrogation window of a pair of consecutive images, a Fast Fourier Transform based cross-correlation was calculated to infer the most probable displacement vector of the particles within the interrogation window. The magnitude of each displacement vector was divided by the time interval between two images (20ms) to estimate the velocity. The calculated velocity vectors were loaded into the Open PIV spatial analysis toolbox (<https://github.com/OpenPIV/openpiv-spatial-analysis-toolbox/>) which then allowed to determine the velocity profile of the fluorescent beads flowing in Matrigel within the culture lane of the OrganoPlate.

RESULTS AND DISCUSSION

Gelation of Matrigel

The peculiarity of Matrigel to be liquid at low temperatures and to form a stable gel above a certain temperature T_{gel} is the most important physical property that predestines it for its use as a

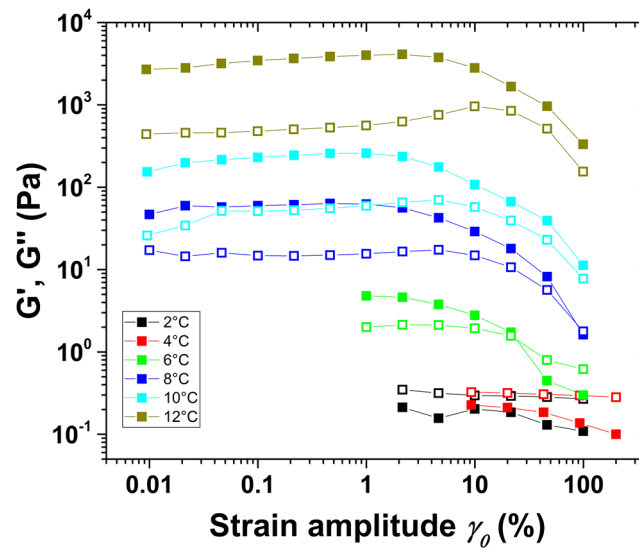


FIG. 4. Determination of the linear response regimes: G' (filled symbols) and G'' (open symbols) as a function of strain amplitude; the strain amplitude runs were carried out under isothermal conditions at the temperatures indicated in the legend.

surrogate extracellular matrix. Therefore, the first step in the characterization of Matrigel for its use in microfluidic cell cultures is the analysis of the gelation process. Rheology, especially small angle oscillatory shear (SAOS) measurements, is best suited for this study. In their seminal work,^{23–25} Winter *et al.* showed that the onset of gelation can be identified in SAOS measurements as the temperature at which both parts of the elastic moduli, i.e. G' and G'' , take the same values, independent of the probe frequency. It has to be stressed that this holds only true if linear response conditions are fulfilled (cf Section: Experimental). We tested this by measuring the elastic moduli as a function of the oscillation amplitude γ_0 (see Fig. 4).

For each temperature, an appropriate maximum strain amplitude in the linear response regime was selected. In the following analysis of the gelation behaviour of Matrigel, these limiting values of the strain amplitudes have been respected.

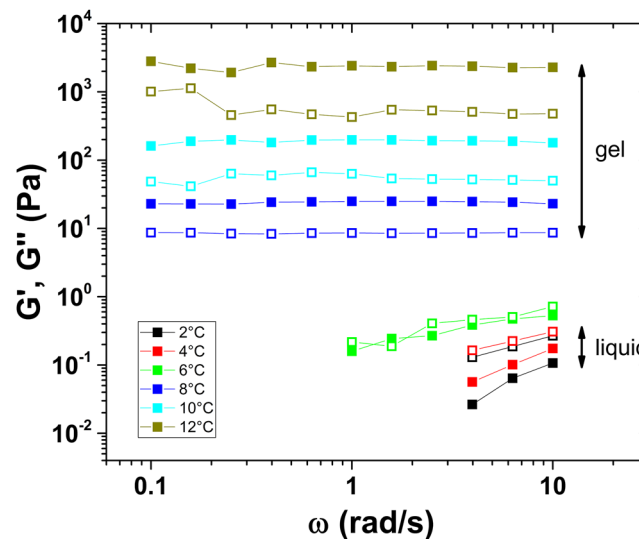


FIG. 5. Gelation of Matrigel: G' (filled symbols) and G'' (open symbols) as a function of oscillation frequency; measured isothermally at the temperatures indicated in the legend. For details see text.

Fig. 5 shows isothermal measurements of the elastic shear moduli as a function of the oscillation frequency. Below 6°C, the storage modulus G' is always smaller than the loss modulus G'' , i.e. the system is in a liquid phase. Above 6°C, G' which corresponds to the fully elastic response of the sample is higher than G'' and is independent of the frequency. This is a clear sign that the system exhibits solid-like behaviour. At 6°C finally, G' equals G'' for all measured frequencies. This indicates that gelation starts around $T_{gel} = 6^\circ\text{C}$. For the use of Matrigel in microfluidic devices, this experimental result indicates that it is important to cool the microfluidic device to a temperature below T_{gel} in order to avoid early gelation.

Flow of Matrigel in a rheometer

The flow behaviour and especially the viscosity of Matrigel is of special interest because it gives information about the shear stress that will act on embedded cells when filling the channels of a microfluidic device. Many materials such as dispersions, emulsions, polymer solutions or gels do not have a constant viscosity but show a dependency of viscosity on the shear rate:¹⁸ $\eta = \eta(\dot{\gamma})$. The shear rate that a fluid is exposed to when it flows through a pipe or a microfluidic device is not constant along the cross-section of the device. Therefore, it is of great importance to determine the viscosity of Matrigel as a function of shear rate. Using state-of-the-art rheological equipment, flow behaviour can be analysed at different temperatures for a wide range of different shear and strain rates. Fig. 6 shows the viscosity of Matrigel as a function of applied shear rate at different temperatures. Please note that the absolute values of the viscosity greatly depend on the filling process (please see section Experimental).

First, a scan with increasing shear rates was conducted (filled symbols in Fig. 6). This scan was directly followed by a second scan with decreasing shear rates starting at the highest shear rate of about 10 s^{-1} (open symbols in Fig. 6). As a result of this procedure, an influence of the shear history on the flow curves for temperatures equal or higher than 6°C can be stated. This was expected since the start of gelation at 6°C is also the start of structure formation (gel network) inside Matrigel (see Fig. 5). Shearing Matrigel at temperatures higher than 6°C leads to a competition between network formation due to gelation and network destruction due to shearing. Since network formation takes more time, the measured viscosities depend on the shear history. The temperature of 6°C above which this behaviour occurs, is a confirmation of the results of the determination of the gelation temperature from the isothermal frequency sweeps described in the previous paragraph (Fig. 5). The flow curves depict also that Matrigel behaves like a liquid at temperatures lower than 6°C. This is evidenced by the observation that the viscosity decreases with increasing temperature below 6°C, which is a behaviour expected for liquids.

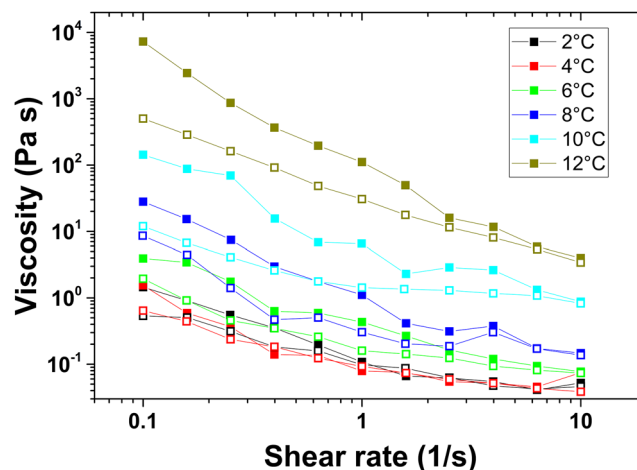


FIG. 6. Flow curves. First scan with increasing shear rates (\blacktriangleright): filled symbols. Second scan with decreasing shear rates (\blacktriangleleft): open symbols. For more details see text.

TABLE I. Power law exponents (see text).

Temp.	2°C	4°C	6°C	8°C	10°C	12°C
$n \nearrow$	0.20	0.33	0.10	-0.17	-0.12	-0.62
$k \nearrow$	0.16	0.14	0.45	1.33	8.3	109
$n \searrow$	0.40	0.40	0.34	0.19	0.48	-0.09
$k \searrow$	0.13	0.12	0.23	0.54	2.12	35

The overall behaviour of the flow curves illustrated in Fig. 6 clearly shows non-Newtonian behaviour. This holds also true for the liquid phase below 6°C which is very unusual at first sight. It could be explained by precursors of the gel already present at lower temperatures. This experimental finding at lower temperatures certainly deserves further investigation.

The non-Newtonian behaviour of the flow curves can be modelled by a power law model:¹⁸

$$\sigma = k\dot{\gamma}^n = k\dot{\gamma}^{n-1}\dot{\gamma} \quad (1)$$

with σ and $\dot{\gamma}$ being the shear stress and the shear rate respectively. k is a constant, n is the power law exponent and the term $k\dot{\gamma}^{n-1}$ corresponds to an apparent viscosity of Matrigel. Table I exhibits the power law parameters deduced from fits of the flow curves shown in Fig. 6.

In case of the first scans with increasing shear rates (\nearrow), the exponents n are positive up to the gelation temperature. Above T_{gel} they become negative, i.e. the destruction of the gel structure induced by the shear forces becomes more dominant. The second scans with decreasing shear rates (\searrow) yield exponents which do not show a systematic behaviour due to the fact that the first applied shear stress which is the highest shear stress for this study already destroys the gel structure.

Flow of Matrigel in a microfluidic device

The flow behaviour of Matrigel retrieved from rheological measurements (Fig. 6 and Table I) can now be used to analyse the flow profile of Matrigel in a microfluidic device.

For the following analysis, the power law parameters of the decreasing shear rate curves have been used since they better reflect the state of Matrigel after it has been filled into the microfluidic device using a pipette. Fig. 7 shows the flow profile determined by PIV measurements at 8°C. Due to the asymmetric geometry of the microfluidic device (Fig. 2), only the left part of the data opposite to the phaseguide was used for fitting (filled symbols). The right side (empty symbols) have not been

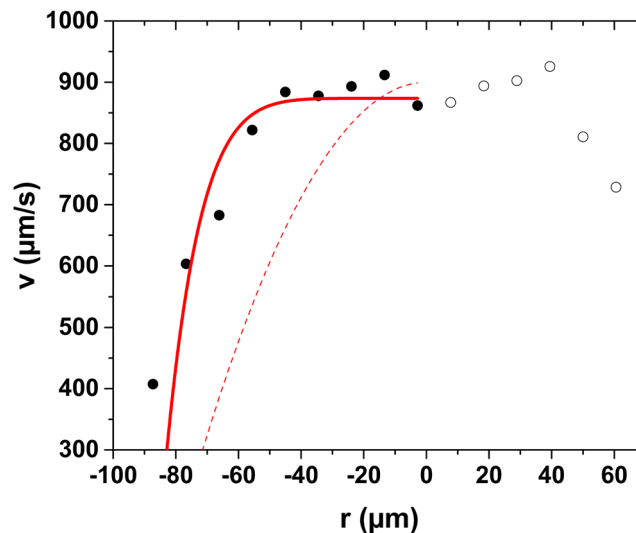


FIG. 7. Velocity profile across the culture lane (for the definition of the r -axis see Fig. 2). Filled symbols: PIV data used for fitting. Empty symbols: PIV data not used for fitting (see text). Solid line: Fit using a power law model function. Dashed line: Fit using a Hagen-Poiseuille model. For all fits: $R=87\mu\text{m}$.

considered for fitting. The dashed line in Fig. 7 shows a fit according to a Hagen-Poiseuille law for Newtonian fluids flowing in a circular pipe^{18,26}

$$v = v_{max} \left(1 - \frac{r^2}{R^2} \right) \quad (2)$$

that did not fit the PIV data. The flow profile of a power law fluid takes the form:²⁶

$$v = \frac{\sigma_{wall}^{\frac{1}{n}} R^{\frac{1}{n}+1} - |r|^{\frac{1}{n}+1}}{kR \left(\frac{1}{n} + 1 \right)} \quad (3)$$

Using this model, there is a much better fit to the PIV data (solid line in Fig. 7) and the resulting exponent $n=0.15$ is close to the value of 0.19 obtained from the rheological measurements.

Consequences for the use of Matrigel in microfluidic cell culture

A key parameter for the survival rate of cells during the filling process is the shear rate $\dot{\gamma} = d\gamma_{fluid}/dt = dv/dr$ which can be directly deduced from the fit of the velocity profile (black solid line in Fig. 8).

Assuming that the cells can survive a maximum shear rate of 50 s^{-1} (dashed horizontal red line in Fig. 8), all cells would survive filling of the microfluidic device at 8°C . To analyse the situation at another temperature for which no PIV data has been measured, we first use the shear stress at the wall ($\sigma_{wall} = 1.03 \text{ Pa}$) obtained from the fit of the PIV data at 8°C (Fig. 7, eq. 3) in order to calculate the pressure difference Δp along the microfluidic device ($L=2.5 \text{ mm}$) during the experiment:

$$\Delta p = \frac{2L \sigma_{wall}}{R} = 59 \text{ Pa} \quad (4)$$

For the same pressure difference and using the power law parameters from Table I, the shear rates at 2°C can now be calculated (dashed blue line in Fig. 8). Assuming again a maximum shear rate of 50 s^{-1} , all cells being closer to the borders than $40 \mu\text{m}$ would not survive. A similar calculation (cf [supplementary material](#)) can be made for the more realistic situation that not the pressure difference but the flow rate Q across the microfluidic device is constant for all temperatures (e.g. by using automated pipettes). The corresponding results are also shown for 2°C in Fig. 8 (solid blue line). Again, many cells would not survive, when the filling of the microfluidic device would be performed at this temperature.

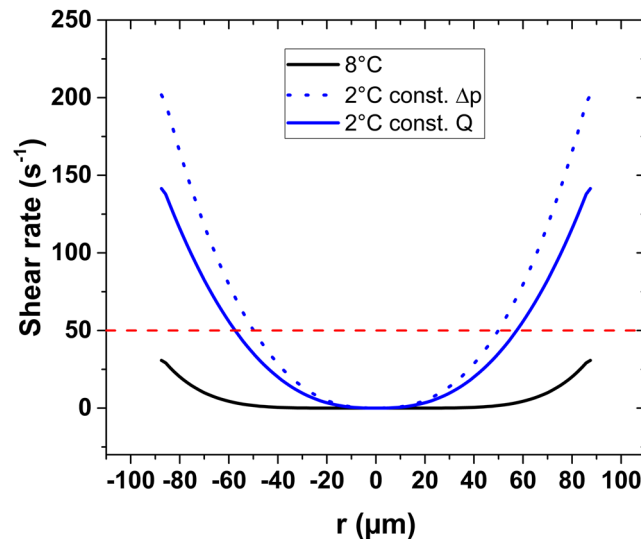


FIG. 8. Shear rates at 8°C and 2°C . Shear rates at 8°C are determined from the velocity profiles. Shear rates at 2°C are calculated from the 8°C curves with the help of the flow curves (Fig. 6). ΔP =pressure drop, Q =volumetric flow rate.

Thus, a single PIV measurement of Matrigel in a microfluidic device can be used in combination with standard rheological characterization to predict the shear rate that cells are imposed to during the filling of a microfluidic device. There are two competing parameters to optimise the loading in 3D microfluidic channels: the need to lower the temperature to avoid the early gelation of Matrigel and promote its flow through narrow lanes; and the need for higher temperatures to increase the viscosity and the non-Newtonian characteristic of Matrigel. Increasing the non-Newtonian characteristic leads to flatter velocity profiles, minimising the shear stress experienced by the cells during loading into microfluidic channels. This study suggests that the optimum loading temperature of Matrigel in microfluidic cell culture lies between 8°C and 10°C, with a lower temperature more suited to longer microfluidic channels, and a higher temperature for shorter channels where early gelation is less of a concern. This allows one to minimise the trial and error experimental efforts required to optimise survival rates of loaded cells.

CONCLUSIONS

We characterised the rheological properties of a hydrogel (Matrigel) during a process representative of seeding a three-dimensional microfluidic cell culture device (OrganoPlate, Mimetas B.V.) with live cells. We could show that Matrigel is a liquid at temperatures below 8°C. Above 8°C, the rheological measurements showed the typical signs of a solid (real part of shear modulus higher than imaginary part). Moreover it could be shown that the viscosity of Matrigel can be well described by a power law model. The PIV measurements lead to the conclusion that the minimum amount of shear stress is obtained when the hydrogel is loaded at a temperature between 8°C and 10°C. Higher temperatures lead to greater shear due to temperature induced gelation, while lower temperatures lead to greater shear stress due to temperature induced liquefaction leading to loss of non-Newtonian fluid flow behaviour. Our interdisciplinary approach of rheological characterisation combined with *in situ* particle image velocimetry is applicable for other types of microfluidic devices and other hydrogels. This is an important step towards rational optimisation of three dimensional microfluidic cell culture protocols.

SUPPLEMENTARY MATERIAL

See [supplementary material](#) for a movie of the PIV measurements and a description of the combination of PIV and rheological data.

ACKNOWLEDGMENTS

KIWK and ELM received funding from the SysMedPD project from the European Union's Horizon 2020 research and innovation program under grant agreement No. 668738. ELM and SH were also supported by an Aides à la Formation-Recherche training allowance from Fonds National de la Recherche Luxembourg ref. 10099424.

- ¹ P. Lu, V. M. Weaver, and Z. Werb, *J. Cell Biol.* **196**(4), 395–406 (2012).
- ² J. H. Miner, *Extracellular Matrix in Development and Disease* (Elsevier, 2005).
- ³ S. R. Caliari and J. A. Burdick, *Nat. Methods* **13**(5), 405–414 (2016).
- ⁴ S. Van Vlierberghe, P. Dubruel, and E. Schacht, *Biomacromolecules* **12**(5), 1387–1408 (2011).
- ⁵ E. Lucumi Moreno, S. Hachi, K. Hemmer, S. J. Trietsch, A. S. Baumuratov, T. Hankemeier, P. Vulto, J. C. Schwamborn, and R. M. T. Fleming, *Lab Chip* **15**(11), 2419–2428 (2015).
- ⁶ S. Halldórsson, E. Lucumi Moreno, R. Gómez-Sjöberg, and R. M. T. Fleming, *Biosensors and Bioelectronics* **63**, 218–231 (2015).
- ⁷ I. Meyvantsson and D. Beebe, *Annu. Rev. Anal. Chem.* **1**, 423–449 (2008).
- ⁸ J. W. Haycock, in *3D Cell Culture*, No. 695, edited by J. W. Haycock (Humana Press, 2011), pp. 1–15.
- ⁹ X. Zhang, L. Li, and C. Luo, *Lab Chip* **16**(10), 1757–1776 (2016).
- ¹⁰ F. Yanagawa, S. Sugiura, and T. Kanamori, *Regenerative Therapy* **3**, 45–57 (2016).
- ¹¹ S. J. Trietsch, G. D. Israël's, J. Joore, T. Hankemeier, and P. Vulto, *Lab Chip* **13**(18) (2013).
- ¹² J. M. Jang, S. H. T. Tran, S. C. Na, and N. L. Jeon, *ACS Appl. Mater. Interfaces* **7**(4), 2183–2188 (2015).
- ¹³ P. Worthington, D. J. Pochan, and S. A. Langhans, *Frontiers in Oncology* **5** (2015).
- ¹⁴ J. M. Zuidema, C. J. Rivet, R. J. Gilbert, and F. A. Morrison, *J Biomed Mater Res B Appl Biomater* **102**(5), 1063–1073 (2014).

- ¹⁵ J. Chen, *Interface Focus* **4**(2) (2014).
- ¹⁶ D. R. Lide and W. M. Haynes, *CRC Handbook of Chemistry and Physics*, 90 ed. (CRC press, 2009).
- ¹⁷ C. W. Macosko, VCH, New York (1994).
- ¹⁸ H. A. Barnes, J. F. Hutton, and K. Walters, *An introduction to rheology* (Elsevier, 1989).
- ¹⁹ T. G. Mezger, *The rheology handbook: for users of rotational and oscillatory rheometers* (Vincentz Network GmbH & Co KG, 2006).
- ²⁰ H. A. Barnes, *Journal of Non-Newtonian fluid mechanics* **70**(1), 1–33 (1997).
- ²¹ J. Mewis and N. J. Wagner, *Colloidal suspension rheology* (Cambridge University Press, 2012).
- ²² J. C. Crocker and B. D. Hoffman, in *Methods in Cell Biology* (Academic Press, 2007), pp. 141-178.
- ²³ F. Chambon and H. H. Winter, *Polym. Bull. (Berlin)* **13**(6), 499–503 (1985).
- ²⁴ H. H. Winter, *Polym. Eng. Sci.* **27**(22), 1698–1702 (1987).
- ²⁵ H. H. Winter and F. Chambon, *Journal of Rheology* **30**(2), 367–382 (1986).
- ²⁶ E. J. Hinch, *Lecture Notes Woods Hole GFD Summer School* **1**(5), 1–19 (2003).

3. Passive controlled flow for neuronal cell culture in 3D microfluidic devices

Title	Passive controlled flow for neuronal cell culture in 3D microfluidic devices
Author(s) & Affiliation(s)	<p>K. I. W. Kane¹, Javier Jarazo¹, E. Lucumi Moreno¹, Paul Vulto² Ronan M.T. Fleming^{1,3}, Bas Trietsch², Jens Schwamborn¹</p> <p>¹Luxembourg Centre for Systems Biomedicine, University of Luxembourg, 7 avenue des Hauts-Fourneaux, L-4362 Esch-sur-Alzette, Grand-Duchy of Luxembourg.</p> <p>²Mimetas B.V, PO Box 11002, 2301EA Leiden, The Netherlands.</p> <p>³Analytical BioSciences Division, Leiden Academic Centre for Drug Research, Leiden University, Einsteinweg 55, 2333CC Leiden, The Netherlands.</p>
Publication Outlet	N/A
Publication Type	N/A
Publication Year	N/A
Publication Status	Draft
Preface	<p>In this paper, we passively controlled the flow of media in a three-dimensional microfluid device to optimise the media exchange for neuronal cell culture. Controlled flow within a lab-on-a-chip is a critical element of successfully implementing culture protocols of dopaminergic derived neurons within a microfluidic device. There have been a multitude of passive pumping technologies that have been successfully used to control the flow within a lab-on-a-chip. However, most of which were only able to generate flow for very few minutes, while the most successful ones were able to achieve around an hour of</p>

flow. This is not convenient for culture protocols requiring constant flow, as hourly media changes will have to be conducted. Herein, we present a design technique adapted for the OrganoPlate, a cell culture plate fully compatible with laboratory automation, which allows its re-dimension to achieve over 24h of flow. This technique uses a similarity model of a target cell type and a simple fluid flow mathematical prediction model to iterate the most optimum dimensions within some manufacturing constraints. This technique has the potential to be applied to many cell types to generate optimum design for their culture. We applied this technique to design a 3D microfluidic device optimised for neuronal cell culture. I contributed to this paper by completing all the modelling work. I wrote all the algorithms utilised in the study. I designed the optimised microfluidic device. Together with Bas Trietsch, we fine-tuned the design for manufacturing. I shaped the overall direction of the analysis and the narrative of the manuscript. I wrote the manuscript.

Draft: Passive controlled flow for neuronal cell culture in 3D microfluidic devices

Khalid I.W. Kane¹, Javier Jarazo¹, Edinson Lucumi Moreno², Paul Vulto³

Ronan M.T. Fleming^{1,2}, Bas Trietsch³, Jens Schwamborn¹

2nd April 2019

¹Luxembourg Centre for Systems Biomedicine, University of Luxembourg, 7 avenue des Hauts-Fourneaux, L-4362 Esch-sur-Alzette, Grand-Duchy of Luxembourg. ²Analytical BioSciences Division, Leiden Academic Centre for Drug Research, Leiden University, Einsteinweg 55, 2333CC Leiden, The Netherlands. ³Mimetas B.V, PO Box 11002, 2301EA Leiden, The Netherlands.

Abstract

Controlled flow within a lab-on-a-chip is a critical element of successfully implementing culture protocols of dopaminergic derived neurons within a microfluidic device. There have been a multitude of passive pumping technologies that have been successfully used to control the flow within a lab-on-a-chip. However, most of which were only able to generate flow for very few minutes, while the most successful ones were able to achieve around an hour of flow. This is not convenient for culture protocols requiring constant flow, as hourly media changes will have to be conducted. Herein, we present a design technique adapted for the OrganoPlate, a cell culture plate fully compatible with laboratory automation, which allows its re-dimension to achieve over 24h of flow. This technique uses a similarity model of a target cell type and a simple fluid flow mathematical prediction model to iterate the most optimum dimensions within some manufacturing constraints. This technique has the potential to be

applied to many cell types to generate optimum design for their culture. We applied this technique to design a 3D microfluidic device, dynamically optimised for neuronal cell culture.

Nomenclature

- R =hydraulic resistance
- μ =viscosity
- L =length of the lane
- w =width of the medium lane
- h =height of the medium lane
- ΔP = difference of pressure
- Q =volumetric flow rate
- ρ =density
- g =gravity
- δt =time interval
- A_w = medium well area
- SBS = Society for Biomolecular Screening

1 Introduction

Microfluidic cell culture concerns the design and implementation of devices and protocols for the culture, maintenance and perturbation of cells in micro-scale fluid volumes. The reasons behind the popularity of microfluidic cell culture are both economic and scientific. Cell culture reagents are expensive, and the amounts used in microfluidic cell cultures are much less than in macroscopic

cell culture [1, 2]. Microfluidic cell culture also has the potential to lower the ratio of extracellular to intracellular fluid volumes, thereby decreasing the temporal lag in extracellular response to molecules transported across cell membranes, e.g., in exometabolomic analyses [3–5]. Microfluidic cell culture also enables the generation of perfused three dimensional cell cultures [6–8]. Moreover, miniaturisation enables multiple experimental replicates within a geometrically confined experimental footprint. Furthermore, the combination of automation, microfluidics and cell culture technologies allows the screening of multiple environmental conditions in parallel [9, 10] as well as enabling regular live cell culture monitoring [11, 12], at a temporal resolution impractically in a manual setting. Therefore, laboratory automation technology can be a key to unleash the full potential of microfluidic cell culture.

Parkinson’s disease is the second most common neurodegenerative disease with more than 10 million people affected worldwide [13, 14]. Parkinson’s disease is characterised by cell death in selectively vulnerable parts of the nervous system [13]. These neuronal losses include cholinergic neurons in the pedunculopontine nucleus, noradrenergic neurons in the locus coeruleus and dopaminergic neurons from the substantia nigra pars compacta [15, 16]. Dopaminergic neurons play a critical role in brain function by releasing a neurotransmitter called dopamine [17–19]. The loss of dopaminergic neurons is the main reason behind the motor symptoms (rigidity, tremors and postural instability) of Parkinson’s disease patients [20]. The study of Parkinson’s disease at the cellular level has been facilitated by the use of *induced pluripotent stem cells* (iPSCs) technology [21, 22]. An iPSC is a technology that allows for the reprogramming of somatic cells into stem cell state that is capable of differentiation into many types of human cell [23]. Reinhardt et al. [24] developed a protocol to generate human neuroepithelial stem cells (hNESCs) from iPSC. These hNESCs can in turn be differentiated into many neuronal cell types, including midbrain-specific dopaminergic neurons, critical to the *in vitro* modelling of Parkinson’s disease pathogenesis.

Laboratory automation is becoming increasingly prevalent in the life sciences [25, 26]. Automated cell culture has the potential to increase the quantity and the quality of experiments that can be completed in parallel and enables long-term cell culture maintenance with reduced manual labour [27]. Once an automated protocol is established, a robot can be operated continuously without

fatigue and with the same consistency and accuracy [26]. Likewise, once established an automated imaging system can take repeated measurements over a long period without intervention [28]. The combination of robotic cell culture and automated imaging has a wide range of biological applications. A leading example is their use to distinguish causation from correlation in the pathogenesis of neurodegenerative diseases by longitudinal measurement of human *in vitro* disease models [29]. Laboratory automation requires precise specification of, and enables fine control over, many experimental protocol parameters, such as dispensing speed, cell culture conditions, fluid temperature and measurements. This enhances experimental reproducibility by reducing variance between replicates [30]. *In vitro* cell culture automation facilitates faithful replication of certain physiological conditions as it enables quantitative control over key experimental parameters, e.g., perfusion rate [31]. This increases the validity of employing an *in vitro* model to represent an *in vivo* system, in health or disease, thereby accelerating biomedical research.

We previously developed a microfluidic titer plate, stratified with three dimensional microfluidic cell culture chips, in a form that is fully compatible with laboratory automation [7]. Subsequently, we implemented the differentiation of hNESCs into three dimensional networks of electrophysiologically active dopaminergic neurons in these microfluidic cell culture chips [32]. A 2-lane *Organo-Plate* consists of a stratified array of 96 chips embedded in a customised 384-well plate format [7]. Each chip consists of a single microfluidic chip contained between two pieces of glass: a top plate with holes corresponding to the underside of selected wells, and a bottom plate. Each chip has 4 wells and 2 lanes: one *gel inlet well* for loading of gel-embedded cells into the culture lane, one *medium inlet well* connected to one *medium outlet well* through a medium lane where the flow of media is driven by a pressure drop between the 2 wells, and one well used as an *observation window* for monitoring the quality of cells through an inverted microscope. The culture and medium lanes are separated by a *phaseguide*, preventing the gel-embedded cells from flowing into the medium lane forcing it to stay on the culture lane. A phaseguide is a patterned pinning barrier that controls the liquid-air interface by forcing it to align with the ridge, hence guiding the fluid flow into the needed lane [6]. The microfluidic titer plate was designed for compatibility with laboratory automation, which we have previously demonstrated with the differentiation of dopaminergic neurons [33].

Microfluidic technology is well established. In addition, the use of microfluidics with controlled flow rates is widespread [34–36]. However, most of the microfluidic technologies with controlled flow conditions use active pumping [36, 37]. In other terms, an external pump is usually utilised to regulate the flow rate inside the microfluidic device. However, this is not fully compatible with standard laboratory automation which requires the use of stand-alone standard culture plate such as a microtiter plate used in the OrganoPlate. Therefore, the OrganoPlate has the potential to unleash microfluidic cell culture with controlled flow conditions in a standard laboratory automation. However, the flow in the OrganoPlate is not well understood, and its flow capabilities not fully exploited.

Herein, we combined engineering principles with cell biology to re-design the OrganoPlate into a 3D microfluidic device optimised for neuronal cell culture. First, the biological requirements for neuronal cell culture is combined with a dynamic similitude model of cerebral blood flow to elaborate on the target flow rate requirements to dynamically replicate cerebral flow in the OrganoPlate. Second, these were used to optimise the design of the OrganoPlate, that allows the flow of media constantly between media changes for the culture of midbrain like dopaminergic neurons. The re-designed OrganoPlate was manufactured, and the biological compatibility was proven with the culture of human neuroepithelial stem cells into dopaminergic neurons.

2 Materials and Methods

2.1 Flow physical modelling

The general continuum description of the flow of an incompressible, Newtonian fluid flow with variable properties and no body forces other than gravity is expressed with the following general equations:

the incompressible continuity equation,

$$\frac{\partial u_i}{\partial x_j} = 0 \tag{1}$$

the momentum equation,

$$\rho \left(\frac{\partial u_j}{\partial t} + u_i \frac{\partial u_j}{\partial x_i} \right) = \frac{\partial \tau_{ij}}{\partial x_i} + \rho b_j \quad (2)$$

where the fluid stress is given by Stokes' law of viscosity,

$$\tau_{ij} = -p\delta_{ij} + \mu \left(\frac{\partial u_i}{\partial x_j} + \frac{\partial u_j}{\partial x_i} \right) \quad (3)$$

Where u_i represents the i th component of the velocity vector in the direction of flow, p is the pressure, and ρ is the mass fluid density, μ is the dynamic viscosity and b_j is the body force per unit mass.

If a long parallel channel with the x-direction along the axis of the channel and the coordinates y and z in the plane perpendicular to the axis of the channel is considered. The entering fluid flow velocity profile undergoes a transition along the stream wise direction. This continues until the flow becomes independent of the stream wise position. The distance from the channel entry to this position is known as the entrance length. After the entrance length, the flow velocity profile is said to be fully developed, and the velocity field is unidirectional. In other terms, $u(x) = [u(y, z), 0, 0]$. In addition, there is no change in velocity magnitude along a streamline. Assuming that the entering flow is only driven by gravitational body force, pressure head, through the difference in height between the inlet reservoir and the plane formed by the channel; the fully developed incompressible fluid flow needs to be analysed. The above systems of equations become simply:

$$\rho \frac{\partial u}{\partial t} = -\frac{dp}{dx} + \rho g_x + \frac{\partial}{\partial y} \left(\mu \frac{\partial u}{\partial y} \right) + \frac{\partial}{\partial z} \left(\mu \frac{\partial u}{\partial z} \right) \quad (4)$$

If we assume that throughout any cell culture, all the physical parameters of the media remain

constant, and that there is no streamwise acceleration then equation 4 can be further simplified:

$$\frac{\partial^2 u}{\partial y^2} + \frac{\partial^2 u}{\partial z^2} = \frac{1}{\mu} \frac{d}{dx} (p - \rho g x) \quad (5)$$

If we assume that throughout the experiment all the physical parameters of the media remain constant, that there is streamwise deceleration of the fluid particle, and that the characteristic length is the hydraulic diameter of the OrganoPlate cross section; then equation 5 can be rewritten in terms of changes of momentum terms in the streamwise direction:

$$m \frac{\partial u}{\partial t} = (P_1 A - P_2 A) + (m g \sin \theta) - (\tau_w \pi D_h L) \quad (6)$$

where θ represents the difference in height between the inlet reservoir and the outlet of the medium lane, A is the cross-sectional area, and P the wetted perimeter of the cross-section.. The first term on the right hand side is the net pressure force, the second term is the streamwise component of the weight and the final term is the wall friction force. Equation 6 can be further simplified into the piezometric head and the friction head loss:

$$\frac{L}{g} \frac{du}{dt} = \frac{P_1^* - P_2^*}{\rho g} - f \frac{L}{D_h} \frac{u |u|}{2g} \quad (7)$$

where $P^* = P + \rho g z$ is the piezometric pressure.

The no-slip boundary condition can be assumed since there is no electrokinetic effects and the shear rate is less than $10^{12} s^{-1}$.

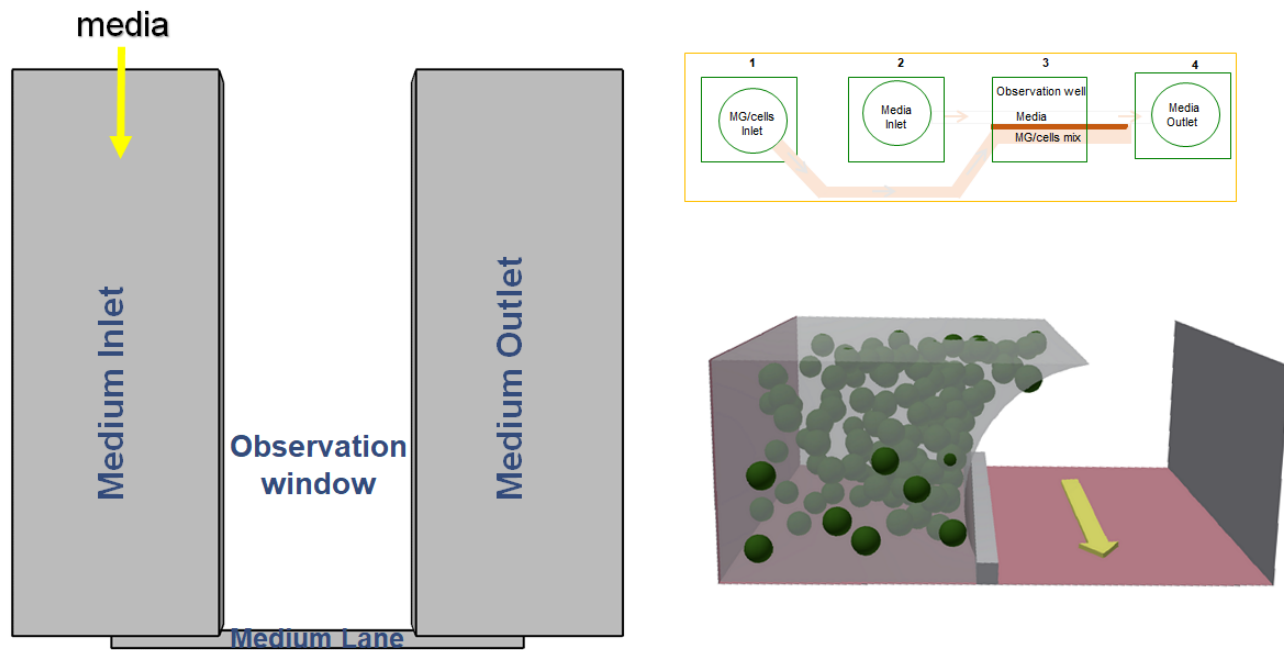


Figure 1: Schematic representation of the media section of the media lane. Scheme of a single 2-lane bioreactor composed of a gel inlet (1), a perfusion inlet (2), an optical readout window (3) and a perfusion outlet (4)

2.2 Original microfluidic geometry

2.2.1 The OrganoPlate

The geometry (#9603-200B, Mimetas BV, Leiden, The Netherlands) investigated (Figure 1) consisted of two lanes: one for the flow of the mixture of matrigel and cells called the gel lane, the other one for the flow of media called medium lane [7]. The gel lane consists of a 12.154mm long channel with an inlet, without an outlet and three elbows. The medium lane consists of a 9mm long channel with square inlet and outlet reservoirs with sides of 4.5mm . Both lanes have a width of 0.2mm and a height of 0.12mm . The two lanes are separated by a phaseguide that provides matrigel flow surface tension, and precludes an overflow of matrigel into the medium lane [38].

2.2.2 Flow physical modelling applied to the geometry of the OrganoPlate

Equations 2 to 7 are solved for a steady state flow with no-slip boundary conditions at all the boundaries except for the inlets and outlets of the lanes. The hydraulic resistance between the

inlet and outlet wells on the medium lane can be calculated with the following equation, assuming rectangular cross-section:

$$R_h = \frac{12\mu L}{wh^3 (1 - 0.630h/w)} \quad (8)$$

Where: μ is the media viscosity, L is length of the lane, w is width of the medium lane and h is height of the medium lane. Using equation 8, the difference of pressure, ΔP , and the flow rate, Q , in the medium lane can be calculated using the following equation:

$$\Delta P = R_h Q \quad (9)$$

Let n be the interval between two measurements, the following equation can be written as:

$$\Delta P (n + 1) = \Delta P (n) - 2\rho g \cdot \delta h \quad (10)$$

Where δh is the change in height between the time interval.

$$\delta h = \frac{Q \cdot \delta t}{A_w} \quad (11)$$

Where δt is the time interval between two measurements of the flow rate. Equation 10 is a geometric series, and can be re-written as:

$$Q_n = \left(\frac{R_h A_w - 2\rho g \cdot \delta t}{R_h A_w} \right)^n Q_0 \quad (12)$$

The laminar characteristic of the flow was verified by calculating the *Reynolds number*, Re . The Reynolds number is a dimensionless number used in fluid mechanics to determine the fluid

flow patterns. It compares the convective inertial effects to the shear effects on the fluid flow. On one hand, when the Reynolds number is very large, the flow is dominated by inertial effects and is characterised by more random patterns such as fluid particles rotating around their own axes or even moving in the direction opposite to the overall direction of flow. The flow is said to be turbulent. On the other hand, for smaller Reynolds number the shear effects dominate the pattern of flow, therefore, the flow moves in a straight profile. The flow is said to be laminar. The characteristic Reynolds number have been empirically determined for different geometries. The hydraulic diameter, D_h , of the micro channel was calculated, and subsequently the highest value of the Reynolds number which corresponds to the highest flow rate was computed to determine the fluid flow pattern:

$$D_h = \frac{4A}{P}$$

$$Re = \frac{\rho u D_h}{\mu} \quad (13)$$

2.3 Similarity model

In order to find the target flow rate that needs to be achieved, we used the principles developed by Edgar Buckingham and Joseph Bertrand [39] on dimensional analysis called the Buckingham π theorem. This theorem allows to find a set of dimensionless numbers that one can utilise to scale up or down a prototype and/or change the physical parameters because of the availability of certain substances or because they are easier to measure in a laboratory setting. For instance, in the aerospace industry, one can find a set of dimensionless numbers that can be kept constant to correlate experimental data from models to prototype whether the model is smaller than prototype and/or the fluid used in the experiment is different than the fluid in normal operating conditions

of the product. Similarly, dynamic similarity has been extensively used in engineering fluid flow conditions of scaled models. Dynamic similarity theorem dictates that the fluid flow dynamics of two systems are identical if and only if three conditions are met. First, the two systems are geometrically similar in terms of shape only. Second, the boundary conditions of the two systems are similar. Third, the Reynolds and *Wormsley numbers* are the same between the two systems. The Wormsley number determines the pulsatility of flow.

2.3.1 Design constraints

A set of design constraints had to be followed for the effective manufacturing of the 3D microfluidic device:

- The height of the channel must be between 10 and 500 μm , and preferably between 50 and 360 μm .
- The width of the channel must be more than 25 μm , and preferably more than 100 μm .
- The length of the channel must fit the dimension of a Society for Biomolecular Screening (SBS) 384 standard plate.
- The channel aspect ratio which is the ratio between the width and the height of the channel must be more than 1.

2.3.2 Optimisation of existing design parameters for neuronal culture

Sensitivity analysis The partial derivative of R_h using Equation 8 was obtained with respect to the viscosity of media, length, width and height of the medium lane respectively. The sign of the partial derivative of R_h with respect to each variable was studied to investigate how each variable influenced the time dependent flow of media in the medium lane.

Geometric parameters iteration

In order to optimise the geometric parameters of the OrganoPlate with respect to cerebral flow, the variables of the hydraulic resistance from Equation 8, and the loading conditions were

iterated to find the best combination of variables that would yield the flow rate closest to the target dynamic conditions. Briefly, the desired physiological systems was used as an input to find the best geometric parameters of the OrganoPlate to achieve dynamic similarity between the target cell types and the flow characteristic in the biological system. the following steps were repeated until the right dimensions were found:

Step1 Equation 13 was used to calculate the target flow rate Q_t by comparing the Reynolds number in the brain (prototype) with the Reynolds number in the medium lane (model).

Step2 Equation 8 was used to calculate the hydraulic resistance in the the medium lane.

Step3 Equation 12 was used to obtain the time dependent solution of flow in the medium lane.

Step4 The maximum and minimum deviations, Q_{max} and Q_{min} respectively, from the target flow rate were calculated as $2Q_t$ and $0.2Q_t$ respectively.

Step5 The initial and the final flow rates (after flow of 24hours, chosen for change of media convenience) were calculated.

Step6 The initial and the final flow rates, Q_0 and Q_f respectively, were compared with the maximum and minimum deviations from the target flow rate.

The calculations were started with the existing OrganoPlate design parameters. Then, the length of the medium lane, the loaded amount of media and the viscosity of the used media were increased in small increments, while in parallel decreasing by increments the width and height of the cross-section of the medium lane. These values were iterated up until the point where $[Q_0, Q_f,] \subset [Q_{max}, Q_{min},]$.

2.4 Biological validation

2.4.1 Human neuroepithelial stem cell culture

In order to validate the biological utility of the new optimised 3D microfluidic design, we used a human neuroepithelial stem cell line from a healthy donor (#hNESC K7) and a human neuroepithelial stem cell line with an inserted PINK1-I368N mutation (#40066C5V). These cells were maintained and differentiated into midbrain-specific dopaminergic neurons within the old and new design of the OrganoPlate, by using an existing macroscopic cell culture protocol [24] that we previously adapted for microfluidic cell culture in an automation setting [33]. In brief, to culture hNESC in an OrganoPlate, hNECs were harvested from wells of a 6 well plate, the harvested hNESC were then re-suspended on Matrigel (catalogue number 354277, lot number 3318549, Discovery Labware, Inc., Two Oak Park, Bedford, MA, USA). 0,2 μ L of this Matrigel-cell mix was loaded in assigned chips of the OrganoPlate at a density of 0.03 million cells/ μ L. After seeding the cells, the plate was incubated at 37 °C and 5% CO₂.

2.4.2 Dopaminergic neuronal differentiation

The culture medium preparation “N2B27 medium” consisted of mixed equal amounts of Neurobasal medium (invitrogen/life technologies) and DMEM/F12 medium (invitrogen/life technologies) supplemented with 1% penicillin/streptomycin (life technologies), 2 mM L-glutamine (life technologies), 0.5 X B27 supplement without Vitamin A (life technologies) and 0.5 X N2 supplement (life technologies). The medium to maintain the hNESC in culture “maintenance medium” consisted on N2B27 medium with 0.5 μ M PMA (Enzo life sciences), 3 μ M CHIR (Axon Medchem) and 150 μ M Ascorbic Acid (Sigma Aldrich). The differentiation medium formulation to induce the differentiation of hNECs towards midbrain dopaminergic neurons “differentiation medium with PMA” consisted in N2B27 medium with 200 μ M ascorbic acid, 0.01 ng/ μ L BDNF (Peprotech), 0.01 ng/ μ L GDNF (Peprotech), 0.001 ng/ μ L TGF β 3 (Peprotech), 2.5 μ M dbcAMP (Sigma Aldrich) and 1 μ M PMA. The function of PMA in this medium preparation was to stimulate the sonic hedghog (SHH)

pathway in the cultured hNESCs. Differentiation medium with PMA was changed, everyday during the first 6 days of culture in the differentiation process. For the maturation of differentiated neurons PMA was no longer added to the differentiation medium “differentiation medium without PMA” from day 7 onwards, this differentiation medium without PMA was changed everyday during 1 week. To monitor cellular morphology during differentiation, bright field images were acquired automatically in an epifluorescence microscopy station.

2.4.3 Immunofluorescence staining assay

Immunostaining for the dopaminergic neuronal markers class 3 beta tubulin (TUB β III) and tyrosine hydroxylase (TH), the penultimate enzyme in the biosynthesis of dopamine [24, 40, 41], was performed on representative chips at day 24 of differentiation. Differentiated cells were fixed with 4% paraformaldehyde (PFA) in 1 \times phosphate-buffered saline (PBS) for 15 min, by manually adding 70 μ L in medium well inlet and 30 μ L in medium well outlet followed by permeabilisation with 0.05% Triton-X 100 in 1 \times PBS (3 min on ice), and blocking with 10% fetal calf serum (FCS) in 1 \times PBS (1h). After washing with 1 \times PBS, the primary antibodies mouse anti-TUB β III (1:2000, Covance) and rabbit anti-TH (1:2000, Santa cruz biotechnology), were incubated for 90 min at room temperature. After washing with 1 \times PBS, the secondary antibodies Alexa Fluor 488 Goat Anti-Mouse and Alexa Fluor 568 Goat Anti-Rabbit together with a stain DNA (Hoechst 33342, Invitrogen), were incubated for 2 hours at room temperature. After washing with 1 \times PBS and water, confocal images of representative culture chambers were acquired using a confocal microscope (Zeiss LSM 710).

2.4.4 Statistical Analysis

Three representative chips (n=3) were selected to illustrate the results of this study, in which the statistical analyses were performed by determination of the mean value and the standard deviation of the proportion of dopaminergic neurons within the overall neuronal population.

3 Results and Discussion

3.1 OrganoPlate time dependant flow rate

In our previous protocol to differentiate hNESCs into DNs in the OrganoPlate, $80\mu l$ and $40\mu l$ were added into the medium inlet and outlet respectively. This is equivalent to a pressure drop between the medium inlet and medium outlet of $\sim 20Pa$. The equivalent pressure was computed and the time dependent solution was subsequently obtained using equations 10, 11 and 12.

The time interval, $\delta t = 10s$, is chosen such that the changes of pressure, P , is less than 2% between two measurements, so that 10 is still valid and can be used to calculate the flow rate of the media every 10s. The graph of which is shown in figure 2.

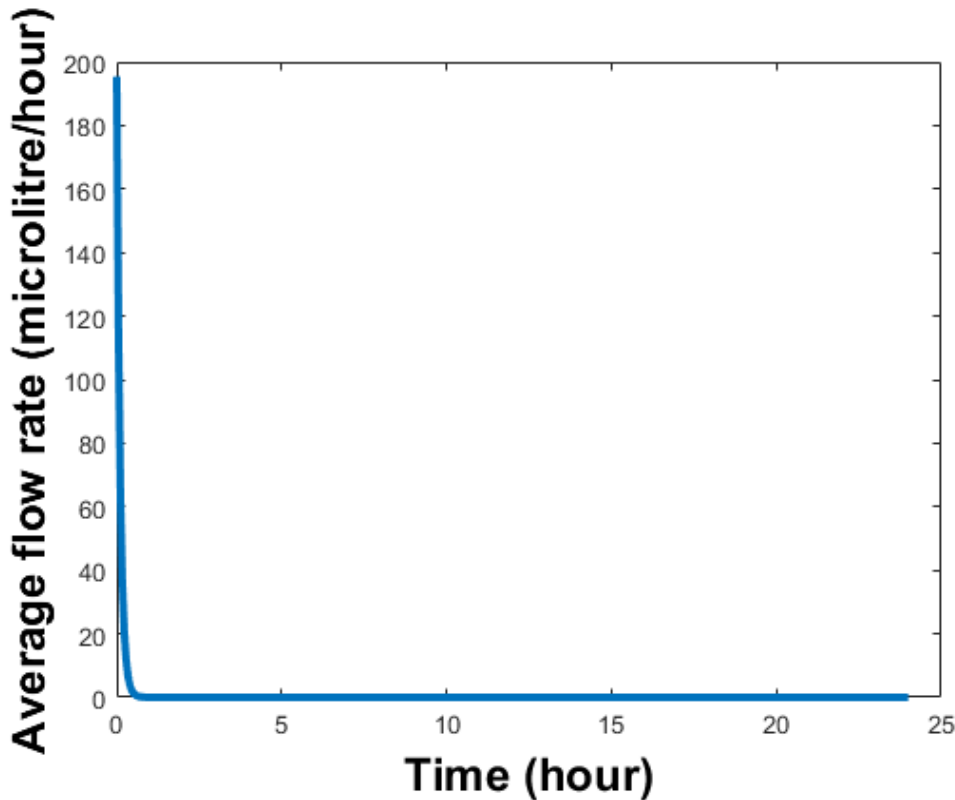


Figure 2: Flow rate in the medium lane for 24 hours

It was found that for the highest flow rate of $Q = 201\mu l/hour$, the Reynolds number was $Re = 0.5$ which was well below the threshold to transition from Laminar to turbulent flow. In fact,

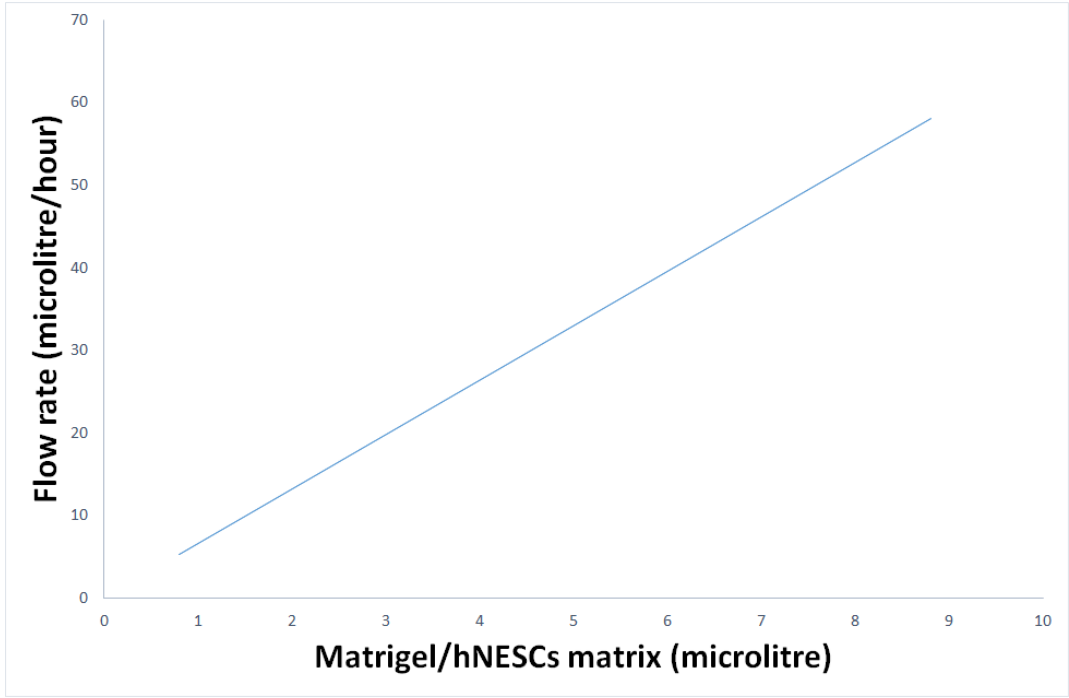


Figure 3: Targeted flow rate for dynamic similarity between the brain and the OrganoPlate

with such small Reynolds number, we are more into the creeping flow regime where viscous forces are very important and the inertial effects less so. Therefore, the inertial terms of the Navier-Stokes equation can be neglected in any computational fluid simulation analysis resulting in Stokes flow.

The average flow rate over 24h is $0.80 \mu\text{l}/\text{hour}$, which is in agreement with the earlier reported flow rate in the OrganoPlate [7].

3.2 Similarity model

Cerebral blood flow was assumed to be $750\text{ml}/\text{min}$, which is equivalent to $54\text{ml}/100\text{g}\cdot\text{min}$ [42]. Step 1 of the geometric parameters iteration was used to calculate the target flow rate that should be achieved in order to dynamically mimic the flow of brain in the geometry of the OrganoPlate. The target flow rate obtained for different amounts of matrigel/hNESCs mixture is summarised in Figure 3.

For the current design of the OrganoPlate, the target flow rate is $5.3\mu\text{l}/\text{hour}$ and the maximum and minimum deviations are $10.6\mu\text{l}/\text{hour}$ and $1.1\mu\text{l}/\text{hour}$ respectively. The target flow rate is

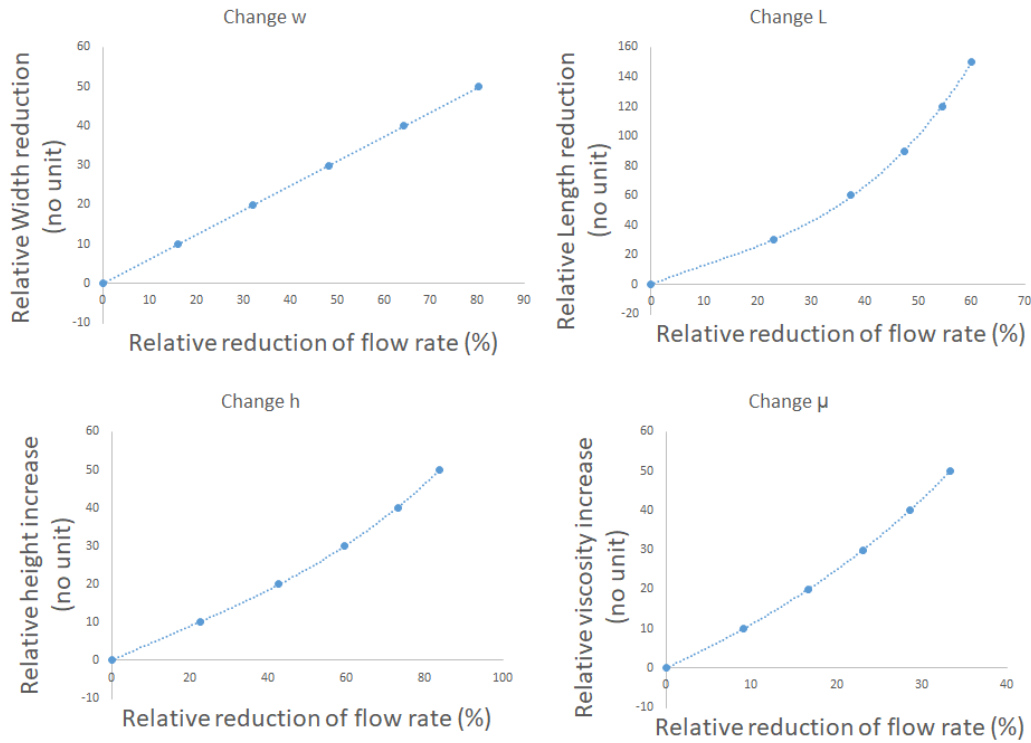


Figure 4: Sensitivity analysis of the design variable

achieved only for 13.5 minutes out of the 1440 minutes, assuming media change every 24hours. Therefore, in order to dynamically mimic cerebral flow in the OrganoPlate, it must be re-designed.

3.3 Optimisation of existing design parameters for neuronal culture

How each variable in Equation 8 influences the hydraulic resistance was investigated and the results are summarised in Figure 4.

Then, the ease of change of each variable was also investigated (Figure 5), the outcome of which allows to optimise the variables in order to yield the desire flow rate in the medium lane over a span of 24hours.

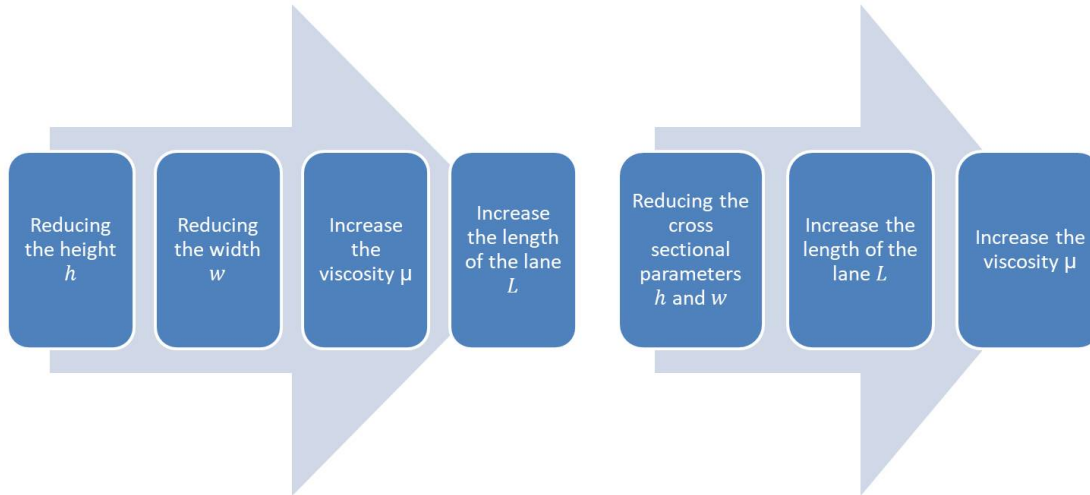


Figure 5: Ease of change ranking of parameters of hydraulic resistance

System manufacturing and Design

The optimisation analysis was applied in conjunction with the geometric parameters iteration steps to find the most optimum dimensions of the culture lane that would yield the desired flow rate over 24hours, and a final design that could be manufactured. It was found that the optimum dimensions of one bioreactors and loading conditions to satisfy the similarity model and the design constraints are:

- Target flow rate is 5.68 μ l/hour.
- Upper limit of target flow rate is 10.56 μ l/hour.
- Lower limit of target flow rate is 1.06 μ l/hour.
- Number of wells used: 6 for one bioreactor.
- Width and height of gel lane and position of gel inlet well is unchanged relative to culture lane. However, the length will increased to accommodate for longer channel.
- Medium lane width is 100 μ m
- Medium lane height is 50 μ m
- 2 consecutive wells used as medium inlet. Medium inlet becomes a rectangle of 4.5X9.0mm.

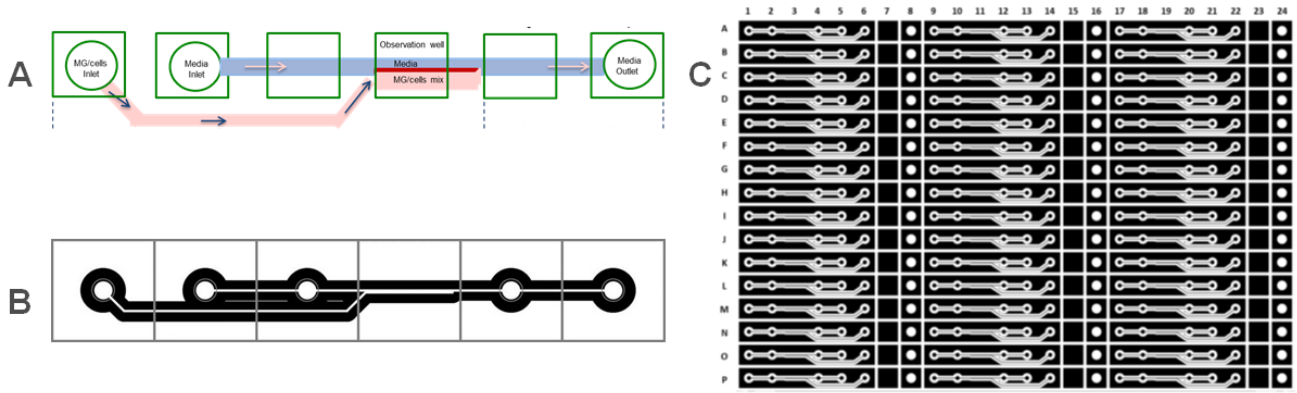


Figure 6: 3D microfluidic device optimised for neuronal cell culture. (A) Optimum design. (B) Modification for manufacturing of a bioreactor. (C) The new design applied to a 384 microtiter plate

- 2 consecutive wells used as medium outlet. Medium outlet becomes a rectangle of 4.5X9.0mm.
- Loaded media into medium outlet is 20 μ l.
- Loaded media into medium inlet is 236 μ l.

The optimum design schematic is shown in Figure 6A, however, the design was slightly modified (Figure 6B) by dis-joining the medium inlet and outlet wells into distinct ones to ease the manufacturing. The modified design was combined with a 384 microtiter plate to build a 3D microfluidic cell culture plate with 64 bioreactors. The layout of which is shown in Figure 6C.

The flow rate over 24 hours is shown in Figure 7. The laminar characteristic of the flow was verified by calculating the Reynolds number, Re . The hydraulic diameter, D_h of the micro channel was calculated, and subsequently the highest value of the Reynolds number with characteristic length D_h , which corresponds to the highest flow rate was computed. It was found that for the highest flow rate, the Reynolds number was $Re = 1$ which is well below the threshold to transition from Laminar to turbulent flow. Therefore, with such small Reynolds number, we are more into the creeping flow regime, except for the initial maximum flow rate, where viscous forces are very dominant compared with the inertial effects. Therefore, the inertial terms of the Navier-Stokes

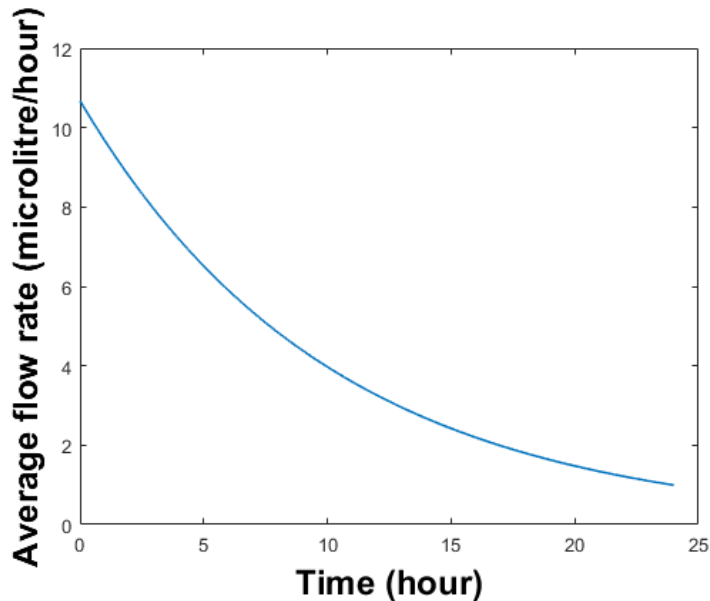


Figure 7: Flow rates inside the new microfluidic medium lane

equation can be neglected, resulting in Stokes flow. The no-slip boundary condition is still valid since there is no electrokinetic effects and the shear rate is less than $10^{12} s^{-1}$ [43].

4 Conclusions

Advanced experimental models of human cells, e.g., microfluidic culture of human pluripotent stem cell-derived neuronal cells, involves a complex interaction between a solid, inorganic microfluidic cell culture device, a gelatinous composite of living cells embedded in an extracellular matrix, and a perfusive flow of fluid cell culture medium that continuously exchanges certain biochemical species with cells, each of which contains a network of biochemical reactions. We achieved the first step into controlling over the rate of exchange of key biochemical species by dynamically optimising the medium lane within the microfluidic cell culture device. We developed a microfluidic device for culture of patient-derived neuronal cells in conditions dynamically optimised for those of the normal and diseased human brain. We biologically validated the 3D microfluidic device design by differentiating human neuroepithelial stem cells into dopaminergic neurons. We hope that this design can be used to develop new treatments for neurodegenerative diseases, with special focus on Parkinson’s disease.

Acknowledgements ELM received funding from the SysMedPD project from the European Union’s Horizon 2020 research and innovation program under grant agreement No. 668738.

Conflict of interest statement *The authors certify that they have no relevant financial interests in this manuscript and that any/all financial and material support for this research and work are clearly identified in the Acknowledgements section of this manuscript.*

References

- [1] Gómez-Sjöberg R, Leyrat AA, Pirone DM, Chen CS, Quake SR. Versatile, Fully Automated, Microfluidic Cell Culture System. *Analytical Chemistry*. 2007 Nov;79(22):8557–8563. 00446. Available from: <http://pubs.acs.org/doi/abs/10.1021/ac071311w>.
- [2] Lecault V, Vaninsberghe M, Sekulovic S, Knapp D, Wohrer S, Bowden W, et al. High-throughput analysis of single hematopoietic stem cell proliferation in microfluidic cell culture arrays. *Nat Methods*. 2011 Jul;8(7):581–586. 00174. Available from: <http://www.hubmed.org/display.cgi?uids=21602799>.
- [3] Croushore C, Supharoek S, Lee C, Jakmunee J, Sweedler J. Microfluidic device for the selective chemical stimulation of neurons and characterization of peptide release with mass spectrometry. *Anal Chem*. 2012 Nov;84(21):9446–9452. Available from: <http://www.hubmed.org/display.cgi?uids=23004687>.
- [4] Shintu L, Baudoin R, Navratil V, Prot J, Pontoizeau C, Defernez M, et al. Metabolomics-on-a-chip and predictive systems toxicology in microfluidic bioartificial organs. *Anal Chem*. 2012 Feb;84(4):1840–1848. 00053. Available from: <http://www.hubmed.org/display.cgi?uids=22242722>.

- [5] Oedit A, Vulto P, Ramautar R, Lindenburg PW, Hankemeier T. Lab-on-a-Chip hyphenation with mass spectrometry: strategies for bioanalytical applications. *Current Opinion in Biotechnology*. 2015 Feb;31:79–85. 00000. Available from: <http://www.sciencedirect.com/science/article/pii/S0958166914001517>.
- [6] Vulto P, Podszun S, Meyer P, Hermann C, Manz A, Urban GA. Phaseguides: a paradigm shift in microfluidic priming and emptying. *Lab Chip*. 2011 May;11(9):1596–1602. 00031. Available from: <http://pubs.rsc.org/en/content/articlelanding/2011/lc/c01c00643b>.
- [7] Trietsch SJ, Israëls GD, Joore J, Hankemeier T, Vulto P. Microfluidic titer plate for stratified 3D cell culture. *Lab on a Chip*. 2013;13(18):3548. Available from: <http://xlink.rsc.org/?DOI=c31c50210d>.
- [8] van Duinen V, Trietsch SJ, Joore J, Vulto P, Hankemeier T. Microfluidic 3D cell culture: from tools to tissue models. *Current Opinion in Biotechnology*. 2015 Dec;35:118–126. Available from: <http://www.sciencedirect.com/science/article/pii/S0958166915000713>.
- [9] Grossmann G, Guo W, Ehrhardt D, Frommer W, Sit R, Quake S, et al. The RootChip: an integrated microfluidic chip for plant science. *Plant Cell*. 2011 Dec;23(12):4234–4240. Available from: <http://www.hubmed.org/display.cgi?uids=22186371>.
- [10] Antia M, Herricks T, Rathod P. Microfluidic modeling of cell-cell interactions in malaria pathogenesis. *PLoS Pathog*. 2007 Jul;3(7):0939–0948. 00064. Available from: <http://www.hubmed.org/display.cgi?uids=17658948>.
- [11] Ho SY, Chao CY, Huang HL, Chiu TW, Charoenkwan P, Hwang E. NeurphologyJ: An automatic neuronal morphology quantification method and its application in pharmacological discovery. *BMC Bioinformatics*. 2011 Jun;12:230. Available from: <http://www.ncbi.nlm.nih.gov/pmc/articles/PMC3121649/>.
- [12] Vedel S, Tay S, Johnston DM, Bruus H, Quake SR. Migration of cells in a social context. *Proceedings of the National Academy of Sciences*. 2013 Jan;110(1):129–134. Available from: <http://www.pnas.org/cgi/doi/10.1073/pnas.1204291110>.

- [13] Lees AJ, Hardy J, Revesz T. Parkinson's disease. *The Lancet*. 2009 Jun;373(9680):2055–2066. Available from: <http://www.sciencedirect.com/science/article/pii/S014067360960492X>.
- [14] Abdullah R, Basak I, Patil KS, Alves G, Larsen JP, Møller SG. Parkinson's disease and age: The obvious but largely unexplored link. *Experimental Gerontology*. 2015 Aug;68:33–38. Available from: <http://www.sciencedirect.com/science/article/pii/S053155651400271X>.
- [15] Surmeier DJ, Schumacker PT. Calcium, Bioenergetics, and Neuronal Vulnerability in Parkinson's Disease. *J Biol Chem*. 2013 Apr;288(15):10736–10741. Available from: <http://www.jbc.org/content/288/15/10736>.
- [16] Bellucci A, Mercuri NB, Venneri A, Faustini G, Longhena F, Pizzi M, et al. Review: Parkinson's disease: from synaptic loss to connectome dysfunction. *Neuropathol Appl Neurobiol*. 2016 Feb;42(1):77–94. Available from: <http://onlinelibrary.wiley.com/doi/10.1111/nan.12297/abstract>.
- [17] Chinta SJ, Andersen JK. Dopaminergic neurons. *The International Journal of Biochemistry & Cell Biology*. 2005 May;37(5):942–946. 00102. Available from: <http://www.sciencedirect.com/science/article/pii/S1357272504003711>.
- [18] Schöndorf DC, Aureli M, McAllister FE, Hindley CJ, Mayer F, Schmid B, et al. iPSC-derived neurons from GBA1-associated Parkinson's disease patients show autophagic defects and impaired calcium homeostasis. *Nat Commun*. 2014 Jun;5. 00002. Available from: <http://www.nature.com/ncomms/2014/140606/ncomms5028/full/ncomms5028.html>.
- [19] Muñoz P, Huenchuguala S, Paris I, Segura-Aguilar J. Dopamine Oxidation and Autophagy. *Parkinsons Dis*. 2012;2012. 00000. Available from: <http://www.ncbi.nlm.nih.gov/pmc/articles/PMC3433151/>.

- [20] Pfeiffer RF, Wszolek ZK, Ebadi M. Parkinson's Disease, Second Edition. CRC Press; 2012. Available from: <https://www.crcpress.com/Parkinsons-Disease-Second-Edition/Pfeiffer-Wszolek-Ebadi/p/book/9781439807149>.
- [21] Hillje AL, Schwamborn JC. Utilization of stem cells to model Parkinson's disease – current state and future challenges. *Future Neurology*. 2016 Apr;11(2):171–186. Available from: <http://www.futuremedicine.com/doi/abs/10.2217/fnl.16.7>.
- [22] Bahnassawy L, Nicklas S, Palm T, Menzl I, Birzele F, Gillardon F, et al. The Parkinson's Disease-Associated LRRK2 Mutation R1441G Inhibits Neuronal Differentiation of Neural Stem Cells. *Stem Cells and Development*. 2013 Apr;22(18):2487–2496. 00002. Available from: <http://online.liebertpub.com/doi/abs/10.1089/scd.2013.0163>.
- [23] Han DW, Tapia N, Hermann A, Hemmer K, Höing S, Araúzo-Bravo MJ, et al. Direct Reprogramming of Fibroblasts into Neural Stem Cells by Defined Factors. *Cell Stem Cell*. 2012 Apr;10(4):465–472. 00226. Available from: <http://www.sciencedirect.com/science/article/pii/S1934590912001142>.
- [24] Reinhardt P, Glatza M, Hemmer K, Tsytsyura Y, Thiel CS, Höing S, et al. Derivation and Expansion Using Only Small Molecules of Human Neural Progenitors for Neurodegenerative Disease Modeling. *PLoS ONE*. 2013 Mar;8(3):e59252. 00023. Available from: <http://dx.plos.org/10.1371/journal.pone.0059252>.
- [25] Dunn DA, Feygin I. Challenges and solutions to ultra-high-throughput screening assay miniaturization: submicroliter fluid handling. *Drug Discovery Today*. 2000 Dec;5(12, Supplement 1):84–91. Available from: <http://www.sciencedirect.com/science/article/pii/S1359644600000647>.
- [26] Kong F, Yuan L, Zheng YF, Chen W. Automatic Liquid Handling for Life Science: A Critical Review of the Current State of the Art. *J Lab Autom*. 2012 Jun;17(3):169–185. Available from: <http://dx.doi.org/10.1177/2211068211435302>.

- [27] Dauwalder O, Landrieve L, Laurent F, de Montclos M, Vandenesch F, Lina G. Does bacteriology laboratory automation reduce time to results and increase quality management? *Clinical Microbiology and Infection*. 2016 Mar;22(3):236–243. Available from: <http://www.sciencedirect.com/science/article/pii/S1198743X15009787>.
- [28] Arrasate M, Finkbeiner S. Automated microscope system for determining factors that predict neuronal fate. *Proc Natl Acad Sci U S A*. 2005 Mar;102(10):3840–3845. Available from: <http://www.ncbi.nlm.nih.gov/pmc/articles/PMC553329/>.
- [29] Skibinski G, Finkbeiner S. Longitudinal measures of proteostasis in live neurons: Features that determine fate in models of neurodegenerative disease. *FEBS Letters*. 2013 Apr;587(8):1139–1146. Available from: <http://onlinelibrary.wiley.com/doi/10.1016/j.febslet.2013.02.043/abstract>.
- [30] Triaud F, Clenet DH, Cariou Y, Le Neel T, Morin D, Truchaud A. Evaluation of Automated Cell Culture Incubators. *JALA: Journal of the Association for Laboratory Automation*. 2003 Dec;8(6):82–86. Available from: <http://journals.sagepub.com/doi/abs/10.1016/s1535-5535%2803%2900018-2>.
- [31] Halldorsson S, Lucumi E, Gómez-Sjöberg R, Fleming RMT. Advantages and challenges of microfluidic cell culture in polydimethylsiloxane devices. *Biosensors and Bioelectronics*. 2015 Jan;63:218–231. 00126. Available from: <http://www.sciencedirect.com/science/article/pii/S0956566314005302>.
- [32] Lucumi Moreno E, Hachi S, Hemmer K, Trietsch SJ, Baumuratov AS, Hankemeier T, et al. Differentiation of neuroepithelial stem cells into functional dopaminergic neurons in 3D microfluidic cell culture. *Lab Chip*. 2015 May;15(11):2419–2428. Available from: <http://pubs.rsc.org/en/content/articlelanding/2015/lc/c5lc00180c>.
- [33] Kane KIW, Moreno EL, Hachi S, Walter M, Jarazo J, Oliveira MAP, et al. Automated microfluidic cell culture of stem cell derived dopaminergic neurons. *Scientific Reports*. 2019 Dec;9(1). Available from: <http://www.nature.com/articles/s41598-018-34828-3>.

- [34] Uguz I, Proctor CM, Curto VF, Pappa AM, Donahue MJ, Ferro M, et al. A Microfluidic Ion Pump for In Vivo Drug Delivery. *Advanced Materials*. 2017 Jul;29(27):1701217. Available from: <http://doi.wiley.com/10.1002/adma.201701217>.
- [35] Clime L, Brassard D, Geissler M, Veres T. Active pneumatic control of centrifugal microfluidic flows for lab-on-a-chip applications. *Lab on a Chip*. 2015;15(11):2400–2411. Available from: <http://xlink.rsc.org/?DOI=C4LC01490A>.
- [36] Shemesh J, Jalilian I, Shi A, Heng Yeoh G, Knothe Tate ML, Ebrahimi Warkiani M. Flow-induced stress on adherent cells in microfluidic devices. *Lab on a Chip*. 2015;15(21):4114–4127. Available from: <http://xlink.rsc.org/?DOI=C5LC00633C>.
- [37] Boyd-Moss M, Baratchi S, Di Venere M, Khoshmanesh K. Self-contained microfluidic systems: a review. *Lab on a Chip*. 2016;16(17):3177–3192. Available from: <http://xlink.rsc.org/?DOI=C6LC00712K>.
- [38] Yildirim E, Trietsch SJ, Joore J, Berg Avd, Hankemeier T, Vulto P. Phaseguides as tunable passive microvalves for liquid routing in complex microfluidic networks. *Lab Chip*. 2014 Jul;14(17):3334–3340. 00000. Available from: <http://pubs.rsc.org/en/content/articlelanding/2014/lc/c4lc00261j>.
- [39] Heller V. Scale effects in physical hydraulic engineering models. *Journal of Hydraulic Research*. 2011 Jun;49(3):293–306. Available from: <https://www.tandfonline.com/doi/full/10.1080/00221686.2011.578914>.
- [40] Daadi MM, Grueter BA, Malenka RC, Jr DER, Steinberg GK. Dopaminergic Neurons from Midbrain-Specified Human Embryonic Stem Cell-Derived Neural Stem Cells Engrafted in a Monkey Model of Parkinson’s Disease. *PLOS ONE*. 2012 Jul;7(7):e41120. Available from: <http://journals.plos.org/plosone/article?id=10.1371/journal.pone.0041120>.
- [41] Yan Y, Yang D, Zarnowska ED, Du Z, Werbel B, Valliere C, et al. Directed Differentiation of Dopaminergic Neuronal Subtypes from Human Embryonic Stem Cells. *Stem Cells*. 2005

Jun;23(6):781–790. 00390. Available from: <http://doi.wiley.com/10.1634/stemcells.2004-0365>.

[42] Roher A, Debbins, Malek-Ahmadi M, Pipe, Maze, Belden, et al. Cerebral blood flow in Alzheimer’s disease. *Vascular Health and Risk Management*. 2012 Oct;p. 599. Available from: <http://www.dovepress.com/cerebral-blood-flow-in-alzheimer-s-disease-peer-reviewed-article-VHRM>.

[43] Munson BR, Okiishi TH, Huebsch WW, Rothmayer AP. *Fundamentals of Fluids Mechanics*, 7th Edition; 1990. 00000. Available from: https://www.academia.edu/8267810/Fundamentals_of_Fluids_Mechanics_7th_Edition.

4. Automated microfluidic cell culture of stem cell derived

Title	Automated microfluidic cell culture of stem cell derived
Author(s) & Affiliation(s)	<p>Khalid I.W. Kane¹, Edinson Lucumi Moreno¹, Siham Hachi¹, Moriz Walter², Javier Jarazo¹, Thomas Hankemeier³, Paul Vulto⁴, Jens C. Schwamborn¹, Martin Thoma², Ronan M.T. Fleming¹.</p> <p>¹Luxembourg Centre for Systems Biomedicine, University of Luxembourg, 7 avenue des Hauts-Fourneaux, L-4362 Esch-sur-Alzette, Grand-Duchy of Luxembourg.</p> <p>²Fraunhofer Institute for Manufacturing Engineering and Automation IPA, Stuttgart, Germany.</p> <p>³Analytical BioSciences Division, Leiden Academic Centre for Drug Research, Leiden University, Einsteinweg 55, 2333CC Leiden, The Netherlands. ⁴Mimetas B.V, PO Box 11002, 2301EA Leiden, The Netherlands.</p>
Publication Outlet	Scientific Reports
Publication Type	Peer Reviewed Journal
Publication Year	2019
Publication Status	Published
Preface	<p>In this paper, we establish an automated platform optimised mainly for the differentiation and long-term monitoring of stem cell, Parkinson's disease patient derived dopaminergic neurons. Parkinson's disease is a slowly progressive neurodegenerative disease characterised by dysfunction and death of selectively vulnerable midbrain dopaminergic neurons and the</p>

	<p>development of human in vitro cellular models of the disease is a major challenge in Parkinson's disease research. We constructed an automated cell culture platform optimised for long-term maintenance and monitoring of different cells in three-dimensional microfluidic cell culture devices. The system can be flexibly adapted to various experimental protocols and features time-lapse imaging microscopy for quality control and electrophysiology monitoring to assess cellular activity. Using this system, we continuously monitored the differentiation of Parkinson's disease patient derived human neuroepithelial stem cells into midbrain specific dopaminergic neurons. Calcium imaging confirmed the electrophysiological activity of differentiated neurons and immunostaining confirmed the efficiency of the differentiation protocol. This system is the first example of an automated Organ-on-a-Chip culture and has the potential to enable a versatile array of in vitro experiments for patient-specific disease modelling. Martin Thoma, Moris Walter and I designed and built the automated platform. Ronan Fleming, Edinson Lucumi Moreno and I proposed and designed the experiments. With the help of Ronan Fleming and Edinson Lucumi Moreno, I mainly wrote the manuscript. Edinson Lucumi Moreno and I run the experiments. Siham Hachi, Edinson Lucumi Moreno and I generated the calcium data.</p>
Citation	<p>Kane KIW, Moreno EL, Hachi S, Walter M, Jarazo J, Oliveira MAP, et al. Automated microfluidic cell culture of stem cell derived dopaminergic neurons. Scientific Reports [Internet]. 2019 Dec [cited 2019 Feb 12];9(1). Available from: http://www.nature.com/articles/s41598-018-34828-3</p>

SCIENTIFIC REPORTS



OPEN

Automated microfluidic cell culture of stem cell derived dopaminergic neurons

Khalid I. W. Kane¹, Edinson Lucumi Moreno^{1,3}, Siham Hachi¹, Moriz Walter², Javier Jarazo¹, Miguel A. P. Oliveira¹, Thomas Hankemeier³, Paul Vulto⁴, Jens C. Schwamborn¹, Martin Thoma² & Ronan M. T. Fleming^{1,3}

Parkinson's disease is a slowly progressive neurodegenerative disease characterised by dysfunction and death of selectively vulnerable midbrain dopaminergic neurons and the development of human *in vitro* cellular models of the disease is a major challenge in Parkinson's disease research. We constructed an automated cell culture platform optimised for long-term maintenance and monitoring of different cells in three dimensional microfluidic cell culture devices. The system can be flexibly adapted to various experimental protocols and features time-lapse imaging microscopy for quality control and electrophysiology monitoring to assess cellular activity. Using this system, we continuously monitored the differentiation of Parkinson's disease patient derived human neuroepithelial stem cells into midbrain specific dopaminergic neurons. Calcium imaging confirmed the electrophysiological activity of differentiated neurons and immunostaining confirmed the efficiency of the differentiation protocol. This system is the first example of an automated Organ-on-a-Chip culture and has the potential to enable a versatile array of *in vitro* experiments for patient-specific disease modelling.

Laboratory automation is becoming increasingly prevalent in the life sciences^{1,2}. Automated cell culture has the potential to increase the quantity and the quality of experiments that can be completed in parallel and enables long-term cell culture maintenance with reduced manual labour³. Once an automated protocol is established, a robot can operate continuously without fatigue and with the same consistency and accuracy². Likewise, once established an automated imaging system can take repeated measurements over a long period without intervention⁴. The combination of robotic cell culture and automated imaging has a wide range of biological applications. A leading example is their use to distinguish causation from correlation in the pathogenesis of neurodegenerative diseases by longitudinal measurement of human *in vitro* disease models⁵. Laboratory automation requires precise specification of, and enables fine control over, many experimental protocol parameters, such as dispensing speed, cell culture conditions, fluid temperature and measurements. This enhances experimental reproducibility by reducing variance between replicates⁶. *In vitro* cell culture automation facilitates faithful replication of certain *in vivo* physiological conditions as it enables quantitative control over key experimental parameters, e.g., perfusion rate⁷. This increases the validity of employing an *in vitro* model to represent an *in vivo* system, in health or disease, thereby accelerating biomedical research.

During manual cell culture, procedures involving liquid handling, such as dispensing media, aspirating media, and movement of liquid samples between containers, are essential to all protocols. Therefore, when a cell culture protocol is automated, a liquid-handler and a robot for transposition of receptacles, are two of the most important devices. There are two types of technologies used in liquid-handler: *contact* and *non-contact dispensing*². On one hand, to dispense a precise volume, contact dispensing requires the head of the tip holding the fluid to touch the bottom of the substrate; for instance, the bottom of a well or to touch the liquid surface. On the other hand, non-contact dispensing does not require any contact between the tip and the substrate or liquid surface for liquid release. Dispensing can require the handling of very small volumes, as low as a few nano-litres, so the

¹Luxembourg Centre for Systems Biomedicine, University of Luxembourg, 7 avenue des Hauts-Fourneaux, L-4362, Esch-sur-Alzette, Luxembourg. ²Fraunhofer Institute for Manufacturing Engineering and Automation IPA, Stuttgart, Germany. ³Division of Systems Biomedicine and Pharmacology, Leiden Academic Centre for Drug Research, Leiden University, Einsteinweg 55, 2333CC, Leiden, The Netherlands. ⁴Mimetas B.V, PO Box 11002, 2301EA, Leiden, The Netherlands. Khalid I. W. Kane and Edinson Lucumi Moreno contributed equally. Correspondence and requests for materials should be addressed to R.M.T.F. (email: ronan.mt.fleming@gmail.com)

technological advances in liquid handlers have focused more on dispensing than on aspiration². Low volume dispensing and aspiration are especially required for microfluidic cell culture⁷. The robot to move receptacles can be a robotic arm or a gantry robot with a gripper for receptacles². A gantry robot only moves in Cartesian coordinates, where the three principal axes of control have linear actuators.

The choice of devices used in laboratory automation should be based on their intended uses, flexibility, purchase costs and maintenance costs. Selecting the components of an automated plant usually entails having to purchase devices from different manufacturers, as no single firm supplies all of the devices that might be required to automate a laboratory protocol. Therefore, all of the components must be amenable to software integration in order to be able to function as a single autonomous plant. *Computer scripting* achieves integration by assigning a master software that communicates directly with all devices⁸. In this approach, assuming that all the devices are able to send and receive commands, a communication protocol must be implemented that is compatible with each individual device. However, this approach requires the master device software to recognise every other device using an idiosyncratic communication protocol. This approach can be very expensive and challenging to implement. Alternatively, *Standardisation in Laboratory Automation* (SiLA, <http://www.sila-standard.org/>) is a consistent and efficiently extensible approach for integration of laboratory automation devices, based on a standard protocol specification for exchanging structured information in a client-server model of communication. Furthermore, SiLA defines over 30 standard device classes used in the field of life sciences, including incubators, microscopes, de-lidders and liquid handlers⁹. For each device class, a list of required and optional functions are proposed to standardise the software communication within a laboratory automation plant. This approach standardises the communication between all of the devices of a plant, regardless of the manufacturer, and a SiLA compatible process management software can then be used to control each SiLA compatible device, without any modification.

Parkinson's disease is characterised by cell death in selectively vulnerable parts of the nervous system^{10,11}. These neuronal losses include cholinergic neurons, noradrenergic neurons and dopaminergic neurons which play a critical role in brain function by releasing a neurotransmitter called dopamine^{12–16}. The loss of dopaminergic neurons is the main reason behind the motor symptoms of Parkinson's disease patients¹⁷. The study of Parkinson's disease at the cellular level has been facilitated by the use of *induced pluripotent stem cells* (iPSCs) technology¹⁸. iPSCs are embryonic-like stem cells that have been derived from somatic cells, skin fibroblast, via reprogramming¹⁹. Reinhardt *et al.*²⁰ developed a protocol to generate human neuroepithelial stem cells (hNESCs) from iPSCs. These hNESCs can in turn be differentiated into many neuronal cell types, including midbrain-specific dopaminergic neurons, critical to the *in vitro* modelling of Parkinson's disease pathogenesis.

Microfluidic cell culture concerns the design and implementation of devices and protocols for the culture, maintenance and perturbation of cells in micro-scale fluid volumes. The reasons behind the popularity of microfluidic cell culture are both economic and scientific. Cell culture reagents are expensive, and the amounts used in microfluidic cell cultures are much less than in macroscopic cell culture^{21,22}. Microfluidic cell culture also has the potential to lower the ratio of extracellular to intracellular fluid volumes, thereby decreasing the temporal lag in extracellular response to molecules transported across cell membranes, e.g., in exometabolomic analyses^{23–25}. With the advent of Organ-on-a-Chip technology²⁶, microfluidic cell culture has developed tremendously and includes examples of perfusion culture, co-culture and three dimensional cell cultures^{27–29}. Moreover, miniaturisation enables multiple experimental replicates within a geometrically confined experimental footprint. Thus far, no examples are known of an Organ-on-a-Chip operation in an automated setting, although few hold the promise to do so³⁰. Even though the combination of automation, microfluidics and cell culture technologies allows the screening of multiple environmental conditions in parallel^{31,32}, as well as enabling regular live cell culture monitoring^{33,34} at a temporal resolution impractically in a manual setting. Therefore, laboratory automation technology is key to unleash the full potential of microfluidic cell culture. We previously developed a microfluidic titer plate for three dimensional microfluidic cell culture, called an OrganoPlate²⁸. Subsequently, we implemented the differentiation of hNESCs into three dimensional networks of electrophysiologically active dopaminergic neurons into the OrganoPlate³⁵. The microfluidic titer plate was designed for compatibility with laboratory automation, but this has yet to be exploited. The manual culture of human pluripotent stem cell derived cells within the microfluidic titer plate has also been established, but the potential for automation has also not yet been exploited.

Herein, we report the integration of developmental biology, microfluidic cell culture and laboratory automation technology to generate a flexible automated, enclosed microfluidic and macroscopic cell culture observatory, termed the *Pelican*. We elaborate on each device in the Pelican, as well as the SiLA software integration approach used to realise an automated system. We illustrate the functionality of the Pelican for automated cell culture and differentiation of human neuroepithelial stem cells into dopaminergic neurons, within a three-dimensional microfluidic device²⁸. We monitored the health of the cells throughout the experiment with an automated image acquisition pipeline. After 24 days in culture, we assessed the outcome by characterising known features of dopaminergic neurons by calcium imaging and immunofluorescence assays. Three dimensional imaging revealed mature and interconnected neuronal populations within microfluidic cell culture chips. The Pelican is a modular automation system, compatible with implementation of a variety of automation platforms, where cost-effective flexibility is maximised to allow for replacement or further expansion of platforms by integration of new devices. Microfluidic cell culture has already been manually integrated with iPSC technology³⁵. Our work integrates an automated system with an Organ-on-a-Chip stem cell culture.

Results

System Construction and Design. Figure 1 illustrates the automated cell culture enclosure (see Supplementary Figs S1 and S2), constructed and assembled according to the hardware design and the plant control architecture. The different devices and their use in the automated system are detailed in the Supplementary Experimental Procedures.

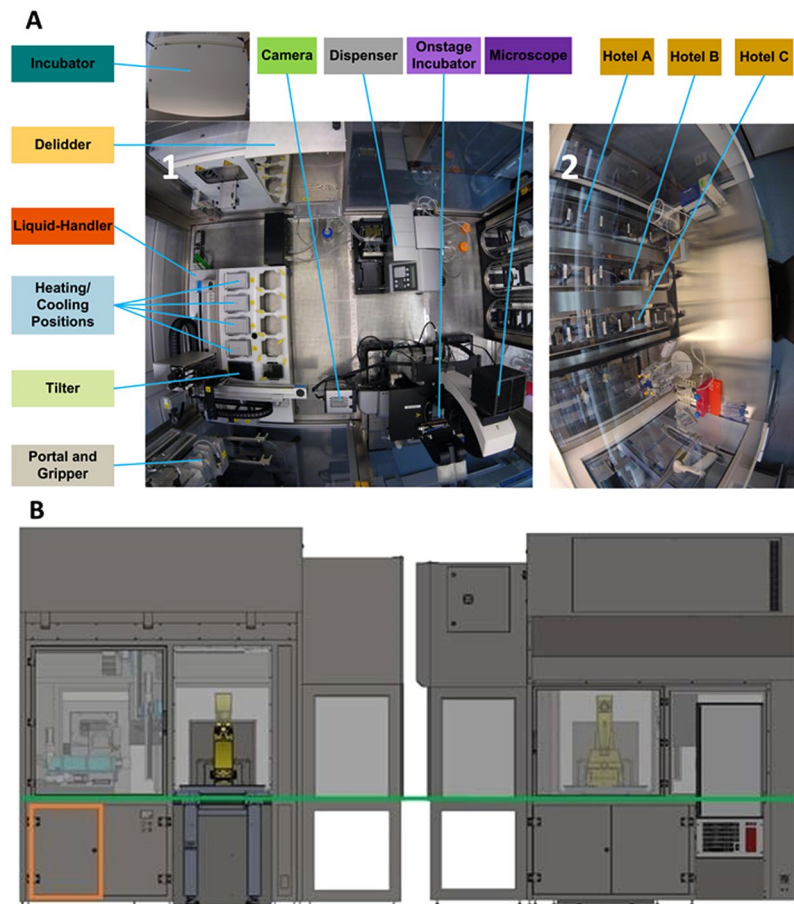


Figure 1. Pelican automated cell culture observatory. **(A)** Top view inside the Pelican automation workstation without housing: (1) Wide angle lens image of the automated enclosure. (2) Wide angle lens image of the adjacent manual cell culture bench. **(B)** Outside view of automated culture system (top). Front (bottom left) and rear (bottom right) views of Pelican with housing. Yellow (imaging station), light blue (liquid handling station), green (level of stainless steel work surface) and orange (waste containers). The colour codes of the devices labels in **(A)** and Fig. S1 match.

Hardware selection. In brief, in the Pelican, a four-axis (X - Y - Z - θ) gantry robot is used in combination with a gripper, that allows many types of substrates to be handled and services all devices with substrate from above. The robot was attached to the top of the stainless steel frame support inside the housing through rails that allow the movement of the robotic arm along three axes. This maximised the modular capacity of the Pelican because the rails determine the robotically *useful space* of the system, in contrast to other automated systems with a fixed rotating robot arm, which often has limited reach. The useful space is the space that is available to potentially hold new devices, adding to the functions of the automated platform.

In the Pelican, a ZEUS pipetting module (Hamilton Inc.) with disposable tips combines the precision of contact dispensing with the versatility of non-contact dispensing. In addition, a liquid dispenser with only non-contact dispensing was also implemented in the system. The liquid dispenser is less precise than the liquid-handler. However, it is much faster as it can handle up to 96 wells per step compared to 4 wells per step for the pipetting modules. Despite its shortcomings, the contact dispensing function of the ZEUS is especially useful for microfluidic cell culture where very small volumes must be dispensed. In addition, the contact dispensing helps to make sure that the dispensed media is bubble free. This is very important as with low flow rate non-contact dispensing, bubbles that arise can impeded the flow of fresh media, which could ultimately starve the cells in a chip. Contact dispensing is very precise for dispensing small volumes. However, this precision is dependent on dispensing at an exact location, which is not always possible as the dispensing tip cannot always physically access the well to make contact with the liquid¹.

With contact dispensing, well cross-contamination is a risk as there is direct contact between the tip and the liquid in the destination well. Therefore, a cleaning protocol was implemented after each dispensing step. This does not promote speed and high-throughput capabilities so sought after in laboratory automation, however, the contact dispensing was only utilised for the initial loading of media to avoid the introduction of bubbles in the dry medium lane. Non-contact dispensing does not require any contact between the dispensing tip and the liquid. This helps to avoid cross-contamination, and promotes the integrity of the well. Non-contact dispensing is very popular in laboratory automation because it is versatile, and it is easy to dispense to any area of a well regardless of

geometry such as undercuts, so long as there is an opening on the well³⁶. As a result, the non-contact dispensing methodology was utilised for all subsequent media changes.

Software integration. Each of the devices of the Pelican are physically connected via Ethernet to a computer (Precision T7600, Dell Sa, Mamer, Luxembourg), according to the plant architecture illustrated in Fig S1. The SiLA standard was consistently implemented for networking and integrating the devices and components. A driver development kit (DDK, Fraunhofer IPA, <http://www.sila-standard.org/driver-information-platform/fraunhofer-ipa/sila-driverdevelopment-kit/>) enabled the development of SiLA compliant drivers for each of the devices, if it was not available from the manufacturer. Incorporating a driver and converting the commands occurred in Laboratory Automation Control Suite (LACS, Fraunhofer IPA).

In brief, LACS is a programming environment for laboratory automation. It incorporates three software packages: LacsDriverCore, LACS graphical user interface (GUI) and LACS Config Editor. LacsDriverCore reads the SiLA drivers of the devices generated by the DDK, hence, it connects the devices to a computer. The LACS GUI is the process management software, the interface between a device and an operator (via the computer) through a loaded SiLA driver. The running of all existing protocols through LACS GUI merely requires the identification of the required protocol and the input of the required plate name by the operator. LACS Config Editor is used to draft automated protocols. LACS does not make any process-specific decisions, nor does it analyse any data. In the occurrence of an unexpected event (a device failure or any other error), the operator is always prompted to assess and rectify the error or the event.

The safety features around the housing, the hotels and the incubator of the Pelican (sensors to read the states of the components), and the operations of the de-lidder and the stage incubator were all controlled through a digital and analogue logic module (UR20-FBC-MOD 1334930000, Weidmuller GmbH & Co. KG, Germany). A digital and analogue logic device has a binary set; a binary input and binary output. It is usually used for a maintenance device or to control a device with a simple binary command such as for a valve ON/OFF and a light switch. A single weidmuller SiLA driver was installed to control all devices connected to one logic module.

Software (Labware Manager, Fraunhofer IPA) handles all positions inside the Pelican plant and all substrates. In the first case it holds the information, which position is occupied and with which substrate and which free position could potentially hold which type of substrate. The software knows each position and status as well as each substrate in the plant including position and type. All data are stored in an open source PostgreSQL database (PostgreSQL, <https://www.postgresql.org/>). Like the hardware devices, this virtual device has a SiLA communication interface and a Windows 7 graphical user interface to view the stored data.

The integration of new devices requires two or three steps depending on the complexity of the device and the availability of compatible drivers. The first step requires the generation of a driver for the new devices. If a SiLA driver is already available through the device manufacturer, open source, or if a commercial software that can be referenced in Microsoft Visual basic is available, then one can directly use the existing driver and move to the second step. Otherwise, one has to use the Driver Development Kit to generate a SiLA compatible driver. The DDK already possesses the framework to easily write the driver for most laboratory devices such as a camera, a microscope or a liquid dispenser. One needs only to add the commands provided by the manufacturer of the device. The second step is completed by assigning the new device a SiLA IP/Port. Once the SiLA driver of the new device is written and tested, the final step is to integrate it into the Pelican. This is done, by opening the driver in LACS Configuration Editor and saving the device in the list of working devices in the Pelican.

Microfluidic device. A 2-lane *OrganoPlate* (#9603-200B, Mimetas BV, Leiden, The Netherlands) consists of a stratified array of 96 microfluidic chips embedded in a customised 384-well microtiter plate format²⁸ (Fig. 2). Each chip consists of a single microfluidic chip contained between two pieces of glass: a top plate with holes corresponding to the underside of selected wells, and a bottom plate. Each chip is connected through 4 neighbouring wells and 2 lanes: one *gel inlet well* for loading of gel-embedded cells into the culture lane, one *medium inlet well* connected to one *medium outlet well* through a medium lane. The flow of media is driven by a pressure drop between the aforementioned 2 wells. The fourth well is used as an *observation window* for monitoring the quality of cells through an inverted microscope. The culture and medium lanes are separated by a *phaseguide*, preventing the gel-embedded cells from flowing into the medium lane. A phaseguide is a patterned pinning barrier that controls the liquid-air interface by forcing it to align with the ridge, hence, guiding the fluid flow into the appropriate lane²⁷.

Automating the differentiation of human neuroepithelial stem cell into dopaminergic neurons.

In order to biologically validate the automated system, and the ability of the Pelican to differentiate cells in microfluidic device, the assay developed by Reinhardt *et al.*²⁰ and adapted into the *OrganoPlate* by Lucumi *et al.*³⁵ was used to develop an automated pipeline to differentiate hNESCs into three dimensional networks of electrophysiologically active dopaminergic neurons in the *OrganoPlate*. The first step of the assay involve loading 0.8 µl of matrigel/hNESCs mixture into the culture lane.

The day after loading the gel-embedded hNESCs into the culture lane of the *OrganoPlate*, a *semi-automated image acquisition protocol* was executed through LACS to qualitatively assess the health of the cell culture. An appropriate field of view was selected manually and focussed. The subsequent automated image acquisition protocol (Fig. 3) consisted of first setting the environmental condition of the onstage incubator to 5% CO₂ and to a temperature of 37 °C. Second, the robotic arm moved the plate from the storage incubator to the microscope. Third, the microscope scanned through all the observation windows of the *OrganoPlate*, and the camera took an image of each observation window. Fourth, the plate was transported back to the incubator by the robotic arm. Immediately after the automated image acquisition, the *automated differentiation of hNEESC into dopaminergic neurons protocol* (Fig. 4) was executed through LACS. This protocol consisted of first instructing the robotic arm

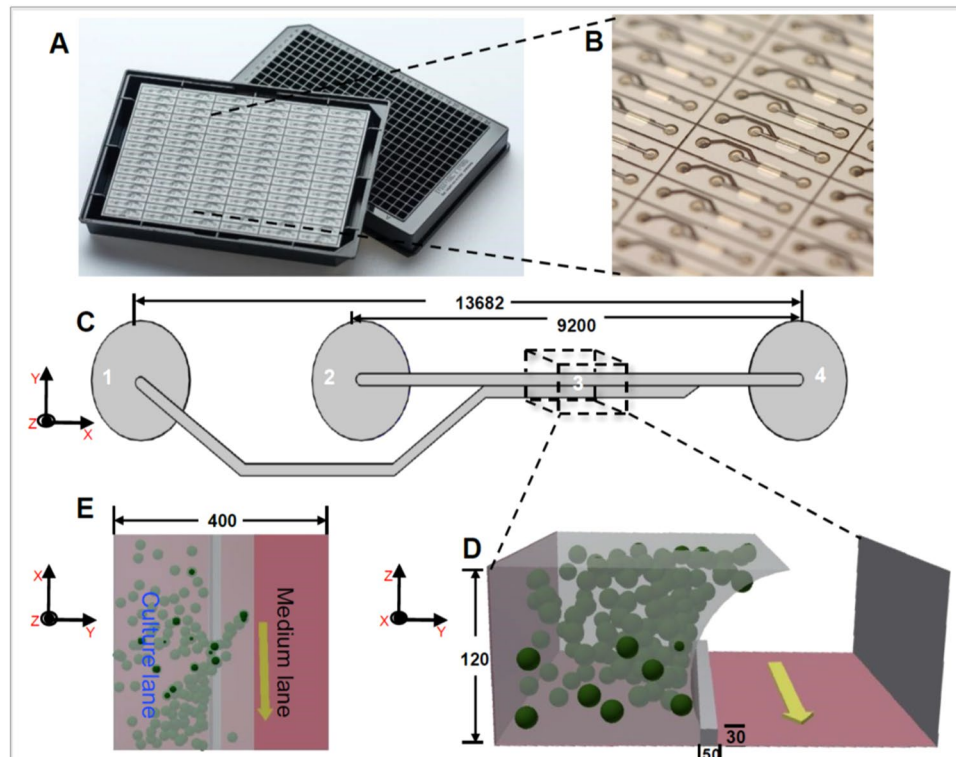


Figure 2. Microfluidic cell culture device: OrganoPlate. (A) Photograph of underside (left) and upper views (right) of an OrganoPlate. (B) bottom plate of OrganoPlate with selective chips. (C) A schematic of a single 2-lane chip; 1 = Gel inlet, 2 = Medium inlet, 3 = Observation window, 4 = Medium outlet. (D) A transverse section of a culture chamber showing the direction of the flow in the medium lane (yellow arrow), the phaseguide and the culture lane with suspended spheres representing cells embedded in Matrigel. (E) Top view of transverse section of a culture chamber with phaseguide, medium and culture lanes. All dimensions in μm .

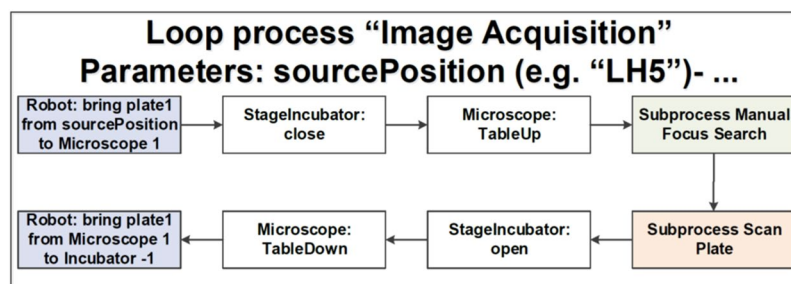


Figure 3. Semi-automated image acquisition pipeline. See Supplementary Fig. S5 for more details.

to move the plate from the storage incubator to the de-lidder to remove the lid from the plate, before moving it to the liquid dispenser. Second, the dispenser aspirated media from each medium inlet and outlet well. Third, the dispenser replenished the media in each medium inlet and outlet well respectively. Fourth, the robotic arm moved the plate to the de-lidder to put the lid back before placing the plate inside the storage incubator (Supplementary Video 1). These two protocols were run in this order every two days for 24 days.

Human neuroepithelial stem cell culture differentiation. We utilised the Pelican and the existing protocol described by Reinhardt *et al.* and Lucumi *et al.*^{20,35} to fully automate the differentiation of hNESC into dopaminergic neurons inside a stratified three-dimensional microfluidic device. After manually seeding hNESC in an OrganoPlate, a microfluidic cell culture device with 3D capabilities compatible with laboratory automation, the hNESC were distributed in three dimensions within the culture lane, but also adjacent to the meniscus (Fig. 5A). Thereafter the Pelican executed an automated differentiation protocol to start and maintain the differentiation process. Initially, this required a liquid dispenser to aspirate the maintenance medium and dispense the differentiation medium with PMA, into inlet and outlet wells of the OrganoPlate. Thereafter, it required incubation and regular media replenishment.

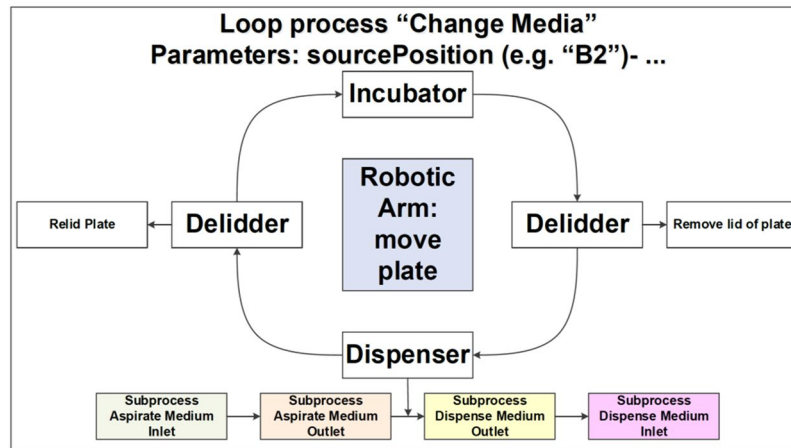


Figure 4. Automated media change pipeline. See Supplementary Fig. S4 for more details.

During the differentiation, cells started to form aggregates, and morphological changes started to appear, such as acquisition of cellular polarity and projection of processes representative of neuronal morphology (Fig. 5B). An automated protocol replaced the medium with PMA with medium without PMA, and differentiated neurons started a maturation process accompanied by acquisition of a more evident neuronal morphology (Fig. 5C). Differentiated neurons projecting their processes can be observed in the culture lane and in the area occupied by the meniscus, located in part of the medium lane. Neuronal activity of differentiated cells was tested using calcium imaging (Fig. 5D) and morphological and phenotypic characteristics like neuronal processes positive for TUB β III (green) and the amount of tyrosine hydroxylase positive neurons (red) were characterised using an immunostaining assay (Fig. 5E). A top view of the culture chamber of a chip with hNESc (Fig. 6A), shows that cells were distributed in the entire culture chamber, Hoechst nuclear staining (blue). Furthermore, their processes have been projected in all directions of the culture lane, as well as on the meniscus part in the medium lane. It can also be seen that the neuronal networks and the level of connectivity of the differentiated neurons is homogeneous in the entire culture chamber, denoting an even effect of the differentiation protocol, as well as the efficiency of perfusion in the medium lane (Fig. 6A).

Figure 6B enlarges the view of a specific area of one chip with differentiated neurons from hNESc. Neurons positive for TUB β III (green) and positive for tyrosine hydroxylase (red) are located in both culture and medium lanes. However, all cells appear to migrate towards the medium lane. This is confirmed in the front view of the enlarged area (Fig. 6C), where the extent of the area occupied by the meniscus in the medium lane is clear, in addition to the degree of cells located on the meniscus on the medium lane. On average, the efficiency of differentiation for tyrosine hydroxylase positive neurons in 3 chips of the OrganoPlate with hNESc differentiated neurons was 15% of all neurons (Fig. 6D), which is in accordance with values reported previously in analogous manual, microfluidic and macroscopic cell culture systems^{20,35}.

After 24 days, we were able to obtain midbrain-like, mature dopaminergic neurons in 96 three-dimensional self-contained microfluidic chips. Regular pictures were taken during differentiation for quality control and morphological study (Fig. 5A–C), and end point assays are represented in Fig. 5D,E to illustrate the fate of the differentiation.

Calcium imaging and immunostaining assays. To probe the neuronal activity of cells cultured in an OrganoPlate within the Pelican, we used Fluo-4-based calcium imaging. We acquired time-series of representative culture chambers of WT and PINK1 p.I368N-mutated populations at day 24 of differentiation (Supplementary Video 2). Analysis of those calcium imaging data revealed spontaneous neuronal activity in differentiated control and PINK1-mutant neurons in an OrganoPlate, within the Pelican. We detected individual cells by applying an automated cell segmentation algorithm³⁷ to the raw calcium imaging data. Figure 6E,G illustrate segmented mean fluorescence frames of representative culture chambers of an OrganoPlate with WT and PINK1-mutated neurons respectively. Fluorescence traces were then measured for each segmented cell to assess their activity (Fig. 6F,H). Some of the fluorescence traces reveal calcium transients indicating neuronal firing events (Fig. 6F e.g. signal #2, 3, 9 and Fig. 6H e.g. signal #8, 14, 27). Fluorescence traces revealed different firing patterns of the differentiated neurons. Some of these traces exhibited regular firing patterns, as opposed to other ones, corresponding probably to dopaminergic neurons, similar to what has been previously reported by Lucumi *et al.*³⁵ in adjacent manual culture.

Discussion

We assembled an automated cell culture observatory, termed the Pelican. It was optimised for the long-term cell culture maintenance of neurons inside three-dimensional microfluidic devices. The implementation followed a modular automation design, with generous space for further devices, and is flexible in terms of the automation platforms that can be implemented. For example, the system allows the automation of seeding, feeding and other cell culture processes that could initiate and maintain cell lines in any standard microtiter plate format. In this

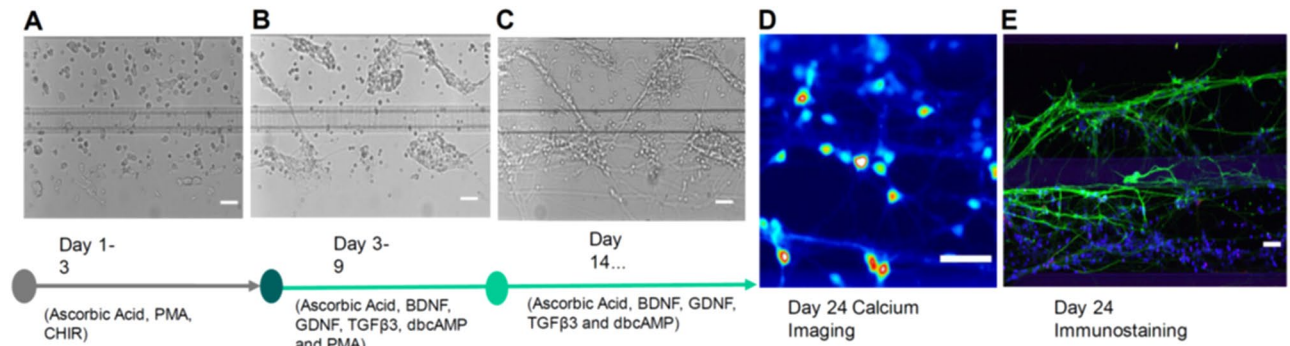


Figure 5. Dopaminergic neuronal differentiation. Bright field images of hNESCs with media components at (A) 1 day (B) 4 days and (C) 21 days after seeding. (D) Calcium imaging frame of a firing event taken at day 24 after seeding. (E) Immunofluorescence image illustrating the neuronal composition inside a culture chamber. All scale bars are 50 μm . Legend as in Fig. 6.

regard, we carefully selected the robotic system, the pipetting technologies and the techniques to integrate all the components of the system into a single plant.

Many methods have been developed over the years to address the issue of standardisation and easy integration of new devices into existing laboratory automated plants^{8,9,38–41}. In the Pelican, Standardisation in Laboratory Automation (SiLA) was chosen for the integration of the devices. SiLA standardises the interfacing, integration and data representation in a simple single XML schema for all devices^{9,42}. SiLA standardises the communication between process management software and one or more devices. SiLA defines common commands per *device class* and the common *device states*. SiLA defines the device classes to achieve these functionalities such as an incubator and a liquid-handler. Each device class will have the required commands for the core functionalities as well as *optional commands* for extended functionalities that are not necessarily present in every device of the same class. In this regard, a SiLA standard common command dictionary was developed for every single device class where the commands such as `setParameter` and `getParameter` and the expected return are known. This allows a process management software to automatically generate the required commands for every device class. Each component of the Pelican was chosen based on cell culture needs without taking into account the manufacturer of each device. The integration of any new device would require sufficient space within the useable area and possibly the development of a SiLA driver (tutorial in user manual available upon request). The modular hardware and software integration flexibility is a key advantage of the Pelican design compared to other automated cell culture systems^{43–48}.

In order to demonstrate the biological utility of the Pelican, control and PINK1-mutant human neuroepithelial stem cell lines were automatically differentiated into midbrain specific dopaminergic neurons. Calcium imaging of spontaneously firing neurons, as well as immunostaining for neuronal markers demonstrate that, neuroepithelial stem cells could be successfully maintained and were spontaneously active within the OrganoPlate inside the Pelican. Further analysis of fluorescence traces for additional cell lines with different genetic backgrounds would be necessary to quantify any difference in phenotypic characteristics of neuronal activity between control and PINK1 mutant neurons. The differentiated neurons can be maintained inside the OrganoPlate for at least 100 days. The Pelican demonstrates proof-of-concept for automated generation of personalised *in vitro* neuronal models from human neuroepithelial stem cells via a microfluidic cell culture approach.

The Pelican is designed for longitudinal analysis of many personalised cellular models exposed to a few perturbations, rather than single, end-point analysis of one cellular model exposed to a large number of perturbations, as for instance is the focus in high throughput drug screening. Therefore, we envisage that such automated system be applied to stratification of patients with complex diseases. In addition, the Pelican can be used of automated cell culture to enable comprehensive phenotyping of large, parallel sets of personalised, *in vitro*, midbrain-specific, dopaminergic neuronal models of Parkinson's disease. By integrating the data generated with a generic mechanistic computational model of the underlying biochemical network of a dopaminergic neuron, each personalised computational model then becomes a coherent representation of our information about the cell autonomous characteristics of Parkinson's disease in each patient. Such personalised computational models, and thereby the corresponding patients, are then amenable to stratification with a range of powerful stratification tools. Stratification based on personalised computational models of data is statistically superior to stratification based on the personalised data alone, as the former explicitly incorporates the wealth of prior biochemical information known about midbrain dopaminergic neurons. Ultimately, this will accelerate the translation of basic biomedical knowledge from the laboratory to the therapies with clinical impact.

Increasing demands for reproducibility, parallelisation and longitudinal observations are driving cell culture research toward automation. We developed a novel automated cell culture observatory that enables long-term maintenance and longitudinal optical measurement of cellular parameters in Organ-on-a-Chip platforms. We demonstrate the use of this platform to successfully automate the generation of personalised *in vitro* neuronal models from human neuroepithelial stem cells. We demonstrate the feasibility of semi-automated image acquisition on this platform and compatibility with different real-time and end-point assays. It is the first time that an

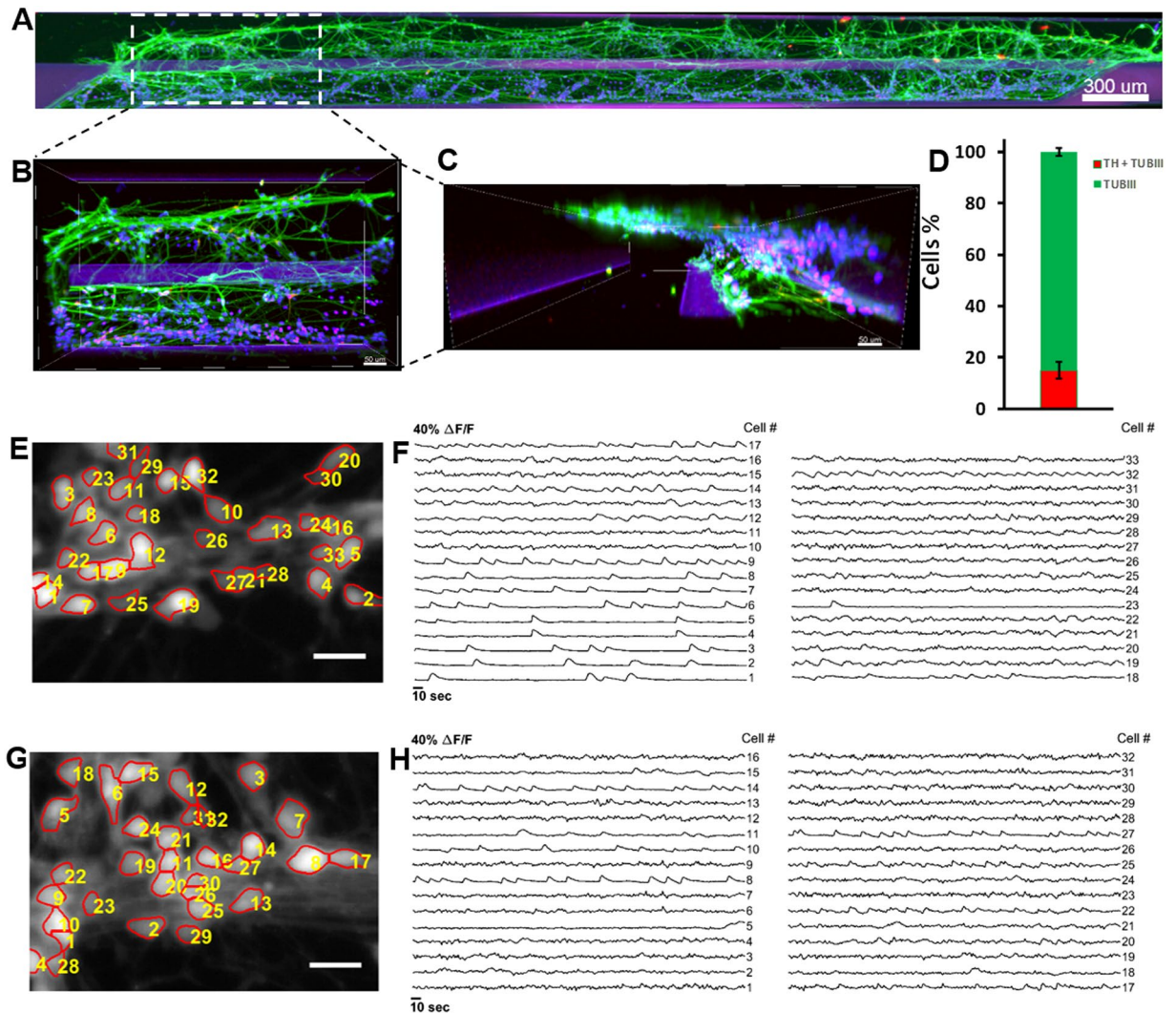


Figure 6. Immunostaining and automated cell segmentation of calcium time-series hNESc differentiated in chips of the OrganoPlate inside the Pelican. (A) Top view of an entire chip in the OrganoPlate showing differentiated wild type neurons (K7 cell line) immunostained for nuclei with Hoechst (blue), TUBβIII (green) and tyrosine hydroxylase (red); scale bar 300 μm. (B) Enlarge top (B) and front (C) views of selected area; scale bar 50 μm. (D) Differentiation efficiency of neurons positive for TUBβIII and tyrosine hydroxylase. (E) Mean fluorescence frame of a calcium time-series of WT population with segmented regions of interest corresponding to individual neurons and (F) their corresponding fluorescence traces. (G) Mean fluorescence frame of a calcium time-series of PINK1 mutants with segmented regions of interest corresponding to individual neurons and their corresponding fluorescence traces (H).

Organ-on-a-Chip platform is applied in an automated setting. It holds great promise for patient stratification by enabling comprehensive phenotyping of large, parallel sets of personalised, *in vitro*, models of complex diseases.

Methods

System Construction and Design. The Pelican is composed of a sterile automation enclosure that abuts a sterile manual enclosure on one side and an incubator on another. The automation enclosure contains a set of devices that may physically communicate via a four-axis gantry robot within a customised housing support. The manual enclosure is a cell culture hood, adapted for restricted communication of material with the automation enclosure. The automation enclosure currently includes a de-lidder, eight-fold and 96fold parallel dispenser, three-axis fourfold liquid handling robot (pipettor) with disposable tips, confocal microscope, and camera. The assembly (Fig. 7a,b), all of the components are described in the Supplementary Experimental Procedures.

Cell culture. All work with human iPSCs and thereof derived cells has been approved by the Ethics Review Panel (ERP) of the University Luxembourg as well as by the Luxembourgish Comité National d’Ethique de Recherche (CNER). The CNER reference number is 201305/04. All experiments were performed in accordance

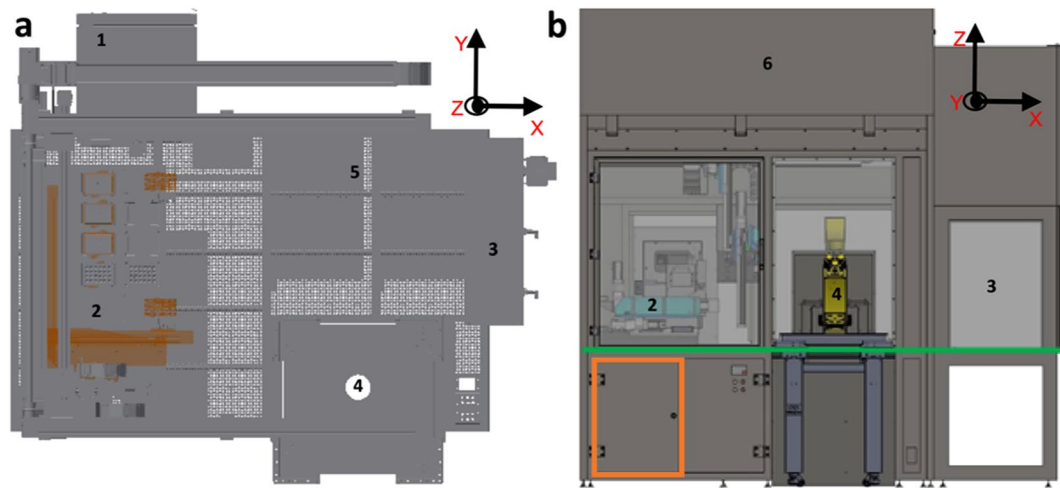


Figure 7. CAD drawing of automated workstation. **(a)** Top view inside the Pelican without housing. **(b)** Front view of the Pelican with housing. Yellow (imaging station), light blue (liquid handling station), green (level of stainless steel work surface) and orange (waste containers). Perforated surface = work surface. (1) Storage incubator. (2) Liquid-handler. (3) Hotels (manual working bench). (4) Position of microscopy station. (5) Position of liquid dispenser. (6) Automated work bench. Coordinates shown here are consistent with the remainder of the manuscript. See also Figs S1 and S2.

with relevant guidelines and regulations. We confirm that written informed consent was obtained, by our cell line suppliers, for the establishment of stem cell lines, from all donors.

Human neuroepithelial stem cell culture. In order to demonstrate the capability of the automated system to maintain and monitor many types of cells including PD specific cell lines, we used a human neuroepithelial stem cell line from a healthy donor (hNESK K7) and a human neuroepithelial stem cell line derived from a patient carrying the Parkinson's disease related mutation p.I368N in PINK1 (40066C5N). These cells were maintained and differentiated into midbrain-specific dopaminergic neurons within an OrganoPlate, by automating an existing macroscopic cell culture protocol²⁰, that we previously adapted for microfluidic cell culture³⁵. In brief, to culture hNESCs in an OrganoPlate, they were harvested from wells of a 6 well plate. The harvested hNESCs were then re-suspended on Matrigel (catalogue number 354277, lot number 3318549, Discovery Labware, Inc., Two Oak Park, Bedford, MA, USA). 0.7 μ L of this Matrigel-cell mix was loaded in assigned chips of the OrganoPlate at a density of 0.03 million cells/ μ L. After seeding the cells, the plate was loaded into position B3 in the hotel of the Pelican. Afterwards, the plate was moved by the robotic arm to the storage incubator, at 37 °C and 5% CO₂.

Dopaminergic neuronal differentiation. The culture medium preparation "N2B27 medium" consisted of mixed equal amounts of Neurobasal medium (invitrogen/life technologies) and DMEM/F12 medium (invitrogen/life technologies) supplemented with 1% penicillin/streptomycin (life technologies), 2 mM L-glutamine (life technologies), 0.5 X B27 supplement without Vitamin A (life technologies) and 0.5 X N2 supplement (life technologies). The medium to maintain the hNESK in culture "maintenance medium" consisted of N2B27 medium with 0.5 μ M PMA (Enzo life sciences), 3 μ M CHIR (Axon Medchem) and 150 μ M Ascorbic Acid (Sigma Aldrich). The differentiation medium formulation to induce the differentiation of hNESCs towards midbrain dopaminergic neurons "differentiation medium with PMA" consisted of N2B27 medium with 200 μ M ascorbic acid, 0.01 ng/ μ L BDNF (Peprotech), 0.01 ng/ μ L GDNF (Peprotech), 0.001 ng/ μ L TGF β 3 (Peprotech), 2.5 μ M dbcAMP (Sigma Aldrich) and 1 μ M PMA. The function of PMA in this medium preparation was to stimulate the sonic hedgehog (SHH) pathway in the cultured hNESCs. Differentiation medium with PMA was changed, every 2 days during the first 6 days of culture in the differentiation process. For the maturation of differentiated neurons, PMA was no longer added to the differentiation medium "differentiation medium without PMA" from day 7 onwards, which was changed every 2 days during 3 weeks. To monitor cellular morphology during differentiation, bright field images were acquired automatically in the Pelican using the microscopy station.

Calcium imaging assay. A calcium imaging assay was done on 15 representative chips of the OrganoPlate at day 24 of differentiation. At room temperature, 50 μ L of 5 μ M cell permeant Fluo-4 AM (Life technologies) in neurobasal medium (Invitrogen/Life technologies) was manually added to the medium inlet well and 20 μ L to the medium outlet well of selected chips of the OrganoPlate. Then, the plate was incubated for 30 min at 37 °C and 5% CO₂. The plate was then placed in an onstage incubator within the microscope. Calcium time-series of spontaneously firing hNESK-derived neurons were then automatically acquired. Images were sampled at a rate of 1 Hz for approximately 5 min, stored as image stacks and analysed using custom Matlab (version 2016b; MathWorks Inc.) scripts. Regions of interest corresponding to individual cells were automatically segmented with an established technique³⁷ and fluorescence traces were generated for each segmented cell and presented as relative changes in fluorescence intensity $\Delta F/F$.

Immunofluorescence staining assay. Immunostaining for the dopaminergic neuronal markers class 3 beta tubulin (TUB β III) and tyrosine hydroxylase (TH), the penultimate enzyme in the biosynthesis of dopamine^{20,49,50}, was performed on representative chips at day 24 of differentiation. Differentiated cells were fixed with 4% paraformaldehyde (PFA) in 1 × phosphate-buffered saline (PBS) for 15 min, by manually adding 70 μ L in medium well inlet and 30 μ L in medium well outlet followed by permeabilisation with 0.05% Triton-X 100 in 1 × PBS (3 min on ice), and blocking with 10% fetal calf serum (FCS) in 1 × PBS (1 h). After washing with 1 × PBS, the primary antibodies mouse anti-TUB β III (1:2000, Covance) and rabbit anti-TH (1:2000, Santa cruz biotechnology), were incubated for 90 min at room temperature. After washing with 1 × PBS, the secondary antibodies Alexa Fluor 488 Goat Anti-Mouse and Alexa Fluor 568 Goat Anti-Rabbit together with a stain DNA (Hoechst 33342, Invitrogen), were incubated for 2 hours at room temperature. After washing with 1 × PBS and water, confocal images of representative culture chambers were acquired using a confocal microscope (Zeiss LSM 710).

Automating the differentiation of human neuroepithelial stem cell into dopaminergic neurons. LACS Config Editor was used to develop automated pipelines for the differentiation of hNESCs into dopaminergic neurons and time-lapse imaging microscopy. The automated pipelines were drafted according to the SiLA communication protocol and command format as previously described^{9,42,51}. In brief, SiLA uses a Simple Object Access Protocol (SOAP) and a Web Service Description Language (WSDL) documentation, both of which are based on XML. A full library of commands for each device is downloaded once and stored in LACS as a configuration document of the Pelican. LACS Config Editor was used to incorporate the automated pipelines in this configuration file used herein to automate the differentiation of hNESCs into dopaminergic neurons. On the workbench, gel-embedded hNESCs were manually loaded into the culture lanes of a 2-lane OrganoPlate as described above. Then, the plate was put inside the Pelican through Hotel B, and placed inside the storage incubator by the robotic arm. The dispenser was fitted with a 5 μ L cassette from Biotek and used as a dispensing medium for the media change.

Statistical Analysis. Three representative chips (n = 3) were selected to illustrate the results of this study, in which the statistical analyses were performed by determination of the mean value and the standard deviation of the proportion of dopaminergic neurons within the overall neuronal population.

Data Availability

All data used within this study are available.

References

- Dunn, D. A. & Feygin, I. Challenges and solutions to ultra-high-throughput screening assay miniaturization: submicroliter fluid handling. *Drug Discovery Today*. **12**, 84–91, [https://doi.org/10.1016/S1359-6446\(00\)00064-7](https://doi.org/10.1016/S1359-6446(00)00064-7) (2000).
- Kong, F., Yuan, L., Zheng, Y. F. & Chen, W. Automatic liquid handling for life science: a critical review of the current state of the art. *J. Lab. Autom.* **3**, 169–185, <https://doi.org/10.1177/2211068211435302> (2012).
- Dauwalder, O. *et al.* Does bacteriology laboratory automation reduce time to results and increase quality management? *Clinical Microb. Infec.* **3**, 236–243, <https://doi.org/10.1016/j.cmi.2015.10.037> (2016).
- Arrasate, M. & Finkbeiner, S. Automated microscope system for determining factors that predict neuronal fate. *Proc. Natl. Acad. Sci. USA* **10**, 3840–3845, <https://doi.org/10.1073/pnas.0409777102> (2005).
- Skibinski, G. & Finkbeiner, S. Longitudinal measures of proteostasis in live neurons: features that determine fate in models of neurodegenerative disease. *FEBS Letters*. **8**, 1139–1146, <https://doi.org/10.1016/j.febslet.2013.02.043> (2013).
- Triaud, F. *et al.* Evaluation of automated cell culture incubators. *J. Lab. Autom.* **6**, 82–86, [https://doi.org/10.1016/s1535-5335\(03\)00018-2](https://doi.org/10.1016/s1535-5335(03)00018-2) (2003).
- Halldorsson, S., Lucumi Moreno, E., Gomez-Sjoberg, R. & Fleming, R. M. T. Advantages and challenges of microfluidic cell culture in polydimethylsiloxane devices. *Biosensors and Bioelectronics*. **63**, 218–231, <https://doi.org/10.1016/j.bios.2014.07.029> (2015).
- Carvalho, M. C. Integration of analytical instruments with computer scripting. *J. Lab. Autom.* **4**, 328–333, <https://doi.org/10.1177/2211068213476288> (2013).
- Bar, H., Hochstrasser, R. & Papenfub, B. SiLA: Basic standards for rapid integration in laboratory automation. *J. Lab. Autom.* **2**, 86–95, <https://doi.org/10.1177/2211068211424550> (2012).
- Lees, A. J., Hardy, J. & Revesz, T. Parkinson's disease. *The Lancet*. **9680**, 2055–2066, [https://doi.org/10.1016/S0140-6736\(09\)60492-X](https://doi.org/10.1016/S0140-6736(09)60492-X) (2009).
- Abdullah, R. *et al.* Parkinson's disease and age: the obvious but largely unexplored link. *Experimental Gerontology*. **68**, 33–38, <https://doi.org/10.1016/j.exger.2014.09.014> (2015).
- Surmeier, D. J. & Schumacker, P. T. Calcium, Bioenergetics, and neuronal vulnerability in Parkinson's disease. *J. Biol. Chem.* **15**, 10736–10741, <https://doi.org/10.1074/jbc.R112.410530> (2000).
- Bellucci, A. *et al.* Review: Parkinson's disease: from synaptic loss to connectome dysfunction. *Neuropathol. Appl. Neurobiol.* **1**, 77–94, <https://doi.org/10.1111/nan.12297> (2016).
- Chinta, S. J. & Andersen, J. K. Dopaminergic neurons. *The International Journal of Biochemistry & Cell Biology*. **5**, 942–946, <https://doi.org/10.1016/j.biocel.2004.09.009> (2005).
- Schondorf, D. C. *et al.* iPSC-derived neurons from GBA1-associated Parkinson's disease patients show autophagic defects and impaired calcium homeostasis. *Nat. Commun.* **5**, 4028, <https://doi.org/10.1038/ncomms5028> (2014).
- Munoz, P., Huenchuguala, S., Paris, I. & Segura-Aguilar, J. Dopamine oxidation and autophagy. *Parkinsons Dis.*, <https://doi.org/10.1155/2012/920953> (2012).
- Pfeiffer, R. F., Wszolek, Z. K. & Ebadi, M. *Parkinson's Disease, Second Edition* (ed. Pfeiffer, R.) (CRC Press, 2012).
- Hillje, A. L. & Schwamborn, J. C. Utilization of stem cells to model Parkinson's disease – current state and future challenges. *Future Neurology*. **2**, 171–186, <https://doi.org/10.2217/fnl.16.7> (2016).
- Takahashi, K. *et al.* Induction of pluripotent stem cells from adult human fibroblasts by defined factors. *Cell*. **5**, 861–872, <https://doi.org/10.1016/j.cell.2007.11.019> (2007).
- Reinhardt, P. *et al.* Derivation and expansion using only small molecules of human neural progenitors for neurodegenerative disease modeling. *PLoS ONE*. **3**, 59252, <https://doi.org/10.1371/journal.pone.0059252> (2013).
- Gomez-Sjoberg, R., Leyrat, A. A., Pirone, D. M., Chen, C. S. & Quake, S. R. Versatile, fully automated, microfluidic Cell culture system. *Analytical Chemistry*. **22**, 8557–8563, <https://doi.org/10.1021/ac071311w> (2007).
- Lecault, V. *et al.* High-throughput analysis of single hematopoietic stem cell proliferation in microfluidic cell culture arrays. *Nat. Methods*. **7**, 581–586, <https://doi.org/10.1021/ac071311wi> (2011).

23. Croushore, C., Suphahroek, S., Lee, C., Jakmunee, J. & Sweedler, J. Microfluidic device for the selective chemical stimulation of neurons and characterization of peptide release with mass spectrometry. *Anal. Chem.* **21**, 9446–9452, <https://doi.org/10.1021/ac302283u> (2012).
24. Shintu, L. *et al.* Metabolomics-on-a-chip and predictive systems toxicology in microfluidic bioartificial organs. *Anal. Chem.* **4**, 1840–1848, <https://doi.org/10.1021/ac2011075> (2012).
25. Oedit, A., Vulto, P., Ramautar, R., Lindenburg, P. W. & Hankemeier, T. Lab-on-a-Chip hyphenation with mass spectrometry: strategies for bioanalytical applications. *Current Opinion in Biotechnology.* **31**, 79–85, <https://doi.org/10.1016/j.copbio.2014.08.009> (2015).
26. Huh, D. *et al.* Reconstituting organ-level lung functions on a chip. *Science.* **5986**, 1662–1668, <https://doi.org/10.1126/science.1188302> (2010).
27. Vulto, P. *et al.* Phaseguides: a paradigm shift in microfluidic priming and emptying. *Lab on a Chip.* **9**, 1596–1602, <https://doi.org/10.1039/c0lc00643b> (2011).
28. Trietsch, S. J., Israels, G. D., Joore, J., Hankemeier, T. & Vulto, P. Microfluidic titer plate for stratified 3D cell culture. *Lab on a Chip.* **18**, 3548, <https://doi.org/10.1039/C3LC50210D> (2013).
29. van Duinen, V., Trietsch, S. J., Joore, J., Vulto, P. & Hankemeier, T. Microfluidic 3D cell culture: from tools to tissue models. *Current Opinion in Biotechnology.* **35**, 118–126, <https://doi.org/10.1016/j.copbio.2015.05.002> (2015).
30. Junaid, A., Mashaghi, A., Hankemeier, T. & Vulto, P. An end-user perspective on Organ-on-a-Chip: assays and usability aspects. *Current Opinion in Biomedical Engineering.* **1**, 15–22, <https://doi.org/10.1016/j.cobme.2017.02.002> (2017).
31. Grossmann, G. *et al.* The RootChip: an integrated microfluidic chip for plant science. *Plant Cell.* **12**, 4234–4240, <https://doi.org/10.1105/tpc.111.092577> (2011).
32. Antia, M., Herricks, T. & Rathod, P. Microfluidic modeling of cell-cell interactions in malaria pathogenesis. *PLoS Pathog.* **7**, 0939–0948, <https://doi.org/10.1371/journal.ppat.0030099> (2007).
33. Ho, S. Y. *et al.* NeurphologyJ: An automatic neuronal morphology quantification method and its application in pharmacological discovery. *BMC Bioinformatics.* **12**, 230, <https://doi.org/10.1186/1471-2105-12-230> (2011).
34. Vedel, S., Tay, S., Johnston, D. M., Bruus, H. & Quake, S. R. Migration of cells in a social context. *Proceedings of the National Academy of Sciences.* **1**, 129–134, <https://doi.org/10.1073/pnas.1204291110> (2013).
35. Lucumi Moreno, E. *et al.* Differentiation of neuroepithelial stem cells into functional dopaminergic neurons in 3D microfluidic cell culture. *Lab Chip.* **11**, 2419–2428, <https://doi.org/10.1039/C5LC00180C> (2015).
36. Piracci, A. Advantages of Non-Contact Dispensing in SMT Assembly Processes. *SMTA International Conference Proceedings*, http://www.smta.org/knowledge/proceedings_abstract.cfm?PROC_ID=619 (2000).
37. Diego, F., Reichinnek, S., Both, M. & Hamprecht, F. A. Automated identification of neuronal activity from calcium imaging by sparse dictionary learning. *IEEE International Symposium on Biomedical Imaging*, <https://doi.org/10.1109/ISBI.2013.6556660> (2013).
38. American Society for Testing and Material. Standard specification for transferring information between clinical instruments and computer systems. *Annual Book of ASTM Standards*, <https://www.astm.org/DATABASE.CART/WITHDRAWN/E1394.htm> (2002).
39. Smith, B. & Ceusters, W. HL7 RIM: an incoherent standard. *Stud. Health Technol Inform.* **124**, 133–138 (2006).
40. Joshi, S. & Pillai R. *LECIS Commentary*, https://www.ergotech.com/lecis.org/documents/UserSpace/LECIS_commentary.pdf (2002).
41. Roth, A., Jopp, R., Schafer, R. & Kramer, G. W. Automated generation of Animl documents by analytical instruments. *J. Lab. Autom.* **4**, 247–253, <https://doi.org/10.1016/j.jala.2006.05.013> (2006).
42. Bar, H. & Syre, U. Infoteam SiLA library simplifies device integration. *J. Lab. Autom.* **5**, 371–376, <https://doi.org/10.1016/j.jala.2011.05.003> (2011).
43. Paull, D. *et al.* Automated, high-throughput derivation, characterization and differentiation of induced pluripotent stem cells. *Nat. Meth.* **9**, 885–892, <https://doi.org/10.1038/nmeth.3507> (2015).
44. Konagaya, S., Ando, T., Yamauchi, T., Suemori, H. & Iwata, H. Long-term maintenance of human induced pluripotent stem cells by automated cell culture system. *Scientific Reports.* **5**, 16647, <https://doi.org/10.1038/srep16647> (2015).
45. Soares, F. A. C. *et al.* Investigating the feasibility of scale up and automation of human induced pluripotent stem cells cultured in aggregates in feeder free conditions. *Journal of Biotechnology.* **173**, 53–58, <https://doi.org/10.1016/j.jbiotec.2013.12.009> (2014).
46. Kami, D. *et al.* Large-scale cell production of stem cells for clinical application using the automated cell processing machine. *BMC Biotechnology.* **13**, 102, <https://doi.org/10.1186/1472-6750-13-102> (2013).
47. Thomas, R. J. *et al.* Automated, scalable culture of human embryonic stem cells in feeder-free conditions. *Biotechnol Bioeng.* **6**, 1636–1644, <https://doi.org/10.1002/bit.22187> (2009).
48. Terstegge, S. *et al.* Automated maintenance of embryonic stem cell cultures. *Biotechnol Bioeng.* **1**, 195–201, <https://doi.org/10.1002/bit.21061> (2007).
49. Daadi, M. M., Grueter, B. A., Malenka, R. C., Redmond, D. E. Jr & Steinberg, G. K. Dopaminergic neurons from midbrain-specified human embryonic stem cell-derived neural stem cells engrafted in a monkey model of Parkinson's disease. *PLOS ONE.* **7**, 41120, <https://doi.org/10.1371/journal.pone.0041120> (2012).
50. Yan, Y. *et al.* Directed Differentiation of Dopaminergic Neuronal Subtypes from Human Embryonic Stem Cells. *Stem Cells.* **6**, 781–790, <https://doi.org/10.1634/stemcells.2004-0365> (2005).
51. McIntosh, R. L. & Yau, A. A Flexible and Robust Peer-to-Peer Architecture with XML-Based Open Communication for Laboratory Automation. *J. Lab. Autom.* **1**, 38–45, <https://doi.org/10.1016/S1535-5535-04-00240-0> (2003).

Acknowledgements

KIWK, ELM, TH and PV received funding from the SysMedPD project from the European Union's Horizon 2020 research and innovation program under grant agreement No. 668738. ELM, SH and JJ were also supported by an Aides a la Formation-Recherche training allowance from Fonds National de la Recherche Luxembourg ref. 10099424. The authors thank Miguel Oliveira for his assistance with generation of photographs. The authors also thank Christophe Bouillon for his help to setup the platform.

Author Contributions

R.F. conceived the project. K.I.W.K., R.F. and E.L.M. proposed and designed the experiments, and wrote the manuscript. J.J. and J.C.S. provided the cells. K.I.W.K. and E.L.M. run the experiments. K.I.W.K., S.H. and E.L.M. generated the calcium data and S.H. analysed the data. M.T. and M.W. designed the automated platform. M.T., M.W. and K.I.W.K. built the automated platform. All the authors discussed the results and commented on the manuscript.

Additional Information

Supplementary information accompanies this paper at <https://doi.org/10.1038/s41598-018-34828-3>.

Competing Interests: M.T. and M.W. disclose that they are employees of Fraunhofer IPA. T.H. and P.V. disclose that they are co-founders of Mimetas BV. None of the other authors have potential conflicts of interest to be disclosed. The other authors certify that they have no relevant financial interests in this manuscript and that any/all financial and material support for this research and work are clearly identified in the Acknowledgements section of this manuscript.

Publisher's note: Springer Nature remains neutral with regard to jurisdictional claims in published maps and institutional affiliations.



Open Access This article is licensed under a Creative Commons Attribution 4.0 International License, which permits use, sharing, adaptation, distribution and reproduction in any medium or format, as long as you give appropriate credit to the original author(s) and the source, provide a link to the Creative Commons license, and indicate if changes were made. The images or other third party material in this article are included in the article's Creative Commons license, unless indicated otherwise in a credit line to the material. If material is not included in the article's Creative Commons license and your intended use is not permitted by statutory regulation or exceeds the permitted use, you will need to obtain permission directly from the copyright holder. To view a copy of this license, visit <http://creativecommons.org/licenses/by/4.0/>.

© The Author(s) 2019

5. Neuronal hyperactivity in a LRRK2-G2019S cellular model of Parkinson's Disease

Title	Neuronal hyperactivity in a LRRK2-G2019S cellular model of Parkinson's Disease
Author(s) & Affiliation(s)	<p>Siham Hachi¹, Edinson Lucumi Moreno¹, Sarah L. Nickels¹, Khalid I.W. Kane¹, Masha Moein¹, Jens C. Schwamborn¹, Alex Skupin¹, Pieter Vanden Berghe², Ronan M.T. Fleming¹</p> <p>¹Luxembourg Centre for Systems Biomedicine, University of Luxembourg, 6 avenue du Swing, L-4367 Belvaux, Luxembourg.</p> <p>²Laboratory for Enteric Neuroscience, Translational Research in Gastrointestinal Disorders, Department of Clinical and Experimental Medicine, University of Leuven, Leuven, Belgium.</p>
Publication Outlet	N/A
Publication Type	N/A
Publication Year	N/A
Publication Status	Draft
Preface	<p>In this paper, we assessed the neuronal activity of induced pluripotent stem cell derived neurons from Parkinson's Disease patients with LRRK2-G2019S mutations and compared it with isogenic controls. Monogenic Parkinson's Disease can be caused by a mutation in one of several genes, with diverse biochemical functions. The gene encoding the leucine-rich repeat kinase 2 (LRRK2) causes a late onset autosomal dominant inherited form of Parkinson's Disease. The function of the LRRK2 gene is incompletely understood, but several in vitro studies have reported that LRRK2-G2019S mutations affect neurite branching, calcium homeostasis and mitochondrial function, but thus far, there have been no</p>

reports of effects on electrophysiological activity. We assessed the neuronal activity of induced pluripotent stem cell derived neurons from Parkinson's Disease patients with LRRK2-G2019S mutations and isogenic controls. Neuronal activity of spontaneously firing neuronal populations was recorded with a fluorescent calcium-sensitive dye (Fluo-4) and analysed with a novel image analysis pipeline that combined semi-automated neuronal segmentation and quantification of calcium transient properties. Compared with controls, LRRK2-G2019S mutants have shortened inter-spike intervals and an increased rate of spontaneous calcium transient induction. This neuronal hyperactivity in a cellular model of LRRK2-G2019S Parkinson's Disease is reminiscent of the neuronal hyperactivity observed in models of other neurodegenerative diseases, such as Alzheimer's disease. I contributed by writing the algorithm for the acquisition of the calcium images data in the automated platform.

Draft: Neuronal hyperactivity in a LRRK2-G2019S cellular model of Parkinson's Disease

Siham Hachi¹, Edinson Lucumi Moreno¹, Sarah L. Nickels¹, Khalid I.W. Kane¹, Masha Moein¹, Jens C. Schwamborn¹, Alex Skupin¹, Pieter Vanden Berghe², Ronan M.T. Fleming¹

¹Luxembourg Centre for Systems Biomedicine, University of Luxembourg, 6 avenue du Swing, L-4367 Belvaux, Luxembourg. ²Laboratory for Enteric Neuroscience, Translational Research in GastroIntestinal Disorders, Department of Clinical and Experimental Medicine, University of Leuven, Leuven, Belgium.

Abstract

Monogenic Parkinson's Disease can be caused by a mutation in one of several genes, with diverse biochemical functions. The gene encoding the leucine-rich repeat kinase 2 (LRRK2) causes a late-onset autosomal dominant inherited form of Parkinson's Disease. The function of the LRRK2 gene is incompletely understood, but several *in vitro* studies have reported that LRRK2-G2019S mutations affect neurite branching, calcium homeostasis and mitochondrial function, but thus far, there have been no reports of effects on electrophysiological activity. We assessed the neuronal activity of induced pluripotent stem cell derived neurons from Parkinson's Disease patients with LRRK2-G2019S mutations and isogenic controls. Neuronal activity of spontaneously firing neuronal populations was recorded with a fluorescent calcium-sensitive dye (Fluo-4) and analysed with a novel image analysis pipeline that combined semi-automated neuronal segmentation and quantification of calcium transient properties. Compared with controls, LRRK2-G2019S mutants have shortened inter-spike intervals and an increased rate of spontaneous calcium transient induction. This neuronal hyperactivity in a cellular model of LRRK2-G2019S Parkinson's Disease is reminiscent of the neuronal hyperactivity observed in models of other neurodegenerative diseases, such as Alzheimer's disease.

Introduction

Parkinson's disease (PD) is the second most common neurodegenerative disease affecting more than 10 million people worldwide [1, 2]. It is known that cell death in PD occurs at many levels of the nervous system [1], including the loss of cholinergic neurons in the pedunculopontine nucleus, noradrenergic neurons in the locus coeruleus and dopaminergic neurons from the substantia nigra pars compacta (SNc) [3, 4]. In addition, dopaminergic neurons produce the neurotransmitter dopamine, which plays a central role in brain function [5–7]. Moreover, the loss of dopaminergic neurons is responsible for the primary motor symptoms in PD, including rigidity, resting tremors, bradykinesia and postural instability [8]. Further understanding of PD at the cellular level requires advanced patient-derived cellular models that recapitulate the main characteristics of the neurons that are selectively vulnerable to degeneration in PD.

Between 5-10% of PD cases have a genetic or familial origin [9, 10]. Certain mutations in the LRRK2 (leucine rich repeat kinase 2) gene are as-

sociated with familial and sporadic forms of PD [11]. LRRK2 is a multi-domain protein localised in the cytoplasm. It has kinase and GTPase activity in addition to domains for protein-protein interactions that make it a key regulator of cellular function [12–15]. However, its exact function is still incompletely understood. Mutation G2019S is the most common LRRK2 mutation, it has been detected in 1% to 3% of sporadic PD cases and 3% to 6% in familial PD cases world-wide [16, 17]. In addition, clinical symptoms associated with patients with G2019S mutation include tremor, dystonia, cognitive impairment/dementia and anxiety [17, 18]. Mutant LRRK2 proteins impair normal protein phosphorylation in DA neurons and affect cell survival [16]. Over-expression of LRRK2 results in mitochondrial fragmentation [19] and an increase in LRRK2 activity is involved in neuronal apoptosis via mitochondria. Furthermore, LRRK2 deletion protects against mitochondrial dysfunction [12, 20] and a role for this protein in cytoskeletal dynamics has been demonstrated [16, 21, 22]. Several studies reported that LRRK2 mutations alters neuronal morphology, manifested by reduced neurite length as

well as complexity [21, 23]. However, little is known about the effect of LRRK2 mutations on neuronal activity.

The study of PD at the cellular level has been facilitated by the use of induced pluripotent stem cell (iPSCs) technology. Several methods have been developed to reprogram human somatic cells into iPSCs. Reinhardt et al. [24] demonstrated the use of iPSC technology to obtain human neuroepithelial stem (hNESc) using small molecules. These hNESc can then be differentiated into specific neuronal cell types, including midbrain dopaminergic neurons (mDNs). Monogenic patient-derived stem cells can also be genetically modified to repair certain mutations, resulting in isogenic control lines, with the same genetic background as the patient-derived cells. Dopaminergic neurons derived from patient's iPSC with LRRK2 mutation G2019S have shown increased expression and accumulation of alpha synuclein protein, shortening of neurites length together with diminished branching [25], increased susceptibility to oxidative stress [26], mitochondria damage [27] and signs of neurodegeneration in general [25, 27].

In experimental neuroscience there are several options to record electrophysiological activity of neurons *in vitro*. Patch clamp recording techniques provide very accurate measurements, however, they cannot be used to measure the electrophysiological activity of a large population of neurons. An alternative technique is to use various fluorescent indicators of electrophysiological activity, coupled with light microscopy and digital cameras [28]. Fluorescent calcium indicators respond to the binding of calcium ions by changing their fluorescence properties. *Calcium imaging* is the combination of fluorescent calcium indicators with imaging instrumentation, and is a versatile technique for studying neuronal activity and different aspects of cellular development [29, 30]. In particular, fluorescent calcium-sensitive dyes [31] permit simultaneous recording of electrophysiological activity in a large population of neurons. *Calcium imaging* has found widespread applications in neuroscience and its ability to record electrophysiological activity for a large population of neurons simultaneously makes it especially suited to analysing the phenotypic differences between normal and diseased neurons¹.

Neuronal activity is characterised by firing single or bursts of action potentials. During an action potential, intracellular calcium concentration increases transiently [32, 33]. A calcium transient

is characterised by a fast rise in intracellular calcium concentration followed by an exponential decay. Calcium imaging is an accessible option to characterise the neuronal activity of differentiated neurons derived from patient samples [34]. This approach is based on the use of fluorescent indicators that are sensitive to calcium concentration, using either calcium sensitive dyes (e.g. Fura-2 AM and Fluo-4 AM) [35] or genetically encoded calcium sensitive protein sensors [36]. With a suitable microscope and camera, one then obtains a temporal series of fluorescent images.

Calcium imaging can generate a large amount of data, necessitating the development of new computational techniques for processing and analysis to leverage the potential of this technique [37]. Given a temporal series of fluorescent images, individual neurons can be identified by manually selecting regions of interest. However, this method is subjective and laborious when large populations of neurons are being imaged. Therefore, robust and reliable computational approaches are required to automate and facilitate the analysis of calcium imaging data [38]. Automated identification of individual cells is one of the main image analysis challenges. Different methods exist to identify cells, including machine learning [39], non-negative matrix factorisation [40], independent component analysis [41] and sparse dictionary learning [42]. Most of these approaches typically delineate regions of interest corresponding to cell bodies and then generate fluorescence traces for each cell. As these traces represent the dynamics of calcium indicators, which are much slower than the spiking activity of neurons, various algorithms have been developed to deconvolve a fluorescence signal into a spike train [43]. Such methods are based on Markov chain Monte Carlo [44], fast non-negative deconvolution [45], greedy algorithms [46] or finite rate of innovation [47]. Combining these methods together in one pipeline would be useful for the neuroscience community. Patel et al. [38] have recently published a pipeline to measure features of neuronal network activity. It uses a cell segmentation method based on Independent Component Analysis (ICA) that provides rather accurate results. However, it is semi-automated and cannot identify cells that are not active or cells firing synchronously. Additionally, it detects neuronal processes that might not be relevant for the user. Moreover, it is computationally expensive especially when dealing with large neuronal populations.

In this paper, we developed a fully automated

¹@Pieter, would you suggest a citation to one of your papers here please?

pipeline for calcium image analysis and analysis of fluorescence traces from individual neurons. This pipeline was applied to quantitatively characterise the neuronal activity of human neuroepithelial stem cell-derived neurons *in vitro*. We used a sparse dictionary learning based-algorithm [42] to identify single neurons in a spontaneously firing population, enabling the extraction of fluorescence traces for individual neurons. Fluorescence traces were deconvolved into spike trains [45] and calcium transients were identified and extracted to quantify their properties and characterise the neuronal activity of differentiated cells. Applying this image analysis pipeline to calcium time-series of spontaneously firing iPSC-derived wild-type and LRRK2-G2019S mutant neurons, revealed neuronal hyperactivity in mutant neurons. Although the LRRK2-G2019S mutation is associated with neuronal hyperactivity *in vitro*, the causal mechanisms remain to be elucidated in future work.

Materials and methods

hNESc differentiation into dopaminergic neurons

A control human neuroepithelial stem cell-line (K7), and the same cell-line with an introduced LRRK2-G2019S mutation (K7M), in addition to a LRRK2-G2019S patient-derived cell-line (T4) and its isogenic control (T4GC), were maintained and differentiated into midbrain dopaminergic neurons using small molecules and growth factors, in 96 well plates, by using an existing protocol described by Reinhardt et al. [24]. Here we used 3 plates representing 3 biological replicates. In brief, CellCarrier optically clear bottom, black, tissue treated 96 well plates (Perkin Elmer) were coated with Matrigel (catalogue number 354277, lot number 3318549, Discovery Labware, Inc., Two Oak Park, Bedford, MA, USA). At the time of cell seeding, the coating medium was removed from each well of the 96 well plate and the different cell-lines were seeded in selected wells, at a density of 0.3 million cells/ml in 80 μ L of medium, and incubated at 37 rC with 5% CO₂. The medium was changed every other day and this process was repeated throughout the differentiation process for 5 weeks.

The culture medium preparation “N2B27 medium” consisted of mixing equal amounts of Neurobasal medium (Invitrogen/life technologies) and DMEM/F12 medium (Invitrogen/life technologies) supplemented with 1% penicillin/streptomycin (life technologies), 2 mM L-glutamine (life technologies), 0.5 X B27 supplement without Vitamin A (life technologies) and 0.5X N2 supplement (life technologies).

The medium to maintain the hNESc in culture “*maintenance medium*” consisted of N2B27 medium with 0.5 μ M Purmorphamine (PMA) (Enzo life sciences), 3 μ M CHIR (Axon Medchem) and 150 μ M Ascorbic Acid (Sigma Aldrich). The differentiation medium formulation to induce the differentiation of hNESc towards midbrain dopaminergic neurons “*differentiation medium with PMA*” consisted in N2B27 medium with 200 μ M ascorbic acid, 0.01 ng/ μ L BDNF (Peprotech), 0.01 ng/ μ L GDNF (Peprotech), 0.001 ng/ μ L TGF β 3 (Peprotech), 2.5 μ M dbcAMP (Sigma Aldrich) and 1 μ M PMA. 80 μ L of differentiation medium with PMA was changed every 2 days during the first 6 days of culture in the differentiation process. For the maturation of differentiated neurons PMA was no longer added to the differentiation medium “*differentiation medium without PMA*” from day 7 onwards, this differentiation medium without PMA was changed every 2 days during 3 weeks.

Calcium imaging

A calcium imaging assay was done on representative wells of a black CellCarrier optically clear bottom, tissue treated 96 well-plate (Perkin Elmer). Differentiation medium was removed from the wells with differentiated cells. Those wells were washed twice with 100 μ L of neurobasal medium. Afterwards, the washing medium was removed and 80 μ L of 5 μ M cell permeant Fluo-4 AM (Life technologies) in neurobasal medium was added to wells at room temperature and incubated at 37 rC for 30 minutes. The medium with Fluo-4 was removed and replaced by the old differentiation medium and left incubating for 10 more minutes. Images of spontaneously firing hNESc-derived neurons were acquired, using an epifluorescence microscope (Leica DMI6000 B) equipped with a confocal device (Revolution DSD2, Andor) and an sCMOS camera (Neo 5.5, Andor). Images of size 1200 x 1200 pixels were sampled at a rate of 2 Hz for 4 min, stored as separate image files and analysed using custom Matlab (version 2017b; MathWorks) scripts. Four to six calcium time-series of randomly selected fields of view were acquired in three representative wells for each cell-line.

Automated image analysis

Calcium image analysis was achieved by combining published open source algorithms developed in MATLAB into a novel automated pipeline. The pipeline is illustrated in Figure 1 and consists of the following steps: 1) neuronal segmentation, 2) fluorescence trace extraction from the segmented neurons, 3) spike train inference and 4) calcium

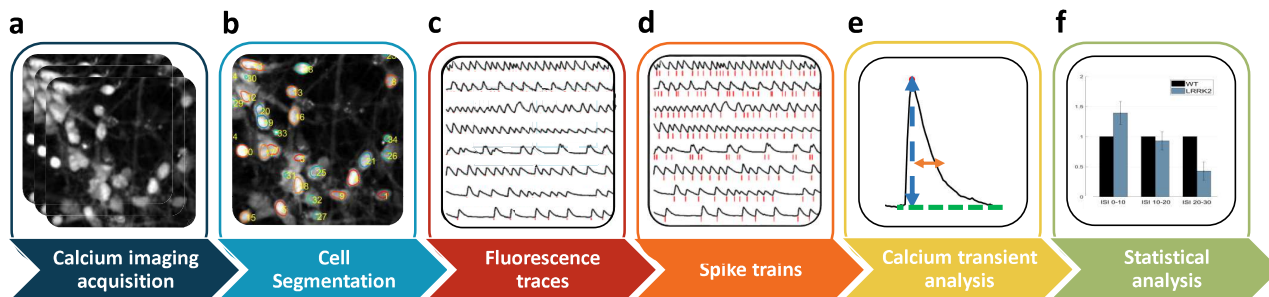


Figure 1: Automated image analysis pipeline for calcium imaging data to quantify neuronal activity. Cells are cultured in an automated cell culture observatory (a). Calcium imaging data of a neuronal population are acquired (b). Regions of interest (ROIs) corresponding to individual neurons are identified (c). Fluorescence traces (black traces) and their underlying spike trains (red lines) are measured for each ROI (d). Calcium transients are detected and their properties are estimated, as shown below in Figure 2 (e). Statistical analysis is performed to estimate differences in calcium transient parameters between two neuronal populations.

spike analysis. We integrated all of these steps in a pipeline to quantify neuronal activity. Calcium imaging datasets for each cell-line were stored in one folder to perform batch analysis, where all datasets were automatically analysed with one click.

Image segmentation: To detect individual neurons in calcium time-series, we employed an automated image segmentation technique, based on sparse dictionary learning [42]. This method was proven to outperform state-of-the-art cell segmentation algorithms in calcium imaging data, particularly the most commonly used method based on independent component analysis and principal component analysis (the CellSort tool) [41].

Briefly, the algorithm reshapes the (2+1)D calcium imaging data into a 2D matrix, then applies a matrix factorisation based on sparse dictionary learning [48] to decompose the data into a spatial and temporal components. This is followed by an image segmentation step where a wavelet transform and watershed algorithm are used to detect single cells. The wavelet functions are based on a cubic B-spline, to remove background noise and enhance fluorescence traces coming from the pixels that belong to neuronal cell bodies over other shapes [37]. The wavelet functions use a convolution mask with the coefficients $[1\ 4\ 6\ 4\ 1]/16$. This function can be extended to different scales and can therefore be applicable to different cell sizes. For a more detailed description of the wavelet functions refer to Reichinnek et al. [37]. Here, we used a wavelet scale of 4, as explained in the Discussion section.

Fluorescence trace generation and spike train inference: Fluorescence traces were extracted from automatically segmented regions of interest, corresponding to neuronal somata, by averaging the intensities of all pixels within each a region of

interest at each frame. These traces are presented as relative changes in fluorescence intensity ($\Delta F/F = (f - f_0)/f_0$) where f is the fluorescence intensity and f_0 the fluorescence baseline defined as the 20th percentile of the fluorescence signal within a sliding window of 10 frames. Thereafter, the user can choose between spike train inference or peak detection corresponding to calcium transient peaks. In the case of spike train inference, fluorescence traces are deconvolved into spike trains using a fast non-negative deconvolution (OOPSI) algorithm described in Vogelstein et al. [45] or the constrained-OOPSI [49]. The output of the OOPSI algorithm is the probability that a spike occurred at a given time frame. We set a probability threshold to exclude improbable spikes.

Calcium transient analysis: After measuring fluorescence traces, we identified and quantified the features of calcium transients using the CaSiAn tool; a JAVA-based application for calcium signal analysis [50], which was integrated into our pipeline. First, transient peaks were detected by finding the local maxima of each fluorescence trace. We used a peak threshold of 20% of the maximum transient amplitude. Subsequently, for each identified calcium transient, a set of features, illustrated in Figure 2, were quantified. The features quantified were the inter-spike interval (time between two transient peaks), spike amplitude, spike width, area under the spike, calcium increasing rate and decreasing rate related to calcium fluxes. Fluorescence traces with less than 5 spikes were excluded.

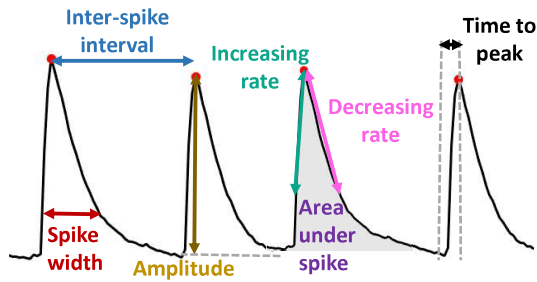


Figure 2: Description of the measured calcium transient features.

Comparison between LRRK2 G2019S mutants and isogenic control cell-lines For each pair of mutant and isogenic control cell lines, the quantified features of calcium transients from sets of fluorescence traces from individual neurons were compared. The fluorescence traces from neurons of the same cell-line in different wells but the same biological replicate, were considered as a single set and subsequently the mean and standard deviation of each quantified feature from that set was estimated. Due to high variability in firing patterns, each fluorescence trace was classified according to its mean inter-spike interval, using intervals of 10 seconds, resulting in three classes (0 - 10, 10 - 20, 20 - 30 seconds). This classification was performed on each biological replicate of each cell-line. Statistical analysis of calcium transient features to calculate differences between wild-type and LRRK2-G2019S-mutated cell-lines. Specifically, a student's t-test was used and $P < 0.05$ was considered statistically significant.

Results

Automated neuronal segmentation of calcium time-series

We implemented an automated analysis pipeline (Figure 1) for quantification of neuronal activity in calcium imaging data and applied it to spontaneously firing hNESc-derived neurons. An automated sparse dictionary learning algorithm was adapted and successfully applied to segment calcium imaging data (Figure 3a). An optimal wavelet scale parameter was identified (scale 4) as smaller wavelet scales yielded inhomogeneous fluorescence intensity within a single region of interest representing a neuron, leading to over-segmentation (Figure 4b scale 3). Larger wavelet scales exceeded the limit of the dimensions of our cells including other cells or parts of their neighbourhood resulting in erroneous segmentation (Figure 4c scale 5). The choice of the wavelet scale parameter strongly depends on cell size (Figure 4b-c). The optimal pixel intensity threshold was determined to be 0.06,

which represents the percentage of the maximum intensity of the smoothed image. After optimising the different parameters, individual neurons were accurately and automatically segmented and their corresponding fluorescence traces were analysed (Figure 3c). These traces revealed calcium transients with different waveforms and different frequencies showing the diversity in firing frequencies and firing patterns in this neuronal culture.

Hyperactivity of LRRK2-G2019S mutant neurons

After neuronal segmentation and fluorescence traces, with more than 5 calcium transients, were obtained from a large number of neurons for each cell-line (1258 ± 336 traces for K7, 1022 ± 421 for K7M, 480 ± 195 for T4GC and 369 ± 267 for T4, $n = 3$ plates). For each biological replicate, inter-spike interval values of a pair of cell-lines (e.g. K7 vs. K7M) were merged together to form one set (Figure 5a). Each set was then classified according to short, medium and long classes of inter spike intervals (Figure 5b). Each class contained average ISI from both control and mutant neurons (Figure 5c). Within the short inter-spike interval class (0 - 10 sec), the proportion of mutant neurons is significantly higher than for controls. The proportion of mutant neurons decreases as the inter-spike intervals increases. Approximately 55% of neurons with a LRRK2-G2019S mutation exhibited inter-spike intervals between 0 - 10 sec against 32% in control (Figure 5d). Figure 5 shows data of one biological replicate for K7 and K7M cell-lines. The same analysis was performed on the other pair of cell-lines (T4 vs. T4GC) and for each biological replicate. No significant differences were observed in other calcium transient features (see Supplementary Material). In summary, compared with isogenic controls, fluorescence traces from LRRK2-G2019S mutant neurons demonstrated reduced inter-spike intervals.

Discussion

Calcium imaging technique Calcium imaging provides a powerful means to monitor the activity of neuronal populations *in vivo* [51] and *in vitro* [52]. In contrast to electrophysiological approaches, such as patch clamp techniques, it allows simultaneous recording of neuronal activity and spatial location of individual neurons for a large population [52]. Calcium imaging generates a large amount of data, which becomes challenging to analyse manually as neuronal population size increases. It is therefore necessary to apply computational methods to partially automate the analysis of calcium imaging

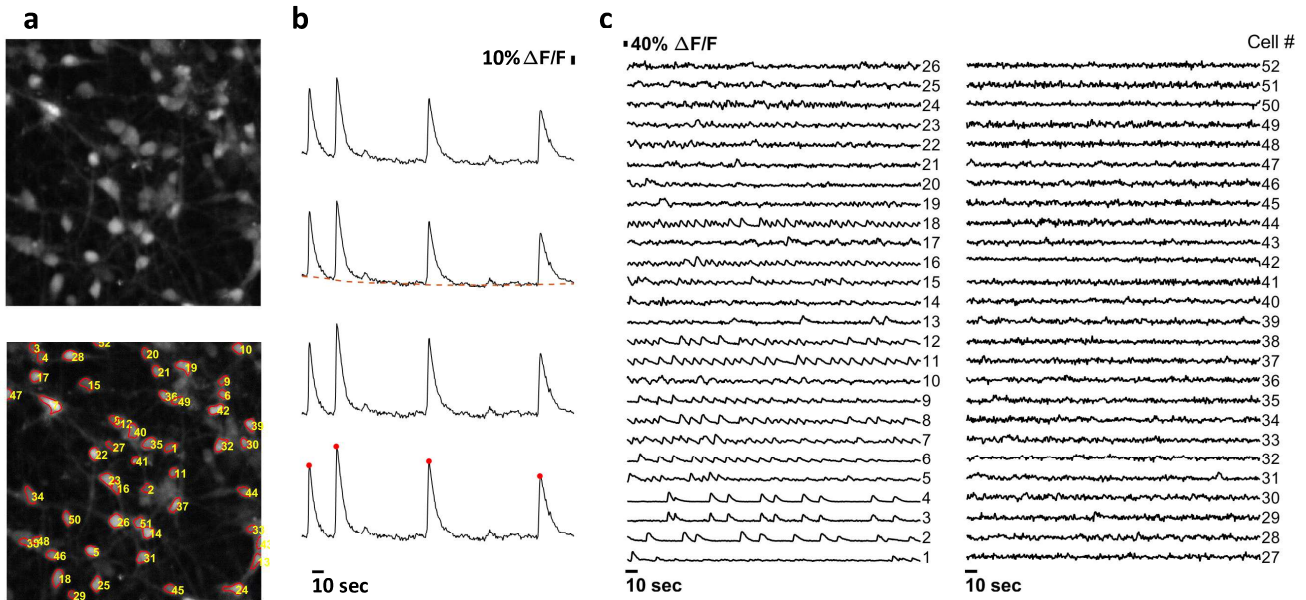


Figure 3: Automated segmentation, fluorescence trace estimation and spike train inference of calcium time-series of a neuronal population. **(a)** Mean fluorescence frame of a calcium time-series (top) and numbered segmentation of individual neuronal somata (bottom). **(b)** Fluorescence baseline correction. **(c)** Fluorescence traces corresponding to the segmented neurons in **(a)**.

data.

Automated computational image analysis for calcium imaging data Computational image analysis is required to efficiently, reliably and quantitatively analyse calcium time-series and activity-dependent fluorescence traces. With the recent developments of several algorithms to segment calcium imaging data, infer spike trains from fluorescence traces and analyse calcium transients [49], it is necessary to establish pipelines of methods as one package. In this study, we established a pipeline that brings together a set of complementary algorithms to analyse calcium imaging data and quantify calcium transient properties to characterise neuronal activity.

In this pipeline, we integrated a sparse dictionary learning-based segmentation algorithm that was shown to be more robust than the CellSort tool [41]. The former achieved a sensitivity of 94.3% while the latter exhibited 83.1% [42]. The sparse dictionary learning-based algorithm provides an accurate segmentation and can discriminate two overlapping cells exhibiting similar firing patterns. In the preprocessing step, this method uses a wavelet transform to intensify the fluorescence traces belonging mainly to cell bodies and not processes. This limits the amount of segmented regions such as neuronal projections that might not be of interest to the user. These wavelet functions are described by a convolution mask with the coefficients [1 4 6 4 1]/16. This function can be extended to different scales by adding zeros between the

coefficients [37]. Choosing the right wavelet scale is crucial to obtain well segmented cells and depends on the size of the imaged cells (Figure 4).

In addition to the wavelet scale, other parameters need to be tuned for an optimal segmentation, such as the intensity threshold. If the threshold is too low, then regions containing pixels with a low intensity that do not belong to a cell body would be considered. On the other hand, if the threshold is too high then cell bodies with lower intensity pixels would be excluded. The requirement for tuning these parameters makes the pipeline semi-automated, rather than fully automated. Tuning these parameters strongly depends on the experimental setup used for calcium imaging recordings, such as type of microscope, camera, fluorescence light source and calcium indicators. However, once these parameters are optimised for a particular calcium imaging acquisition protocol, automated processing of similar datasets is possible. Although there is a significant parameter tuning in this approach, it provides robust segmentation of individual neurons. This pipeline was effectively applied to different cell culture systems, such as organoids [53] and microfluidic cell culture [34].

Hyperactivity of LRRK2-G2019S mutants

Patient-derived neurons are becoming extensively used in neuroscience for modelling and investigating different neurodegenerative diseases, revealing various relevant disease mechanisms [54]. We applied our image analysis pipeline to human neuroepithelial stem cells differentiated into

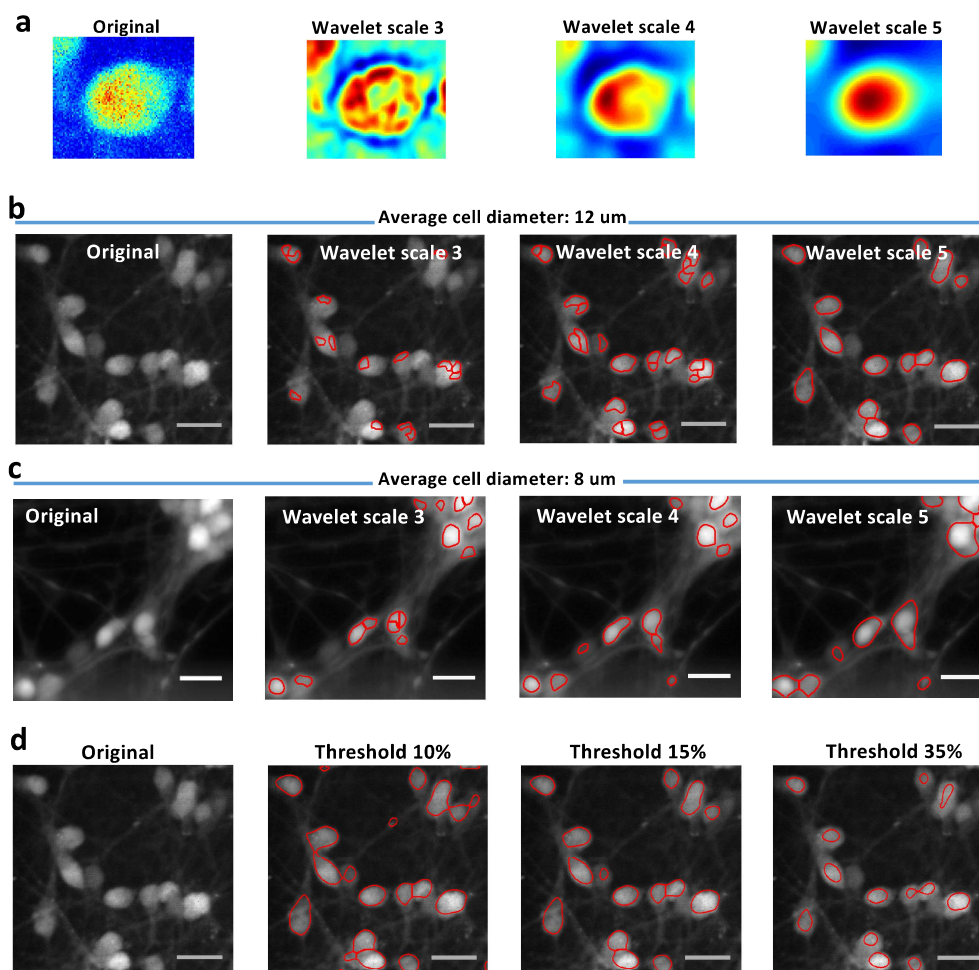


Figure 4: Effect of wavelet scale size on segmentation. **(a)** Different wavelet scale sizes have different effects on the image in the preprocessing step. The purpose of the wavelet function is to smooth the image and give more intensity to round shapes such as cell bodies. **(b)** The effect of different wavelet scales on segmentation of somas of an average diameter of 12 μm . Clearly, wavelet scale 5, compared with 3 and 4, induces a more accurate segmentation as the somata are well delineated. **(c)** The effect of different wavelet scales on segmentation of somas of an average diameter of 8 μm . Clearly, wavelet scale 4 performs better than 3, where some somata are subdivided into several parts and 5, where some somata are merged in one segment. **(d)** Effect of intensity threshold on segmentation.

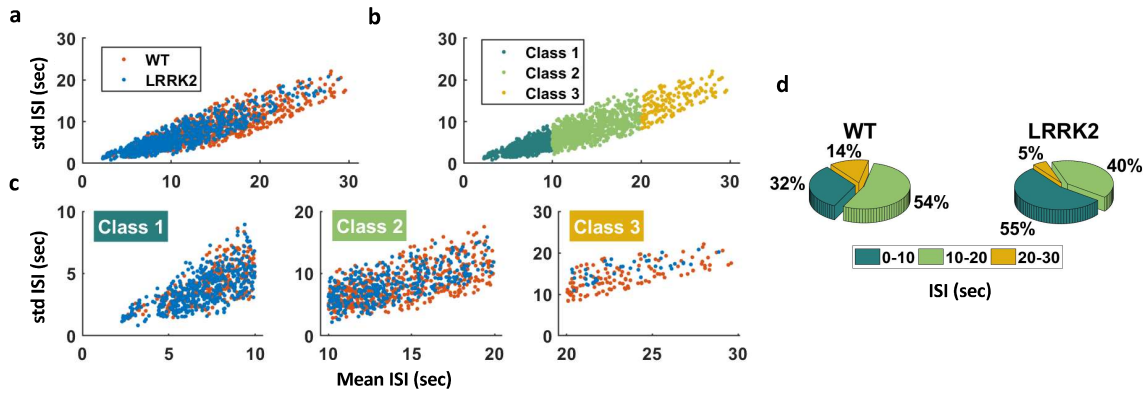


Figure 5: Classification of mean interspike interval (ISI) values (K7 and K7M cell-lines). **(a)** Scatter plot of merged inter-spike intervals (ISI, seconds) from control and LRRK2-G2019S mutants. **(b)** Classification of inter-spike intervals into 10-sec interval groups, colours correspond to individual classes (1 - 3). **(c)** Scatter plots of the merged inter-spike intervals from control and LRRK2-G2019S neurons for each class. **(d)** Pie charts showing relative proportions of neurons in each inter-spike interval class colour-coded same as in **(b)**.

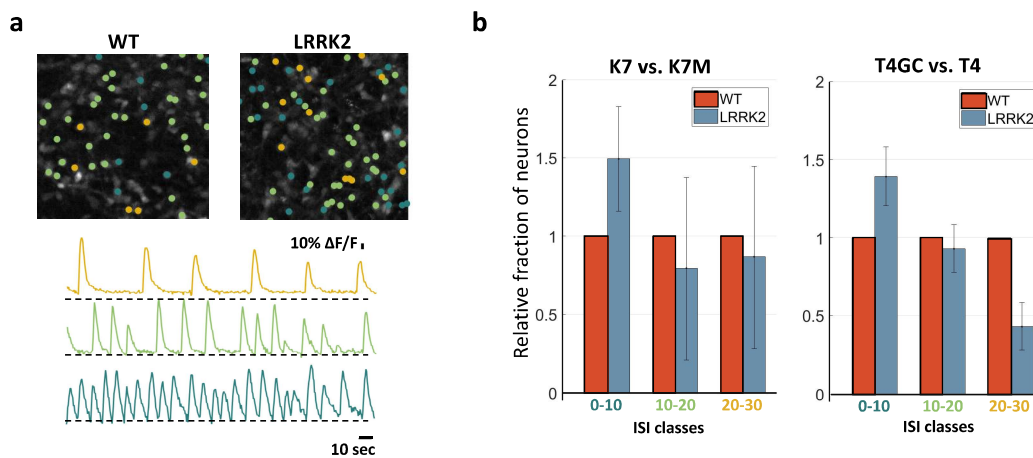


Figure 6: Hyperactivity of LRRK2-G2019S mutant neurons. **(a)** Mean fluorescence frames of K7 (control) and K7M (LRRK2-G2019S) cell-lines overlaid with activity maps (top) and examples of traces from each class (bottom). **(b)** Comparison of the fractions of LRRK2-G2019S neurons in each class relative to wild-type (for both cell-lines).

dopaminergic neurons to measure the effect of a LRRK2-G2019S mutation on neuronal activity. Mutant LRRK2 has been found to be implicated in several cellular dysfunctions including mitochondrial degradation [55], calcium homeostasis impairment [55], synaptic transmission [56] as well as neurite length shortening [21].

We found that LRRK2-G2019S mutated neurons displayed a form of neuronal hyperactivity compared with control neurons. In particular, we demonstrated that the inter-spike interval between action potential-evoked calcium transients was significantly shorter in LRRK2-G2019S mutated neurons. As yet, we do not know the mechanism for this hyperactivity. However, this phenotype has been previously observed in several studies related to neurodegeneration in Alzheimer's disease (AD) [57]. In this respect, an *in vivo* whole-cell patch clamp technique was utilised to assess the electrical activity of neurons vulnerable in AD [58].

This study aimed at linking the dendritic morphological abnormalities, in particular shortening of dendritic length, to neuronal excitability. A full morphological computational model, simulating *in vivo* conditions, predicted high firing frequency subsequent to reduction of dendritic length, making the neuron electrically more compact, thus leading to shorter inter-spike intervals, which was confirmed by patch-clamp recordings [58]. Siskova et al. reported that in a neuron with shortened morphology, synaptic currents would translated faster into postsynaptic currents resulting in hyperexcitability. This structure-dependant cellular mechanism could be a possible explanation to the hyperexcitability of LRRK2-G2019S mutants that we observed, considering that this mutation induces dendritic shortening [55]. In fact, Cherra et al. reported that LRRK2-G2019S mutation decreases the dendritic mitochondrial density thus leading to dendritic area reduction [55]. Moreover, Bolognin et

al. (under review) showed significantly shortened morphology of hNESc-derived neurons carrying a LRRK2-G2019S mutation.

Hyperactivity was previously observed in mouse and patient models of Alzheimer's disease [57, 59]. Moreover, patient-derived motor neurons were shown to exhibit a form of neuronal hyperexcitability in ALS disease [60] as well as cortical neurons in Huntington's disease [61]. It is an interesting question as to why hyperactivity of vulnerable neurons seems to be a common pathological phenotype in these neurodegenerative diseases.

Conclusion

We combined different computational data analysis approaches into one pipeline to analyse calcium imaging data and calcium transients with the aim of quantifying neuronal activity of large neuronal ensembles. The pipeline includes accurate cell segmentation, fluorescence trace measurement, spike train inference and calcium transient analysis. This pipeline will facilitate investigations of neuronal activity with large numbers of neurons. We successfully applied this pipeline to human neuroepithelial stem cells differentiated into dopaminergic neurons carrying LRRK2-G2019S mutation, after 30 days of differentiation.

This provided preliminary evidence for a disease-specific phenotype characterised by neuronal hyperactivity *in vitro*, similar to what has been reported in the most common neurodegenerative diseases such as Alzheimer's disease and ALS. Further studies on neuronal hyperexcitability in LRRK2 mutated neurons can be expanded to investigate whether this phenotype is manifested in other LRRK2 mutations (e.g. R1441C mutation) and whether it persists as neurons mature. We believe that new imaging techniques, computational approaches and iPSC technology taken together have great potential to facilitate identification of disease phenotypes, discovery of potential biomarkers and novel therapeutic strategies.

Acknowledgements

This project has received funding from the European Union's Horizon 2020 research and innovation programme under grant agreement No 668738. SH and ELM were supported by an Aides à la Formation-Recherche training allowance from Fonds National de la Recherche Luxembourg (ref. 10099424). JCS lab is supported by a CORE grant from the Fonds National de la Recherche.²

²All authors check acknowledgements please.

References

- [1] Andrew J Lees, John Hardy, and Tamas Revesz. Parkinson's disease. *The Lancet*, 373(9680):2055–2066, June 2009.
- [2] Rashed Abdullah, Indranil Basak, Ketan S. Patil, Guido Alves, Jan Petter Larsen, and Simon Geir MÅyller. Parkinson's disease and age: The obvious but largely unexplored link. *Experimental Gerontology*, 68:33–38, August 2015.
- [3] D. James Surmeier and Paul T. Schumacker. Calcium, Bioenergetics, and Neuronal Vulnerability in Parkinson's Disease. *Journal of Biological Chemistry*, 288(15):10736–10741, April 2013.
- [4] Arianna Bellucci, Nicola Biagio Mercuri, Annalena Venneri, Gaia Faustini, Francesca Longhena, Marina Pizzi, Cristina Missale, and PierFranco Spano. Review: Parkinson's disease: from synaptic loss to connectome dysfunction. *Neuropathology and Applied Neurobiology*, 42(1):77–94, February 2016.
- [5] Shankar J. Chinta and Julie K. Andersen. Dopaminergic neurons. *The International Journal of Biochemistry & Cell Biology*, 37(5):942–946, May 2005. 00102.
- [6] David C. SchÅúndorf, Massimo Aureli, Fiona E. McAllister, Christopher J. Hindley, Florian Mayer, Benjamin Schmid, S. Pablo Sardi, Manuela Valsecchi, Susanna Hoffmann, Lukas Kristoffer Schwarz, Ulrike Hedrich, Daniela Berg, Lamy S. Shihabuddin, Jing Hu, Jan Pruzsak, Steven P. Gygi, Sandro Sonnino, Thomas Gasser, and Michela Deleidi. iPSC-derived neurons from GBA1-associated Parkinson's disease patients show autophagic defects and impaired calcium homeostasis. *Nature Communications*, 5, June 2014.
- [7] Patricia MuÃoz, Sandro Huenchuguala, Irmgard Paris, and Juan Segura-Aguilar. Dopamine Oxidation and Autophagy. *Parkinson's Disease*, 2012, 2012.
- [8] Johannes Meiser, Daniel Weindl, and Karsten Hiller. Complexity of dopamine metabolism. *Cell Communication and Signaling : CCS*, 11:34, May 2013.

- [9] Christine Klein and Michael G. Schlossmacher. Parkinson disease, 10 years after its genetic revolution: multiple clues to a complex disorder. *Neurology*, 69(22):2093–2104, November 2007. 00175.
- [10] Hardy J. Rideout and Leonidas Stefanis. The neurobiology of LRRK2 and its role in the pathogenesis of Parkinson’s disease. *Neurochemical Research*, 39(3):576–592, 2014.
- [11] Un-Beom Kang and Jarrod A. Marto. Leucine-rich repeat kinase 2 and Parkinson’s disease. *PROTEOMICS*, pages n/a–n/a, December 2016.
- [12] Vera Dias, Eunsung Junn, and M. Maral Mouradian. The Role of Oxidative Stress in Parkinson’s Disease. *Journal of Parkinson’s disease*, 3(4):461–491, 2013.
- [13] Heather Mortiboys, Krisztina K. Johansen, Jan O. Aasly, and Oliver Bandmann. Mitochondrial impairment in patients with Parkinson disease with the G2019s mutation in LRRK2. *Neurology*, 75(22):2017–2020, November 2010.
- [14] Mark R. Cookson. LRRK2 Pathways Leading to Neurodegeneration. *Current Neurology and Neuroscience Reports*, 15(7):1–10, May 2015.
- [15] Brent J. Ryan, Selim Hoek, Edward A. Fon, and Richard Wade-Martins. Mitochondrial dysfunction and mitophagy in Parkinson’s: from familial to sporadic disease. *Trends in Biochemical Sciences*, 40(4):200–210, April 2015.
- [16] M. Ferreira and J. Massano. An updated review of Parkinson’s disease genetics and clinicopathological correlations. *Acta Neurologica Scandinavica*, pages n/a–n/a, June 2016. 00001.
- [17] Lauren R. Kett and William T. Dauer. Leucine-Rich Repeat Kinase 2 for Beginners: Six Key Questions. *Cold Spring Harbor Perspectives in Medicine*, 2(3), March 2012.
- [18] Lorraine V. Kalia, Anthony E. Lang, Lili-Naz Hazrati, Shinsuke Fujioka, Zbigniew K. Wszolek, Dennis W. Dickson, Owen A. Ross, Vivianna M. Van Deerlin, John Q. Trojanowski, Howard I. Hurtig, Roy N. Alcalay, Karen S. Marder, Lorraine N. Clark, Carles Gaig, Eduardo Tolosa, Javier Ruiz-Martínez, Jose F. Martí-Masso, Isidre Ferrer, Adolfo Láspez de Munain, Samuel M. Goldman, Birgitt Schijle, J. William Langston, Jan O. Aasly, Maria T. Giordana, Vincenzo Bonifati, Andreas Puschmann, Margherita Canesi, Gianni Pezzoli, Andre Maues De Paula, Kazuko Hasegawa, Charles Duyckaerts, Alexis Brice, A. Jon Stoessel, and Connie Marras. Clinical Correlations With Lewy Body Pathology in LRRK2-Related Parkinson Disease. *JAMA neurology*, 72(1):100–105, January 2015.
- [19] Rebecca Wallings, Claudia Manzoni, and Rina Bandopadhyay. Cellular processes associated with LRRK2 function and dysfunction. *The Febs Journal*, 282(15):2806–2826, July 2015.
- [20] Ciro Iaccarino, Claudia Crosio, Carmine Vitale, Giovanna Sanna, Maria Teresa Carrà, and Paolo Barone. Apoptotic mechanisms in mutant LRRK2-mediated cell death. *Human Molecular Genetics*, 16(11):1319–1326, June 2007.
- [21] David MacLeod, Julia Dowman, Rachel Hammond, Thomas Leete, Keiichi Inoue, and Asa Abeliovich. The Familial Parkinsonism Gene LRRK2 Regulates Neurite Process Morphology. *Neuron*, 52(4):587–593, November 2006.
- [22] Laurence Borgs, Elise Peyre, Philippe Alix, Kevin Hanon, Benjamin Grobarczyk, Juliette D. Godin, Audrey Purnelle, Nathalie Krusy, Pierre Maquet, Philippe Lefebvre, Vincent Seutin, Brigitte Malgrange, and Laurent Nguyen. Dopaminergic neurons differentiating from LRRK2 G2019s induced pluripotent stem cells show early neuritic branching defects. *Scientific Reports*, 6, September 2016.
- [23] Sharon L. Chan and Eng-King Tan. Targeting LRRK2 in Parkinson’s disease: An update on recent developments. *Expert Opinion on Therapeutic Targets*, April 2017.
- [24] Peter Reinhardt, Michael Glatza, Kathrin Hemmer, Yaroslav Tsytsyura, Cora S. Thiel, Susanne Häußing, Sören Moritz, Juan A. Parga, Lydia Wagner, Jan M. Bruder, Guangming Wu, Benjamin Schmid, Albrecht Röpke, Jürgen Klingauf, Jens C. Schwamborn, Thomas Gasser, Hans R. Schuler, and Jared Sternecker. Derivation and Expansion Using Only Small Molecules of Human Neural

- Progenitors for Neurodegenerative Disease Modeling. *PLoS ONE*, 8(3):e59252, March 2013.
- [25] Anna-Lena Hillje and Jens C Schwamborn. Utilization of stem cells to model Parkinson's disease – current state and future challenges. *Future Neurology*, 11(2):171–186, April 2016.
- [26] Ha-Nam Nguyen, Blake Byers, Branden Cord, Aleksandr Shcheglovitov, James Byrne, Prachi Gujar, Kehkooi Kee, Birgitt SchÄijle, RicardoÄE. Dolmetsch, William Langston, TheoÄD. Palmer, and ReneeÄReijo Pera. LRRK2 Mutant iPSC-Derived DA Neurons Demonstrate Increased Susceptibility to Oxidative Stress. *Cell Stem Cell*, 8(3):267–280, March 2011.
- [27] Laurie H. Sanders, JosÄ'e LaganiÄ're, Oliver Cooper, Sally K. Mak, B. Joseph Vu, Y. Anne Huang, David E. Paschon, Malini Vangipuram, Ramya Sundararajan, Fyodor D. Urnov, J. William Langston, Philip D. Gregory, H. Steve Zhang, J. Timothy Greenamyre, Ole Isacson, and Birgitt SchÄijle. LRRK2 mutations cause mitochondrial DNA damage in iPSC-derived neural cells from ParkinsonÄ's disease patients: Reversal by gene correction. *Neurobiology of disease*, 62, February 2014.
- [28] J. A. Connor. Digital imaging of free calcium changes and of spatial gradients in growing processes in single, mammalian central nervous system cells. *Proceedings of the National Academy of Sciences of the United States of America*, 83(16):6179–6183, August 1986. 00305.
- [29] Santripati Khandai, Ronald A. Siegel, and Sidhartha S. Jena. Probing the microstructure of hydrogels using fluorescence recovery after photobleaching. 2013.
- [30] K Michel, M Michaelis, G Mazzuoli, K Mueller, P Vanden Berghe, and M Schemann. Fast calcium and voltage-sensitive dye imaging in enteric neurones reveal calcium peaks associated with single action potential discharge. *The Journal of Physiology*, 589(Pt 24):5941–5947, December 2011.
- [31] Mayumi Tada, Atsuya Takeuchi, Miki Hashizume, Kazuo Kitamura, and Masanobu Kano. A highly sensitive fluorescent indicator dye for calcium imaging of neural activity in vitro and in vivo. *European Journal of Neuroscience*, 39(11):1720–1728, June 2014.
- [32] Christoph Stosiek, Olga Garaschuk, Knut Holthoff, and Arthur Konnerth. In vivo two-photon calcium imaging of neuronal networks. *Proceedings of the National Academy of Sciences of the United States of America*, 100(12):7319–7324, June 2003.
- [33] Jason N. D. Kerr, David Greenberg, and Fritjof Helmchen. Imaging input and output of neocortical networks in vivo. *Proceedings of the National Academy of Sciences of the United States of America*, 102(39):14063–14068, September 2005.
- [34] E. Lucumi Moreno, S. Hachi, K. Hemmer, S. J. Trietsch, A. S. Baumuratov, T. Hankemeier, P. Vulto, J. C. Schwamborn, and R. M. T. Fleming. Differentiation of neuroepithelial stem cells into functional dopaminergic neurons in 3d microfluidic cell culture. *Lab on a Chip*, 15(11):2419–2428, May 2015.
- [35] Pieter Vanden Berghe, Jan Tack, and Werend Boesmans. Highlighting Synaptic Communication in the Enteric Nervous System. *Gastroenterology*, 135(1):20–23, July 2008.
- [36] Gayane Aramuni and Oliver Griesbeck. Chronic calcium imaging in neuronal development and disease. *Experimental Neurology*, 242:50–56, April 2013.
- [37] Susanne Reichinnek, Alexandra von Kameke, Anna M. Hagenston, Eckehard Freitag, Fabian C. Roth, Hilmar Bading, Mazahir T. Hasan, Andreas Draguhn, and Martin Both. Reliable optical detection of coherent neuronal activity in fast oscillating networks in vitro. *NeuroImage*, 60(1):139–152, March 2012.
- [38] Tapan P. Patel, Karen Man, Bonnie L. Firestein, and David F. Meaney. Automated quantification of neuronal networks and single-cell calcium dynamics using calcium imaging. *Journal of Neuroscience Methods*, 243:26–38, March 2015.
- [39] Ilya Valmianski, Andy Y. Shih, Jonathan D. Driscoll, David W. Matthews, Yoav Freund, and David Kleinfeld. Automatic Identification of Fluorescently Labeled Brain Cells for Rapid Functional Imaging. *Journal of Neurophysiology*, 104(3):1803–1811, September 2010.

- [40] Ryuichi Maruyama, Kazuma Maeda, Hajime Moroda, Ichiro Kato, Masashi Inoue, Hiroyoshi Miyakawa, and Toru Aonishi. Detecting cells using non-negative matrix factorization on calcium imaging data. *Neural Networks*, 55:11–19, July 2014.
- [41] Eran A. Mukamel, Axel Nimmerjahn, and Mark J. Schnitzer. Automated analysis of cellular signals from large-scale calcium imaging data. *Neuron*, 63(6):747–760, September 2009.
- [42] F. Diego, S. Reichinnek, M. Both, and F.A. Hamprecht. Automated identification of neuronal activity from calcium imaging by sparse dictionary learning. In *2013 IEEE 10th International Symposium on Biomedical Imaging (ISBI)*, pages 1058–1061, April 2013.
- [43] Rafael Yuste, Jason MacLean, Joshua Vogelstein, and Liam Paninski. Imaging Action Potentials with Calcium Indicators. *Cold Spring Harbor Protocols*, 2011(8):pdb.prot5650, August 2011.
- [44] Joshua T. Vogelstein, Brendon O. Watson, Adam M. Packer, Rafael Yuste, Bruno Jedynek, and Liam Paninski. Spike Inference from Calcium Imaging Using Sequential Monte Carlo Methods. *Biophysical Journal*, 97(2):636–655, July 2009. 00090.
- [45] Joshua T. Vogelstein, Adam M. Packer, Timothy A. Machado, Tanya Sippy, Bakdash Babadi, Rafael Yuste, and Liam Paninski. Fast Nonnegative Deconvolution for Spike Train Inference From Population Calcium Imaging. *Journal of Neurophysiology*, 104(6):3691–3704, December 2010.
- [46] Benjamin F. Grewe, Dominik Langer, Hans-Jürg Kasper, Björn M. Kampa, and Fritjof Helmchen. High-speed in vivo calcium imaging reveals neuronal network activity with near-millisecond precision. *Nature Methods*, 7(5):399–405, May 2010. 00151.
- [47] Jon Onativia, Simon R Schultz, and Pier Luigi Dragotti. A finite rate of innovation algorithm for fast and accurate spike detection from two-photon calcium imaging. *Journal of neural engineering*, 10(4):046017, August 2013. 00016 PMID: 23860257.
- [48] Julien Mairal, Francis Bach, Jean Ponce, and Guillermo Sapiro. Online Dictionary Learning for Sparse Coding. In *Proceedings of the 26th Annual International Conference on Machine Learning, ICML '09*, pages 689–696, New York, NY, USA, 2009. ACM. 01223.
- [49] Eftychios A. Pnevmatikakis, Daniel Soudry, Yuanjun Gao, Timothy A. Machado, Josh Merel, David Pfau, Thomas Reardon, Yu Mu, Clay Lacefield, Weijian Yang, Misha Ahrens, Randy Bruno, Thomas M. Jessell, Darcy S. Peterka, Rafael Yuste, and Liam Paninski. Simultaneous Denoising, Deconvolution, and Demixing of Calcium Imaging Data. *Neuron*, 89(2):285–299, January 2016.
- [50] Mahsa Moein. *Dissecting the crosstalk between intracellular calcium signalling and mitochondrial metabolism*. PhD thesis, University of Luxembourg, May 2017.
- [51] Weijian Yang and Rafael Yuste. In vivo imaging of neural activity. *Nature Methods*, 14(4):349–359, April 2017.
- [52] Christine Grienberger and Arthur Konnerth. Imaging Calcium in Neurons. *Neuron*, 73(5):862–885, March 2012.
- [53] Anna S. Monzel, Lisa M. Smits, Kathrin Hemmer, Siham Hachi, Edinson Lucumi Moreno, Thea van Wuellen, Javier Jarazo, Jonas Walter, Inga BrÄijggemann, Ibrahim Boussaad, Emanuel Berger, Ronan M.T. Fleming, Silvia Bolognin, and Jens C. Schwamborn. Derivation of Human Midbrain-Specific Organoids from Neuroepithelial Stem Cells. *Stem Cell Reports*, 8(5):1144–1154, April 2017. 00003.
- [54] Sean M. Wu and Konrad Hochedlinger. Harnessing the potential of induced pluripotent stem cells for regenerative medicine. *Nature Cell Biology*, 13(5):497–505, May 2011. 00374.
- [55] Salvatore J. Cherra III, Erin Steer, Aaron M. Gusdon, Kirill Kiselyov, and Charleen T. Chu. Mutant LRRK2 Elicits Calcium Imbalance and Depletion of Dendritic Mitochondria in Neurons. *The American Journal of Pathology*, 182(2):474–484, February 2013.
- [56] Maria D. Cirnaru, Antonella Marte, Elisa Belluzzi, Isabella Russo, Martina Gabrielli, Francesco Longo, Ludovico Arcuri, Luca Murru, Luigi Bubacco, Michela Matteoli, Ernesto Fedele, Carlo Sala, Maria Passafaro, Michele Morari, Elisa Greggio, Franco Onofri, and Giovanni Piccoli. LRRK2 kinase activity regulates synaptic vesicle trafficking and

neurotransmitter release through modulation of LRRK2 macro-molecular complex. *Frontiers in Molecular Neuroscience*, 7, May 2014.

- [57] Marc Aurel Busche and Arthur Konnerth. Neuronal hyperactivity – A key defect in Alzheimer’s disease? *BioEssays*, 37(6):624–632, June 2015. 00024.
- [58] Zuzana ÅšÅškovÅš, Daniel Justus, Hiroshi Kaneko, Detlef Friedrichs, Niklas Henneberg, Tatjana Beutel, Julika Pitsch, Susanne Schoch, Albert Becker, Heinz vonÅšder-ÅšKammer, and Stefan Remy. Dendritic Structural Degeneration Is Functionally Linked to Cellular Hyperexcitability in a Mouse Model of Alzheimer’s Disease. *Neuron*, 84(5):1023–1033, December 2014.
- [59] Laure Verret, Edward O. Mann, Giao B. Hang, Albert M. I. Barth, Inma Cobos, Kaitlyn Ho, Nino Devidze, Eliezer Masliah, Anatol C. Kreitzer, Istvan Mody, Lennart Mucke, and Jorge J. Palop. Inhibitory Interneuron Deficit Links Altered Network Activity and Cognitive Dysfunction in Alzheimer Model. *Cell*, 149(3):708–721, April 2012. 00308.
- [60] Brian J. Wainger, Evangelos Kiskinis, Cassidy Mellin, Ole Wiskow, Steve S.W. Han, Jackson Sandoe, Numa P. Perez, Luis A. Williams, Seungkyu Lee, Gabriella Boulting, James D. Berry, Robert H. Brown, Merit E. Cudkowicz, Bruce P. Bean, Kevin Eggan, and Clifford J. Woolf. Intrinsic Membrane Hyperexcitability of ALS Patient-Derived Motor Neurons. *Cell reports*, 7(1):1–11, April 2014. 00000.
- [61] Carlos Cepeda, Nanping Wu, VÅšronique M. AndrÅš, Damian M. Cummings, and Michael S. Levine. The corticostriatal pathway in Huntington’s disease. *Progress in Neurobiology*, 81(5):253–271, April 2007. 00218.

6. Conclusions and outlook

This Chapter specifies the main contributions, some of the blank and blind spots of the conducted research and delineates perspective on future directions.

In order to achieve the first goal of this thesis, we assembled a fully automated cell culture observatory called the Pelican. The platform was optimised for the long-term cell culture maintenance of neurons inside 3D microfluidic devices. However, the system allows the automation of seeding, feeding and other cell culture processes in order to maintain cell lines in any SBS plate. The two most important design decisions of the Pelican were the liquid handler and the robot. First, we aimed at designing a modular automated platform that was flexible in terms of the functions it can accomplish. Second, we also aimed at giving ourselves the flexibility to improve the system in the future. In this regard, we carefully selected the robotic system, the pipetting technologies and the techniques to integrate all the components of the system into a single plant.

As a result, in the Pelican, a four-axis (X-Y-Z- θ) gantry robot in combination with a gripper were chosen. This was attached to the ceiling of the housing through rails that allow the movement of the robotic arm in the four axes. This maximised the modular capacity of the Pelican. In terms pipetting technology, a Z-Excursion Universal Sampler (with compressed O-ring expansion tip technology) module which combines the precision of contact dispensing and the versatility of noncontact dispensing was chosen. Despite its shortcomings, the contact dispensing function of the ZEUS is especially useful for microfluidic cell culture where very small volumes must be dispensed. In addition, the non-contact dispensing helps to make sure that the dispensed media is bubble free. This is very important as we have observed in some bioreactors, the presence of bubbles in one of the two lanes with low flow rate non-contact dispensing. These bubbles can impede the flow of fresh media, which could ultimately starve the cells. However, the use of the contact dispensing did not come without its set of restrictions mainly the fact that microfluidic systems made from glass bottoms such as the OrganoPlate, are very fragile. The contact between the tip and the bottom of the well usually leads to cracking of the glass. In addition, despite the precision of the ZEUS module, the

dispensing of media is very time consuming which require a trade-off between the time it takes to change the media versus leaving cells exposed to the flow of air from the sterile environment. The effect of which have not been fully investigated yet as part of this thesis.

We successfully used the system to differentiate human neuroepithelial stem cells into dopaminergic neurons in a three-dimensional microfluidic device. Cell culture health through regular automated image acquisition and time-series imaging assays were implemented. All these assays are very important to assess the quality of neuronal differentiation.

In order to address the second goal of this thesis of better understanding the physical properties of the extracellular matrix, Matrigel, used to embed human neuroepithelial stem cells and differentiate them into dopaminergic neurons, a rheometer was used to determine the viscosity as a function of shear stress and temperature. First, it was found that Matrigel was a non-Newtonian fluid for all temperatures. In other words, the viscosity of Matrigel changes with the applied shear stress for all temperatures. Second, Matrigel is a shear thinning fluid for all temperatures, which means that the viscosity of Matrigel decreases as the applied shear stress increases. Third, below 6°C, Matrigel fully behaved as a liquid. Above 6°C, Matrigel has a more solid like behaviour. At 6°C, under shear stress, the energy is evenly distributed between increasing the heat content and the elastic deformation of the sample. Therefore, 6°C is transition temperature above which Matrigel starts forming solid structures. Finally, it was found that the most optimum seeding temperature of human neuroepithelial stem cells into the microfluidic device is 8°C, which maximized the plateau at the centre of the culture lane, hence minimising shear stress on cells, while also allowing the flow of Matrigel in the culture lane. However, there is a clear limitation of this study in the fact that Matrigel is a naturally occurring substance, and its rheological properties are very much batch specific. It means that two batches of Matrigel have a high probability of having slightly different properties. This makes predicting the exact optimal temperature of loading nearly impossible. Therefore, a study where enough batch replicates are utilised to determine the average standard deviation of the rheological properties of Matrigel is such a crucial next step to this work. In doing so, the range of optimum loading temperatures could be determined.

For the completion of the third goal, we applied computational fluid dynamics to model the perfusion of existing bioreactor designs with culture medium in order to exactly quantify the

ideal media and rate of media flow for maintenance of human induced pluripotent stem cell derived neurons in culture. The fluid dynamic simulation was coupled with a similarity model of cerebral flow to optimise the design of a novel 3D microfluidic device that allows to mimic cerebral dynamic conditions. The design was slightly modified to allow the manufacturing of a plate that has 64 of such microfluidic bioreactors. The plate was tested in the differentiation of human neuroepithelial stem cells into dopaminergic neurons. Furthering this work would require looking into other microfluidic designs that are not based on phaseguide technology and not limited to the geometry of the OrganoPlate. In doing so, a new microfluidic system could be built within a clear design parameter of prolonging the flow of media at a given flow rate optimum for dopaminergic neuronal differentiation.

There is great deal of potential in combining the rheological study of Matrigel with the modelling of media to better understand the dynamic and transport interactions between these two substances during differentiation. The first step would be to run a small molecules' experiment to investigate the transport of nutrients, through diffusion, and determine the diffusion coefficient of small molecules into Matrigel. In doing so, we will be able to better refine the target flow rate of media based on the true supply requirements of the human neuroepithelial stem cells in the differentiation into mid brain like dopaminergic neurons using small molecules.

We envisage the use of the optimised microfluidic device (Goal 3) to seed cells at the optimum conditions (Goal 2) in the automated cell culture (Goal 1) to enable comprehensive phenotyping of large, parallel sets of personalised, in vitro, midbrain-specific, dopaminergic neuronal models of Parkinson's disease. By integrating the data generated with a generic mechanistic computational model of the underlying biochemical network of a dopaminergic neuron, each personalised computational model then becomes a coherent representation of our information about the cell autonomous characteristics of Parkinson's disease in each patient. Such personalised computational models, and thereby the corresponding patients, are then amenable to stratification with a range of powerful stratification tools. Stratification based on personalised computational models of the personalised data is statistically superior to stratification based on the personalised data alone as the former explicitly incorporates the wealth of prior biochemical information known about midbrain dopaminergic neurons.

The aetiopathogenic stratification of Parkinson's disease patients, for instance into mitochondrial vs non-mitochondrial Parkinson's disease is an important first step toward targeting the development of therapies toward the underlying dysfunction that is present. Ultimately, this will accelerate the translation of basic biomedical knowledge from the laboratory to the therapies with clinical impact.

7. Supplementary material for Chapter 2

**Determination of the rheological properties of Matrigel for
optimum seeding**

K. I. W. Kane, E. Lucumi Moreno, C. M. Lehr, S. Hachi, R. Dannert, R. Sanctuary, C. Wagner,
R.M.T. Fleming and J. Baller

Supplementary Material

Supplementary information

The following file is provided as supplementary information:

- *BeadsFlowingInMatrigel.avi*: movie of the PIV measurement

Below please find a paragraph describing the combination of PIV and rheological data.

Combination of PIV and rheological data

(equation numbers correspond to the numbers in the manuscript)

The pressure difference Δp of a Newtonian fluid (viscosity η) flowing at a volume flowrate Q across a tube with length L and diameter R is given by the Hagen-Poiseuille equation¹:

$$\Delta p = \frac{8\eta L Q}{\pi R^4} (*)$$

The velocity profile for Newtonian liquids is given by^{1,2}:

$$v = \frac{2Q}{\pi R^2} \left(1 - \frac{r^2}{R^2}\right) (2)$$

which corresponds to a parabolic profile with a maximum velocity of $v_{\max} = \frac{2Q}{\pi R^2}$.

For power-law liquids, the velocity profile reads²:

$$v = \frac{\sigma_{\text{wall}}^{\frac{1}{n}} R^{\frac{1}{n}+1} - |r|^{\frac{1}{n}+1}}{kR} (3) \text{ with } \sigma_{\text{wall}} = \frac{\Delta p R}{2L} (4)$$

The velocity profile recorded during the PIV measurements (Fig. 7) is now fitted with equation (3) and the obtained velocity curve is derived with respect to the time in order to obtain the shear rates (Fig. 8).

The microfluidic device was filled with a pipette and the capillary forces which are the cause for the flow correspond to a pressure difference which can be calculated using eq. (4).

Equation (3) (with eq. 4) contains the pressure difference Δp and the parameters n and k of the power law describing the fluid. Since we now these parameters from the rheological experiments (Table 1), we can now calculate shear rate profiles at different temperatures (Fig. 8) for which we do not have PIV data. The curves can be calculated by assuming that Δp is the same for all temperatures or by assuming that the volume flowrate Q is constant (using eq. (*)).

1. H. A. Barnes, J. F. Hutton and K. Walters, *An introduction to rheology*, Elsevier, 1989.
2. E. J. Hinch, *Lecture Notes Woods Hole GFD Summer School*, 2003, **1**, 1-19.

8. Supplementary material for Chapter 3

**Passive controlled flow for neuronal cell culture in 3D
microfluidic devices**

Khalid I.W. Kane, Javier Jarazo, Edinson Lucumi Moreno, Paul Vulto Ronan M.T. Fleming,
Bas Trietsch, Jens Schwamborn

Supplementary Material

```

%created by Khalid Kane
%Fluid flow analytical model %Hydrostatic model
%-----
%Fluid parameters in SI units
g = 9.81; %g is the gravitation field in m/s2
ro = 1000; %density of water in kg/m3
mu = 0.6913*10^-3; %viscosity of water at 3°C in Pa.s %mu = 1.3*10^-3;
%%viscosity of water at 10°C in Pa.s
%-----
%Add more wells to the medium inlet and outlet in equal proportions, max 10
%wells could be added on each sides
%Change k(a positive integer from 0 to 10 wells, 0 being the current design format)
k=0;
%-----
%Medium lane parameters in SI units
we1_i=0.0045*(k+1);
%loading well width (assume it is a square) in m
we2_i=0.0045;
%loading well width (assume it is a square) in m
l_i = (9.2*10^-3)+(k*2*we2_i);
%length of medium channel in m
%-----
%Medium lane parameters in SI units
w_i = 200*10^-6;
%width of the perfusion lane in m
%-----
d1_i = 120*10^-6;
%height of the channel in both medium and gel channels in m
%-----
vl_i=d1_i*((w_i*l_i));
%total volume of the perfusion lane in terms of space available in m3
%-----
%media loaded into the medium inlet and outlet, can play with these values
%to keep the initial pressure constant while increasing the loading wells
v1_i=80*10^-9*(1+k);
%loaded volume in the first well in m3
v2_i=40*10^-9*(1+k);
%loaded volume in the second well in m3
ca_i=we1_i*we2_i;
%loading well cross-section area
z1_i=(v1_i-vl_i)/ca_i;
%Initial height in first well
z2_i=(v2_i)/ca_i;
%Intial height in second well
h_i=z1_i-z2_i;
%intial driving height
r_i=(12*mu*l_i)/((w_i*(d1_i^3))*(1-((0.630*d1_i)/w_i)));
%hydrodynamic resistance rectangular cross-section
%width w and height h, expression valid when h<w
%Applied pressure
p_i=ro*g*h_i;
dt=1;
%s is the time step can be adjusted if we want more accuracy, but will take longer to
compute
for n=1:86401

```

```

t(n)=n*dt;
q_i(n)=p_i(n)/r_i;
dh_i=q_i(n)*dt/ca_i;
p_i(n+1)=p_i(n)-2*ro*g*dh_i;
%equivalent flow rate
end

%Change k(a positive integer from 0 to 10 wells, 0 being the current design format)
k=1;
%-----
%Medium lane parameters in SI units
we1=0.0045*(k+1);
%loading well width (assume it is a square) in m
we2=0.0045;
%loading well width (assume it is a square) in m
l_p=4.395*10^-3;
%length of phaseguide
l_r = (4.805*10^-3)+(k*2*we2);
%length of medium channel in m
l=l_p+l_r;
%-----
%Medium lane parameters in SI units
w = 100*10^-6;
%width of the perfusion lane (phaseguide section) in m
%-----
d1 = 50*10^-6;
%height of the channel in medium lan (phaseguide section) in m
%-----
w_r = 100*10^-6;
%width of the perfusion lane (phaseguide section) in m
%-----
d1_r = 50*10^-6;
%height of the channel in medium lan (phaseguide section) in m
%-----
r_p=(12*mu*l_p)/((w*(d1^3))*(1-((0.630*d1)/w)));
%hydraulic resistance of phaseguide section of medium lane
r_r=(12*mu*l_r)/((w_r*(d1_r^3))*(1-((0.630*d1_r)/w_r)));
%hydraulic resistance for the remaining section of the medium lane
r=r_p+r_r;
%total hydraulic resistance

v1=d1*((w*l));
%total volume of the perfusion lane in terms of space available in m3
%-----
%media loaded into the medium inlet and outlet, can play with these values
%to keep the initial pressure constant while increasing the loading wells
v1=118*10^-9*(1+k);
%loaded volume in the first well in m3
v2=10*10^-9*(1+k);
%loaded volume in the second well in m3
ca=we1*we2;
%loading well cross-section area
z1=(v1-v1)/ca;
%Initial height in first well
z2=(v2)/ca;

```

```

%Intial height in second well
h=z1-z2;
%intial driving height
% r=(12*mu*1)/((w*(d1^3))*(1-((0.630*d1)/w)));
%hydrodynamic resistance rectangular cross-section
%width w and height h, expression valid when h<w)
p=ro*g*h;
%Applied pressure
dt=1;
% s is the time step can be adjusted if we want more accuracy, but will take longer to
compute
for n=1:86401
t(n)=n*dt;
q(n)=p(n)/r;
dh=q(n)*dt/ca;
p(n+1)=p(n)-2*ro*g*dh;
%equivalent flow rate
end
graph=plot(t/3600,q_i*1000*1000*1000*3600,t/3600,q*1000*1000*1000*3600);
graph(1).LineWidth = 1;
graph(2).LineWidth = 1;
xlabel('Time (hour)', 'FontSize',18, 'FontWeight', 'bold', 'Color', 'black');
ylabel('Average flow rate (microlitre/hour)', 'FontSize',
18, 'FontWeight', 'bold', 'Color', 'black'); ;
title('Average flow rate of the media in the medium lane', 'FontSize',
20, 'FontWeight', 'bold', 'Color', 'r');
legend('Old design', 'New Design')
graph=plot(t/3600,q*1000*1000*1000*3600);
graph(1).LineWidth = 1;
xlabel('Time (hour)', 'FontSize',18, 'FontWeight', 'bold', 'Color', 'black');
ylabel('Average flow rate (microlitre/hour)', 'FontSize',
18, 'FontWeight', 'bold', 'Color', 'black');
%title('Average flow rate of the media in the medium lane', 'FontSize',
20, 'FontWeight', 'bold', 'Color', 'r');

```

9. Supplementary material for Chapter 4

Automated microfluidic cell culture of stem cell derived
dopaminergic neurons

Khalid I.W. Kane, Edinson Lucumi Moreno, Siham Hachi, Moriz Walter
Javier Jarazo, Thomas Hankemeier, Paul Vulto, Jens C. Schwamborn,
Martin Thoma, Ronan M.T. Fleming

Supplementary Material

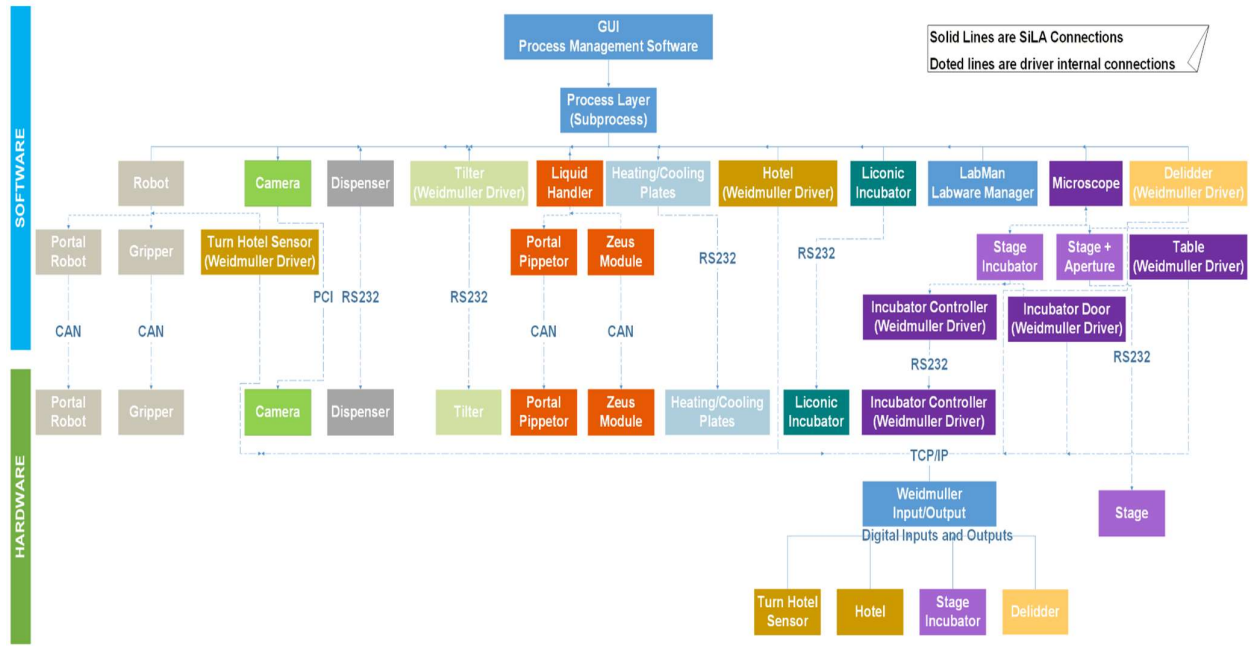


Figure S1: Pelican hardware and software control architecture. Standard on arrow = type of physical connection between a device and the computer. CAN = Controller Area Network. PCI = Peripheral Component Interconnect. RS232 = Recommend Standard number 232. TCP/IP = Transmission Control Protocol/Internet Protocol.

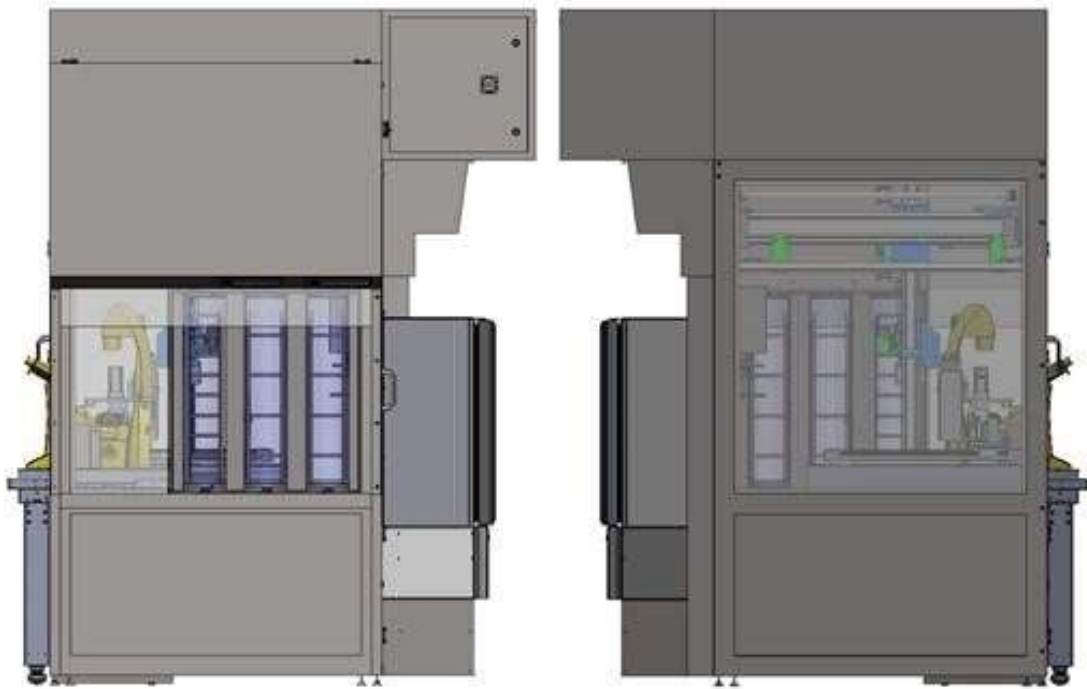
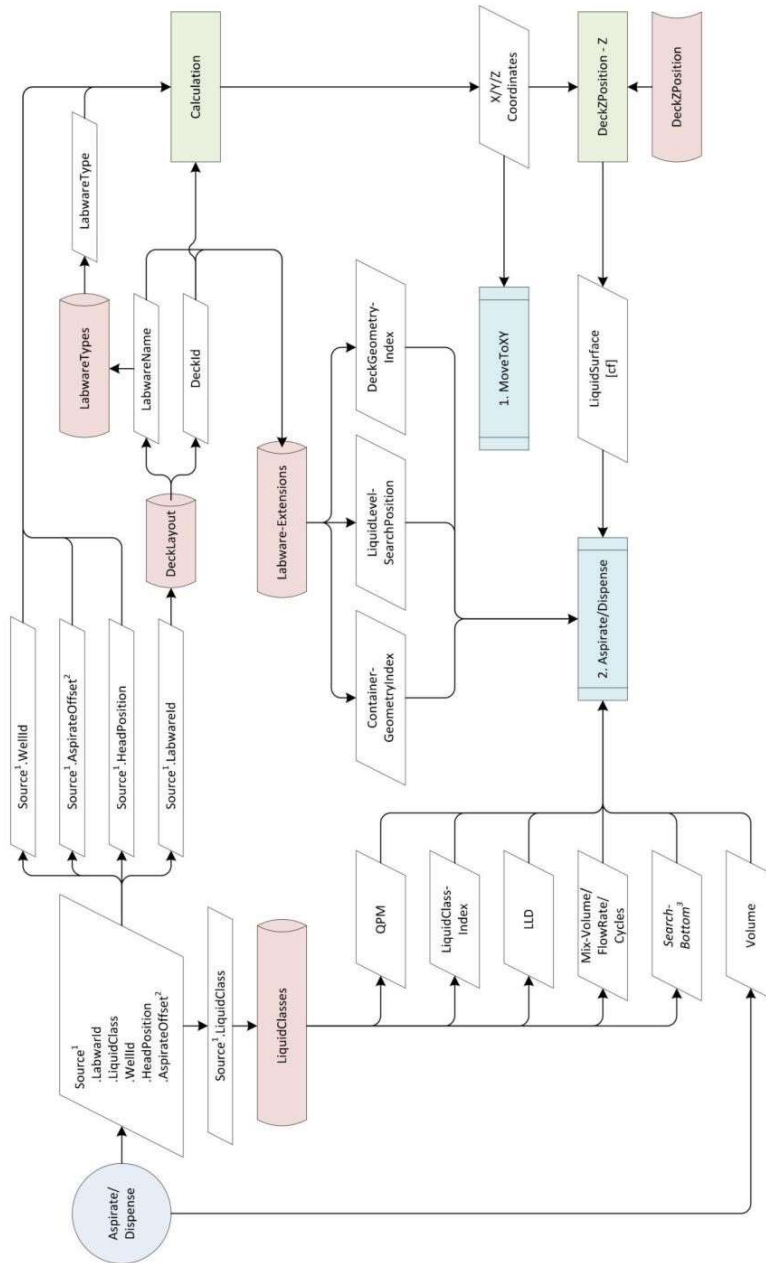


Figure S2: Left and right views of Pelican with housing illustrating the manual work bench and hotels (Left) that connect the Pelican to the outside world and the automated liquid handling station (Right).



- 1: Destination in Dispense
- 2: DispenseOffset in Dispense
- 3: Only in Dispense

Figure S3: Liquid handler data model for pipetting protocols. Blue (physical action of pipette), red (passive action of pipette: reading from liquid-handler database) and green (passive action of pipette: determining well geometry). QPM=Qualitative Pipette Monitoring. LLD=Liquid Level Detection. The automated pipetting follows this order: pickup a disposable tip, detect the liquid level, aspirate liquid, dispense the liquid into the destination well and finally discard the tip.

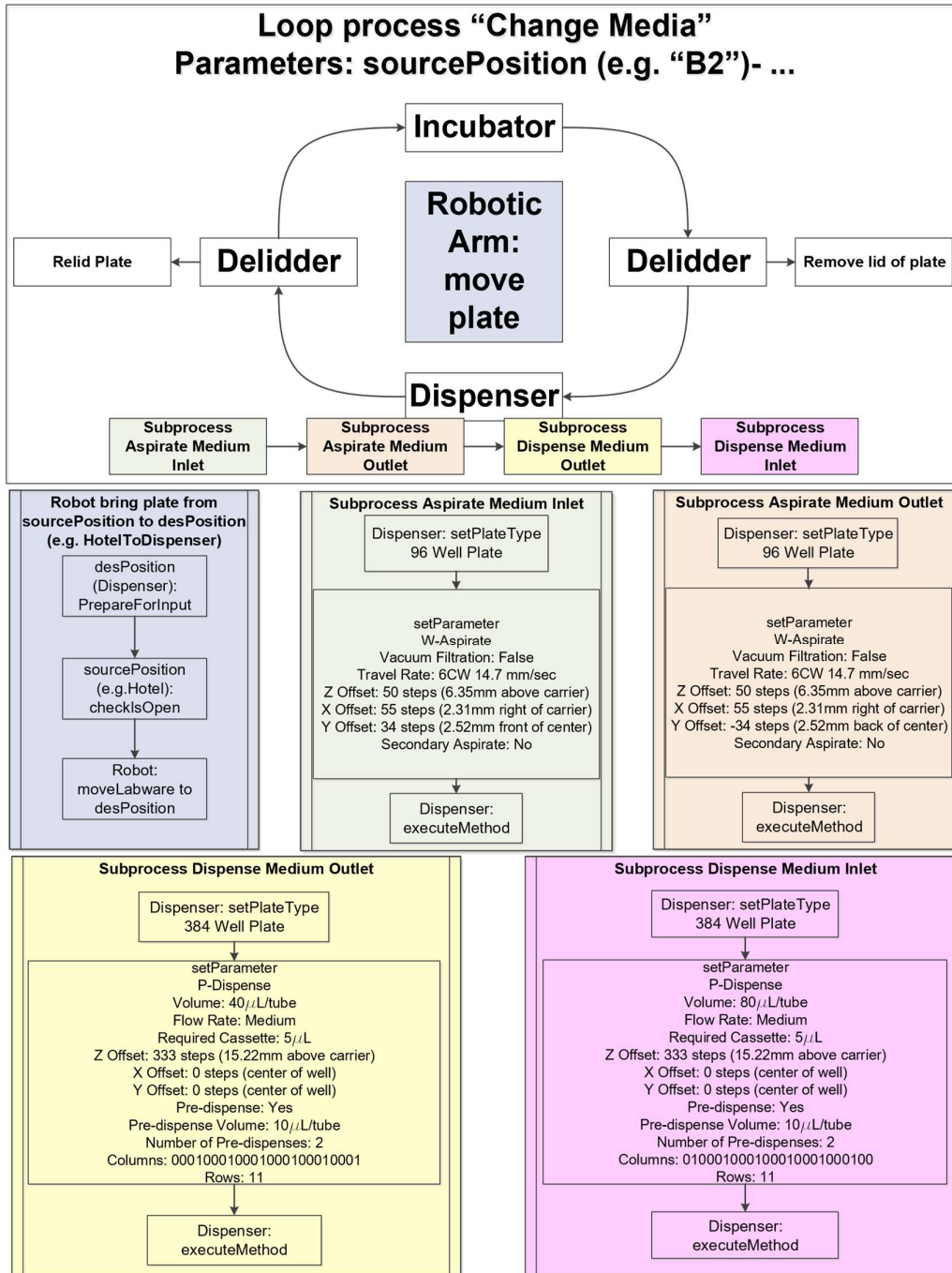


Figure S4: **Automated media change pipeline.** W = Washer, P = Peristaltic, 0 = Method not applied to column, 1 = Method applied to column, -1 = search position. Curved connection = Plate movement. Straight connection = Device specific method.

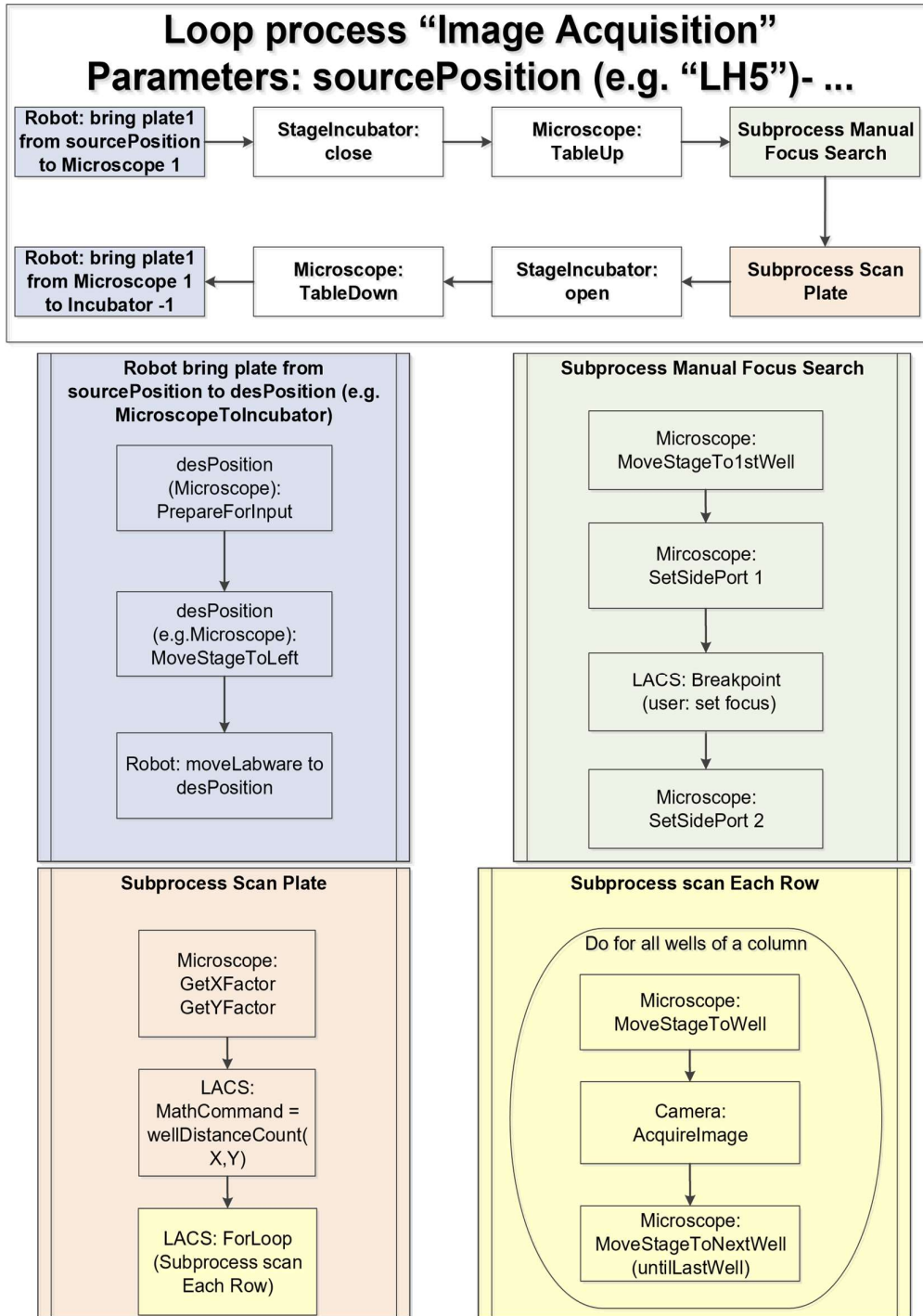


Figure S5: Automated image acquisition pipeline. Abbreviations as in Figure S4.

Supplementary Experimental Procedures

Hardware

Housing

The sterile housing of the Pelican (Figure 6B) consists of a stainless steel frame support. The active components of the system, such as the dispenser, pipettor and de-lidder can be flexibly arranged on a perforated stainless steel work surface in any configuration compatible with accessibility via the four-axis gantry robot (Figure 6). This work surface is laterally bordered by an enclosure that guards against manual collision with any robotic moving parts. Large Plexiglas 360° viewing windows enable observation of enclosed processes. The passive components of the Pelican such as the control system, switch cabinets and a variable collection of waste containers (Figure 6B), are housed beneath the work surface.

Robot and grippers

A customised four-axis gantry robot (Festo GmbH & Co. KG, Karlsruhe, Germany) was incorporated and mounted at the top of the stainless steel frame support inside the housing. The robot is used to transport any Society for Biomolecular Screening (SBS) format plate (ANSI SLAS 4-2004) and consumables by way of a gripper. The plates were processed at the individual stations, then transported by the robotic arm. The robot and the gripper perform all handling and transport functions of the platform that are not already covered by an individual device. Customised gripper jaws (Fraunhofer IPA, Fraunhofer Society, Stuttgart, Germany) were implemented in order to cover the multitude of plate formats with one gripper. Plates and carriers for consumables can be gripped and stacked by this robot.

Liquid-handler (Supplementary Video 3)

A pipettor transfers various reagents in and out of almost any plate types. Every pipetting step was executed via an air displacement pipetting arm (LiHa-Arm 4x, Hamilton Bonaduz AG, Bonaduz, Switzerland) with disposable tips similar to hand pipettes. Four pipetting

units (Z-Excursion Universal Sampler, Hamilton Bonaduz AG, Bonaduz, Switzerland) called ZEUS modules were mounted in a customised X-Y portal (Festo GmbH & Co. KG, Karlsruhe, Germany). Even though the liquid handling robot can move in the X-Y directions, it cannot transport plates. The transport of plates is realised via the four-axis gantry robot. The liquid handler is equipped with both a capacitive and a pressure liquid level detection system. The capacitive technology is used to detect the liquid level of conductive liquids, while the pressure based technology is for both conductive and non-conductive liquids. Each ZEUS module has an anti-droplet control technology preventing cross contamination from a leaking tip. The pipettor is used to execute precise (pipetting resolution of $\pm 0.1\mu\text{L}$) liquid handling steps. It is able to handle volumes from $1\mu\text{L}$ to $1000\mu\text{L}$ depending on the available tip sizes in the plant. Depending on volume and the liquid used, contact and non-contact dispensing is possible. The liquid handlers is equipped with 5 positions to hold racks of 96 tips each, a tilting module and 4 heating and cooling stations, the latter 2 are described below. A graphical user interface that follows a specific structure (see Figure S3) was implemented to write all pipetting protocols.

Tilter

A Multiflex Tilt Module (Kust, Hamilton Bonaduz AG, Bonaduz, Switzerland) was installed on the liquid handling deck, and is used to tilt SBS plates between a horizontal and a 10° degree incline to completely remove the liquid out of big wells.

Heating and cooling positions

Four CPAC Ultraflat & CPAC Microplate Inheco thermoblocks (INHECO Industrial Heating & Cooling GmbH, Planegg, Germany) units, each fitted with a Flat Bottom Adapter (7900016, INHECO Industrial Heating & Cooling GmbH) with positioning frame were installed on the deck of the pipettor as heating and cooling stations. They are used to control the temperature of four SBS plates (4°C - 80°C) during time consuming liquid handling protocols. The thermoblocks are controlled by a Multi TEC Control Unit (8900030, INHECO Industrial Heating & Cooling GmbH).

Liquid dispenser

A dispenser (EL406, BioTek Instruments Inc, Bad Friedrichshall, Germany) is used to transfer various reagents in and out of SBS plates. It is less precise than the liquid-handler. The liquid dispenser has a dispensing resolution of 2% to 11% depending on the protocol. However, it is much faster than the liquid-handler as it can handle up to 96 wells per step compared to 4 wells per step. For washing steps 96 wells can be filled and emptied simultaneously or with the dispensing unit 8 wells can be filled parallel.

Microscopy

A microscope (DMI6000B, Leica AG, Wetzlar, Germany), fitted with an automated onstage stage incubator in an automated stage (SCAN IM 597382, Marzhauser Wetzlar GmbH & Co. KG, Wetzlar, Germany), and a camera (Neo sCMOS 5.5, Andor Technology Ltd, Belfast, Northern Ireland), is used to record images from culture plates. The microscopy assays can be run for a long period of time without perturbing the optimal cell culture conditions because of the presence of the onstage incubator that regulates the CO₂ and the temperature levels.

Onstage incubator

A small incubator housing (H301-K-Frame, Okolab SRL, Naples, Italy) was installed on the stage of the microscope. This incubator was used to store plates in SBS format under regulated conditions. The temperature and CO₂ of the onstage incubator is controlled during microscopic examination by a temperature controller (H301-T-UNIT-BL-PLUS Boldline, Okolab SRL, Naples, Italy) and a CO₂ controller (0506.000, Pecon GmbH, Erbach, Germany) respectively.

Storage Incubator

An incubator (STX-44, LiCONiC AG, Mauren, Principality of Liechtenstein) is used to store plates in SBS format under regulated conditions in terms of temperature, CO₂ and humidity. A varying number of plates, of varying height, may be stored depending on the format of the racks within the incubator. Two standard Liconic stackers, each with a pitch

of 23mm suitable for plates with a maximum height of 17mm, were mounted inside the incubator. Each stacker can store up to 22 plates.

de-lidder

Two de-lidders are used to remove the lids of up to two SBS plates located in the process at any given time. The lids are kept by the de-lidder while the plates are being processed. Another function of this component is to place the lids back on after the plates were processed. It has an internal pressure-based check that verifies the correct handling of the lids for removal and closure.

Hotel

The hotels are used as a secure transfer station between the outside world and inside the housing. All consumables and culture plates are fed in and discharged via the hotels. There are 3 hotels (A, B, and C). Hotel A and hotel B are intended for the loading and discharge of pipette tip racks. Pipette tips may be incorporated on four racks each with 96 tips. Plates in SBS format may be fed in and discharged in all hotels.

Waste Handling

A waste position on the liquid handling deck is available for tip disposal while running a liquid handling process. Pipette tips exit via a downpipe under the work surface where they are dropped into a collection container, which can easily be pulled forward on a rail between the switch cabinets (Figure 6B). Media waste is collected in SBS plates, and removed through the hotels.

Environmental control

Sterility

All the components of the Pelican were contained within an enclosure housing as described above. Air flows at a rate of pressure 161 Pa and wind speed of 0.45 m/s through a filter at the top of the automation enclosure, with a continuous laminar flow down

through the perforated work surface, except where devices deviate the air flow. This air flow is designed to maintain sterility (biosafety level 1) of the automation enclosure.

Temperature

The temperature levels were controlled on most positions of the Pelican. The temperature was regulated through the four heating and cooling positions (4°C-80°C) while changing the media on the liquid handler deck. It was also controlled on the stage incubator (25°C-45°C), while acquiring images, and the incubator is always kept at 37°C at all times.

Carbon dioxide

The Pelican was fed with pure carbon dioxide (99.99%) at a pressure of 1.5bar. The carbon dioxide levels inside the onstage incubator was regulated (0-7%) and the storage incubator was kept at 5% CO₂ at all times.

Humidity

While plates were stored inside the storage incubator, the relative humidity was kept at 95%.

Practicability

A user manual details the procedure for operation of the Pelican Cell culture Observatory (available upon request). This document detailed not only how to operate the system, but also how to extend the current setup to include more devices, and how to integrate the said devices in terms of hardware and software development.

**Neuronal hyperactivity in a LRRK2-G2019S cellular model of
Parkinson's Disease**

Siham Hachi, Edinson Lucumi Moreno, Sarah L. Nickels, Khalid I.W. Kane,
Masha Moein, Jens C. Schwamborn, Alex Skupin, Pieter Vanden Berghe, Ronan M.T.
Fleming

Supplementary Material

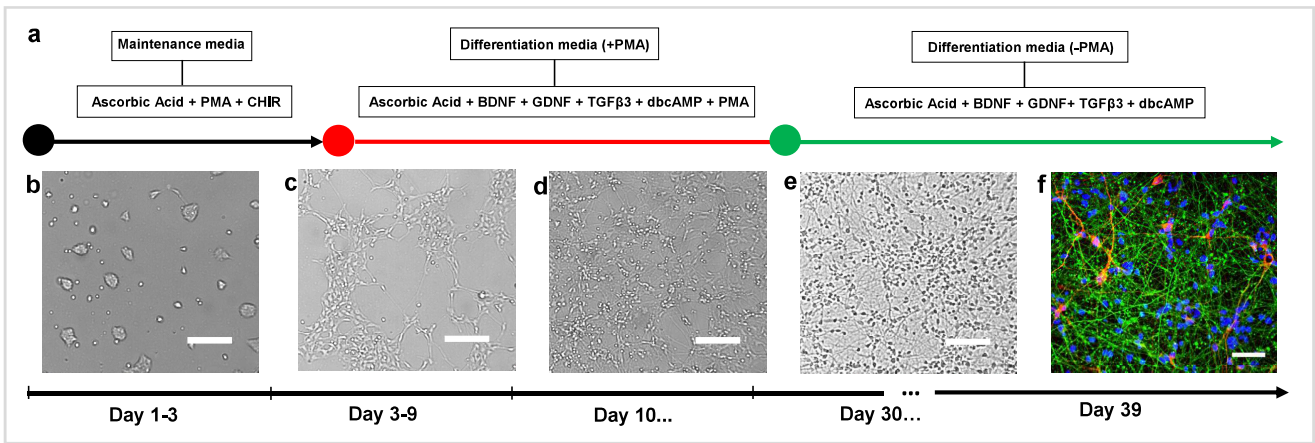


Figure 7: Differentiation of hNESC into dopaminergic neurons. **(a)** Protocol using small molecules. Bright field images of **(b)** hNESCs 1 day after seeding, cultured in maintenance media containing N2B27 medium, ascorbic acid, PMA and CHIR. **(c)** hNESCs 3 days after seeding, cultured in differentiation media containing N2B27 medium, ascorbic acid, BDNF, GDNF, TGF β 3, dbcAMP and PMA. **(d)** hNESCs 10 days after seeding, cultured in differentiation media as in **(c)** but without PMA. **(e)** hNESCs differentiated into neurons in a well of a 96 well plate after 1 month differentiation. **(f)** Immunostaining of selected region in the well, showing neurons positive for nuclei with Hoechst (blue), TUB β III (green) and TH (red); scale bar 50 μ m.

K7 vs. K7M

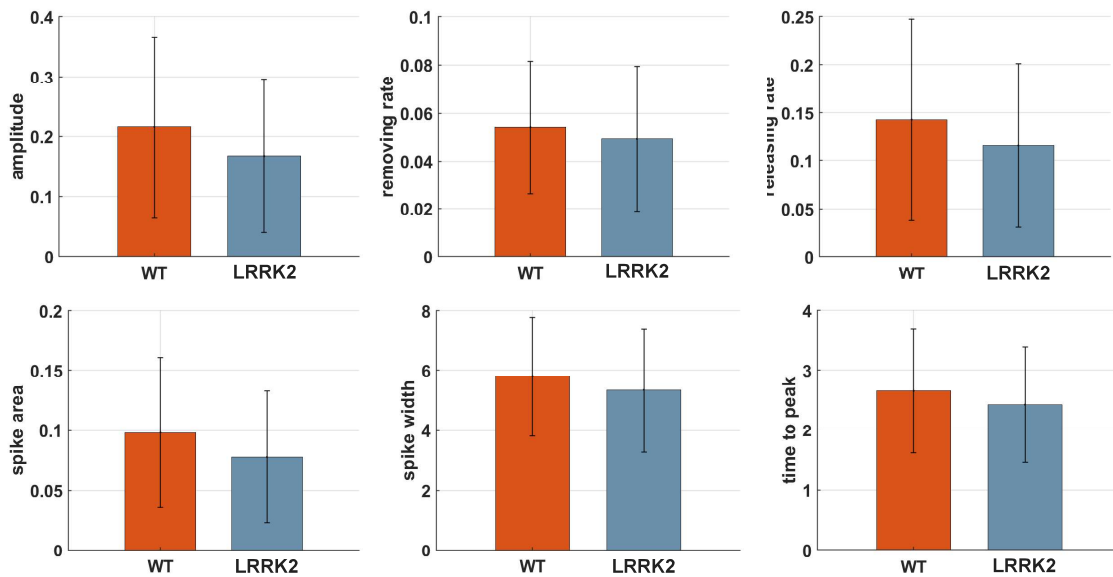


Figure 8: Additional calcium transient features of LRRK2-G2019S mutants and controls (K7 and K7M cell lines). No significant differences were observed.

T4GC vs. T4

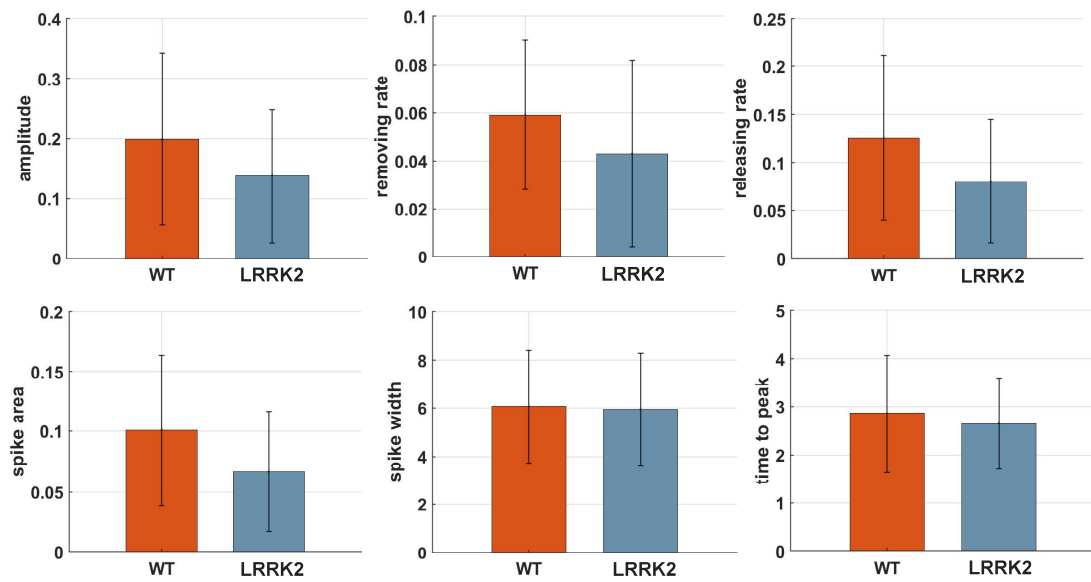


Figure 9: Additional calcium transient features of LRRK2-G2019S mutants and controls, T4 and T4GC cell lines respectively. No significant differences were observed.

Pelican user manual

Khalid I.W. Kane, Moriz Walter, Martin Thoma

Supplementary Material

11.1. Introduction

The Pelican Cell Culture Observatory (PCCO) is a fully automated, sterile cell culture system which is optimised for the long-term maintenance of neuronal cell culture. The PCCO was born from the collaboration between SBG and Fraunhofer IPA. It is composed of six main devices connected through a four-axis Gantry robot which are as follows: Liconic Incubator (STX-44, serial number 1764), Delidder, Dispenser, Microscope, Hamilton three-axis liquid handling robot and Andor Camera. Standardisation in Laboratory Automation (SiLA) compliant drivers were drafted for all of the devices and controlled through a Process Management Software (PMS) developed under the license name Laboratory Automation Control Suite (LACS).

Name	DeviceID	SILA IP/Port	link
Gantry Robot	Luxembourg_Portal	8010	http://127.0.0.1:8010/Provider
LabMan	IpaLabwareManager	8020	http://127.0.0.1:8020/Provider
Liquid Handler	IPA_LuxembourgPipettor	8030	http://127.0.0.1:8030/Provider
Tilter	Hamilton_KUST	8040	http://127.0.0.1:8040/Provider
Temperatur Controller	okoLob_BoldLine	8100	http://127.0.0.1:8100/Provider
Dispenser	SiLA Liquid Handling Cont	8050	http://127.0.0.1:8050/BioTekLHCDevice
Liquid Handler Heating/Cooling	Inheco_MultiTECControl	8060	http://127.0.0.1:8060/Provider
Liconic Incubator	LiconicWebServicesService	8090	http://127.0.0.1:8090/Provider
Pecon Co2 Controller	Pecon_Co2Controller	8110	http://127.0.0.1:8110/Provider
Weidmuller devices	Weidmueller_UR20	8120	http://127.0.0.1:8120/Provider
Camera	Andor_DC	8130	http://127.0.0.1:8130/Provider
Microscope	LeicaDmi6000BLuxembou	8140	http://127.0.0.1:8140/Provider

Figure 1: Pelican devices inventory

11.2. Safety information

11.2.1. General

Hazards may emanate from automatic movements of the system if it is:

Operated by members of staff who have not been trained or instructed

Not used in accordance with its intended use

Not properly maintained and serviced

The system operator is responsible for complying with the safety regulations in the lab and for handling the machine. The operator must ensure that only staff who are sufficiently trained have access to the machine.

11.2.2. Hazard information on the system

Safety labels that are self-explanatory through their symbols or brief text are attached to the hazardous areas of the machine. Make sure that the labels are not covered or removed.

	Warning against a hazardous area
	Warning against hazardous electrical voltage (only accessible to electrical specialists)
	Warning against crushing hazard
	Warning against hot surfaces

Figure 2: Warning information

11.2.3. Information on trouble-free operation of the system

In these operating instructions, we shall use the following symbol to highlight important information on avoiding malfunctions in the process flow or on avoiding damage to the system.

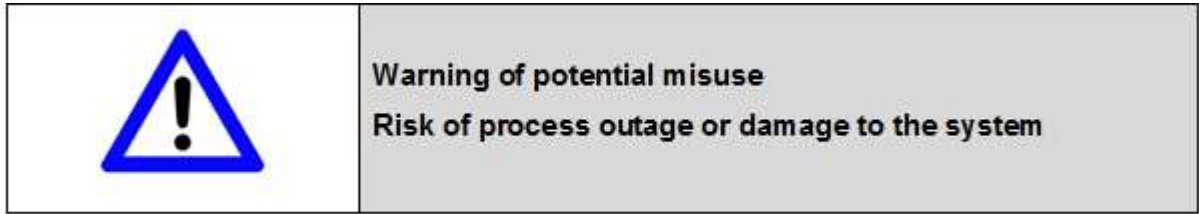


Figure 3: Warning of potential misuse Risk of process outage or damage to the system

11.2.4. Safety technology

The inner area of the system poses risks due to automatic movements, thereby prohibiting access during operation. All risk-generating functions due to moving parts may only be executed on a secured system. The inner area is secured via doors with a safety door switch (see Figure 4).

Mechanical installation areas

Access only for qualified and trained specialist staff. Access is secured via key.

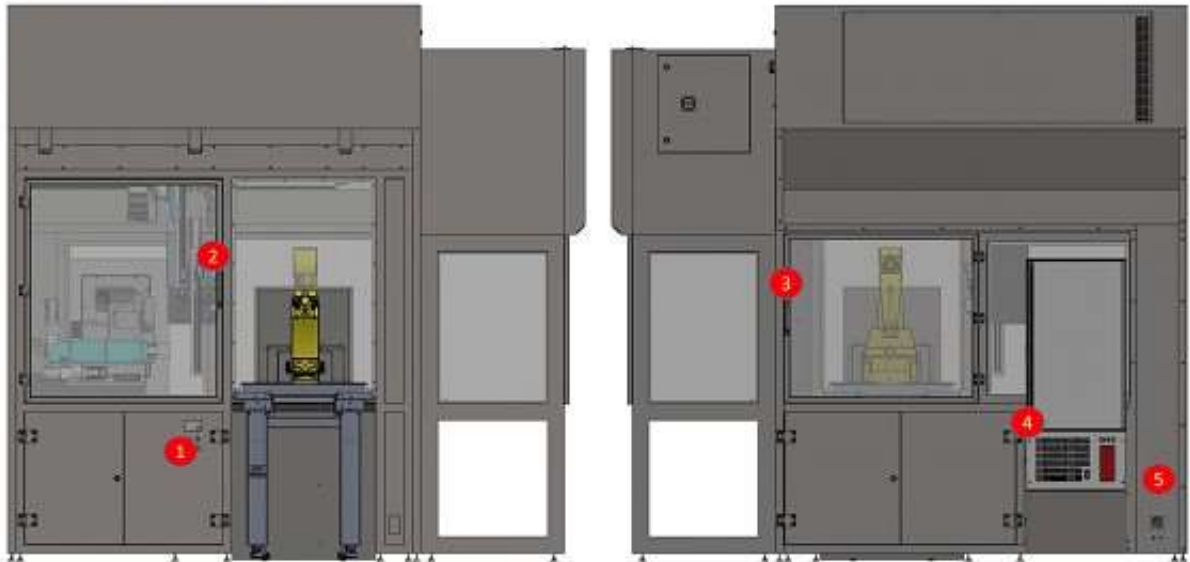


Figure 4: View of safety technology elements of the Pelican. PSENmag=Non-contact, magnetic safety switches (http://brochures.pilz.nl/bro_pdf/PSEN_Safety_Switches_Technical_Catalogue_EN.pdf). 1: Mode selection switch, system ON and enable button 2: PSENmag safety switch – contactless (upper front doors) 3: PSENmag safety switch –

contactless (upper rear doors) 4: PSENmag safety switch – contactless (incubator) 5: Main current switch

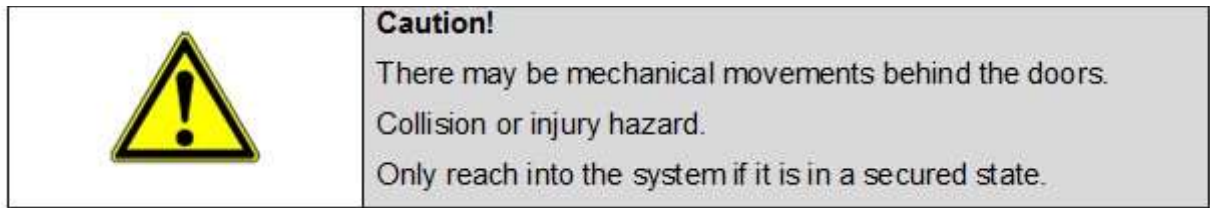


Figure 5: Mechanical installation areas

Electrical installation areas

Access only for qualified and trained electrical specialists. The electrical installation areas are labelled on the outside with an e-arrow symbol. Access is only granted via key.

11.2.5. Occupational safety

With regards to personal protective equipment, the clothing and equipment regulations that apply in the laboratory area must be observed. The system operator is responsible for monitoring this compliance.

11.3. Pelican technical data

11.3.1. Media connection:

Compressed air for pneumatic system: >8bar<10bar

CO2: >1bar <10bar

11.3.2. Voltage:

230 V, 16 A, 50 Hz (32 A fuse) and a main switch for the system's power supply

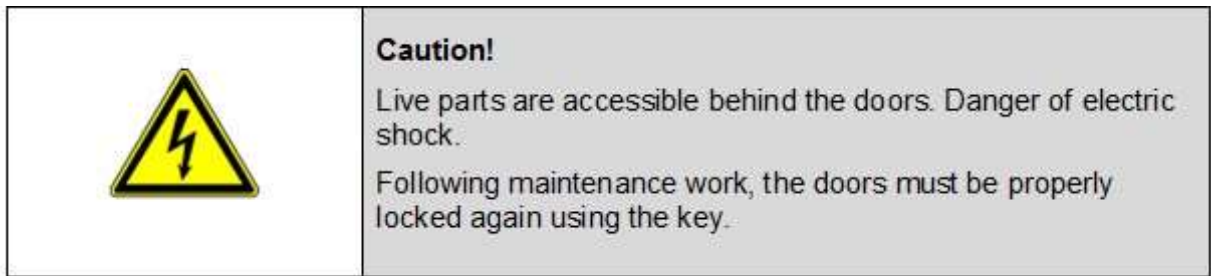


Figure 6: Electrical installation areas

11.3.3. Network:

Ethernet TCP/IP

11.3.4. Other:

USB 2.0, proprietary camera connection

In terms of mechanics, the system is not connected to any other systems (stand-alone operation).

11.3.5. Environmental conditions

The system is intended for operation in laboratory areas of S1/S2 safety classification.

Temperature range: 18 – 27 C Moisture range: 30 – 65% RH 3.4

11.3.6. Noise emission

The sound pressure level emitted by the system is under 75 dB (A).

11.4. Pelican components

The Pelican is structured into the following main assemblies (see Figure 7)

The Pelican assemblies, the components used and the software are described in the following sections.

Housing The housing of the Pelican consists of a base frame that is topped off with the work surface. The active components of the system, such as the portal, pipettor, delidder etc. are arranged above the work surface. The work surface is bordered by a safety enclosure which functions as a safety feature as well as helping to guide the air flow. The system is bordered by a filter system at the top. The safety enclosure is made of stainless steel. Large viewing windows made from Plexiglas are installed to adequately observe the process flow. The lower section of the system contains the control system and switch cabinet. Furthermore, the collection container for waste is located under the work surface. The housing is equipped with an adequate number of opening options in the upper and lower area. The housing stands on height-adjustable feet.

11.4.1. Robots and grippers

A 3-axis portal from Festo is incorporated and mounted on the ceiling inside the system. The portal is used to transport microtiter plates and consumables by way of the installed gripper. The vessels are processed at the individual stations and then transported on by the robotic gripper system. The gripper performs all handling functions of the system that are not already covered by the components on the device. Gripper jaws developed in-house have been implemented in order to cover the multitude of plate formats with one gripper. The plate and consumables carriers are gripped and interlocked by the jaws.

11.4.2. Pipettor

The pipettor transfers the various reagents in and out of the various plates. The pipetting step is executed via a liquid handling arm (LiHa-Arm, 4x) with exchangeable tips. The Zeus pipetting units from Hamilton are mounted in an X-Y portal from Festo.

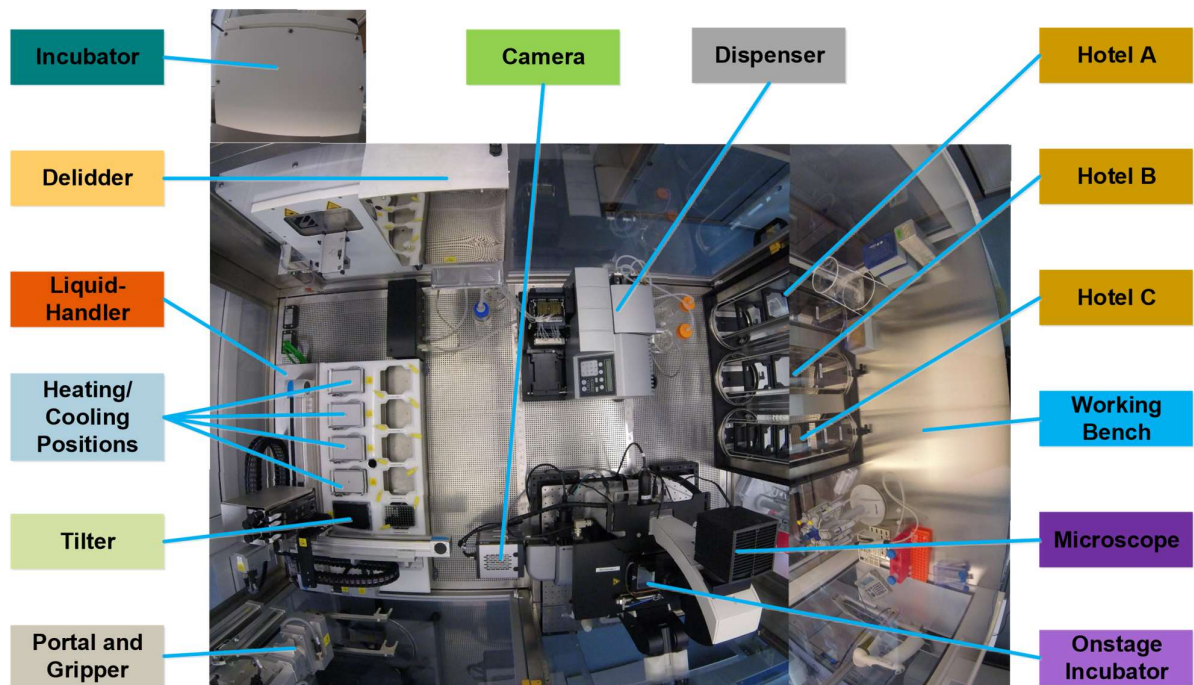


Figure 7: Top view inside the Pelican Automation Workstation without housing. For more clarity, the colour codes of Figures 7 and 9 are matched.

11.4.3. Delidder

The delidder is used to remove the lids of all plates located in the process at a given time. The lids are kept by the delidder while the plates are processed. Another function of this component is to place the lids back on after the plates are processed. The delidder is able to simultaneously process 2 lids. The delidder has an internal, pressure-based check that verifies the correct handling for removal and closure.

11.4.4. Incubator

The incubator is used to store plates in SBS format under regulated conditions in terms of temperature, Co2 and moisture. A varying number of plates may be stored subject to the racks implemented and the associated plates that can be stored.

11.4.5. Onstage incubator

Small incubator housing on the mobile microscope table (stage).

11.4.6. Incubator

The incubator is used to store plates in SBS format under regulated conditions in terms of temperature and Co2 during microscopic examination.

11.4.7. Waste

The waste position is used to dispose of tips during the process. Microtiter plates are removed via the hotels. Pipette tips are fed via a downpipe under the system level where they drop into a collection container. This can easily be pulled forward on a rail between the switch cabinets.

11.4.8. Microscope

The microscope is used to record images from Mimetas plates. These may be observed in the onstage incubator on the stage for a longer time.

11.4.9. Hotel

The “hotels” are used as a secure transfer position between the outside world and the system interior. All consumables are fed in and discharged via the hotels, whereby the used pipette tips are removed via the waste (4.2.7). There are 3 hotels (A, B, and C). Hotel A and hotel B are intended for the infeed and discharge of pipette tip racks. Hamilton pipette tips or smaller pipette tips may be incorporated on 4 racks each with 96 1000 l per rack. Plates in SBS format may be fed in and discharged in all hotels. Hotel C is preferred for this with 9 positions.

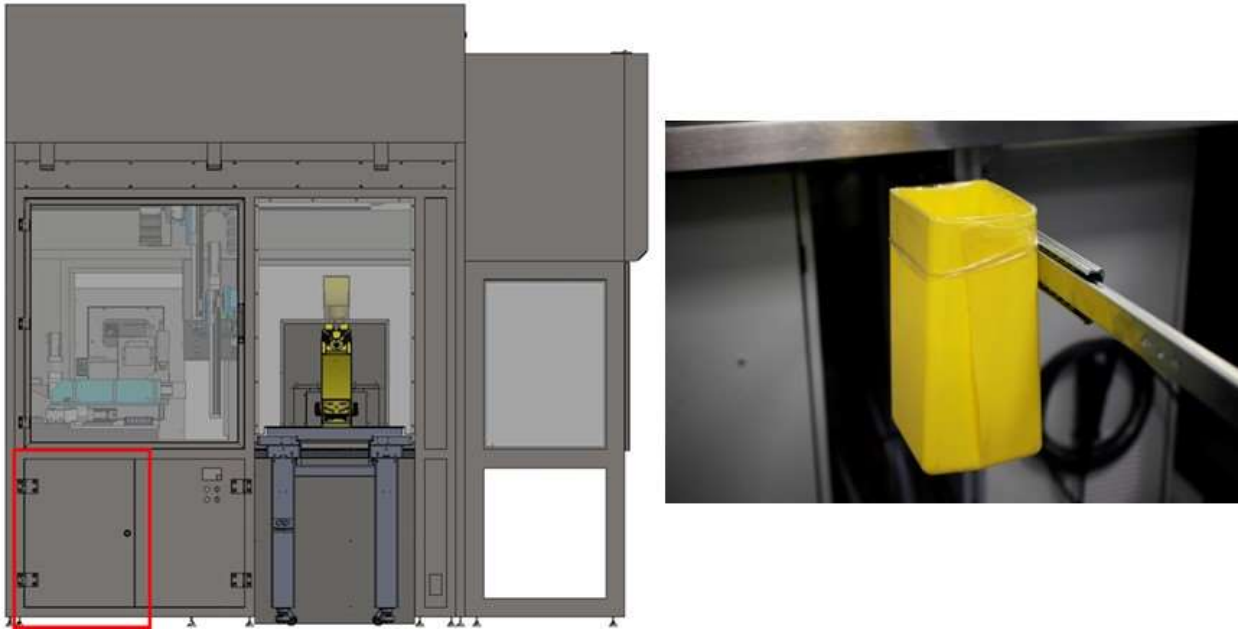


Figure 8: Tips waste station

11.4.10. Tilter

The tilter installed on the pipettor is used to tilt SBS plates (0-10).

11.4.11. Heating and cooling positions

There are 4 heating and cooling positions on the pipettor, which control the temperature of SBS plates (4 C-80 C).

11.4.12. Control system and GUI

The SiLA standard is consistently implemented for networking and integrating the devices and components. Devices, which do not feature a SiLA driver as included by the manufacturer, shall have one added. Incorporating the driver and converting the process occurs in LACS (Laboratory Automation Control Suite) – a programming environment developed by IPA for laboratory automation. The Pelican software does not make any process-specific decisions and does not analyse any data. In the event of unexpected events (device failures or other errors), the operator is always prompted to assess and rectify the error or the event.

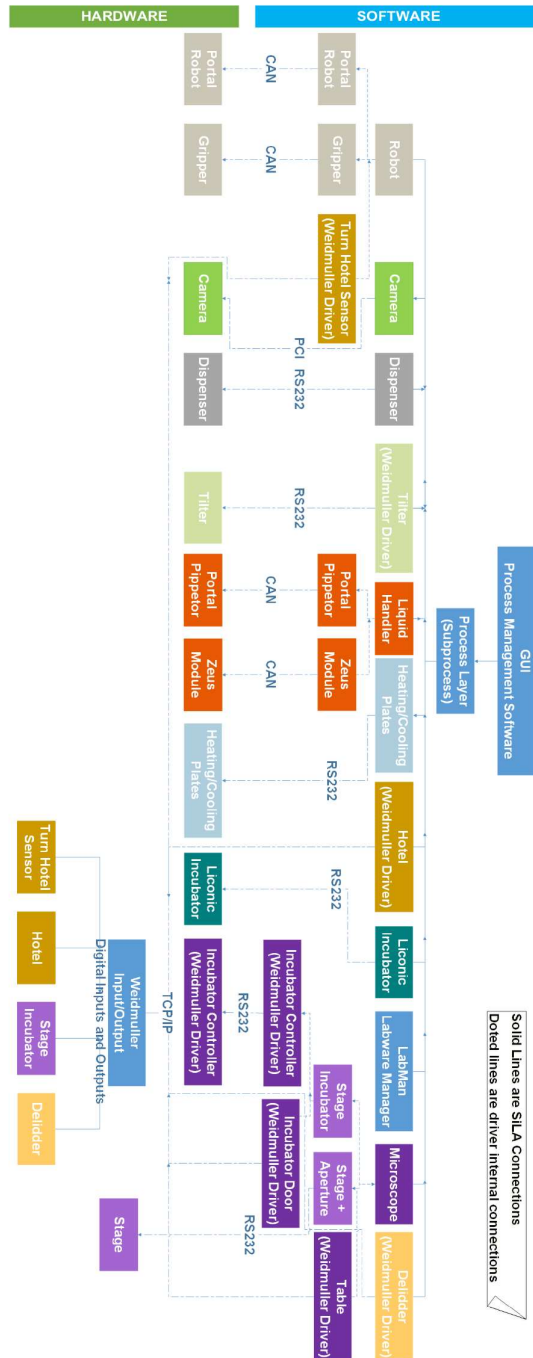


Figure 9: Pelican hardware and software control architecture. Standard on arrow = type of physical connection between a device and the computer. CAN = Controller Area Network. PCI = Peripheral Component Interconnect. RS232 = Recommend Standard number 232. TCP/IP = Transmission Control Protocol/Internet Protocol. For more clarity, the colour codes of Figures 7 and 9 are matched.

Short name	Name	Manufacturer	Product number	VE	Features
Corning_Costar_24Well		Corning			
Corning_Costar_96Well_Round		Corning			
Hamilton1000ul_WO_Filter		Hamilton			
Hamilton300ul_WO_Filter		Hamilton			
Mimetas_OrganoPlate_9601		Mimetas	9601		
Nunc_Nuncleon_96Well_Flat		Mimetas			
Trough		ND	ND		

Figure 10: List of consumables. List to be continuously updated as more labware are added to the Pelican

11.5. Description of operating elements

11.5.1. Main switch Figure

The main switch is situated at the rear of the system on the right next to the incubator. It is used to separate the electrical equipment from the network. It only has an ON and an OFF setting and is clearly marked with I for ON and 0 for OFF

11.5.2. Operating button

The Pelican has 3 operating buttons (see Figure 12), located on the system operating panel.

ON: The system equipment is switched on and started up.

OFF: The system equipment is disconnected from the network.

Enable: Approval from the operator that the system is ready for operation.



Figure 11: Main switch



Figure 12: Operating button and emergency stop button

11.5.3. Emergency stop button

The Pelican has an emergency stop button on the front side. The emergency stop button is located directly next to the operating buttons. The dead man switch also has 2 position

switches in setup mode. All emergency stop buttons are pressure-actuated switches with automatic engagement of the mechanical latch. The operating button is RED and its background YELLOW. If actuated, the whole system is shutdown, i.e. drives are braked to a halt and switched off and/or interrupted. The power supply to the system is maintained. If it is not possible to enable the system after resetting the emergency stop switch, although all requirements are met, the emergency stop switch must be actuated again and reset. If this is not successful, contact the manufacturer or qualified service personnel.



Figure 13: Mode selection switch (left) and acknowledgement button (right)

11.5.4. Mode selection switch and acknowledgement button

Operating mode 1 Automatic is intended to be the standard operation mode for the Pelican, whereas operating mode 2 Setup mode is intended for setting up and tuning in new positions. The system is ultimately switched on via the button sequence ON, Enable and all devices are ready for operation provided that all doors are closed and the emergency stop switch has not been pressed.

Operating mode 1 – System operation mode

This mode is the normal operating mode. All components are activated, and this mode is selected by default by the Pelican. The system is ultimately switched on via the button

sequence ON, Enable and all devices are ready for operation provided that all doors are closed and the emergency stop switch has not been pressed.

Operating mode 2 – System setup mode

The system can be switched to setup mode using the mode selection switch. There is a modified safety circuit in operating mode 2. The following points must be observed in mode 2/setup mode:

The door contacts are deactivated so that the doors can remain open during operation.

If the doors remain open, the acknowledgement button must be held down after the first and before the second click stop.

If the doors are closed, the portal can, however, be operated at a reduced speed, as in automatic mode, without the acknowledgement button being held down.

All devices are deactivated up to the following:

Microscope

Portal, whose speed is restricted to 50 mm/s To enable the system, the enabling must be confirmed while keeping the acknowledgement button pressed down half-way.

There is a sensor technology on the STORAGE system. The operating mode is exclusively intended for setting up the system. It is not possible to have an automatic mode for the system in operating mode 2 as important devices are not functioning. In operating mode 2, the portal is restricted to speeds below 250 mm/s. If it travels faster than this, the emergency stop activates immediately.

Operating mode 3 – routine for setting up the liquid handling processes

There is a modified safety circuit in operating mode 3. This includes all elements specified in section [5.4.2 Safety technology](#). To allow access to the liquid handling processes while

the safety circuit is closed, the upper left system door may however be temporarily opened using an acknowledgement button (see Figure 15 on the right). In operating mode 3, only the pipettor is online. To be able to activate operating mode 3, the acknowledgement button (see Figure 8 2 on the right) must first be mounted on the operating panel (screw-in connection on the bottom). This operating mode selection chip may be removed as below and exchanged for operating mode selection chip 3. Operating mode 3 may subsequently be selected. Since the device control system and the enable button cannot be performed in operating mode 3 via the Robot GUI, this operating mode is reserved for technically trained personnel.



Figure 14: Operating mode selector switch with operating mode selector chip 2

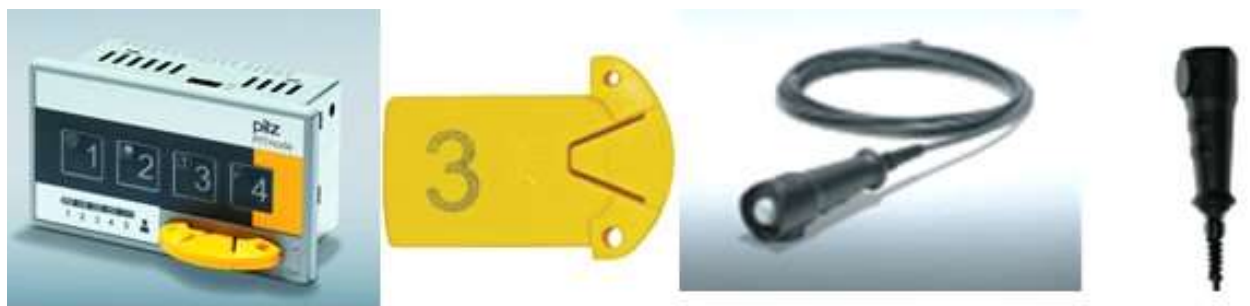


Figure 15: Control elements for operating mode 3

Loading the Pelican

The Pelican is loaded and unloaded via the 3 hotels: Hotel A, Hotel B and Hotel C. These can be found on the right-hand side of the system in the workbench. When the portal is at a standstill, each of the 3 hotels can be opened up to the workbench. To do so, the locking mechanism (Figure 16B) must be rotated to the right into position as shown in Figure 16C. Then, the Plexiglas body can be opened with a 180 turn. Hotel A is intended for 9 multi-well plates. Hotel B and Hotel C are each provided with 4 tip racks, whereby the tips may not extend further than 84 mm below the rack and the racks may only be unloaded from top to bottom via the portal and loaded from bottom to top via the portal.

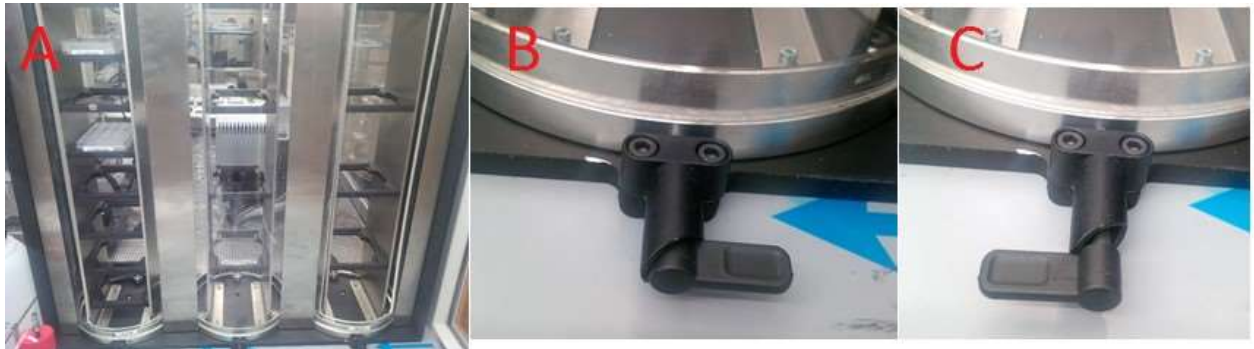


Figure 16: Loading of samples and tips into the Pelican. A: Hotels. B: Closed hotel locking mechanism. C: Open hotel locking mechanism

11.6. Starting the Pelican Cell Culture Observatory

All of the drivers and software relevant to the PCCO are located in the D drive of the Pelican computer in `~D/experimental/AutomatedCellCultureObservatory`.

You should only attempt to run (LACS), amend and generate (LACS Config Editor) protocols after starting all of the SiLA drivers, LACS and initialising all of the devices. If these steps are not followed, this increases the risk of corrupting the PCCO's configuration file which would render the devices unrecognisable by LACS (further explanation can be found in the LACS User Documentation).

11.6.1. Turn on the devices

In order to start the PCCO, all of the devices must be powered on. Some devices, such as the microscope or the stage incubator, should be switched on through the main circuit board underneath the dispenser. The main circuit is protected by a locked door underneath the dispenser and it can be accessed by a provided key.

11.6.2. Start all drivers

The SiLA drivers for all devices must be loaded into the computer in order for them to be recognised. This is accomplished by dragging the .dll file for the named device (the name of the device will always be followed by the extension .dll; i.e. for the microscope it would be `LeicaMicrosystems Dmi6000BLuxembourg.dll`) into the executable file `LacsDriverCore.exe`. `LacsDriverCore.exe` reads the .dll file and connects the device to the computer. Once this step is complete, the device is ready to run commands.

Once all of the drivers are loaded through the `LacsDriverCore.exe`, the PMS (LACS) can be started. LACS is the interface between the device and the operator (via the computer) through the loaded SiLA driver.

All of these steps have been implemented through a batch script located in `~D/experimental/Automated CellCultureObservatory/SilaDrivers` under the name `StartAllDevices.bat`.

By double-clicking on this batch file, all of the drivers can be started through `LacsDriverCore` which initiates the LACS PMS. The following steps in LACS PMS are presented in this order (you must visually ensure that all of the SiLA devices are connected by referring to the list at the bottom left of your screen):

For this purpose, the Reset button is actuated first. All devices load settings in sequence.

Initialise (this step can take up to five minutes to finish); the devices are actively switched via “initialize” in the software, a link is created and the relevant data is

written to the controller. if this step is successful then all of the devices will be loaded and ready to run the protocols. All of the devices should also have 'idle' next to them, meaning that they are ready to run commands. Initialisation is performed after the system is successfully switched on and started in LACS.

To perform an initialisation run, e.g. after a loss of power to the axis controller, the MainProtocol Home script must be executed. As a result, the following devices are initialised in the specified sequence: Liquid handler

Portal

Delidder

On-top incubator on the microscope

Moves the portal into the home position

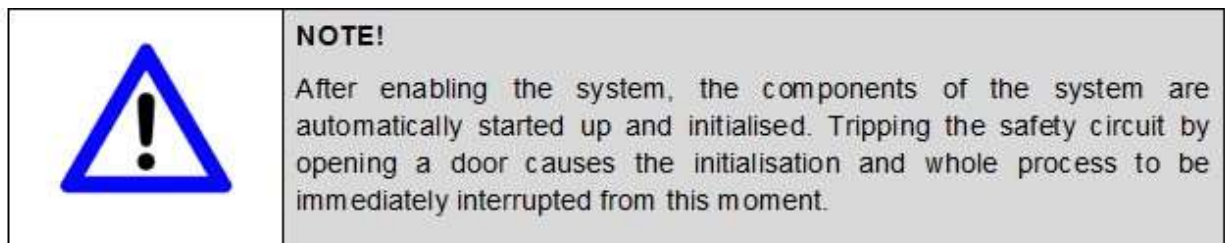


Figure 17: Safety feature while system enabled

11.7. Script execution: running protocols

11.7.1. Enabling the system

Enabling the system concludes the preparation of the experiment. The enabling is divided into 4 sections. The operator is notified and instructed via the relevant dialogues on the process steps:

Checking the system

Closing the safety circuit (doors, etc.)

Resetting the emergency stop button

Switching on the system

As a first step, a final check is made by the operator as to whether the system was loaded as specified above. Check that:

There are no foreign objects in the system (e.g. tools, waste, consumables)

The waste container has been emptied

The system has been loaded properly

There are no plates from prior runs in the system

The database in Labware Manager was modified with the amended plate assignment

The safety enclosure is intact

11.7.2. Processes

The processes are specified according to the following nomenclature and require different levels of knowledge.

Devices

The processes labelled “device” contain just one function and therefore form one method of a device.

Functions

The processes labelled “Fkt.” offer a single function used multiple times.

Loops

The processes labelled “Loop” are called within a loop in another protocol. They may be invoked independently multiple times one after the other subject to the relevant preparation of the system and input values and executed.

Main protocol

The protocols labelled “Main Protocol” may be executed with the relevant input parameters on the system at any time. The requirement is that all positions are populated up to the incubator or the hotels according to the protocol. All other positions in the system must be empty.

Sub-protocols

The protocols labelled “Sub” form a sub-process. They are invoked in loop processes or main processes.

Sub MoveLabware This sub-protocol takes care of the preparation and follow-up processing of plate transport. All of the relevant entries in Labware Manager and decisions are made here.

Test protocols

The protocols labelled “Test” are intended exclusively for system tests and are not considered for use in production. Continuous runs or other types are illustrated here.

11.7.3. Defined Processes

Once all of the devices are initialised, all of the implemented protocols in the PCCO will appear on the left-hand side of the LACS PMS screen. Each of these protocols will require inputting certain parameters. Below is the list of all of the useful implemented protocols, their parameters and their functions. It is very important to refrain from changing the name of any protocols as some of the codes are reused in other protocols and any changes will corrupt the dependencies.

Device Delidder DelidPlate

This protocol uses the delidder to remove the lid from a plate. The input for this protocol is a real positive integer: 1 or 2.

Device Delidder Home

This protocol homes the delidder by moving the delidder up and resetting all of the hold positions to confirm that it is ready to host a new plate.

Device Lid LidPlate

This protocol uses the delidder to close the lid on a plate. The input for this protocol is a real positive integer: 1 or 2.

Device Delidder PrepareForInput

This protocol ensures that a delidder position is ready to host a new plate and that the seek after position is free. The input for this protocol is a real positive integer: 1 or 2.

Device Delidder PrepareForOutput

This protocol ensures that the robot can drive into the delidder by moving it up. The input for this protocol is a real positive integer: 1 or 2.

Device Dispenser Execute

This protocol executes a liquid handling script using the Biotek dispenser. The input for this protocol is the string name of the script. For example, Mimetas OrganoPlate 9601 2 Add100 Media.LHC can be used as a methodName. The scripts for this dispenser are located in `~experimental/AutomatedCellCultureObservatory/SilaDrivers/Dispenser/Scripts`. In order to add a working script for the dispenser, the following steps must be followed (the name given to the new dispensing script is highlighted in green):

open the Liquid Handling Control 2.18 (LHC) software create a new script and save it in
~experimental/AutomatedCellCultureObservatory/SilaDrivers/Dispenser/Scripts
modify the protocol Device Dispenser Execute (as explained in the "Implement new
protocols" section) open Device Dispenser Execute

create an IfThenElse statement; the Expected value is a string value (the script name
.LHC created earlier from the LHC), the ActualValue is the value at the ID
methodName (defined as a variable in the protocol), the comparison type is the
same

```
define constraint hit; set a string variable <?xml version="1.0"  
encoding="utf8"?><ResponseData  
xmlns:xsi="http://www.w3.org/2001/XMLSchema-instance"
```

```
xsi:noNamespaceSchemaLocation="http://sila.coop/schemata/ResponseType  
1.2.xsd"><ParameterSet> <Parameter name="cStringProtocolFilename"  
parameterType="String"><String>
```

```
Mimetas OrganoPlate 9601 MediaExchange  
Media.LHC</String></Parameter></ParameterSet>
```

</ResponseData>, the response value is dispenserParams

```
use the SiLA Liquid Handling Control to setParameters as <?xml version="1.0"  
encoding="utf-8"?><ResponseData  
xmlns:xsi="http://www.w3.org/2001/XMLSchema-instance"  
xsi:noNamespaceSchemaLocation="http://sila.coop/schemata/ResponseType  
1.2.xsd"><ParameterSet> <Parameter name="cStringProtocolFilename"  
parameterType="String"><String>
```

```
Mimetas OrganoPlate 9601 MediaExchange  
Media.LHC</String></Parameter></ParameterSet> </ResponseData>
```

Device LiquidHandler Execute

This protocol executes a liquid handling script using the Hamilton liquid handler. The inputs for this protocol are:

sourceLabwareID: the plate you are aspirating the fluid

from destLabwareID: the plate you are dispensing the fluid to

methodName: the string name of the script, for example, Mimetas OrganoPlate 9601 2 Rem Media, and the scripts are located in ~experimental/AutomatedCellCultureObservatory/SilaDrivers/LiquidHandler/Scripts

aspVolume: the volume aspirated from the sourceLabwareID, this can only be a real positive integer from 1 to 1000 (units: μ l)

dispVolume: the volume dispensed into the destLabwareID, this can only be a real positive integer from 1 to 1000 (units: μ l)

Device TopStage Close

This protocol closes the door of the microscope stage incubator.

Device TopStage PrepareForInput

This protocol ensures that the microscope stage incubator is ready to host a plate and the door is opened, enabling the function of the robot gripper.

Device TopStage PrepareForOutput

This protocol ensures that the microscope stage incubator is ready for a plate retrieval and the door is opened, enabling the function of the robot gripper.

Loop 96WellPlate MediaExchange

This protocol utilises the dispenser to exchange the media of a single Perkin Elmer 96-well plate. The delidder, dispenser and robot are used to move a culture plate from a given position (e.g. the hotel) to complete all of the required steps for media exchange. The protocol finishes with moving the culture plate to a free position in the Liconic incubator. The inputs for this protocol are:

labwareID: the name of the culture plate
dispenserProtocol: the dispenser liquid
handling script string name

Loop MediaExchangeOfFloatingOrganoids

It is important to confirm that there are 24-well type waste and media plates on the liquid handling deck as this loop does not complete these steps. This protocol uses the Hamilton liquid handler to exchange the media of a single 24-well plate. Firstly, it moves the plate to the tilter device position on the liquid handler deck and then it tilts the culture plate and removes its media in this tilted position (spent media is dispensed into the waste plate). Following on from this, the plate is returned to a horizontal position and the media is replenished from the media plate to the culture plate. Finally, the culture plate is moved to a source position, i.e. its initial position. The inputs for this protocol are:

labwareIDWaste: the name of the
waste plate labwareIDMedia: the
name of the media plate labwareID:
the name of the culture plate

This loop will not move the waste plate to the correct position on the liquid handler deck. Therefore, in order to use this loop on its own, you must move the waste plate manually to the desired position in the liquid handler and then manually update the pipettor GUI and the labware manager.

OrganoPlate based loop protocols

Loop Mimetas AddMediaWithDispenser This protocol uses the dispenser in adding media to the medium outlet wells of a single Mimetas plate. The delidder, dispenser and robot are utilised to move a Mimetas plate from a given position (e.g. the hotel) to complete all of the required steps for media exchange. Once all of the initial steps are complete, the Mimetas plate is moved to a free position in the Liconic incubator. The inputs for this protocol are:

labwareID: the name of the Mimetas plate
dispenserProtocol: the dispenser liquid
handling script string name

Loop Mimetas ExchangeMediaInOutlet This protocol uses the Hamilton liquid handler to initially remove 50 μ l of media from the medium outlet and inlet wells of a single Mimetas plate. It uses the dispenser to transfer 15 μ l and 90 μ l of media into the medium outlet and inlet wells respectively and then the Mimetas plate is moved to a free position in the incubator. The inputs for this protocol are:

labwareID: the name of the Mimetas
plate labwareIDWaste: the name of the
waste plate

Loop Mimetas ImageAcquisition This protocol moves a single Mimetas plate to the microscope, which is then scanned and an image is taken of each bioreactor's observation window. In the final step, the Mimetas plate is moved to a free position in the incubator. The inputs for this protocol are:

labwareID: the name of the Mimetas plate imageFolder: the
location where the images are stored (e.g.
~experimental/Images)

Loop PerkinElmer 96 ImageAcquisition

This protocol moves a single Perkin Elmer 96-well plate to the microscope which is then scanned and an image is taken of each well. In the final step, the plate is moved to a free position in the incubator. The inputs for this protocol are:

labwareID: the name of the Mimetas plate imageFolder: the location where the images are stored (e.g. ~experimental/Images)

MainProtocol 96WellPlate MediaExchange

This protocol uses the Loop 96WellPlate MediaExchange method to change the media of 96-well plates. The input variables are the plate names.

Main protocols of data management from the labware manager

The inputs for this protocol are:

1. hotelName: HotelA, HotelB or HotelC
2. labwareTypes: the TypeId defined through the labware manager
3. labwareIDs
4. labwareDescriptions: e.g. the types of cells in the plate or experiment number

MainProtocol CreateAndImportPlates Hotel-Incubator This protocol verifies the number of free positions in the incubator racks and moves plates (as a batch) loaded in any of the hotels to the incubator. If the number of plates is larger than the number of available positions in the incubator, the protocol will not run.

MainProtocol CreateAndImportTips Hotel-Liquidhandler This protocol verifies the number of free positions in the Hamilton liquid handler tip positions (max. of 5) and moves tips (as a batch) loaded in any of the hotels to the incubator. Please be advised that:

If the number of tips is larger than the number of available positions in the liquid handler, the protocol will not run.

The 1000 μ l tips can only be loaded in HotelB, and can only be parked in liquid handler position 5.

You must only load one 1000 μ l tip rack at one time.

MainProtocol CreateBatchLabware This protocol allows the user to create labware IDs in batch instead of manually using the labware manager. It requires the user to input the information about the labware as it would appear in the labware manager GUI.

MainProtocol CreateLabware This protocol uses labware manager to create a labware. In addition to inputs

2, 3 and 4, labware position must also be defined. This position can be any of the positions present in the Pelican.

MainProtocol Home

This protocol homes the liquid handling and the gantry robots, top stage incubator and delidder. The gantry robot is then moved to the centre of the Pelican (safe position). The gantry robot must be at the centre of the Pelican and you must ensure that it will not hit the microscope when it moves sideways.

MainProtocol MediaExchangeOfFloatingOrganoids

This protocol uses Loop MediaExchangeOfFloatingOrganoids to exchange the media of floating organoids. Unlike the loop, this protocol is fully automated. It requires the user to input the IDs of the culture, media and waste plates; all of which should be 24-well plates. This protocol requires an upgrade to include other types of plates.

OrganoPlates based main protocols

MainProtocol Mimetax 1 AddMediaToOutlet This protocol uses the dispenser to add media to the outlets of OrganoPlates.

MainProtocol Mimetas 2 AddMediaToInlet This protocol uses the dispenser to add media to the inlets of OrganoPlates.

MainProtocol Mimetas 3 ImageAcquisition This protocol moves OrganoPlates to the microscope and takes .tiff pictures of all of the observation windows of the plate and saves them in the image folder.

MainProtocol Mimetas 4 ExchangeMediaInOutlet This protocol uses the liquid handler to exchange the media in the Outlets of OrganoPlates.

MainProtocol Mimetas MediaChangeDispenser This protocol uses the dispenser to maintain the differentiation of human neural epithelial stem cells (hNESc) into dopaminergic (DA) neurons in OrganoPlates. It is fully automated and requires the user to input the name of the plates.

MainProtocol MovePlates -Hotel

This protocol moves plates with given IDs to a specified hotel as a batch.

MainProtocol PerkinElmer 96 ImageAcquisition

This protocol moves 96-well plates to the microscope, takes .tiff pictures of all of the wells and then stores the plate inside of the Liconic Incubator.

MicroscopeManualFocus

An automated focus hardware is not incorporated in the DMI6000B microscope. In order to run an automated image acquisition script, a focus point must be defined for every plate. This protocol allows the definition of a focus within an automated image acquisition by:

1. activating the oculars of the microscope
2. moving the stage to the first well of the plate
3. applying a break point to allow the user to find the focus point by adjusting the z position of the stage

4. activating the camera to continue the automated image acquisition whilst keeping the focus point throughout the script

This is optimised for a 96-well plate. However, an upgrade should be performed in order to allow the user to input the coordinates of the first well; optimising the use for any plate type.

Sub CheckExpectedLabwarePosition

There are instances when you will need to ensure that a plate is in a defined position before running a process, such as inside the incubator. This protocol allows the user to define the expected position of a plate. If the plate is not at this position, the protocol will not run.

Sub DelidLabware

This protocol moves a plate to the delidder, removing the lid and moving the plate to a given position. You must input the desired delidder position to be used (1 or 2).

Sub LidLabware

This protocol moves a plate to the delidder, then places the lid onto the plate. You must input the desired delidder position to be used (1 or 2).

Sub Mimetas 384 ScanPlate yDir Sub1

Each well in the third row (observation window) of an OrganoPlate is automatically pictured. This can be used in line with other protocols to automatically map all or part of the observation windows of an OrganoPlate.

Sub Mimetas 96 ScanPlate

Each observation window of an OrganoPlate is automatically pictured and the image is saved in a folder as specified by the user (e.g. D:\experimental\Images\).

Sub PerkinElmer 96 ScanPlate yDir Sub

Each well in the first row of a 96-well plate is pictured. This can be used in line with other protocols to automatically map all or part of the wells of a 96-well plate.

Sub PerkinElmer 96 ScanPlate

Each well of a 96-well plate is automatically pictured and the image is saved in a folder as specified by the user.

11.8. Implement new protocols

Start PCCO as described in the second section of this manual (Starting the Pelican Cell Culture Observatory). It is imperative to have all of the drivers loaded and all the devices in idle mode (once initialised) prior to any of the following steps. This is due to the LacsConfig XML file being protected with a hashcode which therefore means that loading all of the devices will ensure the appropriate update of the hashcode in the configuration file. This will avoid the configuration file from having an obsolete hashcode so that it will be recognisable by LACS. Once this is accomplished, you must start the LACS config Editor, which will load the configuration file of the Pelican. At this time, you can either modify an existing protocol by clicking on the required protocol on the list, or create a new process by going to the onlet Processes/add new process. After having created or modified a process, you must:

click OK (otherwise all changes will be lost) save configuration and replace the existing LacsConfig.xml close LACS config Editor close LACS,

close all

drivers,

restart all

drivers and

LACS, reset
and initialise
all drivers.

Once these steps have been completed, the created/updated protocol is ready to be used.

11.8.1. The Hamilton Liquid Handling GUI tutorial

go to ~D:\experimental\AutomatedCellCultureObservatory\SilaDrivers\
LiquidHandler START Luxembourg Pipettor GUI

reset/intialise

Labware Editor (do not forget to specify the LabwareType): You can measure all of the dimensions of the Labware manually and input them into the GUI

Extended Labware settings: It is important to decide where each labware could be used on the deck because you will have to define the parameter for each position you choose

1. Position Id is/are the position(s) on the deck that these settings could be used in; * is for all the remaining positions that are not already selected. E.g. 6-8 means for positions 6, 7 and 8; then * is the wildcards that is the settings for * will be used for the remaining positions 1, 2, 3, 4, 5, 9 and 10.
2. Container Id is the Geometry Container Index. For this plant, we can define three container Ids; heated positions, not heated positions and tilt module. The values of the Container Id can be amended in the Zeus Parameter Tables (further explanation is covered later in the manual).
3. Liquid Search Position is the initial distance, from the bottom of the tip to the labware, that the channel must travel before it starts to search for the liquid. It should be just above the labware.
4. Deck Id must always be 0. The Deck Id is the Deck Geometry index and it defines how high the channels must be lifted in order to travel safely, with attached tips for instance. You should not need to modify this value.
5. The Tip Type needs to be specified if it is a tip rack only, otherwise it can be left blank as is it is normally disregarded.

Zeus Parameter Tables: you can define the Geometry Container Index(ces) and Deck Geometry index(ces) and add the different parameters for each well type as specified. Then you can transmit the changes to the table in the Extended Labware settings.

6. Pos. of Container Bottom [ce]: in order to specify this ce, you must drive down the pipettor channel with a tip until you touch the bottom of the plate and you take the current z position. $d1: ce = d1 + 0.5\text{mm}$
7. ZeusLiquidClass: There are liquid classes defined by Hamilton which include liquids that are most often used in everyday laboratory operation such as glycerine, water and ethanol.

New liquid classes can be defined by:

right click on any of the predefined liquid classes copy the one that resembles the most like the new liquid class that you aim to define modify as you see fit save on each module

create the calibration curve for the new liquid class by copying the calibration curves from the predefined liquid class you used to create the new liquid class as follows:

Source Index: the predefined liquid class that you used to create the new liquid class

Destination Index: the new liquid class and copy as appropriate

1. Device layout: Offset is the distance from the reference point in x, y and z directions.
2. ParkPosition: for the initialisation position, prepare for input/output: safe position. Position Range = 1-10 (specified/selected) or * (unspecified/unselected).
3. Head Position: the channel you want to use.

11.8.2. The Gantry Robot GUI tutorial: teaching positions

go to
~D:\experimental\AutomatedCellCultureObservatory\SilaDrivers\Robot, START Luxembourg Portal TeachGUI.exe,

reset and initialise, add a master position (in front of a device), and a subposition (the park position of the plate on the device) for a Master Position:

move the robot arm to a safe position in front of the device, where the arm will not impede with the use of the device, then take the current position and click SaveAll, for a subPosition:

move the gripper with the teaching plate on the plate holder of the aforementioned device until it just touches the bottom (be mindful that it does not touch the bottom too closely as the robot will hit the bottom of the plate holder forcefully with the plate which will break if done continuously). Take the current position as your subposition (this is the position the plate needs to be for executing steps e.g. Delidder.1) and click SaveAll. YOU MUST teach the way out of the subposition otherwise the robot will take the shortest position which will crash the robot into the device. Move the plate up vertically with deltaZ at more or less than 0 followed by deltaX OR deltaY=0. Press the "+" and the same will be accomplished by coming out with deltaX OR deltaY at more or less than 0 and deltaZ=0. Press the "+" and then SaveAll.

define the ungripped and gripped width of the gripper, SaveAll must define a route between the device, and every other device in the plant by going to:

1. routing
2. add New
3. select the Source and Destination
4. ensure the route is safe; if you need to avoid an obstacle, add Way point

How do you use Way points? Click on the route created, then drive to a Way point manually and then Add

Current Position

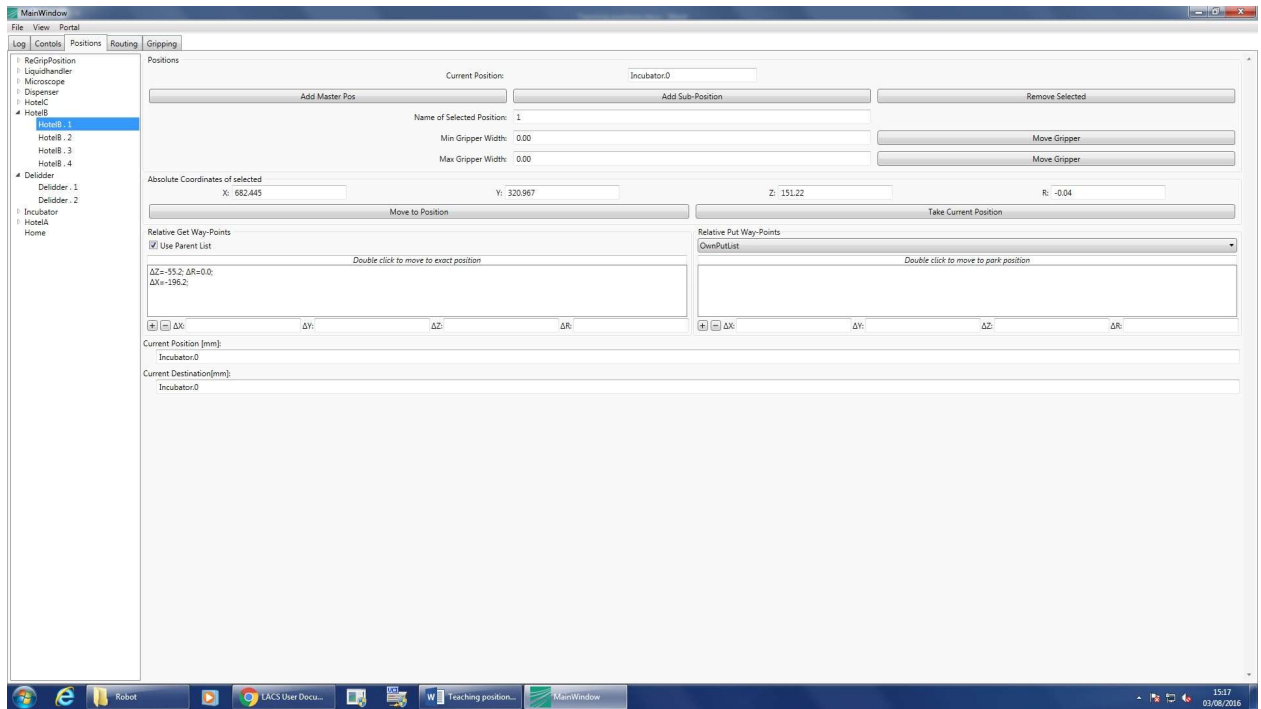


Figure 18: Teaching Master/Sub positions and defining the safe gripping width

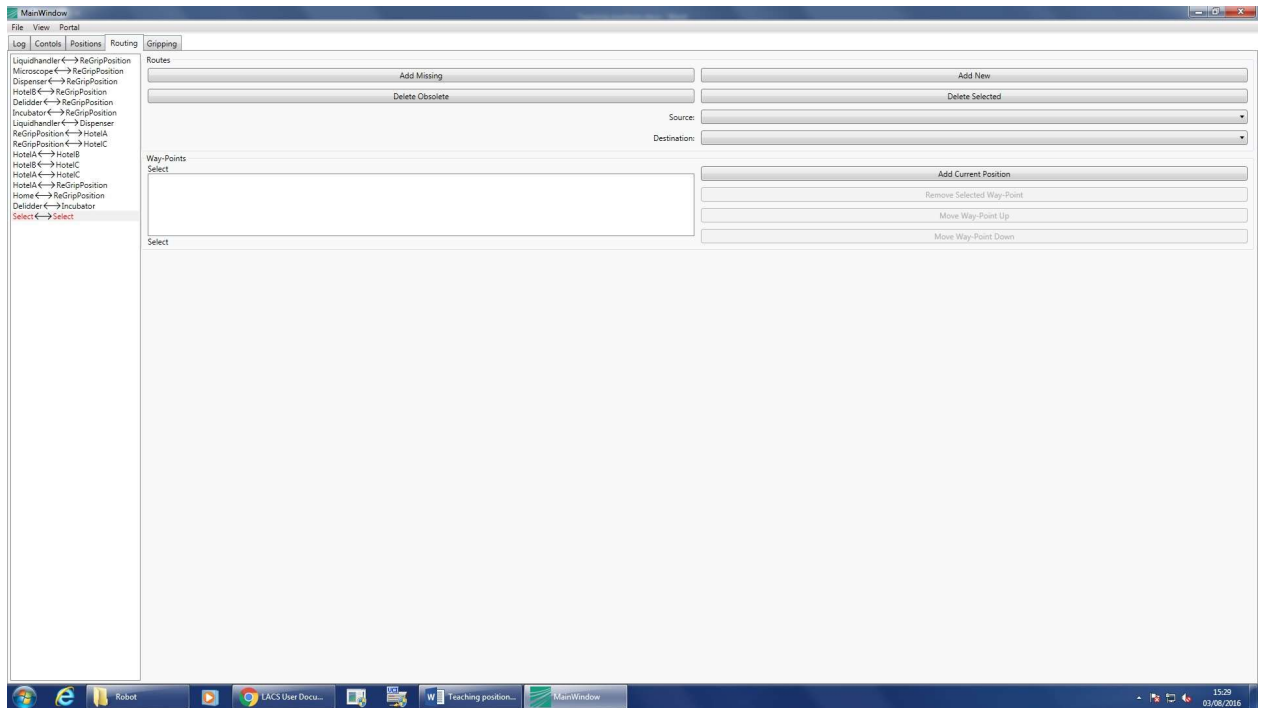


Figure 19: Robot routing in the Pelican

11.9. Writing a SiLA driver

Learning how to write a SiLA driver is easier through using an example. We will use the driver of a shaker (one of the simplest devices in a laboratory) to explain how to write a SiLA driver. A more complex SiLA driver can be written by extending this draft; the syntax and overall layout will be very similar.

Bioshaker SiLA Drive-REPORT

- Connect the device, and make sure that the driver of the adaptor port is properly installed
- Download hterm.zip and install: to Verify the COM port connected
- Download/Install the driver/software the driver/software of the device to make sure that everything works
- Create the Visual studio driver with Fraunhofer IPA. N.B.: VS/View/Task list to see what you need to change to make the device to make the device work in terms of adding commands □ UserMethod1.cs Add the command to replace all the CR commands after public partial ...:

```
private string SendGetCommand(string command)
{
    Interface.Receive();

    string answer = Interface.SendAndReceiveAfterDelay(command + "\r",
200).Trim();    if (answer.Trim().ToUpper() == "E")

        InterpretErrorCode();

    return answer;
}
```

- Repeat the same as last step for all different types of commands for that device. For the

Bioshaker there are three types of commands: *SendGetCommand*,
SendSetCommand,

InterpretErrorCode

```
private void SendSetCommand(string command)
{
    Interface.Receive();

    Interface.Send(command + "\r");
string answer = Interface.ReadLine(2000);
if (answer.Trim().ToUpper() == "OK")

        return;
```

```

        if
(answer.Trim().ToUpper() == "E")
InterpretErrorCode();
else

        throw ExtendedException.Create(EErrorCodes.Unknown, "Command
" + command + " failed with error " + answer);

}

private void InterpretErrorCode()

{

        string answer =
SendGetCommand("getErrorList");          throw
ExtendedException.Create((EErrorCodes)3000);

        }          private string
SendGetCommand(string command)

        {

                Interface.Receive();

                string answer = Interface.SendAndReceiveAfterDelay(command + "\r",
200).Trim();

                if
(answer.Trim().ToUpper() == "E")
InterpretErrorCode();
return answer;

        }

}

```

- Use the Task list to go through the different commands you need to write for the device
 - To write the error list: first, you write all errors in the Errorcodes.cs, then you write the exception *InterpretErrorCode* as shown above:

```
[Description("Error by the DC motor controller.")]
```

```
DcMController = 3000+101,
```

```
[Description("Error due speed failure, for example happens through
mechanical locking.")]
```

```
SpeedFailure = 3000+102,
```

```
....
```

```
[Description("Unknown error")]
```

```
Unknown = 3999
```

- o To write the predefined SiLA commands, go shaker.cs:

```
this.PrepareExecution(ref methodID);
```

```
SendSetCommand("soff");
```

```
Thread.Sleep(5000);
```

```
SendSetCommand("setElmUnlockPos");
```

```
string answer =  
SendGetCommand("getElmStateAsString");  
(answer != "ELMUnlocked")
```

```
if
```

```
{
```

```
InterpretErrorCode();
```

```
}
```

Another SiLA predefined command:

```
this.PrepareExecution(ref methodID);
```

```
SendSetCommand("setElmLockPos");
```

```
SendSetCommand("ssts"+speed);
```

```
SendSetCommand("sonwr"+shakeDuration);
```

```
Thread.Sleep(200);
```

```
string answer =  
SendGetCommand("getShakeState");  
((answer != "3") && !AbortRequested)
```

```
while
```

```
{
```

```
answer =
```

```
SendGetCommand("getShakeState");
```

```
Thread.Sleep(50);
```

```
}
```

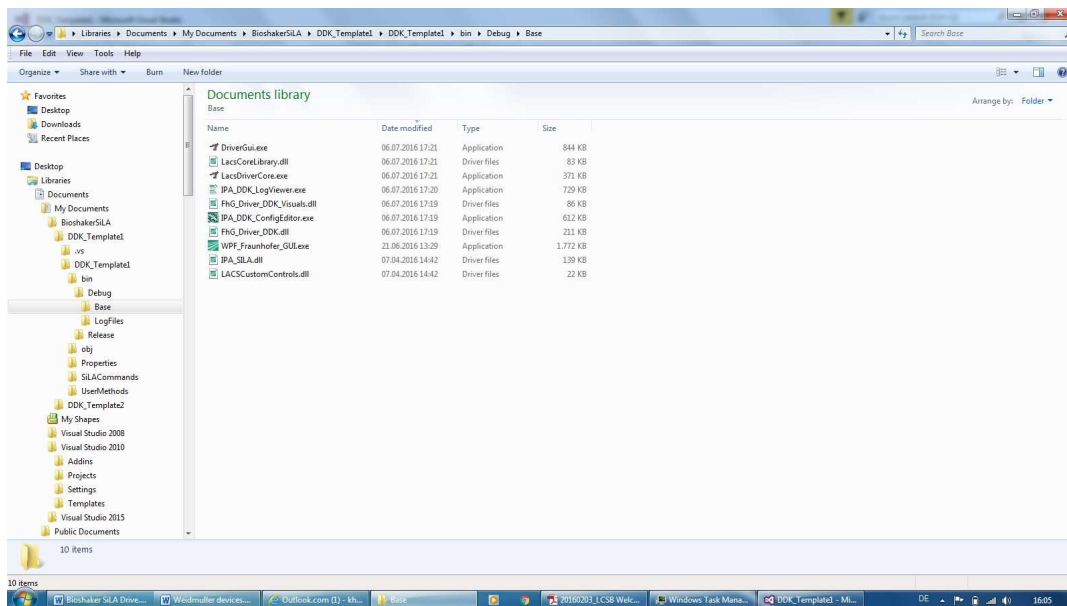
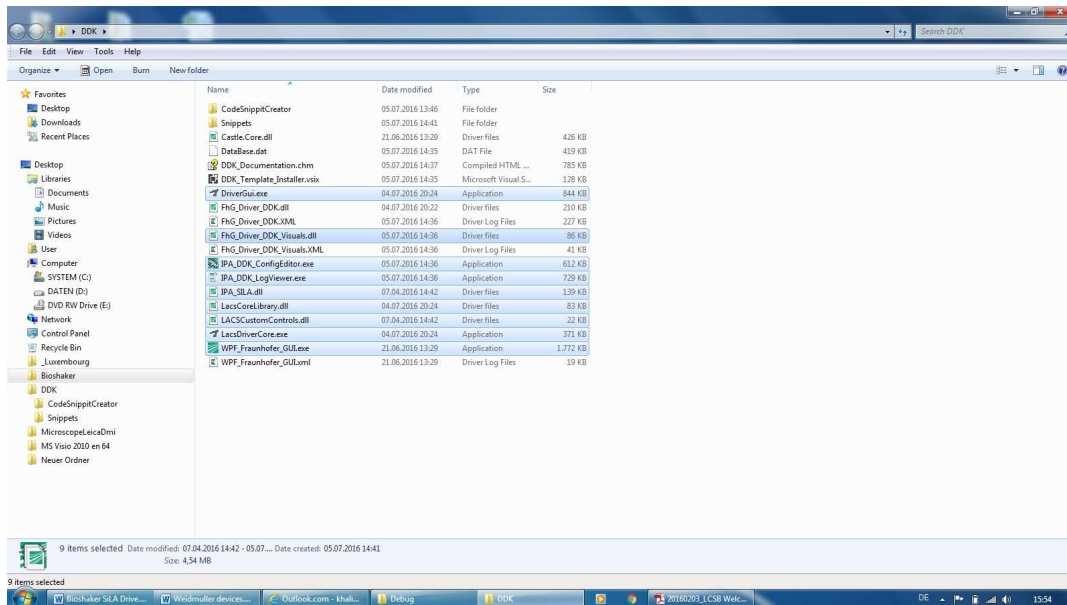
```
        if (AbortRequested) throw new  
AbortException();
```

- Then, you can create the other commands that are optional (not predefined by SiLA) in PublicMethod1.cs: (Don't forget to change the SilaMethod from false to true to be able to use in the driver gui)

```
[SilaMethod(true, ApproximateDuration =  
"PT0S")] public MethodReturnValue  
TemperatureON(int temp)  
  
    {  
  
        int  
methodID = 0;  
try  
  
    {  
  
        // ToDo: Enter the right method name  
this.PrepareExecution(ref methodID);  
SendSetCommand("setTempTarget"+temp);  
  
        SendSetCommand("tempOn");  
  
    }  
  
}
```

- Then you can add more commands into PublicMethod1.cs by: right click , Insert snippet, IPA, Sila Methods

To create the drivergui, LacDriverCore.exe, copy from the ddk to where you wrote the driver



11.9.1. Connect devices into EKI and CAN bus connections

EKI 1524 module

The computers used to control laboratory automation plants usually do not have enough COM ports available in order to control all of the devices. An EKI module solves this issue by featuring two independent Ethernet ports and MAC addresses to provide a redundant network mechanism to guarantee Ethernet network reliability and up to four virtual COM

ports. In the Pelican, an EKI 1524 module with four virtual COM ports is used to connect some devices to the computer, such as the Liconic Incubator and the CO₂ Controller.

In order to establish a connection between a device, the EKI 1524 module and the Pelican computer you must: connect it to the EKI 1524 module, start the software Advanced EKI Device Configuration Utility v2.01 (run as an administrator),

Management/Manual Direct Mapping Virtual COM Port,

Device Type = EKI-1524-BE

Address 1 = 192.168.0.110

Port = the actual port used in the EKI 1524 module

Host COM Port = use an empty virtual port. For the Pelican, we have decided to start with COM Port 30

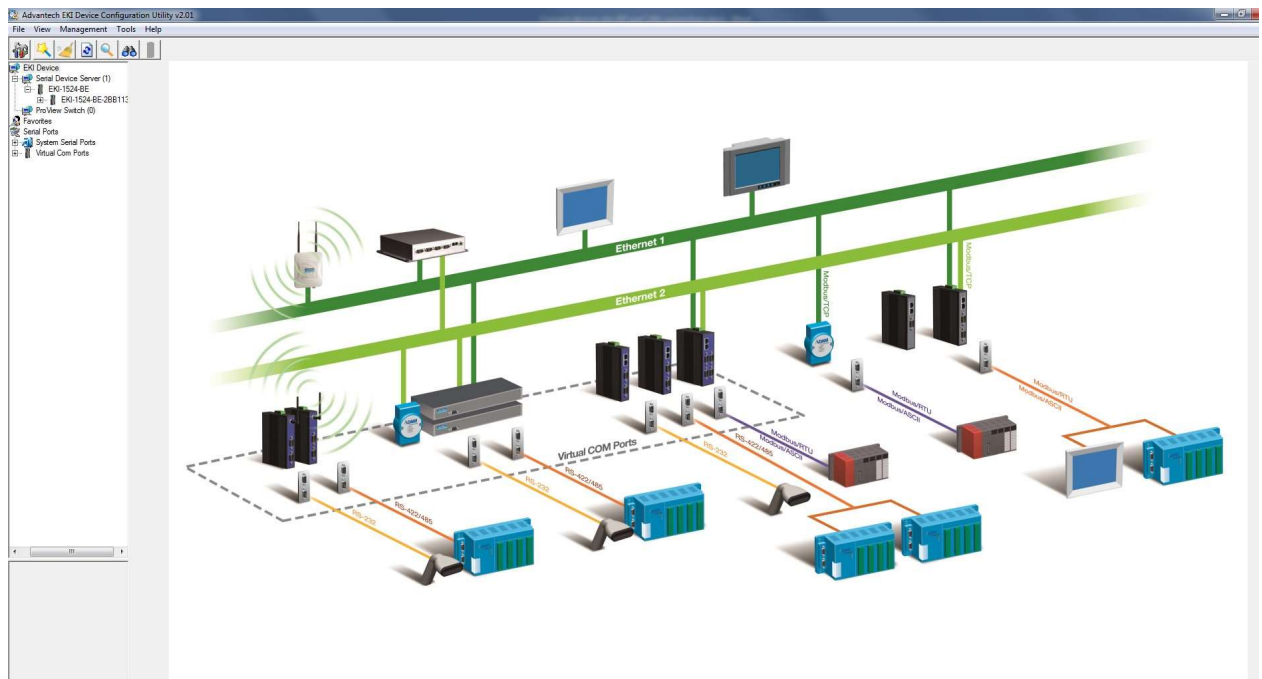


Figure 20: Architecture of the EKI module in the Pelican

CAN bus connections

Some devices in the Pelican, mainly the Hamilton Liquid Handling Robot and the 4-Axis Gantry Robot, require a communication system through their own application without the need of a host computer. A CAN (Controller Area Network) bus allows this message-based protocol. The VCI Device Server Control software allows us to have a programming interface that is independent of the Pelican computer, hence being able to control the liquid handler and the robot simultaneously and independently of the Pelican computer. In the Pelican, to connect the two devices through the CAN bus ports, we need to:

start VCI3 Device Server Control. add the device. add to the running devices in order to initiate desired device.

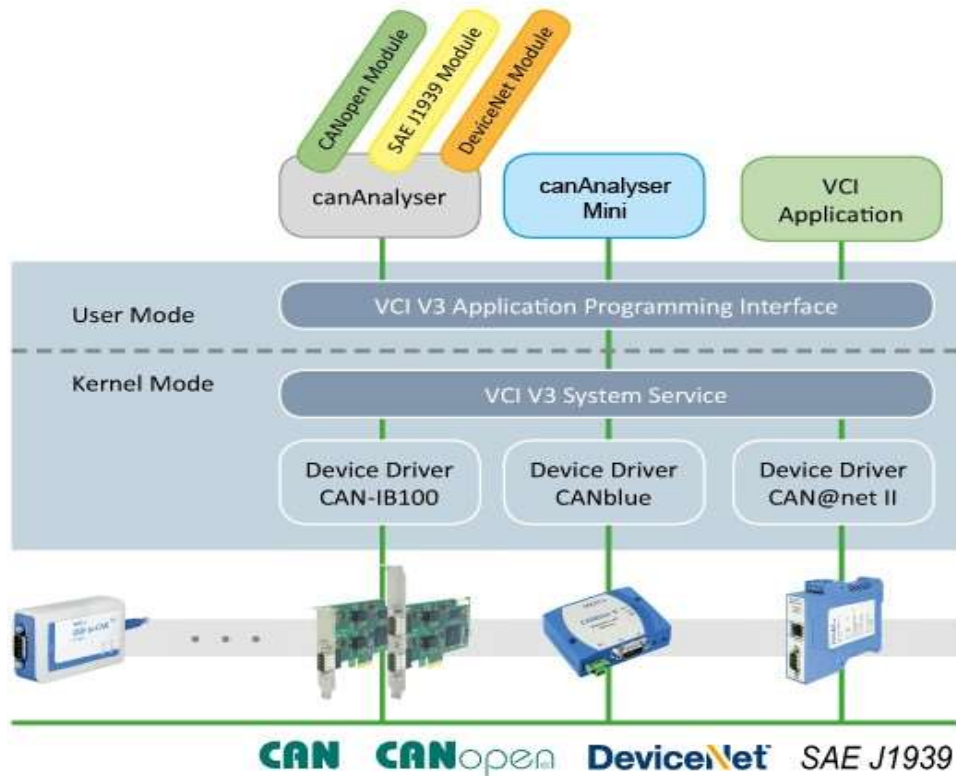


Figure 21: VCI driver interface

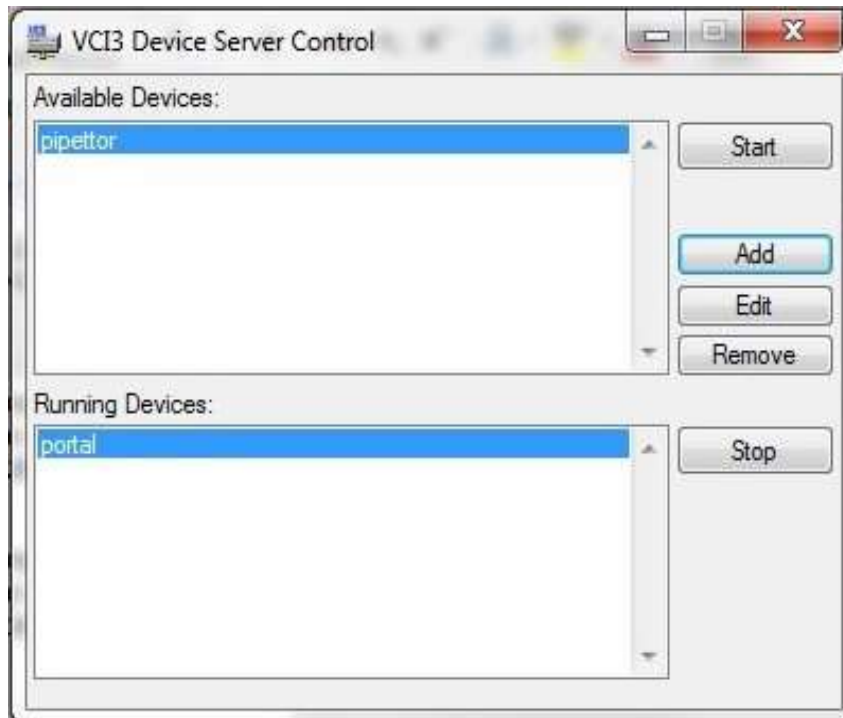


Figure 22: VCI3 Device Server Control

11.9.2. Weidmuller devices

Weidmuller devices have binary sets; binary input and/or binary output. They are usually used for maintenance devices or to control devices with simple binary commands such as ON/OFF, valves ON/OFF, light switch. You will need one single Weidmuller driver to control all of the Weidmuller devices in a plant. You can add a Weidmuller device into the plant by connecting it into the Weidmuller circuit board (Figure 23). If you read the location where the port is connected to the device, you can use the Weidmuller driver to test the device commands .

To control the Weidmuller devices in the Pelican, you need to use the file Fhg Driver Weidmuller UR20.dll to connect to the device. You can start the Weidmuller devices by clicking on weidmueller UR20 GUI.exe, reset and then initialise which enables you to see the digital Input/Output. If the system is ready to accept inputs, it shall display as green. For the outputs, you can activate the different outputs by clicking the circle; red for active and white for inactive.

Valves are usually P switches; you can view the list of devices by opening DeviceConfiguration.xml and modify the switches from P and N or vice versa by opening UR20-ModuleList.xml. In the Pelican plant, two types of digital commands are implemented. There are more than 20 other digital communications and other analog communications that can be bought and integrated into the plant from the Weidmuller website (<http://www.weidmuller.com/>).



Figure 23: weidmuller Hub

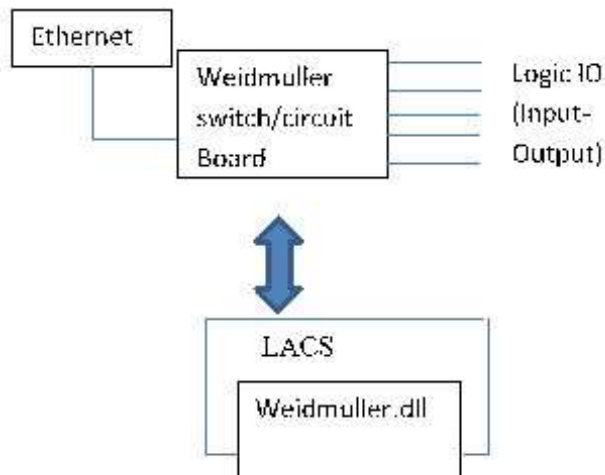


Figure 24: Weidmuller Communication Platform

Appendix

**Laboratory Automation Control Suite (LACS): From
Fraunhofer IPA**

User Documentation LACS

Table of Contents

User Documentation LACS

Introduction

- SiLA Device State Machine
- What is LACS?
- Lacs Pms: Lacs Gui and Lacs Config Editor
- Lacs Core
- What is this documentation about?

Lacs Configuration Editor: Basic operations

- Create a new configuration
- Open an existing configuration
- Save an configuration
- Add an device to an existing Lacs Configuration (Option "Connect to running driver")
- Add an device to an existing Lacs Configuration (Option "Choose driver dll")
- Add a global variable
- Add an process
- Edit an existing process

Lacs Configuration Editor: Editing Processes

- Process Settings
- Local Variables
- Input Parameters
- Currently defined Variables (All available variables)
- Defining a process
 - Add a process step (Command)
 - Add a process step (Subprocess)
 - Remove a process step
 - Configure a process step
- Special Commands
 - PMS Commands
 - Process Commands
 - Subprocess
 - IfThenElse
 - WhileLoop
 - ForLoop
 - StopProcess

List Handling

BuildList

ListItemByIndex

ListItemByValue

ListIterator

Data Handling

BuildComplexType

Parameter Set

DisectComplexObject

MathCommand

SetVariable

UpdateGlobalVariable

ProtocolStep

Using Lacs GUI

Load a config file

Directly connect to a driver

Start a process

Start a device command

Debug a process

Execute commands step by step

Execute commands until stop point

Changing variable values while debugging

Start DDK SiLA Driver

Creating a driver configuration file (.cfg file)

Editing a driver configuration file(.cfg file)

Creating a lacs configuration file

Starting an DDK SiLA driver - (a) manually

Starting an DDK SiLA driver - (b) Via a batch script

General Information: Recommend Proceeding

1. Collect driver configurations
2. Eventually plan distinct control levels
3. Plan the process (A): User Requirements
4. Plan the process (B): Functional Requirements
5. Define Lacs Configuration File(s)

Annex

Does and Don'ts

List of used terms

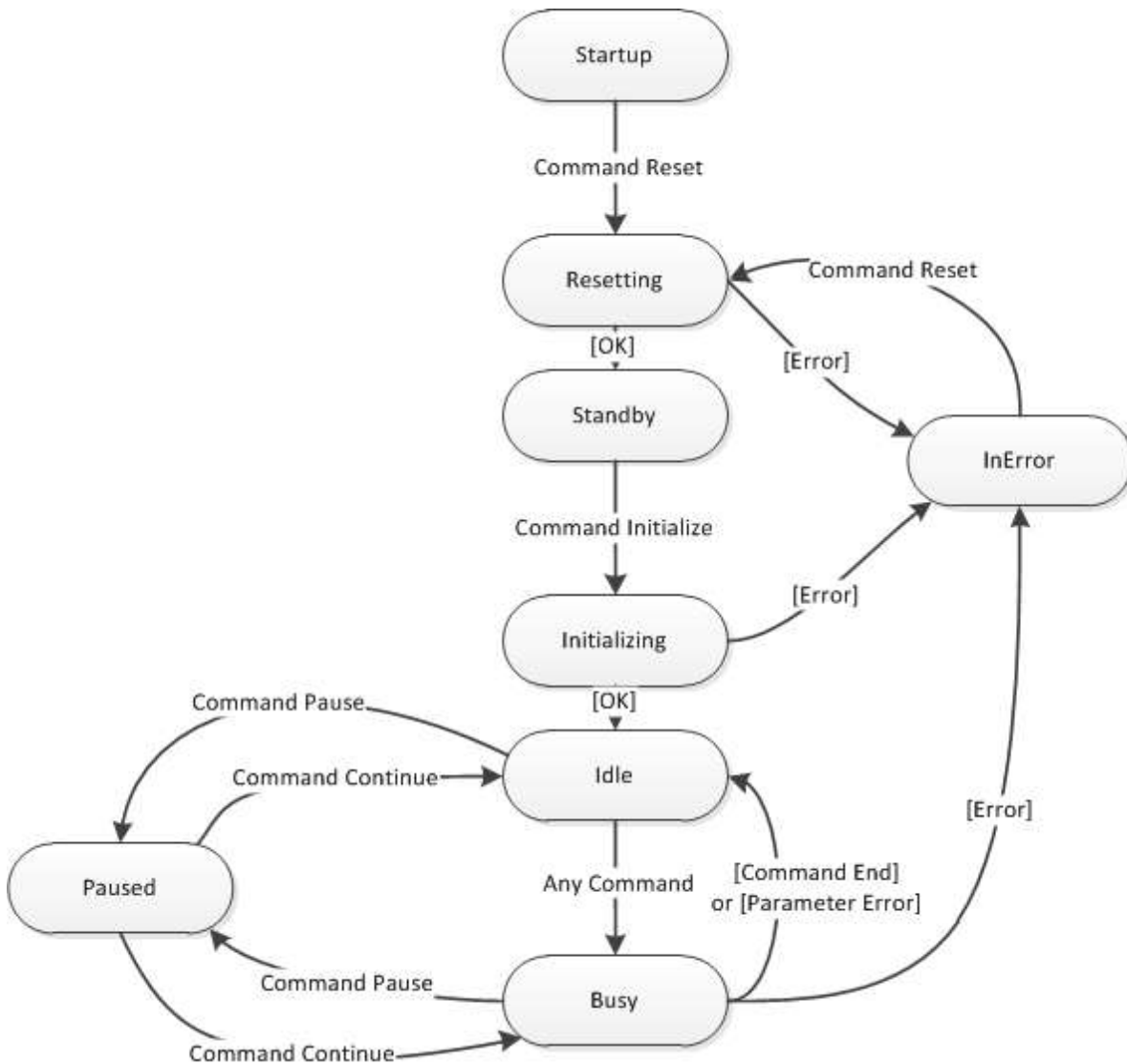
Introduction

To use LACS a basic knowledge of SiLA ("Standardization in Lab Automation") is required. The SiLA association consortium writes about SiLA: "SiLA is aiming to standardize data exchange and command

handling on various levels in the laboratory and from the laboratory towards the enterprise system. SiLA also provides guidelines to implement supplier-specific device commands and parameters, thus enabling unique instrument features” (sila-standard.org/standards). The Standard can be downloaded for free at www.sila-standard.org/ after a registration.

SiLA Device State Machine

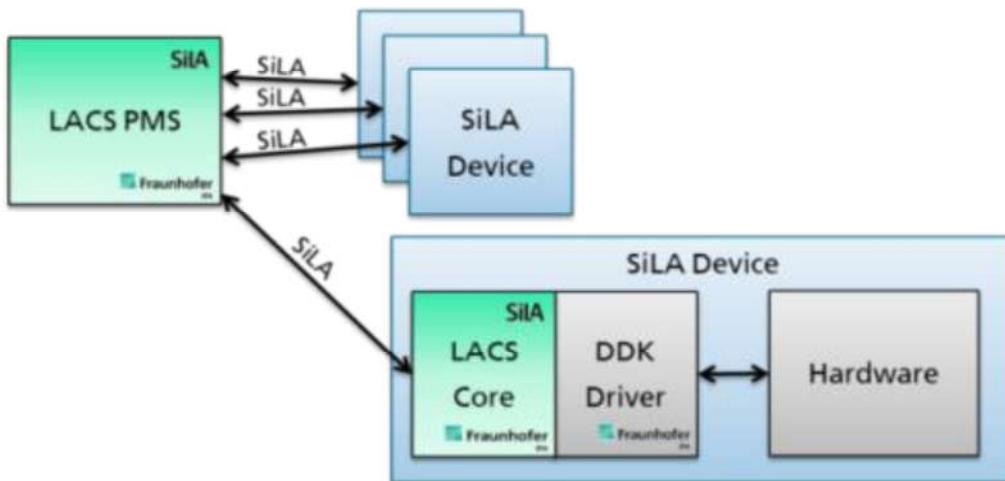
Each SiLA device follows the standardized state machine. Basically this is the following state machine (slightly simplified):



(Detailed state machine: page 37 of [SiLA Device Control & Data Interfaces Specification](#))

What is LACS?

SiLA defines a specified way of communication between devices and the pms (process management software). So both, the pms as well as the device must “speak” SiLA. LACS can be used for both, the device and the pms part of the communication. (The device part is also called “*SiLA Service Provider*”.)



Lacs Pms: Lacs Gui and Lacs Config Editor

The Lacs Pms consists mainly of two programs: *Lacs Gui* (GraphicalUserInterface.exe) and *Lacs Config Editor* (ConfigEditor.exe, also called *Process Editor*).

With *Lacs Config Editor* you can configurate your automation environment with all needed device settings and you can define your processes consisting of device commands. All these data are saved to an xml configuration file (called *Lacs Config File*).

With *Lacs Gui* you can execute and debug the processes, that one has defined in an *Lacs Config File*.

Lacs Core

Lacs Core is a programm which is invisible contained in *Lacs Gui* and *Lacs Config Editor*. It has two main functionalities:

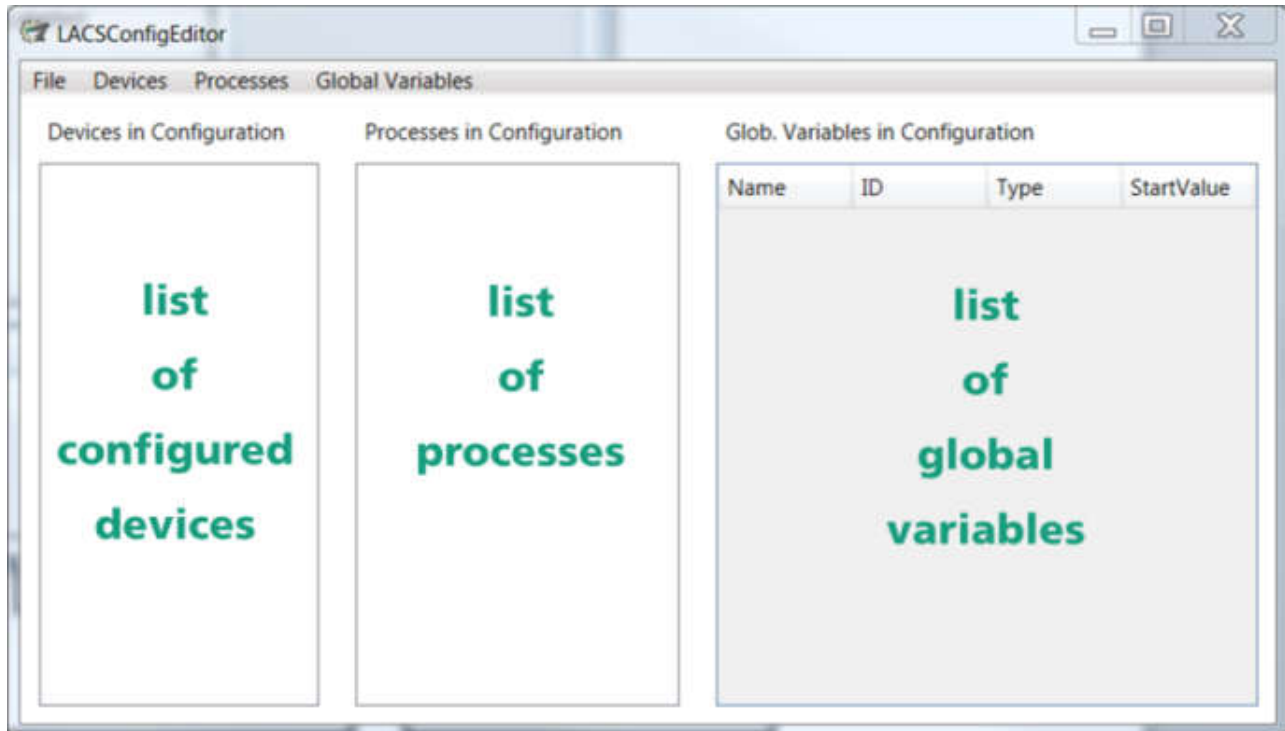
- Pms functionality: Control other SiLA devices
- SiLA Service Provider functionality: To enable an SiLA pms to control this instance of LacsCore.

What is this documentation about?

This documentation describes how to use LACS as a pms (proces management software) and how to use LACS to configure and start a SiLA driver that has been written using DDK.

This documentation does NOT describe how to create a DDK driver.

Lacs Configuration Editor: Basic operations



Create a new configuration

1. Start "ConfigEditor.exe".
2. Click in the menu on "File" > "Save Configuration". Choose a name of your favour.

Open an existing configuration

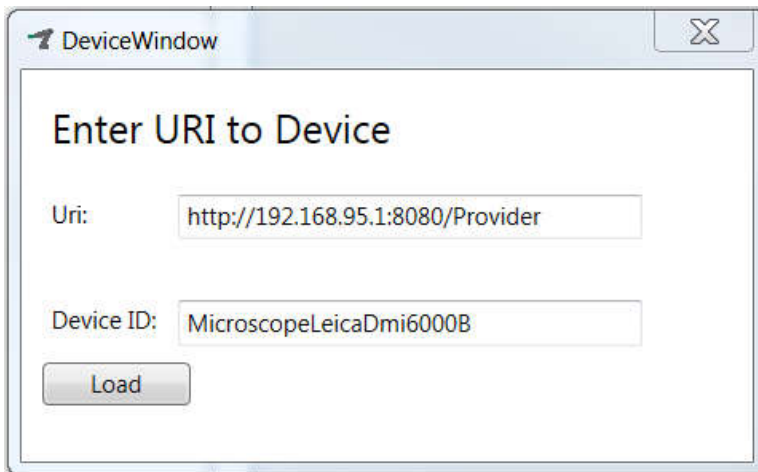
1. Start "ConfigEditor.exe".
2. Click in the menu on "File" > "Open Configuration". Choose the file with the configuration you want to open.

Save an configuration

1. Click in menu on "File" > "Save Configuration". Choose the name of the configuration and click ok.

Add an device to an existing Lacs Configuration (Option "Connect to running driver")

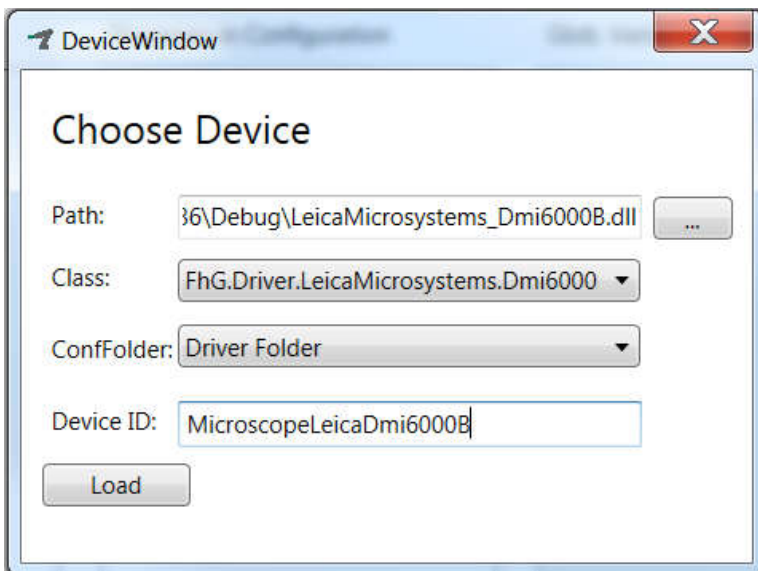
1. Start the SiLA driver of the device you want to add to your configuration.
2. Start "ConfigEditor.exe" and open the configuration you want to edit.
3. Click in the menu on "Devices" > "Connect to a SiLA Device".
4. Insert the Uri (=IP address) and choose an Device ID. In the console window of an DDK driver the Uri can be found after the logging message "Service Provider is starting at [...]".
5. Click on "Load". If the driver can be accessed by Lacs Configuration Editor, the divce will be added to the list "Devices in Configuration"



Add an device to an existing Lacs Configuration (Option “Choose driver dll”)

This option is possible if the driver of the device you want to add has been written with “IPA Driver Development Kit (DDK)” or with “IPA Driver SDK”.

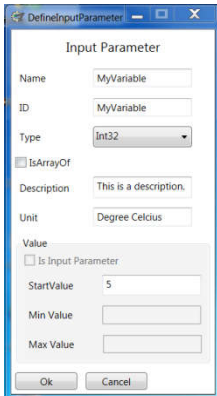
1. Start ConfigEditor.exe and open the configuration you want to edit.
2. Click in the menu on “Devices” > “Load a Driver-DLL”.
3. Choose the path of the driver DLL (for example “LeicaMicrosystems_Dmi6000B.dll” or “FhG_Driver_Weidmueller_UR20.dll”);
4. Insert the Uri (=IP address) and choose an Device ID. In the console window of an DDK driver the Uri can be found after the logging message “Service Provider is starting at [...]”.
5. Click on “Load”. If the driver can be accessed by Lacs Configuration Editor, the device will be added to the list of configured devices.



Add a global variable

1. Click in the menu on “Global Variables” > “Add Variable”.
2. Fill out the fields. It is recommended to use the same Name and ID. The fields “Description” and “Unit” are optional. “Min Value” and “Max Value” are greyed out and cannot be filled. When you are done click “OK”. The window will close and the new variable will be shown in the list of global variables. If you forget to fill a required field, a message box will show you this.

Example:



Tip: Parameters of type String also need a StartValue. If you want to use an empty string as start value, just type a single (or more) space characters into the “StartValue” field. When you click “ok” the spaces (“ ”) will be replaced by an empty string (“”). This is the only case where spaces will be deleted from the StartValue field. If you use other characters in the StartValue field also all spaces will be kept.

Add an process

1. Click in the menu on “Processes” > “Add Process”. The window “ProcessMaker” opens.
2. You now can add and edit process steps
3. If you put in a process name and click ok, the window will close and the new process will be shown at the list of processes.

For details on how to edit a process, look at chapter “Lacs Configuration Editor: Editing Processes”.

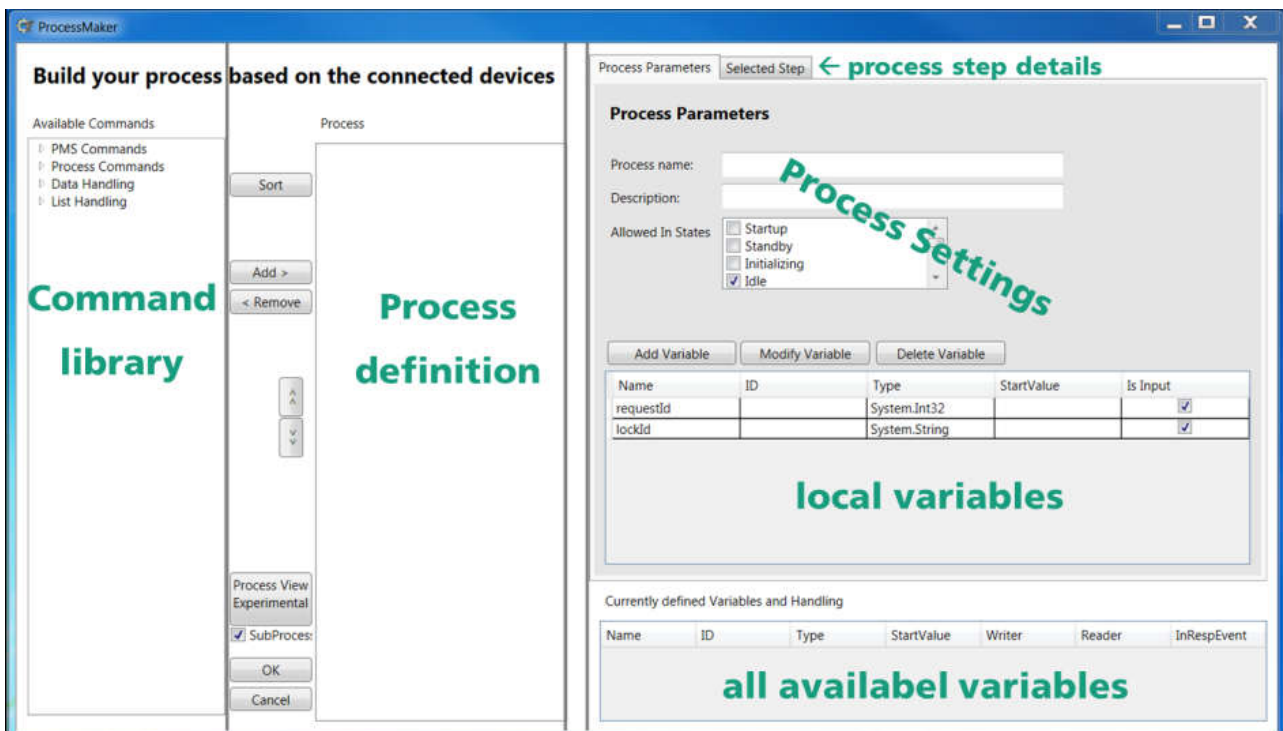
Edit an existing process

1. Click in the menu on “Processes” > “Edit Process”. The window “ProcessMaker” opens.
2. You now can edit the process as described in the next chapter.
3. Click OK

For details on how to edit a process, look at chapter “Lacs Configuration Editor: Editing Processes”.

Lacs Configuration Editor: Editing Processes

When you double click a process to show and edit it, the window “ProcessMaker” opens.



Process Settings

On the right side of the ProcessMaker window is the area with the heading “Process Parameters”. Here you can set and change the process name and a free text description of the process.

The “Allowed In States” setting defines in which pms state the command can be executed. As well as each device the Lacs Pms follows the “SiLA Device State Machine” (see also chapter Introduction). Normally only the state “Idle” should be checked as allowed. – As this is the standard setting you don’t need to change anything after creating a new process.

Local Variables

With the button “Add Variable” you can add a local variable for this process. Use it analogous to adding a global variable (see section “Add a global variable”).

The image shows a dialog box titled "DefineInputParameter". Inside, there is a section titled "Input Parameter". The fields are as follows:

- Name: MyLocalVar
- ID: MyLocalVar
- Type: String
- IsArrayOf:
- Description: This is a description
- Unit: (empty)
- Value section:
 - Is Input Parameter:
 - StartValue: (empty)
 - Min Value: (empty)
 - Max Value: (empty)

At the bottom of the dialog are "Ok" and "Cancel" buttons.

Input Parameters

By means of input parameters you can give a process values when you call it. To add an input parameter click the button "Add Variable". In contrast to adding a local variable you must click the Checkbox "Is Input Parameter". Now you can edit the fields "Min Value" and "Max Value", which are optional. If you fill them, at each call of the process the parameters are checked. If they are out of the range, the process will throw an error. With standard settings this means that the process will stop at this moment.

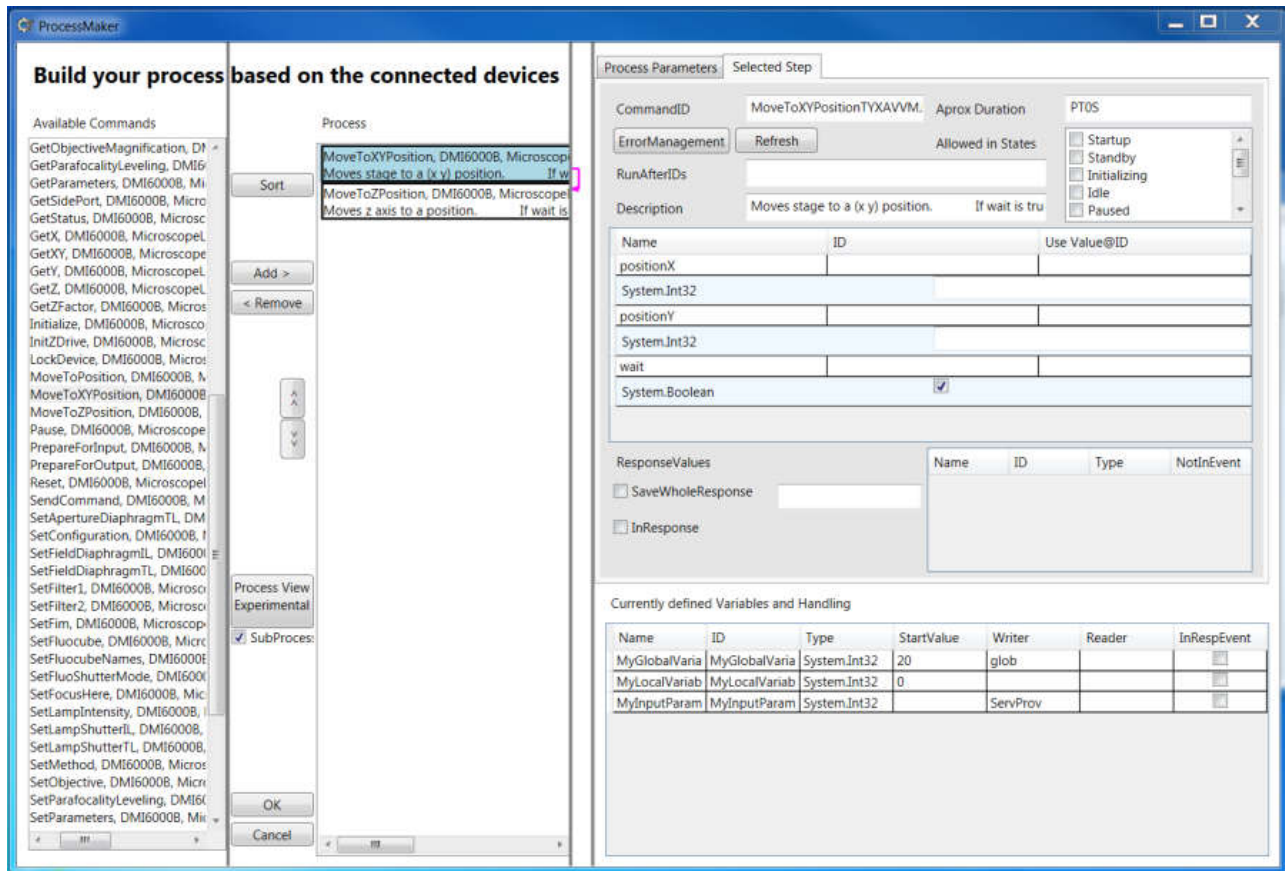
Tip: If you want to set an standard value for an input parameter, you can set "StartValue" before you activate "Is Input Parameter". When you do this and call the process, the input field will be prefilled with the Start Value.

Currently defined Variables (All available variables)

The table of currently defined variables shows all variables, that are visible in the context of this process. That means that there are visible

- all local variables of this process
- all input parameters of this process
- all global variables
- all handles ???

Defining a process



Add a process step (Command)

To add a process step you can browse the command library ("Available Commands"), where all available commands are shown grouped by device. To add a process step double click on a command or mark it with a single click and use the button "Add" afterwards. In the column "Process definition" a new entry for the added command will be shown.

Add a process step (Subprocess)

If you want to call a process the recently programmed, you can select in the command library the section "Process Commands" and then "SubProcess". An Windows will pop up, where you can choose wich process you want to add as a subprocess.

Remove a process step

To remove a process step select the process step in the "Process definition" column and click on the button "Remove".

Configure a process step

Select the Tab "Selected Step" configure a process step. The shown fields are:

- **CommandID:** This Id id identifies a single process step. Normally you should not change it.
- **RunAfterIDs:** Here you can add the Command ID of another process step. This means, that the current process step will only start, when the other process step has finished. To add more than one RunAfterID use a "#" to spereate the command ID's. Each RunAfter-Connection between process

steps is shown as a small coloured arrow to the right of the process definition column. To update the arrows after changing a RunAfterID field, you either must click the button “Sort” or you close and reopen the process (Button “OK”). If you click “Sort”, the displayed order of the process steps may change.

- **Description:** This field will be prefilled with a standard description of the current command. Its content is also shown in the column “Process definition”. So you can use this field to write comments to your process (e.g. “Step 1: Start Incubating”).
- **Input parameters:** The next table with the columns “Name”, “ID” and “Use Value@ID” is used to configure the input parameters of the process step.
 - If you want to use a fixed value, put the desired value in the column “ID” to the right of the variable name.
 - If you want to use a value from a variable or input parameter, then use the column “Use Value@ID” to indicate the ID of the variable (NOT the name). To avoid typos it is recommend to copy and paste the ID. To this you can right-click on desired variable in the table of “all available variables” (“Currently defined Variables”) and select “Copy”. Then you can paste the id to the “Use Value@ID” field.

 **IMPORTANT:** When you insert a value to an “ID” or “Use Value@ID” field you MUST press ENTER to leave the field. If you forget this, your entry will be lost, when you select another process step or leave the ProcessMaker window. If you forgot it and remember before changing the process step or leaving the Process Maker window, you can save the value by again “editing” the field and then clicking Enter.

- **Response values:**
 - Normal case: you can save the response value(s) into an local variable via inserting the variable ID to the field “ID” next to the name of the response value.
 - Special case: SaveWholeResponse: XXXX
 - InResponse: XXXX

 **IMPORTANT:** As at input parameters here the input of the ID must be ended with pressing ENTER.

 **IMPORTANT:** To write an answer to a global variable you afterwards have to use the command “UpdateGlobalVariable” as described in section “Special commands” > “Data handling”.

- **Aprox. Duration:** (advanced feature) XXXX

Special Commands

PMS Commands

- **Breakpoint:** Stops the process and shows a message (in lacs gui a message box). Continues the process either when the user clicks on continue in lacs gui, or when a given timeout duration has elapsed. For the breakpoint you can set a message text and the timeout. The standard timeout is “PT10M” (10 minutes, see below for the duration formatting).
- **Delay:** Waits for a given duration.
- **ChangeFileFlag:** Goes through given text file, removes any occurrences of oldFlag and write newFlag into file.
- **WaitForFileFlag:** Process is blocked, until given text file contains the wished flag, or timeout occurred.

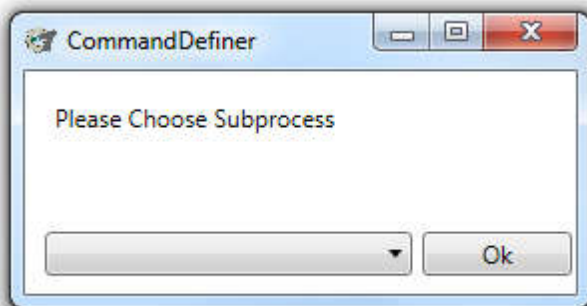
The format for the time durations is the **XML Duration Data Type**, which is defined in ISO 8601. Schema: P[n]Y[n]M[n]DT[n]H[n]M[n]S. Examples:

- P1Y1M --> 1 year and 1 month
- PT1H --> 1 hour
- PT1S --> 1 second
- PT1H5M1S --> 1 hour, 5 minutes and 1 second

Process Commands

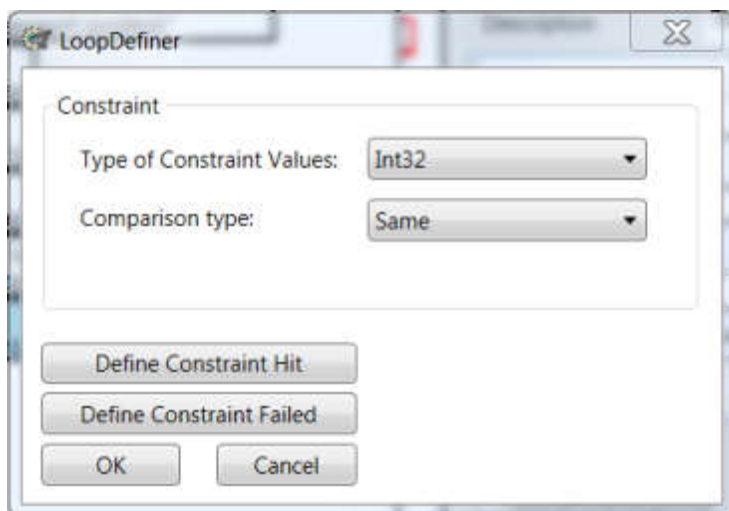
Subprocess

You can call another (recently defined) process via using this command. When you select “SubProcess” and then click “Add” a window opens, where you can choose the process you want to add as a subprocess.



IfThenElse

Compares to given values and decides on that result which protocol steps are performed.



1. **Type of Constraint Values:** Setting the type of the two values, which should be compared.
2. **Comparison type:** The comparison type has to be set (the two compared values are set later on, as well as the comparison type can be changed later on)
3. **Define Constant Hit:** Clicking the button a new process editor window will open, to define the process that is been executed in the case of the comparison result is true.

4. **Define Constrained Failed:** Clicking the button a new process editor window will open, to define the process that is been executed in the case of the comparison result is false.

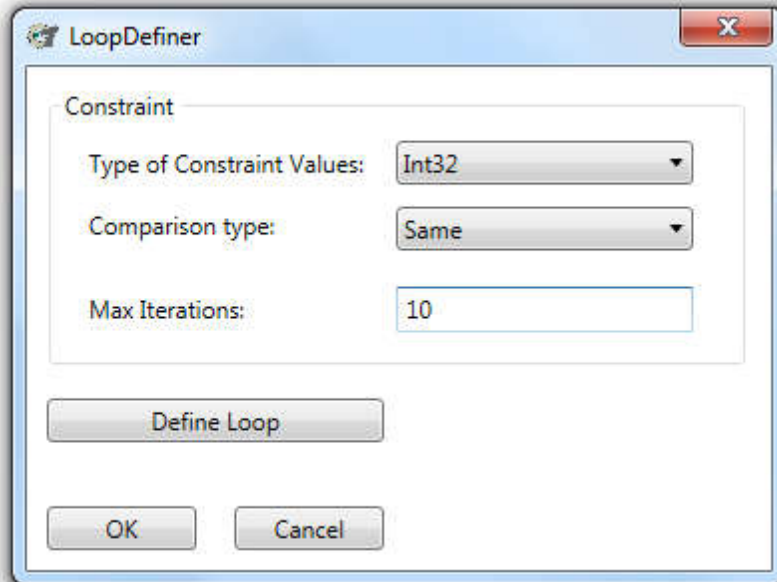
1. **ExpectedValue:** The expected value is normally a fixed value, against the "ActualValue" is been checked.
2. **ActualValue:** The actual value is the variable that should be checked and is the variable part.
3. **ComparisonType:** The comparison type can be edited here.

The constrain can be read like "ExpectedValue" "ComparisonType" "ActualValue", the result goes either to hit or failed.

ComparisonType	True if
Same	"ActualValue" and "ExpectedValue" are equal
Smaller	"ActualValue" is less than "ExpectedValue"
Bigger	"ActualValue" is greater than "ExpectedValue"
In	"ActualValue" is in list of "ExpectedValue"
NotIn	"ActualValue" is not in list of "ExpectedValue"
NotSame	"ActualValue" and "ExpectedValue" are not equala

WhileLoop

This command is used to repeat a process while a defined condition is true. It can be configured similar to "IfThenElse".



1. **Type of Constraint Values:** Setting the type of the two values, which should be compared.
2. **Comparison type:** The comparison type has to be set (the two compared values are set later on, as well as the comparison type can be changed later on)
3. **Max Iterations:** Defines the maximum number of iterations, its like a safety option that the loop will not run for ever if the constrain never fails.

Process Parameters Selected Step

CommandID: WhileLoopWRVSOECMMDOA Aprox Duration: PT05

ErrorManagement: Refresh Allowed in States: [Empty]

RunAfterIDs: ForLoopDWBMLNRWKQCI

Description: This class represents a loop/constraint-check in a l

Name	ID	Use Value@ID
ExpectedValue		
System.Int32	1	
LoopCounter		
System.Int64	0	
ActualValue		
System.Int32		
ComparisonType		

ResponseValues

SaveWholeResponse [Empty]

InResponse

Name	ID	Type	NotInEvent

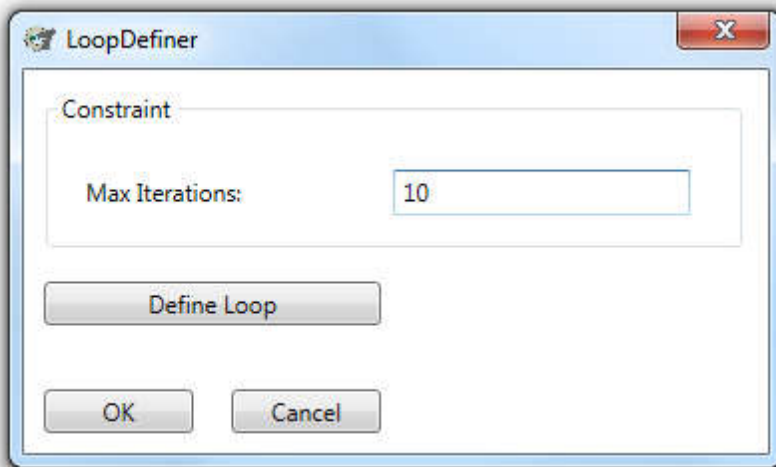
1. **ExpectedValue:** The expected value is normally a fixed value, against the "ActualValue" is been checked.
2. **LoopCounter:** This Variable is been increased each loop round.
3. **ActualValue:** The actual value is the variable that should be checked and is the variable part.
4. **ComparisonType:** The comparison type can be edited here.

The constrain can be read like "ExpectedValue" "ComparisonType" "ActualValue", the result goes either to hit or failed.

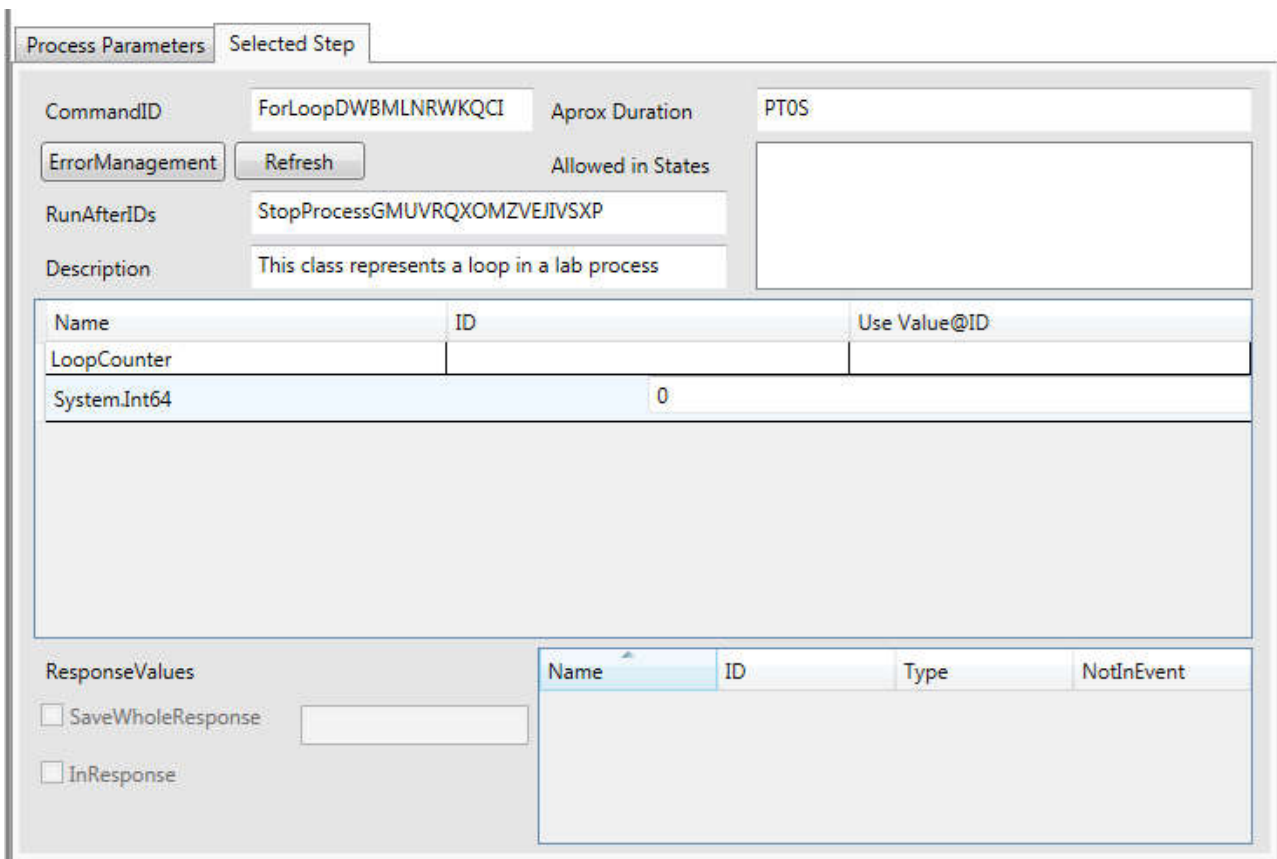
ComparisonType	True if
Same	"ActualValue" and "ExpectedValue" are equal
Smaller	"ActualValue" is less than "ExpectedValue"
Bigger	"ActualValue" is greater than "ExpectedValue"
In	"ActualValue" is in list of "ExpectedValue"
NotIn	"ActualValue" is not in list of "ExpectedValue"
NotSame	"ActualValue" and "ExpectedValue" are not equala

ForLoop

This loop runs for a given count of cycles.



1. **Max Iterations:** Set the number of loop cycles, this can not be set by a variable.



1. **LoopCounter:** This Variable is been increased each loop round.

StopProcess

Stops Process with a given message.

Process Parameters Selected Step

CommandID: StopProcessGMUVRQXOMZV Aprox Duration: PT05

ErrorManagement: Refresh Allowed in States: [Empty]

RunAfterIDs: IfThenElseMPSVEEOVIFDMCEMKUX

Description: Stops Process. Can be used for example inside an i

Name	ID	Use Value@ID
Message		
System.String		

ResponseValues

SaveWholeResponse [Empty]

InResponse

Name	ID	Type	NotInEvent
------	----	------	------------

1. **Message:** The set message is been shown in the process end window.

List Handling

BuildList

With this command you can build up new arrays of data or add items to an existing list.

Process Parameters Selected Step

CommandID: BuildListRAHUDTFDXIHWUTS Aprox Duration: PT55

ErrorManagement: Refresh Allowed in States: [Empty]

RunAfterIDs: WhileLoopWRVSOECMMDOAKXHBZME

Description: builds a list, either adds an item to list, or builds a

Name	ID	Use Value@ID
FirstObjectOrList		
System.Object		
ObjectToAdd		
System.Object		

ResponseValues

SaveWholeResponse [Empty]

InResponse

Name	ID	Type	NotInEvent
generatedList		System.Object	<input type="checkbox"/>

1. **FirstObjectOrList:** Enter here the list where to add an item or the first item of the list.
2. **ObjectToAdd:** Enter here the item that should be added.
3. **GeneratedList:** This is the generated or extended list.

ListItemByIndex

With this method you can get data from a list by the index number.

Process Parameters Selected Step

CommandID: ListItemByIndexUYIFELZEXXG Aprox Duration: PT5S

ErrorManagement: Refresh Allowed in States: [Empty]

RunAfterIDs: BuildListRAHUDTFDXIHWUTSJ

Description: returns item at given position in list

Name	ID	Use Value@ID
ListObject		
System.Object		
IndexOfObject		
System.Int32		

ResponseValues

SaveWholeResponse [Empty]

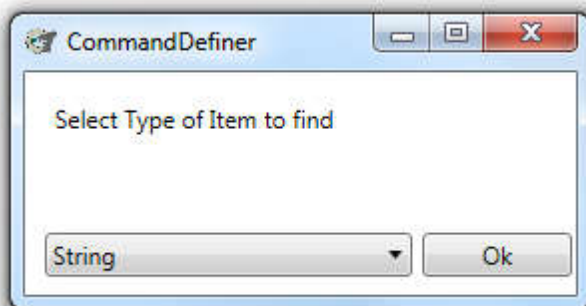
InResponse

Name	ID	Type	NotInEvent
ItemFromList		System.Object	<input type="checkbox"/>

1. **ListObject:** The List from which we want to get the item.
2. **IndexOfObject:** The index number of the item in the list.
3. **ItemFromList:** This is the item of the list on the given index.

ListItemByValue

With this method you can search a specific value in a data list.



1. **Select Type of Item to find:** You have to select the data type of the expected item.

Process Parameters Selected Step

CommandID: ListItemByValueMSMXQQY() Aprox Duration: PT5S

ErrorManagement: Refresh Allowed in States: [Empty]

RunAfterIDs: ListItemByIndexUYIFELZEXXGGREGK

Description: returns a list item identified by a field value

Name	ID	Use Value@ID
ListObject		
System.Object		
FieldName		
System.String		
ValueOfField		
System.String		

ResponseValues

SaveWholeResponse [Empty]

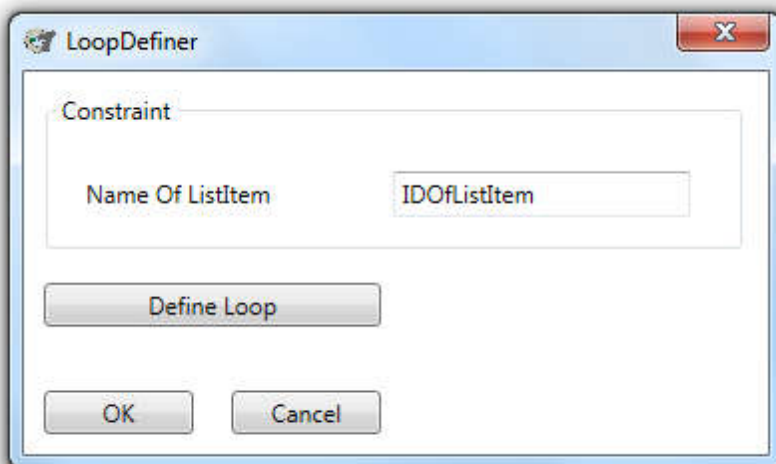
InResponse

Name	ID	Type	NotInEvent
IndexOfItem		System.Int32	<input type="checkbox"/>
ItemFromList		System.Object	<input type="checkbox"/>

1. **ListObject:** The list in which the item should be searched.
2. **FieldName:** ???
3. **ValueOfField:** The value which is search for.

ListIterator

This loop loops through all items in a list.



LoopDefiner

Constraint

Name Of ListItem: IDOfListItem

Define Loop

OK Cancel

1. **Name of ListItem:** Set the name of the variable in the loop, which holds the current item.
2. **Define Loop:** By clicking the button a new process editor window will open and the inner loop process can be programmed.

Process Parameters Selected Step

CommandID: ListIteratorKEVELBSNDYRQO\ Aprox Duration: PT0S

ErrorManagement: Refresh Allowed in States: [Empty Box]

RunAfterIDs: ListItemByValueMSMXQQYQQEEOTO

Description: Loop to Iterate through a list. List is locally copied

Name	ID	Use Value@ID
ListToIterate		
System.Object		
LoopCounter		
System.Int64	0	

ResponseValues

SaveWholeResponse [Empty Box]

InResponse

Name	ID	Type	NotInEvent

1. **ListToIterate:** Set the list from which the items should be loop through.
2. **LoopCounter:** This variable is increased each cycle by one.

Data Handling

BuildComplexType

Builds a string (representing a complex object) from given values. Is directly added to value space.

- - When you add the BuildComplexType command, you must select from a list of different "complex types". The most important types are:
 - For Pipetting: XmlSource, XmlDestination, XmlTipPosition (as defined in sila standard).
 - **SiLA Parameter:**

Parameter Set

Creates an xml parameter set, consisting of a number of sub parameters. This is similar to a Struct in programming languages like C#. When you add a BuildComplexType for a Parameter Set you will be asked to indicate the name and data types of the sub parameters.

DisectComplexObject

This command does the opposite of "BuildComplexType". It splits an complex object into its containing values, and writes them for further handling into variables. You have to select the type of Complex Object, when you add the "DisectComplexObject" command.

MathCommand

Can be used to perform simple mathematical operations. First you have to select the datatypes you want to compute. Possible Computations are "Plus", "Minus", "Times", "Divition" and "Modulo".

SetVariable

Sets a variable to a value. Lists are set separated by #.

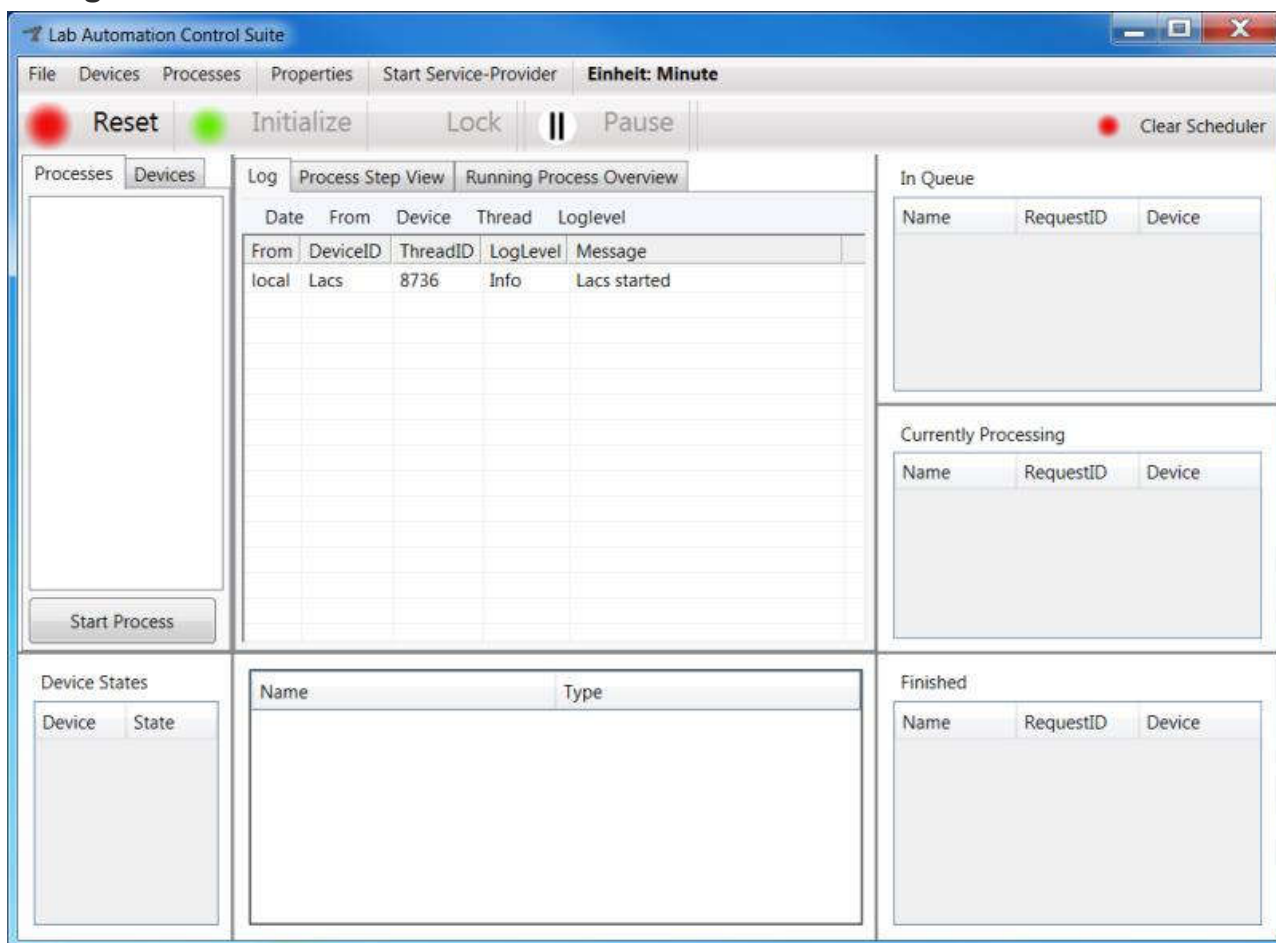
UpdateGlobalVariable

Writes a value to a global variable and/or writes the value from a global variable to a local variable. When adding this command, you must select from the list of global variables wich one you want to update.

ProtocolStep

Creates a log entry with given message and given value.

Using Lacs GUI



Load a config file

1. Click on "File" > "Load Configuration" and select the configuration file.
2. Lacs tries to connect to the configured devices. If this is not possible it will show an error message.

Processes that use commands from devices, that cannot be connected to are not shown in the list of processes. To show a list of unavailable Processes, click on "Processes" > "Show unavailable processes".

Directly connect to a driver

You can directly connect to a single driver without creating a configuration file before:

1. Click "Devices" > "Connect to a SiLA Device"
2. Enter the device URI (e.g. "http://192.168.95.1:8070/Provider") and choose an DeviceID. To jump to the next text field you also can use the TAB-Button.
3. Click "load". Now the commands of this device will be shown in the list on the left side and you can start them.

Start a process

Preperation:

- Before you can start a process, you have to Reset and Initialize the Lacs Pms (see chapter "SiLA Device State Machine"). The red button "Reset" sends a reset command to all connected devices and resets the pms. The green button "Initialize" sends a initialize command to all connected devices and initializes the pms.
- The current pms state can be read via clicking "File" > "Show current pms state".
- You can deactivate the pms state machine via selecting "Properties" > "PMS state machine enabled".

Start a process:

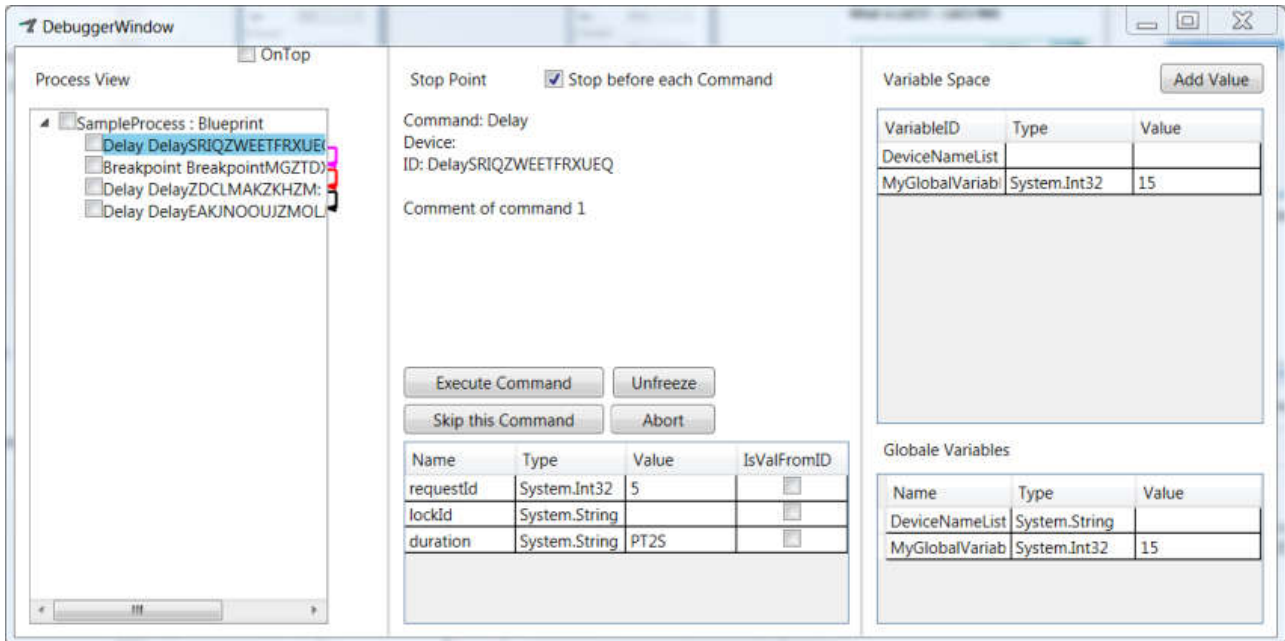
1. Select the process you want to start from the list of processes.
2. Fill the fields with the process parameters you want to use.
3. Click on "Start Process".

The steps of the process will gradually be added to the "In Queue" list. As soon as they are currently executing they are moved to the "Currently processing" list. After finishing the process step, it will be shown in the list "Finished".

Start a device command

1. Reset and Initialize the pms as described in "Start a process".
2. Select the tab "Devices", choose the device.
3. Double click on the command you want to execute. If parameters are required fill the fields.

Debug a process



1. Click on "Processes" > "Debugger" in the Main window.
2. The Debugger Window opens. It will stay on top of all other windows. To disable this functionality, you can deactivate the checkbox "OnTop".
3. DebuggerWindows: Take care that the checkbox "Stop before each Command" is activated (this is the standard value).
4. Main Window: Start a process
5. Debugger: The process will be loaded into the debugger.

Execute commands step by step

1. Make sure that "Stop before each Command" is activated.
2. Click on "Execute Command". The blue highlighted process step will be executed.
3. To skip a single command click on "Skip this Command".

Highlighting colors for process steps:

Color	Meaning
Blue	This process step will be executed next.
Yellow	This process step is currently be executed.
Green	This process step has been finished.

Execute commands until stop point

- To execute many commands without a break, deactivate "Stop before each Command".
- If you want, you can set "stop points". These are defined by selecting the check box before a process step.
- When you now click "Execute Command", the process will be executed until it reaches a stop point.

- If you change your mind, while the process is running, you can select "Stop before each Command". Then the current running process steps will be finished. Afterwards the process waits.

Changing variable values while debugging

You can change the values of variables in the debugger. In the middle column the parameters for the next process step are shown. In the right column the local or global variables are shown. Double click a field to change it. Press enter to save your changes. With the button "Add Value" you can add local variable.

Start DDK SiLA Driver

Before you can start the driver, you have to make sure that the driver configuration file (.cfg) and the lacs configuration file (.lconf) exist.

Creating a driver configuration file (.cfg file)

1. Navigate to the driver folder and identify the driver dll file. The name of the file normally has the form *<Manufacturer><Devicename>.dll* or *<Manufacturer>_<Devicename>.dll*.
2. Drag the driver dll to "DriverGui.exe". The Driver Test Gui window opens. Click on "Commands" > "Reset/Save Configuration" and close the Driver Test Gui window.
3. The file will be created. The name is always the same as the driver dll (except from the file name ending).

Editing a driver configuration file(.cfg file)

1. Navigate to the driver folder and identify the cfg file. The name of the file is identical to the driver dll file (except from the file ending. It normally has the form *<Manufacturer><Devicename>.dll* or *<Manufacturer>_<Devicename>.dll*.
2. Drag the ".cfg" file of the driver to "*IPA_DDK_ConfigEditor.exe*". The config editor window opens. Choose the parameters as described by the supplier of the driver and click save.

Creating a lacs configuration file

1. Navigate to the driver folder and identify the driver dll file.
2. Drag the driver dll to "*LacsDriverCore.exe*". The driver core window opens.
3. The configuration file should have been created now. Ignore the error messages in the driver core window and close the window.
4. Open the configuration file with a text editor (e.g. "Notepad++"). You can edit the fields "IPAdresse", "LogLevel" and "Port".
 - IPAdresse: Set the value to the ip adress of the computer, where the driver is running (*<IPAdresse>XXX.XXX.XXX.XXX</IPAdresse>*). This will be the address where the sila service provider for this driver can be reached
 - Port: Set the port for this driver. Remember that each driver needs its own port and the port must not be occupied by another program. Also remember to configure the port in your firewall, if you want to access the driver from the network.
 - LogLevel: Sets the detail level for the logfile. Allowed values: "Superdebug", "Debug", "Info", "Warning", "Error".

The name of the lacs configuration file is always "*LacsSiLAConfiguration.lconf*".

Starting an DDK SiLA driver - (a) manually

Drag the driver dll or the lacs configuration file onto "*LacsDriverCore.exe*". The driver core window starts and shows some log messages. Warnings are written in yellow, errors in red. After fully starting the driver "The ServiceProvider is starting at [http://ADDRESS:PORT/Provider]" is written in the driver window.

Starting an DDK SiLA driver - (b) Via a batch script

1. Create a text file with the following content and insert the correct paths.

```
START "NAME" "PATH TO LacsDriverCore.exe" "Path to  
LacsSiLAConfiguration.lconf"
```

Example:

```
START "LACS - Bioshake" /MIN "C:\Program Files (x86)\Fraunhofer  
IPA\BioshakeIPA\LacsDriverCore.exe" "C:\Program Files (x86)\Fraunhofer  
IPA\BioshakeIPA\LacsSiLAConfiguration.lconf"
```

2. Save the file with the file ending ".bat".

3. You now can start the driver via double click on the bat file or you can add a link to the bat file to Windows Autostart.

If you start more than one driver in one batch file, you should add an delay between starting the drivers:

```
ping -n 2 localhost> nul
```

Example for a complete batch file:

```
@echo off  
  
echo "Terminate bioshake driver"  
taskkill /F /FI "WINDOWTITLE eq LacsDriverCore BioshakeT_ELM @  
http://192.168.95.1:8060/Provider?wsdl"  
ping -n 2 localhost> nul  
  
echo "Start LACSBioshake"  
START "LACS - bioshake" /MIN "C:\Program Files (x86)\Fraunhofer  
IPA\BioshakeIPA\LacsDriverCore.exe" "C:\Program Files (x86)\Fraunhofer  
IPA\BioshakeIPA\LacsSiLAConfiguration.lconf"  
  
echo "Done starting bioshake driver!"  
ping -n 2 localhost> nul
```

General Information: Recommend Proceeding



This chapter gives a **proposal** how to develop the plant control. Use all this recommendations **ON YOUR OWN RISK AND YOUR OWN RESPONSIBILITY**. We can not assume any responsibility for your actions you derive from this chapter. This tips are useful in many but not in all situations.

1. Collect driver configurations

Write down a list of all device drivers and their SiLA IP address and port. Choose and unique identification for each device („DeviceID“). Example:

Name	DeviceID	SiLA IP / Port
Microscope	LeicaDmi6000B	192.168.95.1:8010
Gantry Robot	GantryRobot	192.168.95.1:8020
Pipettor
...

2. Eventually plan distinct control levels

For example:

Level 1: Transport Layer

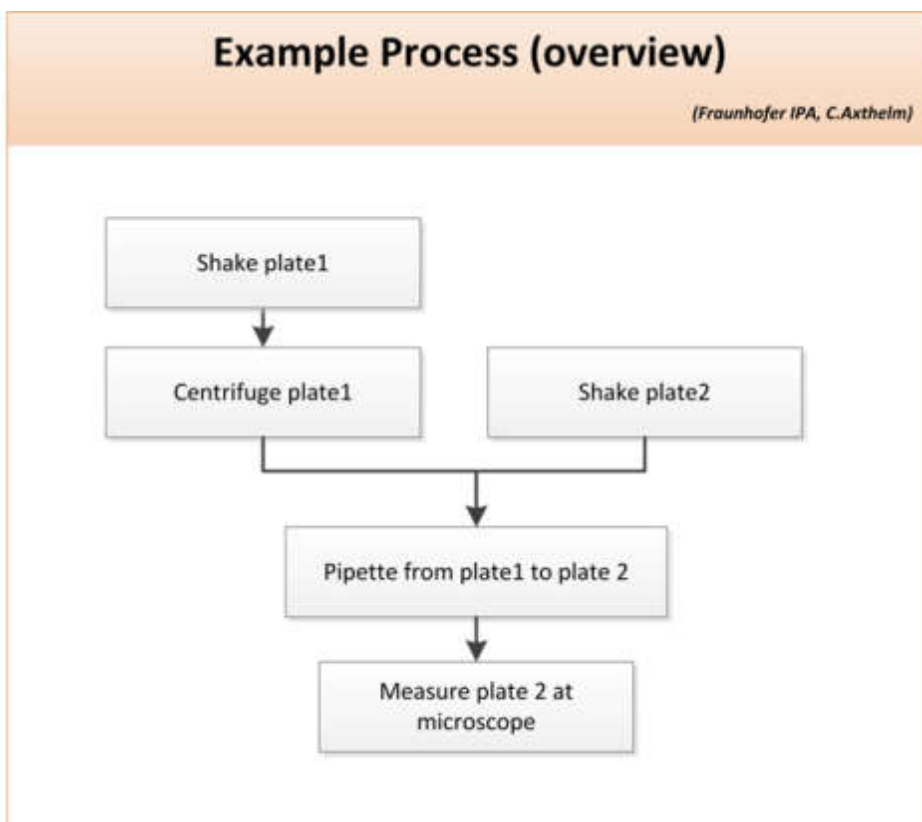
Level 2: Process Layer

Level 3: Only processes that can be used by non-expert laboratory staff without doing any harm to the plant.

3. Plan the process (A): User Requirements

Collect the user requirements for the process. Draw a graphical overview together with the assay expert.

Remember: The assay expert normally is not an expert for the automation. So talk and ask a lot to avoid misunderstandings.

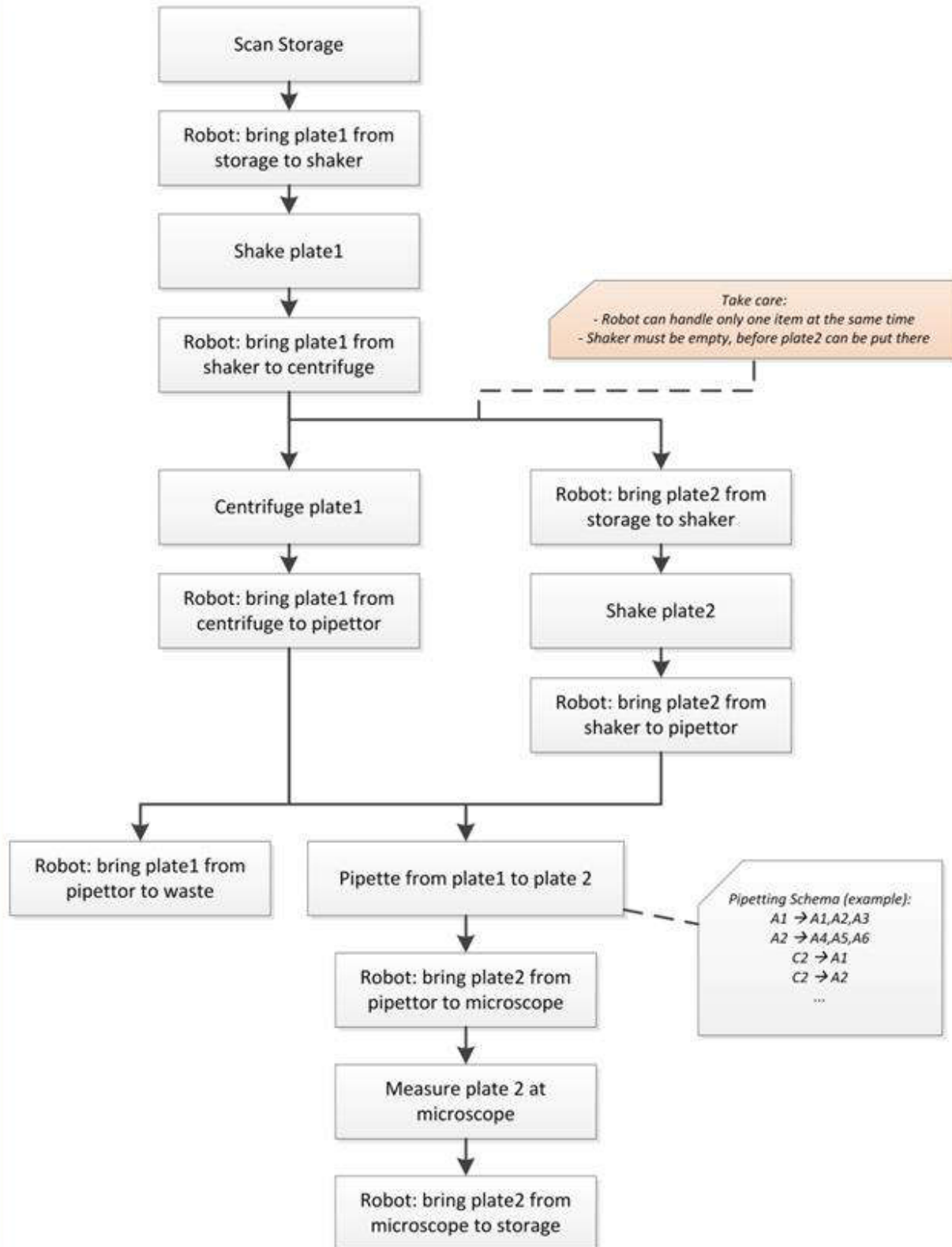


4. Plan the process (B): Functional Requirements

Translate the User Requirements to a technical detailed process flow chart. Write down every single simple step. Visualize eventually parallel executed steps. If it seems necessary define Sub-Processes which collect a bundle of steps.

Example Process (detail)

(Fraunhofer IPA, C.Axthelm)



5. Define Lacs Configuration File(s)

Use Lacs Configuration Editor to define a Lacs Configuration File. Build the previously defined subprocesses and main processes as described in this manual. If you have defined distinct control levels, define an own Configuration File for each level. Start with the lowest level. Make cycles of defining / programming the processes and debugging them with Lacs Pms.

Annex

Does and Don'ts

Don't:

- Don't edit the Lacs Configuration File manually!
- Don't rename processes after you have inserted them as subprocess in other processes! The reference in these processes will then be lost and an runtime error will occur!

Do:

- Choose meaningful names for your processes from beginning on. When they are in use by other processes as subprocess you are not allowed to change the name anymore!
- Use a version management tool for your configuration files (e.g. Git or Subversion).
- Think about your process architecture before you program it. Write it down on paper and discuss it with the assay experts before programming.

List of used terms

- Lacs Gui
- Lacs Core
- Lacs Process Editor
- Lacs Config File
- DeviceID
- SiLA URI

Khalid Ibnou Walid KANE

IsDB, 8111 King Khalid St. AI Nuzlah AI Yamania Dist. Unit No. 1 Jeddah 22332-2444, KSA
Phone: 00966 55 8204166 / 00221 77 463 25 79

khalidkane@hotmail.com

SUMMARY

- ✓ Multi-lingual (English, French) with strong engineering, entrepreneurial background and global experience
- ✓ Demonstrated business leadership, engineering capabilities, new product development (NPD), cross-functional training, and competitive intelligence
- ✓ Research focus with strong analytical, mathematical educational background
- ✓ Effective at combining creative thinking with logical design ideas to develop solutions to challenging engineering, industrial and business-related issues
- ✓ Proven success in self-managed and team-based projects
- ✓ Excellent verbal and written skills with a detail-oriented approach for completing projects and assignments

WORK EXPERIENCE

Islamic Development Bank IsDB - Young Professional Program, Jeddah 2017-Present *Strategy and Transformation Department - Foresight Strategist*

- ✓ Developed the making markets work for development through global value chains methodology as a new strategy for the Bank
- ✓ Applied the GVC approach to include it as the country engagement tool for the Member Country Partnership strategy
- ✓ Completed an RCA analysis for IsDB member countries to come up with the five industries championed by HE The President of IsDB
- ✓ Contributed to his HE the President of IsDB's book: The road to SDGs, a new development model
- ✓ Co-authored an industrialization paper: "The Industrialization Intervention Framework" as a strategy framework for the Bank

Country Relations and services - Global Value Chain (GVC) Expert

- ✓ Led GVC based Member Country Partnership strategy for Gabon: Wood and Manganese Value Chains in the Republic of Gabon
- ✓ On the ground data collection and firm level surveys for GVC analysis
- ✓ Provided GVC inputs for Member Country Partnership strategy of Maldives, Turkey and Morocco
- ✓ Operation Team Leader for Technical assistant grand projects for Trade enhancement program for Suriname and Guyana
- ✓ Led the organization of a GVC workshop in collaboration with Duke University GVCC
- ✓ Missions to Guinea, Niger, Cote d'Ivoire, Malaysia and Indonesia to market the new IsDB Presidency Program based on GVC

LCSB, Luxembourg 2016-2017 *Mechatronic Engineer*

- ✓ Computer programming of Automated Systems using C# and SiLA standards: develop SiLA (Standardisation in Laboratory Automation) compliant drivers, and implement long term protocols into automated plant
- ✓ Maintenance and continuous integration of laboratory robotic system
- ✓ Modelling of complex systems
- ✓ Fully automate cell culture protocols based on three-dimensional microfluidic technology
- ✓ Computational fluid dynamics modelling to optimise the design of micro systems

COGELEC Energy SARL, Senegal 2014-2016 *Project Engineer*

- ✓ Trades: electrical, construction of high and medium voltage lines, construction and engineering of power transformers and power plants

Khalid Ibnou Walid KANE

- ✓ Long-term strategy focused on production of electrical energy with the following technologies (i) concentrated solar (CSP) (ii) classic photovoltaic (PV) and hybrid systems and (iii) small scale hydroelectric systems
- ✓ 150 hectares of land acquired from the municipality of Ndioum, Podor region for the construction of PV and/or CSP plant and a water treatment plant fed by the Senegal River for the cooling of the CSP
- ✓ Negotiating with ASER (Governmental Agency) for the establishment of twenty ERILs (Rural Electrification from Local Initiative) in Thies region where the goal is to give local population (more than 40,000 people) access to electricity. Not enough subsidy provided by the government to allow the project to yield a positive NPV given the low spending power of local population for some villages. However, the project is in an implementation phase in 4 villages in the East of Senegal for rural electrification.

SDK Mining SA, Senegal

2012-2015

Founder and Managing Director

- ✓ Led negotiations with the Senegalese Government
- ✓ Led effort to obtain an exploration permit (Baitilaye) of 258km²
- ✓ Drafted technical mining reports for Baitilaye
- ✓ Drafted Pre- and Post-Prospection financial proposals
- ✓ Led a team, for building geological and geochemical maps of the Baitilaye area
- ✓ Led negotiations, to secure a Joint Venture partnership

Pyramid Group, GCI, Senegal

2012-2012

Management Consultant trainee (Project Management)

- ✓ Drafted technical and financial report for one of the largest fishing factories in Senegal. Restructuring of the management processes and procedures; and a financial projection of the financial profitability over 7 years was also drafted. This helped the fishing company secure 300 million Francs CFA financing from LOCAFRIQUE
- ✓ Drafted a business plan for a mega agricultural project, including the program of activities and the first draft for an agro-pastoral funding. Contacted potential suppliers for the purchase of agricultural equipment
- ✓ Prepared Excel spreadsheets for various projects and clients of the firm
- ✓ Credit Structuring, Project Planning and Structuring
- ✓ Project Viability Analysis

Allianz Insurance PLC, UK

2011-2011

Management Consultant trainee in Commercial Underwriting (Engineering Technical Standards)

- ✓ Completed a report on wind turbines, future trends, help create business plan for Allianz to analyse market entry points for wind turbines business opportunities.
- ✓ Drafted an overview brochure containing short summaries of the services for the Engineering side of Allianz.
- ✓ Created a spreadsheet containing hyperlinks that helped non-engineers understand engineering issues.
- ✓ Provide necessary planning, coordinating activities and created modules from an engineering standards standpoint.
- ✓ Formulated valuable service process maps and programs for ensuring quality financial/engineering delivery. Provide various underwriting and investigating procedures and formulated improvement measures to all accessible inspection onsite procedures. Create proper analytical methods for various client pieces of equipment and determining service and supply requirements. Provide proper time management and tasks to work under tough deadline.

EDUCATION

University of Oxford, UK

2014

MSc in Biomedical Engineering on a full scholarship

Achieved degree class: **Distinction**

University College London and London School of Economics & Political Sciences, UK, 2012

BEng in Engineering with Business Finance (from LSE in London)

Achieved degree class: **First Class Honours** with nomination to the **Dean's List**

Khalid Ibnou Walid KANE

PUBLICATIONS

- ✓ M. F.S. Hamid, **K. I.W. Kane**, A. E. Demirhan, A. Khodary, Making Markets Work for Development through Global Value Chains: Methodology and tools to identify and measure the highest-potential value chains, King Fahd National Library, ISBN: 978-603-32-0354-0 (2019)
- ✓ **K. I.W. Kane**, M. Walter, M. Thoma, Pelican user manual (2017).
- ✓ **K. I.W. Kane**, E. Lucumi Moreno, S. Hachi, M. Walter, J. Jarazo, T. Hankemeier, P. Vulto, J. C. Schwamborn, M. Thoma, R.M.T. Fleming, Automated microfluidic cell culture of stem cell derived dopaminergic neurons, *Scientific Reports*, volume 9, Article number: 1796 (2019); doi: 10.1038/s41598-018-34828-3
- ✓ **K. I.W. Kane**, E. Lucumi Moreno, C. M. Lehra, S. Hachi, R. Dannert, R. Sanctuary, C. Wagner, R. M.T. Fleming and J. Baller, Determination of the rheological properties of Matrigel for optimum seeding conditions in microfluidic cell cultures, *AIP Advances* 8, 125332 (2018); doi: 10.1063/1.5067382
- ✓ **K. I.W. Kane**, Ronan M.T. Fleming, Jens Schwamborn. Invention Disclosure Statement "Neuronal optimum 3D microfluidic device" (*KTT 180052*)
- ✓ **K. I.W. Kane**, Javier Jarazo, Edinson Lucumi Moreno, Paul Vulto, Ronan M.T. Fleming, Bas Trietsch, Jens Schwamborn, Passive controlled flow for neuronal cell culture in 3D microfluidic devices. (*in preparation*)
- ✓ Siham Hachi, Edinson Lucumi Moreno, Sarah L. Nickels, **K. I.W. Kane**, Masha Moein, Jens C. Schwamborn, Alex Skupin, Pieter Vanden Berghe, Ronan M.T. Fleming, Neuronal hyperactivity in LRRK2-G2019S mutation of cellular models of Parkinson's Disease. (*in preparation*)

FURTHER EDUCATION

University of Luxembourg, Luxembourg, 2019

PhD in Bioengineering

Johns Hopkins Carey Business School, US, 2018

Persuasive Communication Executive Education

University of International Business and Economics and World Trade Organization, China, 2018

GVC Workshop

Islamic Research and Training Institute, KSA, 2017

Islamic Finance: Beginner and Intermediate Level

Islamic Development Bank, KSA, 2017

Project Management Professional Executive Education

ACHIEVEMENTS

- ✓ Received offer to complete PhD at the University of Oxford (Declined)
- ✓ Awarded a full scholarship (Yousef Jameel Scholar) to attend Oxford University as an MSc student 2013
- ✓ Member of the Oxford SEH football team 2013
- ✓ Built an accounting software for a local Investment Bank in Senegal 2012
- ✓ UCL's Dean List for Outstanding Achievement 2012
- ✓ Designed a novel Wave Energy Buoy device 2012
- ✓ Awarded the Goldsmid Sessional Prize for Mechanical Engineering 2010-11
- ✓ Chairman of the Engineering Student Committee Board (ESCB) 2011
- ✓ Submitted an innovation idea approved by the UCL Engineering Innovation Review Panel 2011
- ✓ Tutoring young unprivileged students in the East Ham area, London 2010

SKILLS AND OTHER INTERESTS

Languages

Native fluency in French (DALF C2) and English (IELTS 8.0), and two other Senegalese languages (Wolof, Fuula)

Technology

Microsoft Office

Experienced user of programming languages: FORTRAN and MATLAB, both of which are very powerful and similar to C++, C#, AUTOCAD (CATIA and SOLIDWORKS), PVSyst, Finite Element Analysis Package ANSYS

Mathematics

Linear Probability, Probability Methods, Statistics, Advanced Calculus, Optimization